

**UNCLASSIFIED**

---

---

**AD 401 106**

---

*Reproduced  
by the*

**ARMED SERVICES TECHNICAL INFORMATION AGENCY  
ARLINGTON HALL STATION  
ARLINGTON 12, VIRGINIA**



---

---

**UNCLASSIFIED**

NOTICE: When government or other drawings, specifications or other data are used for any purpose other than in connection with a definitely related government procurement operation, the U. S. Government thereby incurs no responsibility, nor any obligation whatsoever; and the fact that the Government may have formulated, furnished, or in any way supplied the said drawings, specifications, or other data is not to be regarded by implication or otherwise as in any manner licensing the holder or any other person or corporation, or conveying any rights or permission to manufacture, use or sell any patented invention that may in any way be related thereto.

**U. S. A R M Y**  
**TRANSPORTATION RESEARCH COMMAND**  
**FORT EUSTIS, VIRGINIA**

TCREC TECHNICAL REPORT 62-63

**RESEARCH PROGRAM TO DETERMINE THE FEASIBILITY AND POTENTIAL  
OF THE GROUND EFFECT TAKE-OFF AND LANDING  
(GETOL) CONFIGURATION**

**VOLUME II**

Task 9R38-11-011-01  
Contract DA 44-177-TC-663

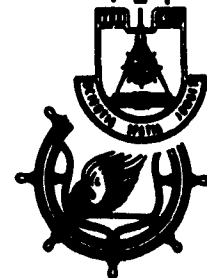
December 1962

APR 17 1963

CATALOGED BY ASTIA  
AD NO. 401106

Agreed by:

- VERTOL DIVISION  
The Boeing Company  
Morton, Pennsylvania



NO. OTS

### DISCLAIMER NOTICE

When Government drawings, specifications, or other data are used for any purpose other than in connection with a definitely related Government procurement operation, the United States Government thereby incurs no responsibility nor any obligation whatsoever; and the fact that the Government may have formulated, furnished, or in any way supplied the said drawings, specifications, or other data is not to be regarded by implication or otherwise as in any manner licensing the holder or any other person or corporation, or conveying any rights or permission, to manufacture, use, or sell any patented invention that may in any way be related thereto.

### ASTIA AVAILABILITY NOTICE

Qualified requesters may obtain copies of this report from

Armed Services Technical Information Agency  
Arlington Hall Station  
Arlington 12, Virginia

This report has been released to the Office of Technical Services, U. S. Department of Commerce, Washington 25, D. C., for sale to the general public.

Reproduction of this document in whole or in part is prohibited except with specific written permission of the Commanding Officer, U. S. Army Transportation Research Command.

The findings and recommendations contained in this report are those of the contractor and do not necessarily reflect the views of the U. S. Army Mobility Command, the U. S. Army Materiel Command, or the Department of the Army.

PROJECT 437-7820  
CONTRACT DA44-177-TC-663  
December 1962

TCREC 62-63

RESEARCH PROGRAM  
TO DETERMINE THE FEASIBILITY AND POTENTIAL  
OF THE  
GROUND EFFECT TAKE-OFF AND LANDING  
(GETOL) CONFIGURATION

VOLUME II

REPORT NO. R276

PREPARED BY  
VERTOL DIVISION  
THE BOEING COMPANY  
MORTON, PENNSYLVANIA

for

U. S. ARMY TRANSPORTATION RESEARCH COMMAND  
FORT EUSTIS, VIRGINIA

## FOREWORD

This report, as presented in Volume I and II, represents a final summary of Boeing-Vertol effort under Contract DA44-177-TC-663 to determine the feasibility and potential of the Ground Effect Take-off and Landing (GETOL) Configuration. This analytical development program was initiated in September 29, 1960 and completed on March 28, 1962 with a preliminary design of a Flight Research Vehicle (FRV).

H. Wahl, F. McHugh and R. Hooper of Boeing-Vertol guided the parametric analysis, development testing, preliminary design and report preparation under the direction of W. Stepniewski. Technical assistance and cooperation was provided by S. Spooner, J. Whitman and G. Smith of USA TRECOM as well as K. Goodsen and R. Kuhn of NASA's Langley Field facility.

Major development testing was performed by NASA at Langley Field. Static room tests were performed from May 22 to June 30, 1961. Tow track testing began May 31, 1961 and was completed June 9 1961, while wind tunnel testing of the GETOL model commenced on July 7 and ended on July 28, 1961. Planform and dynamic model testing was also conducted by Princeton and Toronto Universities.

Special mention for technical service during the life of Contract DA44-177-TC 663 go to T. Sweeney of Princeton University, B. Etkin, J. Liiva, R. Radford, and G. Kurylowich of the University of Toronto, H. Chaplin of DTMB and J. Wosser of ONR. Editorial coordinative assistance for this final report was provided by J. Gaffney.

## CONTENTS

	PAGE
LIST OF ILLUSTRATIONS .....	ii
LIST OF SYMBOLS .....	xii
APPENDICES	
APPENDIX A — STATEMENT OF WORK CONTRACT DA44-177-TC-633 .....	199
APPENDIX B — LITERATURE REVIEW FOR GETOL DESIGN .....	203
APPENDIX C — NASA STATIC ROOM AND WIND TUNNEL TESTS .....	215
APPENDIX D — MOVING MODEL TEST RESULTS (NASA TRACK DATA) .....	319
APPENDIX E — UNIVERSITY OF TORONTO DYNAMIC MODEL DATA .....	325
DISTRIBUTION .....	383

ILLUSTRATIONS

Figure		Page
<u>APPENDIX C - NASA STATIC ROOM AND WIND TUNNEL TESTS FORWARD FLIGHT</u>		
104	Configuration No. 12, $\theta_F = -\theta_R = +30x h/c = .33$ , (Runs 420-422) . . . . .	216
105	Configuration No. 12, $\theta_F = -\theta_R = +30x h/c = .33$ , (Runs 423-424) . . . . .	217
106	Configuration No. 27, $\theta_F = -\theta_R = +30x h/c = \infty$ , (Runs 671-673) . . . . .	218
107	Configuration No. 27, $\theta_F = -\theta_R = +30x h/c = \infty$ , (Run 682) . .	219
108	Configuration No. 36, $\theta_F = -\theta_R = +30x h/c = \infty$ , (Runs 675-677) . . . . .	220
109	Configuration No. 36, $\theta_F = -\theta_R = +30x h/c = \infty$ , (Run 678) . .	221
110	Configuration No. 37, $\theta_F = -\theta_R = +30x h/c = .33$ , (Runs 415-418) . . . . .	222
111	Configuration No. 64, $\theta_F = 0x \theta_R = 0x h/c = .20$ , (Runs 611-613) . . . . .	223
112	Configuration No. 63, $\theta_F = 0x \theta_R = 0x h/c = .33$ , (Runs 607-609) . . . . .	224
113	Configuration No. 34, $\theta_F = 0x \theta_R = 0x h/c = .5$ , (Runs 615-617) . . . . .	225
114	Configuration No. 51, $\theta_F = -60x \theta_R = +60x h/c = .20$ , (Runs 505-508) . . . . .	226
115	Configuration No. 6, $\theta_F = -60x \theta_R = +60x h/c = .33$ , (Runs 511-514) . . . . .	227
116	Configuration No. 6, $\theta_F = -60x \theta_R = +60x h/c = .33$ , (Run 515) . . . . .	228
117	Configuration No. 50, $\theta_F = -60x \theta_R = +60x h/c = .33$ , (Runs 499-503) . . . . .	229
118	Configuration No. 55, $\theta_F = -\theta_R = +60x h/c = .33$ , (Runs 429-430) . . . . .	230

ILLUSTRATIONS (Continued)

Figure		Page
119	Configuration No. 26, $\theta_F = -\theta_R = +60x h/c = \infty$ , (Runs 690-692) . . . . .	231
120	Configuration No. 73, $\theta_F = -\theta_R = +60 h/c = \infty$ , (Runs 683-685) . . . . .	232
121	Configuration No. 81, $\theta_F = -\theta_R = -h/c = .20$ , (Run 404) . . .	233
122	Configuration No. 79, $\theta_F = -\theta_R = -h/c = .20$ , (Run 402) . . .	234
123	Configuration No. 78, $\theta_F = -\theta_R = -h/c = .33$ , (Run 401) . . .	235
124	Configuration No. 80, $\theta_F = -\theta_R = -h/c = .33$ , (Run 403) . . .	236
125	Configuration No. 2, $\theta_F = -30x \theta_R = -30x h/c = .20$ , (Runs 487-490) . . . . .	237
126	Configuration No. 2, $\theta_F = -30x \theta_R = -30x h/c = .20$ , (Run 491) . . . . .	238
127	Configuration No. 15, $\theta_F = -30x \theta_R = -30x h/c = .20$ , (Runs 544-545) . . . . .	239
128	Configuration No. 1, $\theta_F = -30x \theta_R = -30x h/c = .33$ , (Runs 493-495) . . . . .	240
129	Configuration No. 1, $\theta_F = -30x \theta_R = -30x h/c = .33$ , (Runs 496-497) . . . . .	241
130	Configuration No. 4, $\theta_F = -30x \theta_R = -30x h/c = .33$ , (Runs 517-518) . . . . .	242
131	Configuration No. 5, $\theta_F = -30x \theta_R = -30x h/c = .33$ , (Runs 520-521) . . . . .	243
132	Configuration No. 13, $\theta_F = -30x \theta_R = -30x h/c = .33$ , (Runs 547-548) . . . . .	244
133	Configuration No. 28, $\theta_F = -30x \theta_R = -30x h/c = .33$ , (Runs 481-484) . . . . .	245
134	Configuration No. 28, $\theta_F = -30x \theta_R = -30x h/c = .33$ , (Run 485) . . . . .	246
135	Configuration No. 29, $\theta_F = -30x \theta_R = -30x h/c = .33$ , (Runs 556-557) . . . . .	247
136	Configuration No. 30, $\theta_F = -30x \theta_R = -30x h/c = .33$ , (Runs 553-554) . . . . .	248

ILLUSTRATIONS (Continued)

Figure		Page
137	Configuration No. 48, $\theta_F = -30 \times \theta_R = -30 \times h/c = .33$ , (Runs 523-524) . . . . .	249
138	Configuration No. 49, $\theta_F = -30 \times \theta_R = -30 \times h/c = .33$ , (Runs 526-527) . . . . .	250
139	Configuration No. 52, $\theta_F = -30 \times \theta_R = -30 \times h/c = .33$ , (Runs 551-552) . . . . .	251
140	Configuration No. 57, $\theta_F = -30 \times \theta_R = -30 \times h/c = .33$ , (Run 559) . . . . .	252
141	Configuration No. 3, $\theta_F = -30 \times \theta_R = -30 \times h/c = .50$ , (Runs 535-538) . . . . .	253
142	Configuration No. 3, $\theta_F = -30 \times \theta_R = -30 \times h/c = .50$ , (Run 539) . . . . .	254
143	Configuration No. 7, $\theta_F = -30 \times \theta_R = -30 \times h/c = .50$ , (Runs 541-542) . . . . .	255
144	Configuration No. 42, $\theta_F = -30 \times \theta_R = +30 \times h/c = .20$ , (Runs 633-635) . . . . .	256
145	Configuration No. 68, $\theta_F = -30 \times \theta_R = +30 \times h/c = .20$ , (Runs 645-647) . . . . .	257
146	Configuration No. 8, $\theta_F = -30 \times \theta_R = +30 \times h/c = .33$ , (Runs 445-448) . . . . .	258
147	Configuration No. 8, $\theta_F = -30 \times \theta_R = +30 \times h/c = .33$ , (Run 449) . . . . .	259
148	Configuration No. 9, $\theta_F = -30 \times \theta_R = +30 \times h/c = .33$ , (Runs 457-460) . . . . .	260
149	Configuration No. 10, $\theta_F = -30 \times \theta_R = +30 \times h/c = .33$ , (Runs 469-472) . . . . .	261
150	Configuration No. 10, $\theta_F = -30 \times \theta_R = +30 \times h/c = .33$ , (Run 473) . . . . .	262
151	Configuration No. 82, $\theta_F = -30 \times \theta_R = +30 \times h/c = .33$ , (Runs 410-413) . . . . .	263
152	Configuration No. 11, $\theta_F = -30 \times \theta_R = +30 \times h/c = .33$ , (Runs 463-466) . . . . .	264
153	Configuration No. 11, $\theta_F = -30 \times \theta_R = +30 \times h/c = .33$ , (Run 467) . . . . .	265

ILLUSTRATIONS (Continued)

Figure		Page
154	Configuration No. 35, $\theta_F = -30x \theta_R = +30x h/c = .33$ , (Runs 619-622) . . . . .	266
155	Configuration No. 35, $\theta_F = -30x \theta_R = +30x h/c = .33$ , (Run 623) . . . . .	267
156	Configuration No. 46, $\theta_F = -30x \theta_R = +30x h/c = .33$ , (Runs 653-655). . . . .	268
157	Configuration No. 47, $\theta_F = -30x \theta_R = +30x h/c = .33$ , (Runs 657-659) . . . . .	269
158	Configuration No. 66, $\theta_F = -30x \theta_R = +30x h/c = .33$ , (Runs 629-631) . . . . .	270
159	Configuration No. 65, $\theta_F = -30x \theta_R = +30x h/c = .33$ , (Runs 625-627) . . . . .	271
160	Configuration No. 69, $\theta_F = -30x \theta_R = +30x h/c = .33$ , (Runs 649-651) . . . . .	272
161	Configuration No. 43, $\theta_F = -30x \theta_R = +30x h/c = .50$ , (Runs 637-639) . . . . .	273
162	Configuration No. 67, $\theta_F = -30x \theta_R = +30x h/c = .50$ , (Runs 641-643) . . . . .	274
163	Configuration No. 70, $\theta_F = -30x \theta_R = +30x h/c = \infty$ , (Runs 661-665) . . . . .	275
164	Configuration No. 71, $\theta_F = -30x \theta_R = +30x h/c = \infty$ , (Runs 667-669) . . . . .	276
165	Configuration No. 76, $\theta_F = -30x \theta_R = +30x h/c = \infty$ , (Runs 705-709) . . . . .	277
166	Configuration No. 77, $\theta_F = -30x \theta_R = +30x h/c = \infty$ , (Runs 711-713) . . . . .	278
167	Configuration No. 18, $\theta_F = +30x \theta_R = -30x h/c = .20$ , (Runs 587-588) . . . . .	279
168	Configuration No. 18, $\theta_F = -30x \theta_R = +30x h/c = .20$ , (Run 589) . . . . .	280
169	Configuration No. 16, $\theta_F = +30x \theta_R = -30x h/c = .50$ , (Runs 590-591) . . . . .	281
170	Configuration No. 31, $\theta_F = -30 \theta_R = -30 h/c = .33$ , (Runs 405-407) . . . . .	282

ILLUSTRATIONS (Continued)

Figure		Page
171	Configuration No. 31, $\theta_F = -30$ $\theta_R = -30$ $h/c = .33$ , (Run 408) . . . . .	283
172	Configuration No. 58, $\theta_F = -30x$ $\theta_R = -30x$ $h/c = .33$ , (Run 560) . . . . .	284
173	Configuration No. 59, $\theta_F = -30x$ $\theta_F = -30x$ $h/c = .33$ , (Run 561) . . . . .	285
174	Configuration No. 60, $\theta_F = -30x$ $\theta_R = -30x$ $h/c = .33$ , (Runs 563-564) . . . . .	286
175	Configuration No. 44, $\theta_F = -$ $\theta_R = -30x$ $h/c = .33$ , (Run 575) . . . . .	287
176	Configuration No. 45, $\theta_F = -$ $\theta_R = -30x$ $h/c = .50$ , (Runs 576-577) . . . . .	288
177	Configuration No. 32, $\theta_F = -$ $\theta_R = -30x$ $h/c = \infty$ , (Runs 694-696) . . . . .	289
178	Configuration No. 33, $\theta_F = -$ $\theta_R = -30x$ $h/c = \infty$ , (Runs 698-700) . . . . .	290
179	Configuration No. 33, $\theta_F = -$ $\theta_R = -30x$ $h/c = \infty$ , (Run 701) . . . . .	291
180	Configuration No. 21, $\theta_F = 0x$ $\theta_R = -30x$ $h/c = .20$ , (Runs 597-599) . . . . .	292
181	Configuration No. 20, $\theta_F = 0x$ $\theta_R = -30x$ $h/c = .33$ , (Runs 603-604) . . . . .	293
182	Configuration No. 20, $\theta_F = 0x$ $\theta_R = -30x$ $h/c = .33$ , (Run 605) . . . . .	294
183	Configuration No. 19, $\theta_F = 0x$ $\theta_R = -30x$ $h/c = .50$ , (Runs 593-595) . . . . .	295
184	Configuration No. 14, $\theta_F = -$ $\theta_R = -$ $h/c = \infty$ , (Runs 716- 719) . . . . .	296
185	Configuration No. 48, $\theta_F = -30x$ $\theta_R = -30x$ $h/c = .33$ , (Runs 523-524, Roll Angle = 5°) . . . . .	297
186	Configuration No. 49, $\theta_F = -30$ $\theta_R = -30x$ $h/c = .33$ , (Runs 526-528, Roll Angle = 10°) . . . . .	298

ILLUSTRATIONS (Continued)

Figure		Page
<u>HOVER AND TRANSITION</u>		
187	Configuration No. 12, $\theta_F = -\theta_R = +30$ , $h/c = .33$ . . . . .	299
188	Configuration No. 73, $\theta_F = -\theta_R = +60x$ , $h/c = \infty$ . . . . .	300
189	Configuration No. 64, $\theta_F = 0x$ $\theta_R = 0x$ , $h/c = .2$ . . . . .	301
190	Configuration No. 63, $\theta_F = 0x$ $\theta_R = 0x$ , $h/c = .33$ . . . . .	302
191	Configuration No. 20, $\theta_F = 0x$ $\theta_R = -30x$ , $h/c = .33$ . . . . .	303
192	Configuration No. 2, $\theta_F = -30x$ $\theta_R = -30x$ , $h/c = .20$ . . . . .	304
193	Configuration No. 1, $\theta_F = -30x$ $\theta_R = -30x$ , $h/c = .33$ . . . . .	305
194	Configuration No. 4, $\theta_F = -30x$ $\theta_R = -30x$ , $h/c = .33$ . . . . .	306
195	Configuration No. 5, $\theta_F = -30x$ $\theta_R = -30x$ , $h/c = .33$ . . . . .	307
196	Configuration No. 13, $\theta_F = -30x$ $\theta_R = -30x$ , $h/c = .33$ . . . . .	308
197	Configuration No. 28, $\theta_F = -30x$ $\theta_R = -30x$ , $h/c = .33$ . . . . .	309
198	Configuration No. 29, $\theta_F = -30x$ $\theta_R = -30x$ , $h/c = .33$ . . . . .	310
199	Configuration No. 30, $\theta_F = -30x$ $\theta_R = -30x$ , $h/c = .33$ . . . . .	311
200	Configuration No. 31, $\theta_F = -30$ $\theta_R = -30$ , $h/c = .33$ . . . . .	312
201	Configuration No. 3, $\theta_F = -30x$ $\theta_R = -30x$ , $h/c = .50$ . . . . .	313
202	Configuration No. 52, $\theta_F = -30x$ $\theta_R = -30x$ , $h/c = .33$ . . . . .	314
203	Configuration No. 8, $\theta_F = -30x$ $\theta_R = +30x$ , $h/c = .33$ . . . . .	315
204	Configuration No. 10, $\theta_F = -30x$ $\theta_R = +30x$ , $h/c = .33$ . . . . .	316
205	Configuration No. 11, $\theta_F = -30x$ $\theta_R = +30x$ , $h/c = .33$ . . . . .	317
206	Configuration No. 14, $\theta_F = -\theta_R = -$ , $h/c = \infty$ . . . . .	318

ILLUSTRATIONS (Continued)

Figure		Page
<u>APPENDIX D - MOVING MODEL TEST RESULTS</u> <u>(NASA TRACK DATA) HOVERING AND TRANSITION</u>		
207	Configuration No. 70, $\theta_F = -30$ $\theta_R = +30$ , $h/c = \infty$ . . . . .	320
208	Configuration No. 35, $\theta_F = -30$ $\theta_R = +30$ , $h/c = .33$ . . . . .	321
209	Configuration No. 28, $\theta_F = -30$ $\theta_R = -30$ , $h/c = .33$ . . . . .	322
210	Configuration No. 37, $\theta_F = -\theta_R = +30$ , $h/c = .33$ . . . . .	323
211	Configuration No. 31, $\theta_F = -30$ $\theta_R = -30$ , $h/c = .33$ . . . . .	324
<u>APPENDIX E - UNIVERSITY OF TORONTO</u> <u>DYNAMIC MODEL DATA</u>		
212	Probe Layout for Measuring Pressures . . . . .	327
213	Flow Visualization Study (Height = 1/8 inch) . . . . .	328
214	Static Test Rig . . . . .	329
215	Presentation of $V^2$ through the Annular Jet (Graphs No. 1, 2, 3 and 4) . . . . .	331
216	Presentation of $V^2$ through the Annular Jet (Graphs No. 5, 6, 7 and 8) . . . . .	332
217	Presentation of $V^2$ through the Annular Jet (Graphs No. 9, 10, 11 and 12) . . . . .	333
218	Presentation of $V^2$ through the Annular Jet (Graphs No. 13, 14, 15 and 16) . . . . .	334
219	Presentation of $V^2$ through the Annular Jet (Graphs No. 17 and 18). . . . .	335
220	Spanwise Flux Distribution from A to B along Leading Edge of the Model . . . . .	336
221	Spanwise Flux Distribution from B to A along Trailing Edge . . . . .	337
222	Unreduced Record Taken from Flight along Track with No Ramp Installed . . . . .	339
223	Unreduced Record Taken from Flight along Track with No Ramp installed. . . . .	340
224	Flight in Plenum Chamber Configuration over .50 inch Ramp in Track . . . . .	341

ILLUSTRATIONS (Continued)

Figure		Page
225	Flight in Annular Jet Configuration over .125 inch Ramp in Track . . . . .	342
226	Flight in Annular Jet Configuration over .25 inch Ramp in Track . . . . .	343
227	Flight in Annular Jet Configuration over .50 inch Ramp in Track . . . . .	344
228(a)	Cable Sag Parameter . . . . .	358
228(b)	Cable Derivative $C_{2H}^*$ . . . . .	360
228(c)	Cable Derivative $C_{M\theta}^*$ . . . . .	361
228(d)	Cable Derivative $C_{n\psi}^*$ . . . . .	366
228(e)	Drag Component of Cable Tension . . . . .	370
229	Unreduced Record Taken from Flight along Track with No Ramp Installed . . . . .	372
230	Unreduced Record Taken from Flight along Track with No Ramp Installed . . . . .	373
231	Flight in Plenum Chamber Configuration over .50 inch Ramp in Track . . . . .	374
232	Flight in Annular Jet Configuration over .125 inch Ramp in Track . . . . .	375
233	Flight in Annular Jet Configuration over .25 inch Ramp in Track . . . . .	376
234	Flight in Annular Jet Configuration over .50 inch Ramp in Track . . . . .	377
235	Drag Coefficient for Two-Dimensional Flow around a Cylinder . . . . .	379

LIST OF SYMBOLS

<u>Symbol</u>	<u>Description</u>	<u>Unit</u>
A	FLOW AREA BEHIND FAN	SQ FT
A	AUGMENTATION	$\frac{L}{J} = \frac{L}{mV_J} = \frac{CL}{C\mu}$
AR	ASPECT RATIO	
b	MODEL WING SPAN	FT
c	MODEL WING ROOT CHORD	
$C_D$	DRAG COEFFICIENT	$\frac{D}{q S_w}$
$C_L$	LIFT COEFFICIENT	$\frac{L}{q S_w}$
$C_{\ell}$	ROLLING MOMENT COEFFICIENT	$\frac{R}{q S_w b}$
$C_m$	PITCHING MOMENT COEFFICIENT	$\frac{M}{q S_w c}$
$C_{\mu}$	MOMENTUM COEFFICIENT	$\frac{J}{qS} = \frac{mV_J}{qS_w}$
C. P.	CENTER OF PRESSURE	
D	NET DRAG	LB
h	HEIGHT ABOVE GROUND BOARD	FT
HP	AIR HORSEPOWER	$\frac{\Delta PQ}{550}$ HP
j	MOMENTUM FLUX PER UNIT LENGTH	LB/FT
J	MASS FLOW RATE - $m V_J$	$\frac{\text{SLUG FT}}{\text{SEC}^2}$
L	NET LIFT	LB

LIST OF SYMBOLS (Continued)

<u>Symbol</u>	<u>Description</u>	<u>Unit</u>
M	PITCHING MOMENT (MEASURED AT FAN CENTER LINE & WING ROOT QUARTER CHORD)	FT - LB
mac	MEAN AERODYNAMIC CHORD	FT
m	MASS FLOW RATE $Q_{\rho}$	SLUG/SEC
$P_S$	STATIC PRESSURE	IN ALC, LB/SQ IN
$P_T$	TOTAL PRESSURE	IN ALC, LBS/SQ IN
q	FREE STREAM DYNAMIC PRESSURE $\frac{1}{2} \rho v^2$	LB/SQ FT
Q	QUANTITY FLOW RATE MEASURED BEHIND THE FAN	CU FT/SEC
R	ROLLING MOMENT	FT - LB
RPM	REVOLUTION PER MINUTE	
$S_J$	SLOT FLOW AREA	SQ FT
$S_W$	PROJECTED WING AREA	SQ FT
$t_{LE}$	PROJECTED SLOT THICKNESS OF THE LEADING EDGE SLOT	INCH
$t_{TE}$	PROJECTED SLOT THICKNESS OF THE TRAILING EDGE SLOT	INCH
V	FREE STREAM VELOCITY	FT/SEC
$V_J$	AVERAGE JET EXIT VELOCITY AT SLOT $S_J^Q$	FT/SEC
$\beta$	INLET GUIDE VANE ANGLE	DEGREE

LIST OF SYMBOLS (Continued)

<u>Symbol</u>	<u>Description</u>	<u>Unit</u>
$\theta_F$	ANGLE OF THE FRONT SLOT FROM THE VERTICAL (NEGATIVE IN TOWARD THE CENTER OF THE BASE)	DEGREE
$\theta_R$	ANGLE OF THE REAR SLOT FROM THE VERTICAL (NEGATIVE IN TOWARD THE CENTER OF THE BASE)	DEGREE
$\rho$	MASS DENSITY OF AIR	SLUG/CU FT
$\Delta P$	PRESSURE DROP	IN ALC, LBS/SQ IN
$\alpha$	ANGLE OF ATTACK	DEGREE
$\omega$	WING LOADING	$\frac{L}{S_W}$

## APPENDIX A

### STATEMENT OF WORK - CONTRACT DA44-177-TC-663

#### 1. RECITAL

- a. There is a continuing need for U.S. Army aircraft to be made capable of operating under the most adverse conditions. One characteristic which greatly limits the utilization of current Army aircraft is the requirement for relatively smooth and firm airstrips.
- b. As part of its program to bring about a satisfactory solution to the problem of operation from unprepared fields, the Army desires to determine the feasibility and potential of an aircraft landing gear system utilizing the peripheral jet principle to form an air cushion on which an aircraft would operate in the landing and take-off regimes. Such a system may provide the capability for operating independently of prepared landing facilities. An aircraft incorporating this system is referred as a GETOL aircraft (Ground Effect Take-off and Landing).

#### 2. STATEMENT OF WORK

- a. The Contractor as an independent contractor and not as an agent of the Government shall in accordance with the instructions of the Research Contracting Officer (hereinafter referred to as the "Contracting Officer") provide all engineering services, personnel, labor, material and facilities (except as hereinafter indicated) and use its best efforts in the conduct of a research program leading to and including the preliminary design of a research type aircraft to prove the feasibility and potential of an aircraft landing gear system utilizing the peripheral jet principle to form an air cushion on which an aircraft would operate in landing and take-off regimes for operations within the mission of Army aircraft.
- b. To the extent applicable to this research aircraft design pertinent Government specifications shall be used as guides for the structural and functional designs of the aircraft. The design objectives of the research type aircraft shall be as follows:
  - (1) Ground effect take-off and landing with ground clearances of at least three feet with no more than maximum continuous power of the power plant.
  - (2) Take-off and landing over a fifty foot barrier within 500 feet.
  - (3) 250 mph at standard sea level conditions at maximum power.

- (4) Two place (side by side desired), dual controls, with a 600 pound lift capability (crew included, fuel not included).
- (5) Sufficient fuel for 1-1/2 hours at cruise power (maximum continuous) at sea level.
- (6) Handling qualities to fulfill both helicopter and fixed wing requirements in all flight regimes.
- (7) Auxiliary wheels for ground handling.
- (8) All controls shall act in a conventional manner throughout the entire flight range.

c. The Contractor has submitted a proposal for a research program which may generally be followed but specifically the research program shall be accomplished in three (3) Phases as follows:

#### PHASE I - WIND TUNNEL MODEL FABRICATION

Through analysis based on existing experimental data, the Contractor shall establish the configuration and provide the design of a wind tunnel model of a research GETOL aircraft in accordance with the design objectives above specified, to the extent that the same may be applicable and feasible in a wind tunnel model, to demonstrate the nature of GETOL performance attainable. Said model designed shall have a wing spread of approximately 6 feet. The model design will be coordinated with the NASA Langley Laboratory and will be compatible with the requirements for model tests in the NASA facility. Upon completion and coordination of design, the Contractor shall fabricate or have fabricated the wind tunnel model in accordance with the design developed as aforesaid.

#### PHASE II - MODEL TEST AND DATA ANALYSIS

The Contractor shall deliver the wind tunnel model fabricated under Phase I to NASA Langley and render assistance as called upon in the installation of the model in a wind tunnel and shall thereafter provide technical assistance in support of a wind tunnel test program coordinated among the Contractor, the Contracting Officer and the operator of the test facility, and shall obtain and reduce the data obtained from the wind tunnel test. The Contractor shall also render assistance in the installation of the wind tunnel model in an additional test facility to be made available by NASA, and thereafter provide technical assistance in support of this additional work. The Contractor shall obtain data from tests (not to exceed two (2) weeks) to be conducted by the Government on the model in simulated forward flight (moving model) over a stationary ground plane on similar aerodynamic configurations and control settings as the wind tunnel tests. The Contractor is to compare data obtained in this manner with that obtained in the wind tunnel to determine ground plane boundary layer effect encountered in the wind tunnel testing and shall analyze all the test results with respect to the

GETOL potential displayed. The Contractor shall submit all test data and corrections to the Contracting Officer and on the basis of such analyses shall make recommendations as to the sufficiency of the test data to form a basis for the work contemplated under Phase III hereof.

### PHASE III - PRELIMINARY DESIGN OF RESEARCH AIRCRAFT

Utilizing insofar as applicable the results of the work performed under Phases I and II above the Contractor shall make a preliminary design and performance analysis of a research type aircraft incorporating to the maximum achievable the design objectives above stated, capable of demonstrating the GETOL concept through flight testing and providing a basis for evaluation thereof.

- d. The Contractor shall prepare a final report in accordance with USATRECOM Circular 715-10, to be submitted in draft in three (3) copies, to contain a complete description of all work and experimentation accomplished including the test data, a direct comparison of the data obtained in simulated forward flight tests (moving model) with the data of the wind tunnel tests of corresponding configurations, complete details of the methods utilized in the comparison of the simulated forward flight tests of the model with that of the wind tunnel tests, analysis of the test data, and complete preliminary design description, including drawings, of the research vehicle with a presentation of the considerations, data and analysis employed in sufficient detail to clearly justify the design criteria and configuration of the research aircraft. The report shall also contain recommendations for construction of a flight vehicle, ground and flight test programs, and schedules therefor. On approval of the draft, with such revision or augmentation as the Contracting Officer may direct, the Contractor shall prepare one (1) reproducible and five (5) copies for submission to the Contracting Officer.
- e. During the work hereunder, the Contractor shall, upon request of the Contracting Officer, make available any of its personnel engaged in the performance of the work for conferences with the Contracting Officer. Said conferences may include a full discussion of any or all of the work performed hereunder. The Contracting Officer or his representative shall be free to comment on or limit any of the work which is performed by the Contractor, in which event the Contractor shall thereafter take into account any such comments or limitations in performing further work. The Contracting Officer, at the conclusion of each such conference, shall prepare a memorandum setting forth the result of such conference, which memorandum shall serve as a guide for further work. In the event Government personnel visit the Contractor's facility for the purpose of conferences or study of the work, the Contractor shall make available to the Government representatives adequate office space and other facilities as may be necessary at no additional cost to the Government.
- f. The Contracting Officer shall be the sole judge as to the adequacy and completeness of any of the work to be performed hereunder and shall be

at liberty to make suggestions as to further work required or as to other data as the case may be. The Contractor shall perform such other work or revise and augment the work hereunder in such particulars as are requested by the Contracting Officer. No work performed by the Contractor, in order to meet the approval of the Contracting Officer, shall be deemed to constitute a change in this Statement of Work so long as the work is in furtherance of the reports, designs, fabrication, tests, analyses, or other data to be prepared hereunder. Changes in the scope of the contract will be made only by the Contracting Officer by properly executed modifications to the contract.

- g. Project Officer: The Contracting Officer may designate and authorize a representative to act as project officer under this contract. Such representative as may be appointed will be specifically designated in a letter from the Contracting Officer to the Contractor. The project officer shall receive for the Government the reports and other material required under this contract and will represent the Contracting Officer in the technical phases of the work. The project officer will not be authorized to issue change orders, contract supplements, or direct any contract performance requiring contractual modification or adjustment. Changes in the scope of work will be made only by the Contracting Officer by properly executed modifications to the contract.
- h. Plan for Performance: Within twenty (20) days after receipt of written notice from the Contracting Officer of the award of this contract, the Contractor shall deliver to the Contracting Officer its Plan for Performance of the work under the contract for completion of the work within the time specified in Clause 3. entitled "Period of Performance". Said schedule shall be delivered, in duplicate, in sufficient detail to be used as a guide in evaluating the Contractor's performance.
- i. Technical Progress Reports: The Contractor shall submit monthly technical progress reports, in triplicate, to the Contracting Officer by the 20th of each month following the month for which the report is rendered. Such reports shall set forth the general results, progress achieved, and plans for continuing performance of the work hereunder. It shall specify the project name and objective, contract number, and by reference to the plan of performance, a comparison of planned and actual progress and planned and expected completion dates. It shall include a written report of all visits to Governmental agencies or commercial organizations made in connection with this contract and shall also include a brief summary of results and findings obtained therefrom. In addition, the Contractor shall furnish informational copies of this report to such other agencies, and only such other agencies, as may be designated by the Contracting Officer.

APPENDIX B

LITERATURE REVIEW FOR GETOL DESIGN (Sheet 1)

Date	Author	Title	Excerpt	Remarks
February 1959	H. R. Chaplin (DTMB)	Effect of Jet Mixing on the Annular Jet (TMB AD3242) (053)	Annular jet theory, 2 dimensional	Informative only hover only
April 1957	Uwe H. von Glahn (NASA)	Exploratory Study of Ground Proximity Effects on Thrust of Annular and Circular Nozzles (TN 3982)	Scale model studies	Informative ground cushion principles.
September 1959	H. R. Chaplin (DTMB)	TMB-D-3242 (Aero. Rept. 966)	Analytical, general perf. parameters for various "planforms", nozzle angles	Useful, lacks only flow distribution. Has minimum fwd speed information.
November 17, 1960	T. E. Sweeney	The Effect of Planform on the Static Charac- teristics of Peripheral Jet Wings	Scale model tests, various planforms, $\theta$ always $0^\circ$ , various gap ratios	"Plenum" plan- forms, questionable slot internal snapes, indication of $C_p$ shift with gap ratio.
June 1960	Ryan, Aero.	G-42-61	Progress report, GEM structures and manufacturing costs	Did not apply
December 15, 1959	J. E. Loos	ZP-294 (Part D)	400 ft. diameter GEM, close heights. De- sign approach and economics	Did not apply

APPENDIX B  
LITERATURE REVIEW FOR GETOL DESIGN (Sheet 2)

Date	Author	Title	Excerpt	Remarks
August 1958	H. R. Chaplin	TMB-AD-3242 Aero. Rept. 947	Theory, hovering, annular; size, H, power relationships	Informative only.
May 1959	A. A. Tinajero (DTMB)	Aero. Report 954	Circular, $\theta = 45^\circ$ and $0^\circ$ ; test and theory comparison, augmentation loss with forward speed. Very thin slots	Author questions his data when unequal distributions occurred. Tip-off to distribution significance.
June 23, 1960	T. Strand (VRC)	Interim Report on GEM Internal Flow	Discussion of duct and fan principles	Review material only.
May 1960	R. K. Gretif (NASA)	TN D-317	Test, annular, lift moment, drag at fwd speeds. Very thin slot; 0006 air-foil.	Informative only.
January 1960	R. W. Pinnes (BuWeps)	GEM Propulsion (RRSY-60-1)	Questions, which J? Discussion of lift, height and fan points out max. G. W. at some H, not infinitely more as H decreases	Test data did not apply if flow (or fan) characteristics not known. Augmentation ratio a poor item.
October 9, 1959	H. C. Higgins (Boeing)	Surface Geometry of Vehicle Motion on Forces of Ground Pressure Element (Princeton Sympos.) Wichita Tunnel	Model test, thin jet; various good plans, tests at	Good stability and performance data for reasonable GETOL planforms (but stability is bad).

APPENDIX B  
LITERATURE REVIEW FOR GETOL DESIGN (Sheet 3)

Date	Author	Title	Excerpt	Remarks
September 1959	B. Nixon (Princeton)	Report No. 484	2 dimensional jet, hover; smoke vortex instability	Informative photographs.
October 23, 1959	D. Kuhn (NASA)	GEM Research (Princeton Symp.)	Tow tank tests, dynamic stability, 4 and 8 inch diameter nozzles, lab air supply	3% D min jet thickness plenum chamber depth effect noted.
December 1959	C. D. Boehler (Aerophysics Co.)	AR 581-R Aero. Theory Annular Jet	Theory; close and far from ground (see Chaplin's 923, von Glahn TN-3982)	Informative only.
October 23, 1959	Princeton Symp. (Fo Mo Co.)	GEM Role in Trans.	Unprepared and prepared surfaces, power speed relations	Did not apply.
October 1959	Grumman, J. Tucker (Princeton Symp.)	2 Dimensional Study, Low Press Annular Jet GEM at Fwd Speeds (Rm 165)	Theory and test, 2 dimensional and 3 dimensional; plenum	Informative theory test comparison
October 1960 (Ft. Myers Symp.)	T. Strand (URC) R (Report No. 6)	Internal Flow for GEM	Theory	Basic flow review some good vane design information.

APPENDIX B

LITERATURE REVIEW FOR GETOL DESIGN (Sheet 4)

Date	Author	Title	Excerpt	Remarks
June 1960	A. E. Johnson	Interim Data W. T. Tests DTMB GEM #448	Very low aspect ratio, no lateral data; 3 fan, small plenum; fwd fans, all test data.	No use for GETOL configuration.
June 1960	H. R. Chaplin	Theory Correlation DTMB GEM Model 448	See above.	Informative, simple theory for fwd flight.
May 1960	B. Nixon (Princeton)	Maneuvering Capa- bilities of GEM (annular)	Theory, deflection and distribution concepts	Review material only.
June 1960 (Ft. Myers Symp.)	P. K. Chang (Aerophysics)	(AR 60-01) Approximately Solution of 2 D Incomp. Turb. Curved Jets	Theory	Informative, but review material only.
(Ft. Myers Symp.)	C. A. Foltz (U. Wichita)	GEM Inv. at U. of Wichita	Test, annular, jet Plenum, wind tunnel	Review material only.
June 1960	M. F. Gates (Hiller)	(ARD 266) Inv. Special GEM Configs.	Test, stability dif- fuser with Plenum and Recirc.	Review material only.
May 1959	G. Willets	Vertol GEM Proposal (PR 313)	GEM research proposal	Not actuated. Informative only.

APPENDIX B  
LITERATURE REVIEW FOR GETOL DESIGN (Sheet 5)

Date	Author	Title	Excerpt	Remarks
June 23, 1960	L. R. Mack (Iowa Inst. of Hydraulic Res.)	Annular Jet Moving Over Still Water	Varied J, H, V test. Low slot vs, lo fwd speeds (0 to 4 ft/sec.)	Did not apply.
November 1959	(Connel Lab) E. M. Sullivan	SG 1195-5-3 (Truck Test Rig)	Dev. of test truck	A test facility possibility.
October 21, 22, 23, 1959 (Princeton Symposium)	P. Poisson- Quinton	Study of a Current Plan for a Ground Effect Platform	2 dimensional wind, H <sub>2</sub> O; water bubbles for flow visualiza- tion, slots and holes. Very small slots	Information available from a design stand point.
October 21, 22, 23, 1959 (Princeton Symposium)	J. C. M. Frost T. D. Earl (Avro Aircraft, Ltd.)	Flow Phenomena of the Focused Annular Jet	Test, 1/2 annular model, focused jet sheets	Informative only.
October 21, 22, 23, 1959 (Princeton Symposium)	C. Weiland	Labyrinth Seals	Static tests	Informative only.
October 21, 22, 23, 1959 (Princeton Symposium)	M. P. Tulin (Hydronautics, Inc.)	On the Vertical Motions of Edge Jet Vehicles	Jet-wave study, theory	Informative only.

APPENDIX B

LITERATURE REVIEW FOR GETOL DESIGN (Sheet 6)

Date	Author	Title	Excerpt	Remarks
October 21, 22, 23, 1959 (Princeton Symposium)	S. Silverman (North American)	Test Results of an Annular Jet Ground Effect Vehicle	Propeller vs. lab air supply, plenums, skirts	Indication of propeller, close hovering relationship; no design data, but tip-off.
October 21, 22, 23, 1959 (Princeton Symposium)	G. D. Boehler	Forward Flight Characteristics of Annular Jets	Theory	Did not apply
October 21, 22, 23, 1959 (Princeton Symposium)	W. R. Bertelsen	Experience with Several Man-carrying Ground Effect Machines	Homebuilt progress	Interesting remarks no design data
October 21, 22, 23, 1959 (Princeton Symposium)	R. Stanton-Jones	Development of the Saunders-Roe Hovercraft SR-N1	Vehicle description, some test results	Informative only.
October 21, 22, 23, 1959 (Princeton Symposium)	C. S. Cockerell	Some Remarks on the English Channel Crossing of the Hovercraft-annular Jets with Deflectors	Descriptive	Did not apply.
October 21, 22, 23, 1959 (Princeton Symposium)	E. A. Fradenburgh (Sikorsky)	The Helicopter as a Ground Effect Machine	Helicopter vs GEM concludes GEM very limited use	Informative only.

APPENDIX B  
LITERATURE REVIEW FOR GETOL DESIGN (Sheet 7)

Date	Author	Title	Excerpt	Remarks
October 21, 22, 23, 1959 (Princeton Symposium)	J. N. Fresh (DTMB)	Some Tests of a 7-foot GEM Dynamic Model Over Uneven Surfaces	Model (on boom) tests over sine waves	Did not apply.
October 21, 22, 23, 1959 (Princeton Symposium)	A. A. Tinajero (DTMB)	Effect of Vehicle Planform on Augmentation	Test model, planform vary, AR 1.2 to .25 high press thin jets, B for propulsion	Informative - author believes augmentation independent of planform.
October 21, 22, 23, 1959 (Princeton Symposium)	A. E. Johnson (DTMB)	Aerodynamic Characteristics of a 3-foot Diameter Powered Annular Jet Model	Test, annular, jets, hover and cruise	Informative only.
October 21, 22, 23, 1959 (Princeton Symposium)	T. J. Kaario	The Principles of Ground Effect Vehicles	Ram wing, theory principles, vehicle tests	Adequate for ram wings.
October 21, 22, 23, 1959 (Princeton Symposium)	L. R. Mack	Theoretical and Experimental Research on Annular Jets Over Land and Water	Author states augmentation decreases with fwd speed, but reveals no data. Theory and test	Fairly comparison with Higgins.
October 21, 22, 23, 1959 (Princeton Symposium)	W. Z. Stepniewski	Performance Possibilities of Subsonic Airplanes Taking-off and Landing on the Ground Cushion	GETOL concept satisfactory, theory and tunnel tests	Basic presentation of the problem.

APPENDIX B

LITERATURE REVIEW FOR GETOL DESIGN (Sheet 8)

Date	Author	Title	Excerpt	Remarks
October 21, 22, 23, 1959 (Princeton Symposium)	A. E. Hirsch (DTMB)	The Hovering Performance of a Two-dimensional Ground Effect Machine Over Water	Boat, side curtains (Skegs) tests, $H_2O$ 50-70 K	Did not apply.
October 21, 22, 23, 1959 (Princeton Symposium)	National Research Associates	Test Experience and Comments on Air Cushion Vehicles	GEM concepts and philosophy	Did not apply.
October 21, 22, 23, 1959 (Princeton Symposium)	J. E. Sutton (Lockheed)	Propulsion System Experiments	Test, ejectors	Did not apply.
October 21, 22, 23, 1959 (Princeton Symposium)	K. G. Wernicke (Bell helicopter)	Performance Testing of a Five-foot Air Cushion Model	Circular, test, plenum and jets, various H, G. D	First mention over-all eff. (about 50%) (tip-off)
October 21, 22, 23, 1959 (Princeton Symposium)	Thomas M. Clancy ERCO Div. of ACF	Simplified Momentum Theory Solutions for the Augmentation Factor of Hovering Annular Jet Vehicles	Annular, theory; planform applicability; 2 dim. and 3 dim.	Consideration of $\theta$ opt
October 21, 22, 23, 1959 (Princeton Symposium)	Donald G. Sachs (Boeing)	Ground Cushion Flow Visualization Studies	Rest, visual, 18 inch dia. circular annular jet. Base press. dist. 90° and 45° single double slots	All zero $\alpha$ informative.

APPENDIX B  
LITERATURE REVIEW FOR GETOL DESIGN (Sheet 9)

Date	Author	Title	Excerpt	Remarks
April 1959	R. W. Pinnes (BuWeps)	DR-1958 (Power Plant Man's Look at GEM)	Cushion pressure effect on propulsion (fan, etc.) mostly theory, based on Chaplin and Von Glahn	Fan problems.
July 1959	H. R. Chaplin (DTMB)	Aero. Rept. 923 (Annular Nozzle Theory)	Plenum theory	All superseded
September 25, 1958	G. D. Boehler (for AHS forum)	Remarks on GEM	Theory, fund. principles	Interesting - No design application
November 1960	Gyrodyne	Gyrodyne Tests of Model 55 GEM	Annular plenum (liberty bell) theory - test avg. comparison	Did not apply.
November 16-18 1960	G. E. Bowden (Booz-Allen)	Analysis of Recire. GEM	Theory, very close alts.	Inconclusive
November 1960 (Ft. My.)	A. J. Schneider (Grumman)	Power Seal Configs.	Tests, plastic lacerynths	No specific conclusion.
November 1960 (Ft. My.)	H. O. Nay (Hughes)	Hydrostreak	Water curtain 2 dim. test data	Interesting, but did not apply
November 16, 1960 (Ft. My.)	B. H. Carmichael (Aeronutronics)	State of Art Summary for Air Cushion Vehicles	Slight GETOL section. Lots of theory back- ground	Interesting, did not apply.

APPENDIX B

LITERATURE REVIEW FOR GETOL DESIGN (Sheet 10)

Date	Author	Title	Excerpt	Remarks
November 1960 (Ft. Meyers)	Bell Aero Systems	GEM Morphology Study No. 2017-933001	Supposed system for selecting size wt, etc. of GEM large size stuff, but generally agrees with GETOL size, power	Possible design infor. for prelimi- nary estimates.
November 1960 (Ft. Myers)	R. L. Wiegel (Univ. of Calif.)	2nd Status Report on Model Studies on GEM	Determine character of GEM over a tow tank	Did not apply.
November 1960	G. Perrone (AiResearch)	AP 5026-R Progress Report of Design and Fabrication of GEM Fan/ Duct System	Brief description of procedure followed in design of complete fan duct system	Useful possible additional info. for fan system similar to GETOL
November 1960 (Ft. Myers)	AiResearch	AP-5024-R 3rd Prog- ress Report on GEM Propulsion System Study	Detail design infor- mation on fan/duct combination fan flow - fwd speed study	Good
November 1960 (Ft. My.)	B. W. Anderson AiResearch	AP-5025-R Stab and Control	Theory test following annular and AR 1/2	Informative, should be followed.
June 1960	AiResearch	AP-5017-R (Prog. Rept.) AP-5018 (Prog. Rept.)	Prelude to above 3 reports. Theory, design concepts	Informative only.

APPENDIX B

LITERATURE REVIEW FOR GETOL DESIGN (Sheet 11)

Date	Author	Title	Excerpt	Remarks
November 1960 (Ft. My.)	Cleveland Pneumatics	Vol. 1, 2 & 3 Stab and Control of GEM's 1. Elem. Principle 2. Further Considerations 3. Appendices	Theory, 2 dim.	Did not apply.
November 16, 1960 (Ft. My.)	C. A. Fortz (U. of Wichita)	Wing Tunnel Inv. of GEM's (Eng. Rept. 352-2)	Test data, includes data curves, annular $C_{\mu}$ vs. $C_l$ and $C_d$ slot and heights, one GAP, = -5 to +5	Adequate, but annular
November 16, 1960 (Ft. My.)	T. Strand (VRC)	Interim Report on Channel GEM's	Ram wing theory concepts. "Lift power goes to zero" some 2 dim jet flap data	Some possible use
November 1960 (Ft. My.)	Ryan	G-42-62 Final Report GEM's Structures	Aluminum vs. ply- wood, etc. Various sizes of GEM's	Informative only
November 1960 (Ft. My.)	G. Boehler	AR-60-13 GEM Prog. Rept.	Theory and Chaplins test data	Review material only
July 8, 1960	G. A. Hanson (Boeing Seattle)	D2-5515 VTOL Impinging on Plate and Erosion	2 inch dia. jet noz- zles hot ground erosion tests	Good reference material

APPENDIX B

LITERATURE REVIEW FOR GETOL DESIGN (Sheet 12)

Date	Author	Title	Excerpt	Remarks
June 1957	N. R. Augustine (Princeton)	No. 383 Fluid Wings	Jet flap test data	Good
May 1960	K. P. Spreeman (NASA)	TND-363 Aero. Char. Jet Flap and Deflected Slipstream at Zero and Low Fwd Speeds	38% flap with blowing Ground effect was bad	Good
August 1955	Poisson—Quinton (U of W Trans) (No 186)	Lift, Augmentation and Airplane Operation by Circ. Control	Jet flap theory — test	Very good
August 1958	TN 4353 NACA V. E. Lockwood	Wind Tunnel Inv. High Subsonic and Tran- sonic Jet Flaps, Rect. Wings	Jet flap, low mo- mentum coeffs., M = .4 to 1.0	Good A little high speed information
March 2, 1959 (Brussels Present)	Dick Kuhn NASA	Tunnel Wall Effects Associated with VTOL- STOL Model Testing	17 ft section description	Useful information

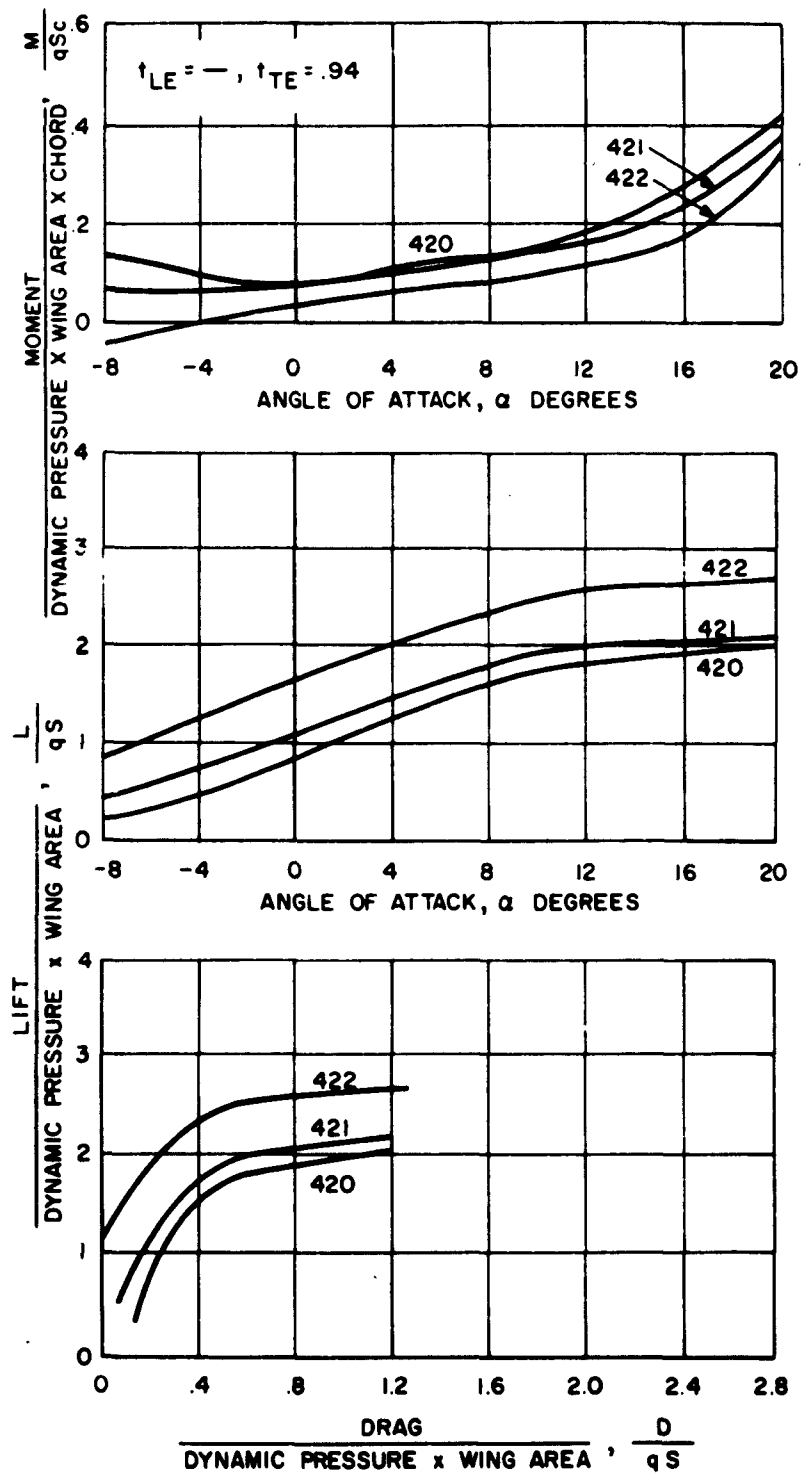
## APPENDIX C

### NASA STATIC ROOM AND WIND TUNNEL TESTS

Appendix C includes the major portion of the data obtained from the development testing performed at NASA with the GETOL wind tunnel model (See Volume I, Page 19). Two methods of presenting data in Figures 104 to 206 are used so as to include two flight regimes. The first method covers forward flight and represents a variation of the conventionally defined aerodynamic coefficients of a model ( $C_L$ ,  $C_D$  and  $C_M$ ) with angle of attack for specific values of momentum

coefficient ( $C_\mu = \frac{\text{Slot Momentum}}{\text{Dynamic Pressure} \times \text{Wing Area}}$ ). The second method covers hover

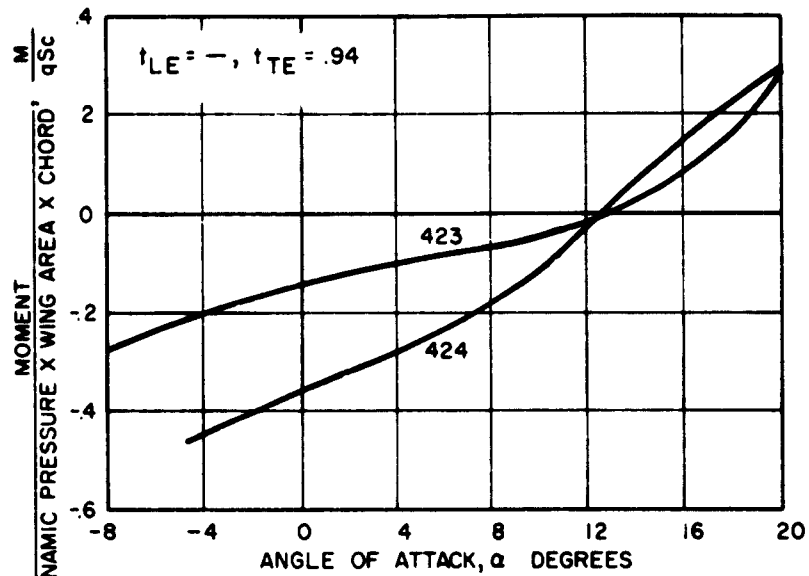
and transition and consists of representing the conventional aerodynamic coefficients divided by the momentum coefficient as a function of the reciprocal of the momentum coefficient. These relationships are presented for constant values of angle of attack. This approach permits finding the value of a conventional aerodynamic coefficient, for instance  $C_L$ , at transition for any angle of attack by dividing the  $C_L/C_\mu$  values represented by ordinates by the  $1/C_\mu$  given by the abscissa.



CONFIGURATION NO. 12

RUN NO.	J/qS
420	.0685
421	.2186
422	.7595

Figure 104. Configuration No. 12,  $\theta_F = -\theta_R = +30 \times h/c = .33$ , (Runs 420-422)



CONFIGURATION NO. 12

RUN NO.	J/qS
423	1.9333
424	3.4811

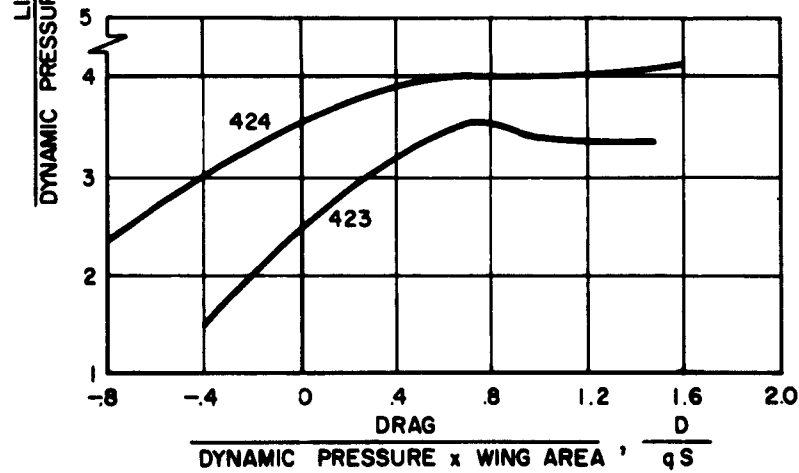
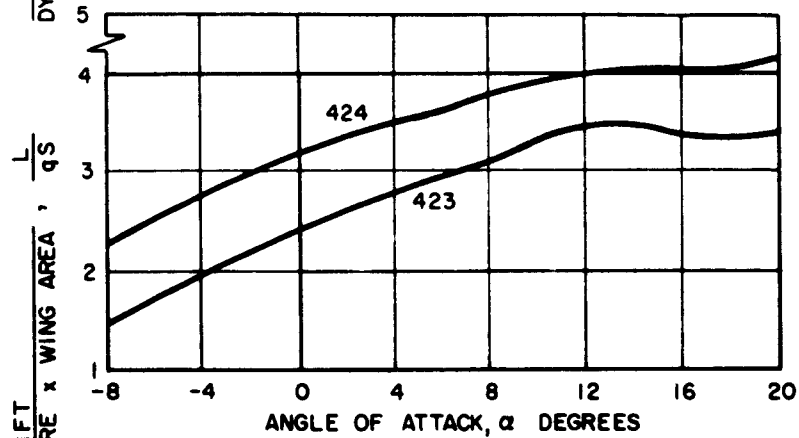


Figure 105. Configuration No. 12,  $\theta_F = -\theta_R = +30^\circ$   $h/c = .33$ , (Runs 423-424)

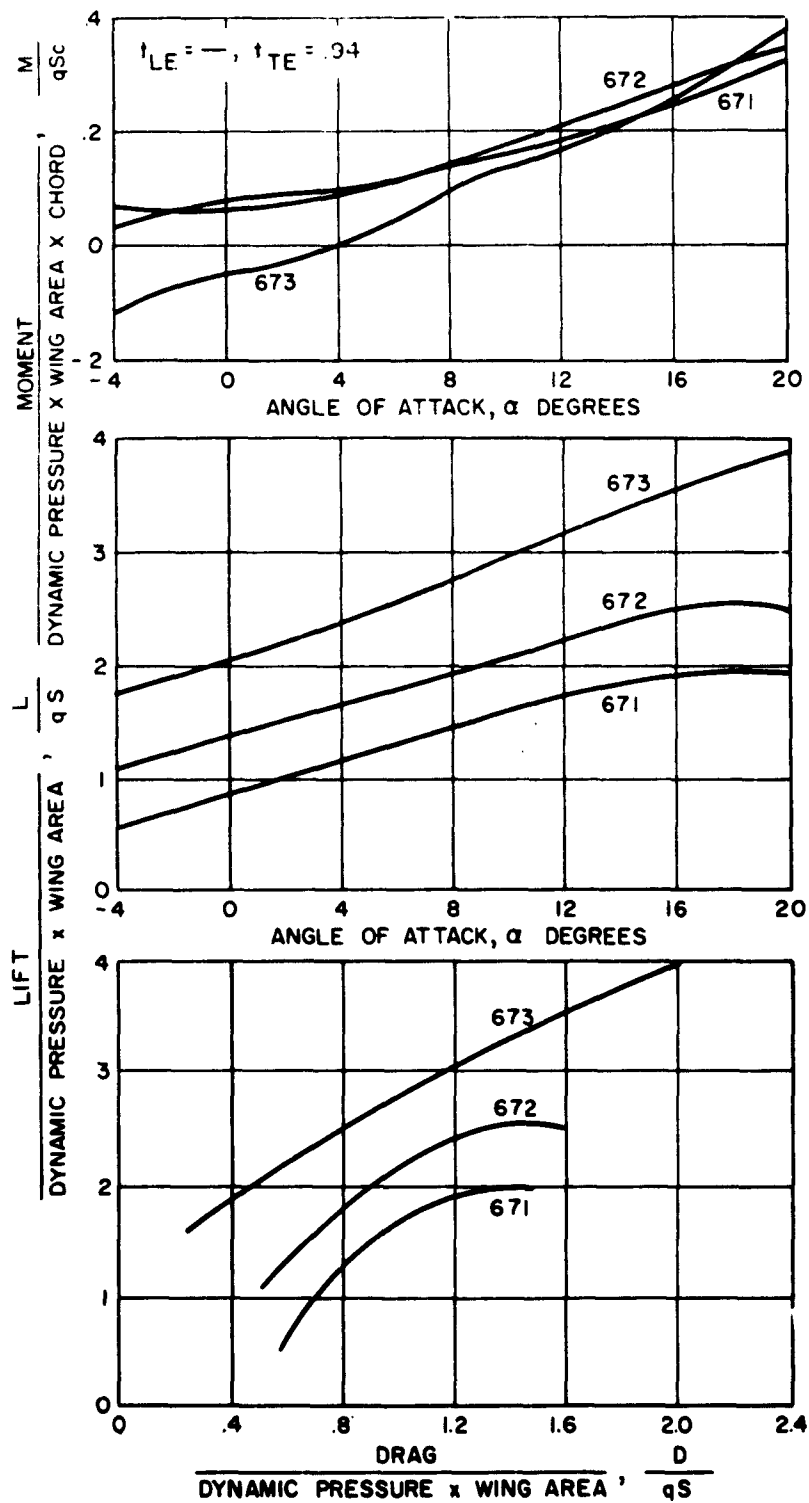
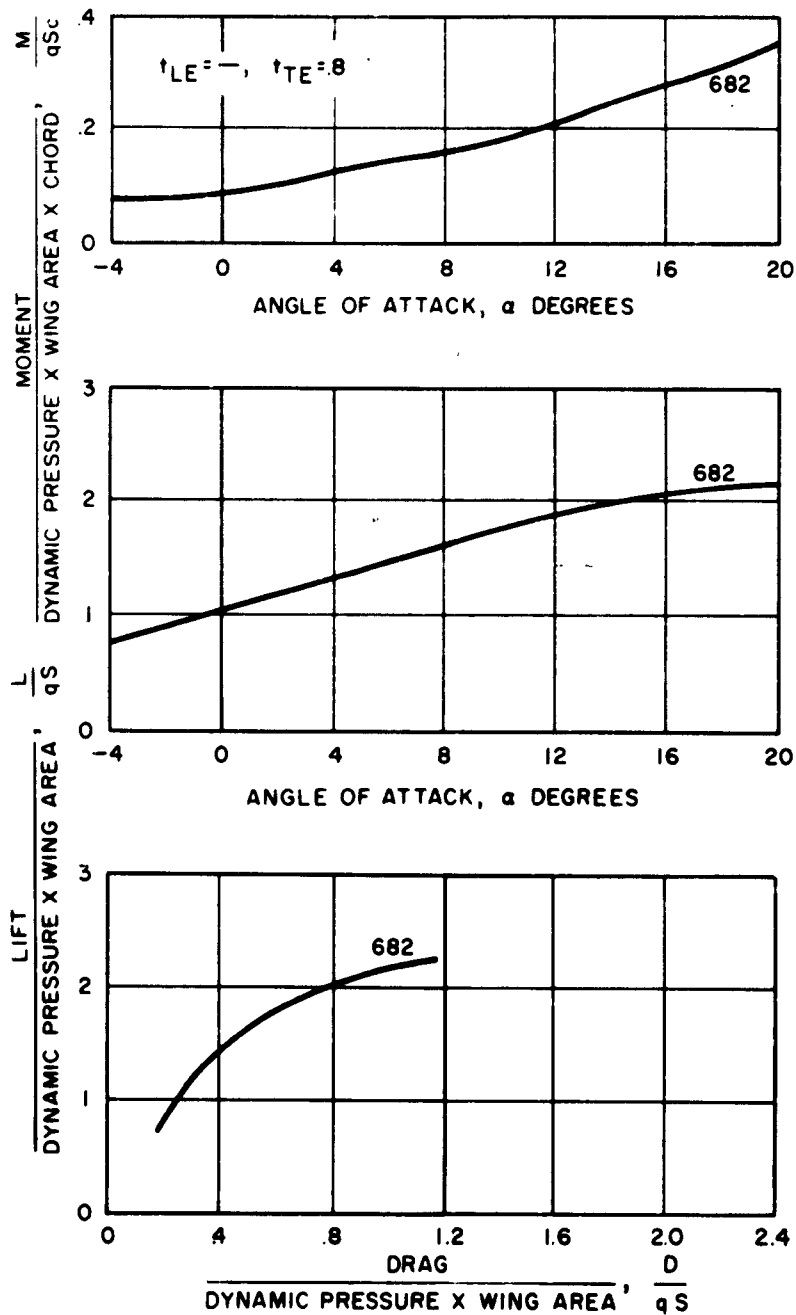


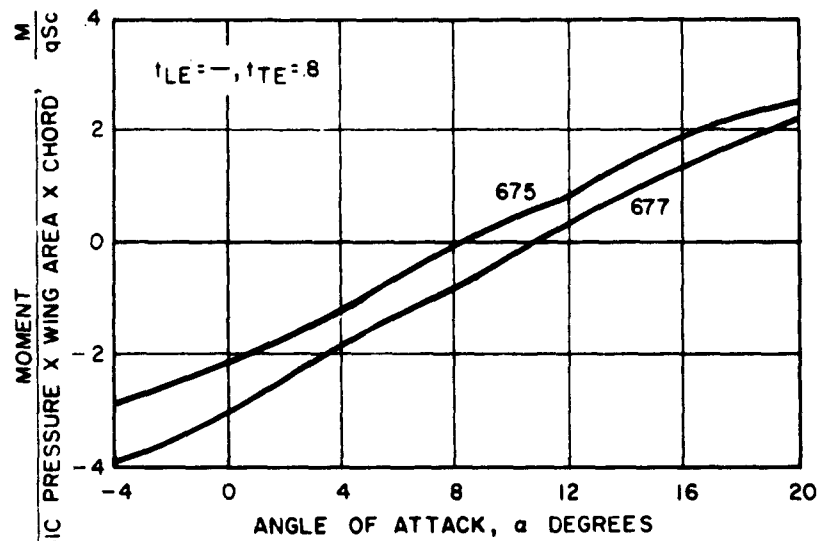
Figure 106. Configuration No. 27,  $\theta_F = -\theta_R + 30 \times h/c = \infty$ , (Runs 671 - 673)



CONFIGURATION NO. 27

RUN NO.	J/qS
682	.292

Figure 107. Configuration No. 27,  $\theta_F = -\theta_R = +30^\circ$   $h/c = \infty$ , (Run 682)



CONFIGURATION NO. 36

RUN NO.	$J/qS$
675	.2784
676	.0697
677	.8853

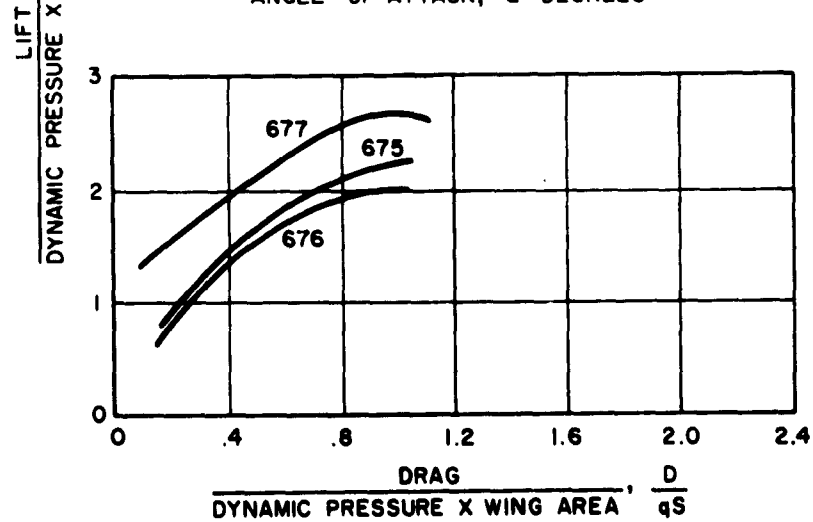
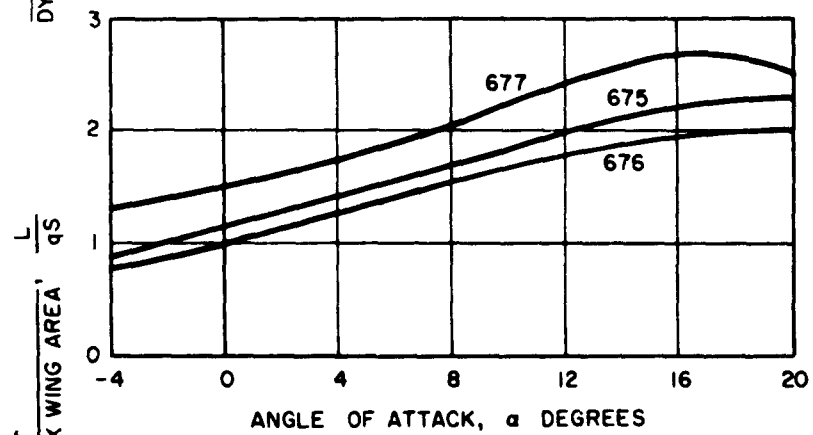
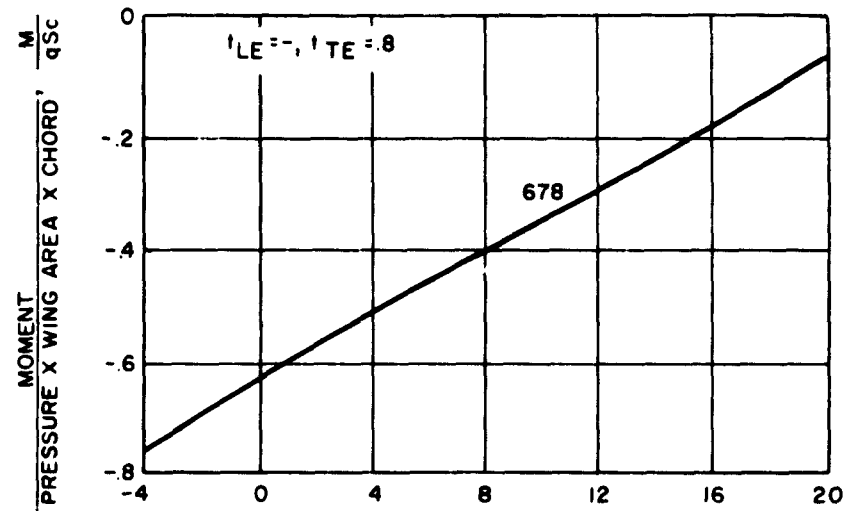


Figure 108. Configuration No. 36,  $\theta_F = -\theta_R + 30x h/c = \infty$ , (Runs 675 - 677)



CONFIGURATION NO. 36

RUN NO.	J/qS
678	2.1834

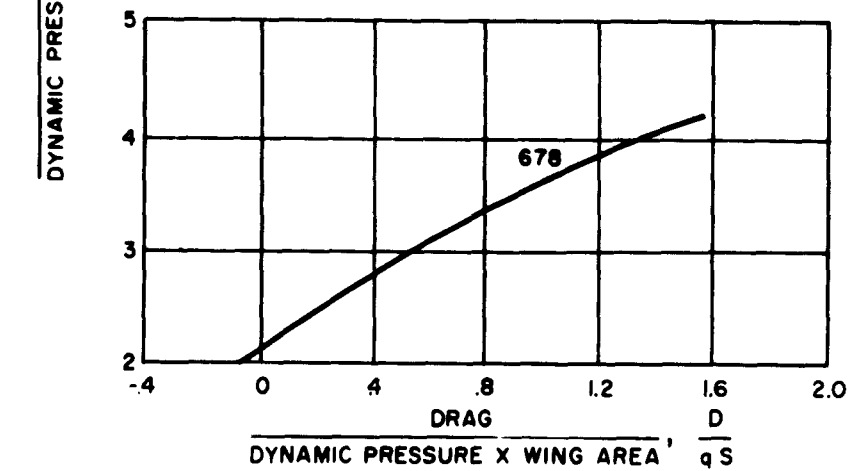
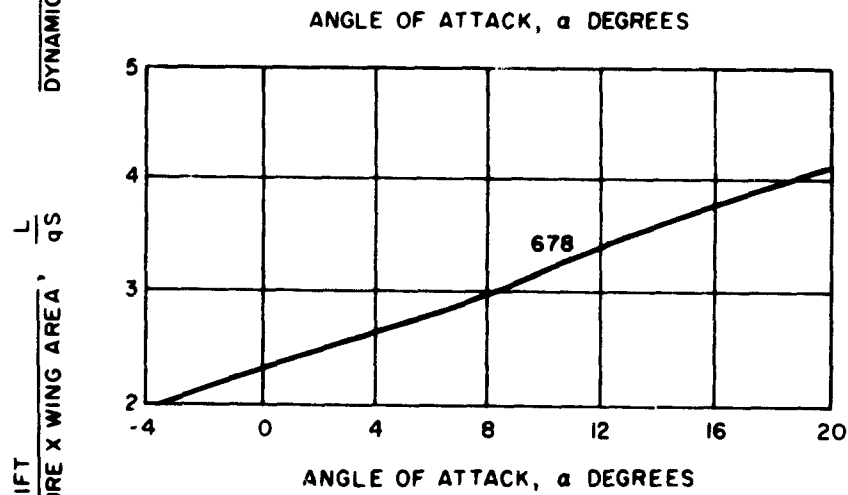
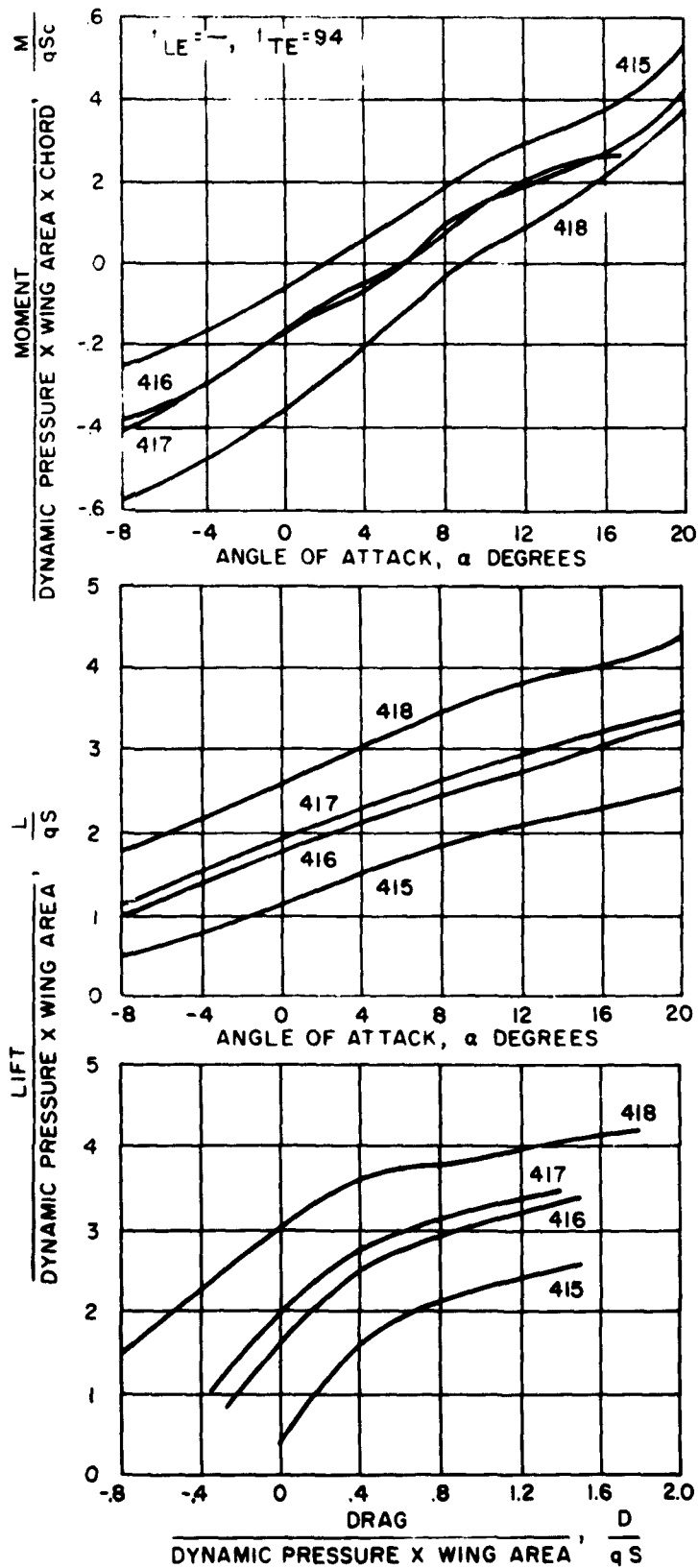


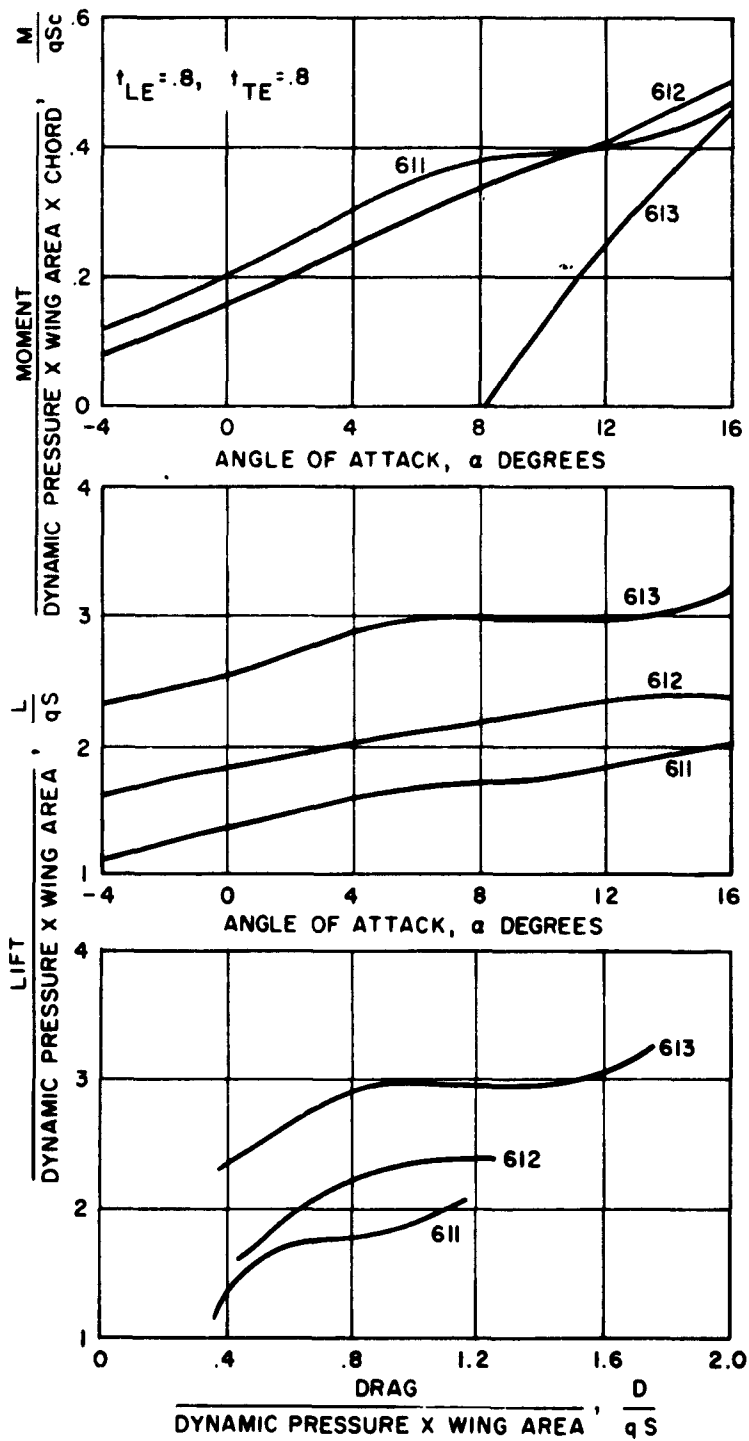
Figure 109. Configuration No. 36,  $\theta_F = -\theta_R = +30^\circ$ ,  $h/c = \infty$ , (Run 678)



CONFIGURATION NO. 37

RUN NO.	J/qS
415	.2682
416	1.0973
417	1.4259
418	2.437

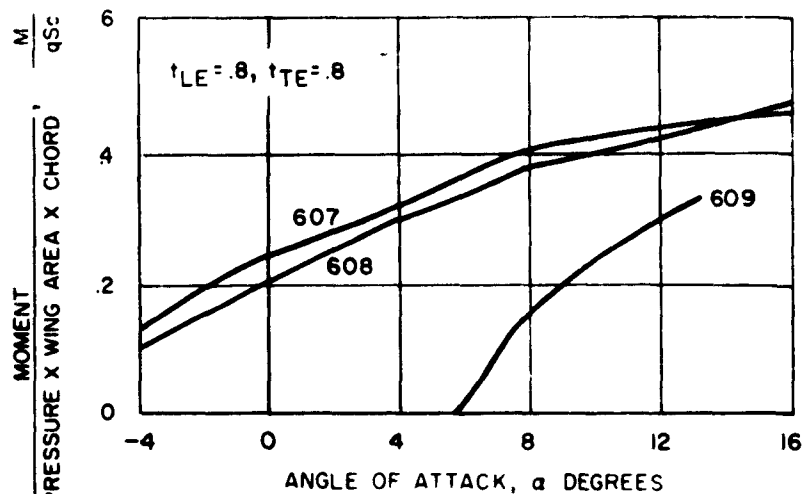
Figure 110: Configuration No. 37,  $\theta_F = -\theta_R = +30^\circ \times h/c = .33$ , (Runs 415 - 418)



CONFIGURATION NO. 64

RUN NO.	J/qS
611	.193
612	.553
613	1.254

Figure 111. Configuration No. 64,  $\theta_F = 0_x \theta_R = 0_x h/c = .20$ , (Runs 611 - 613)



CONFIGURATION NO. 63

RUN NO.	J/qS
607	.190
608	.537
609	1.243

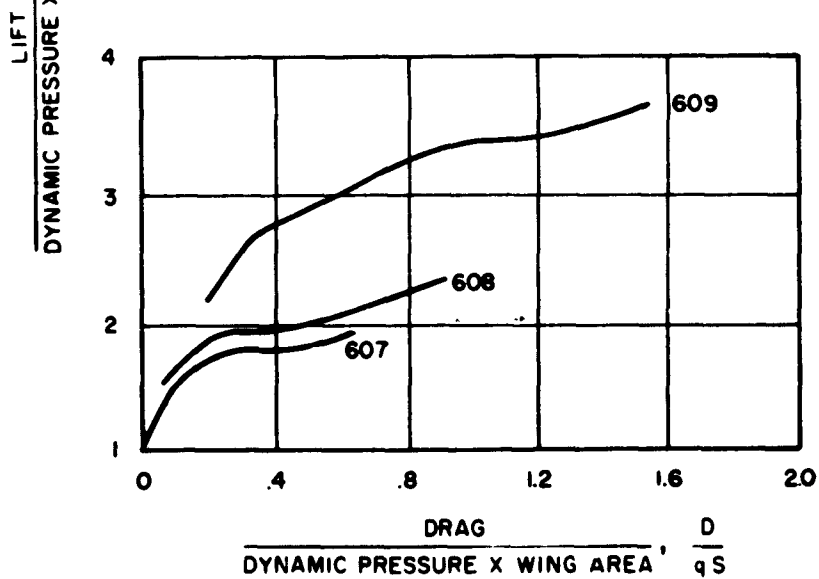
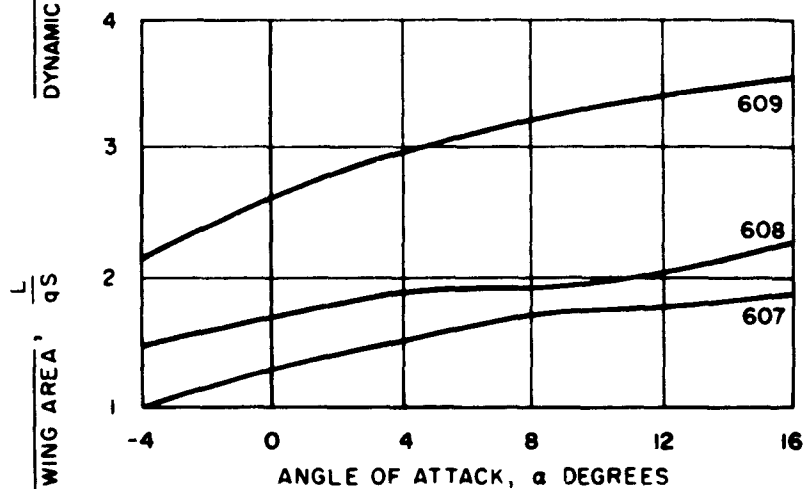
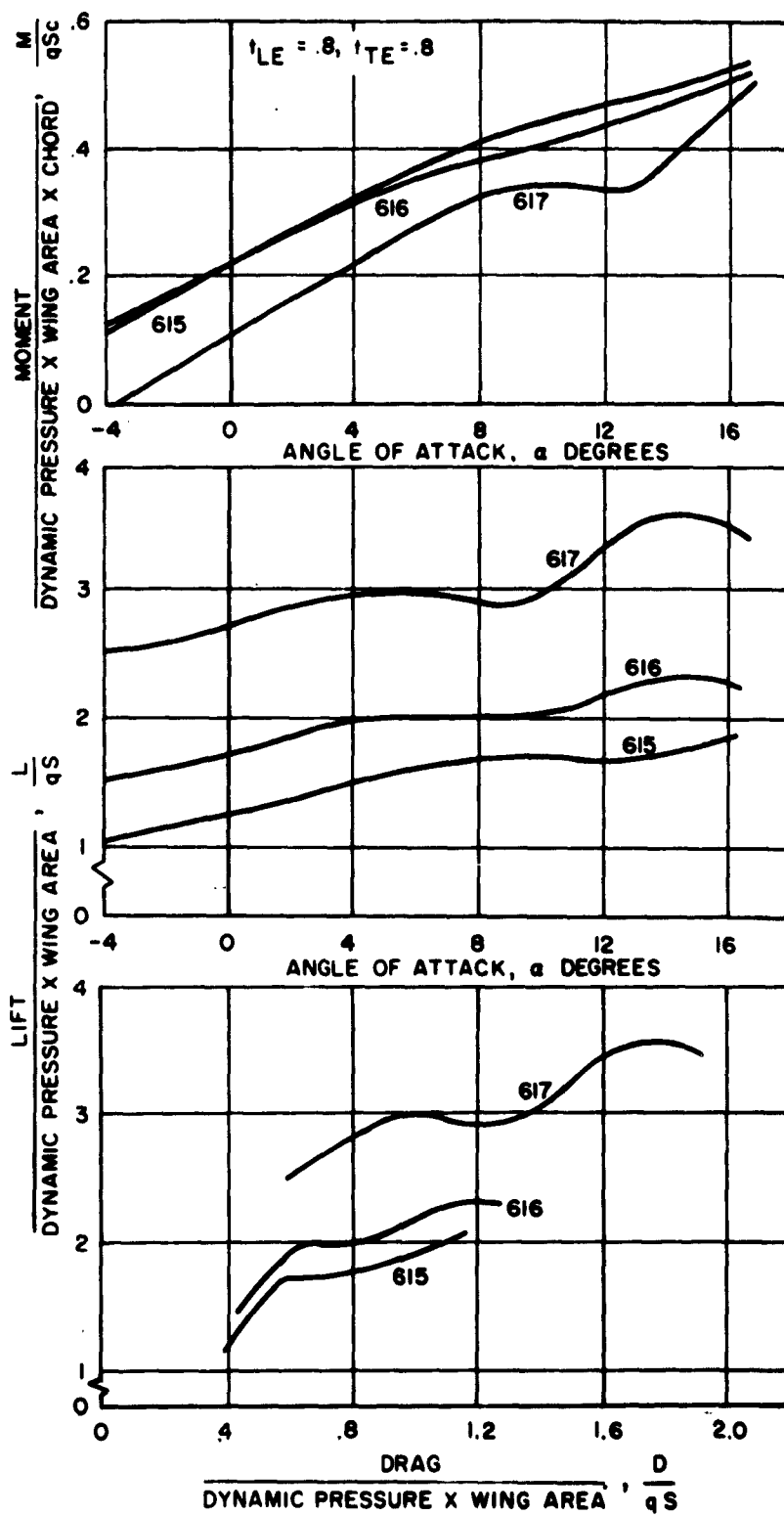


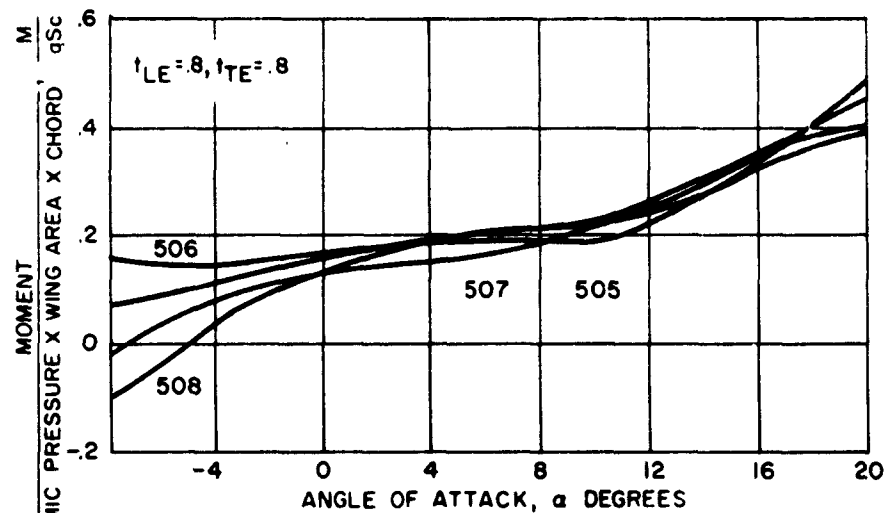
Figure 112. Configuration No. 63,  $\theta_F = 0^\circ$   $\theta_R = 0^\circ$   $h/c = .33$ , (Runs 607 - 609)



CONFIGURATION NO. 34

RUN NO.	J/qS
615	.2095
616	.5810
617	1.3488

Figure 113. Configuration No. 34,  $\theta_F = 0x \theta_R = 0x h/c = .5$ , (Runs 615 - 617)



CONFIGURATION NO. 51

RUN NO.	J/qS
505	.1189
506	.2730
507	.7386
508	1.7776

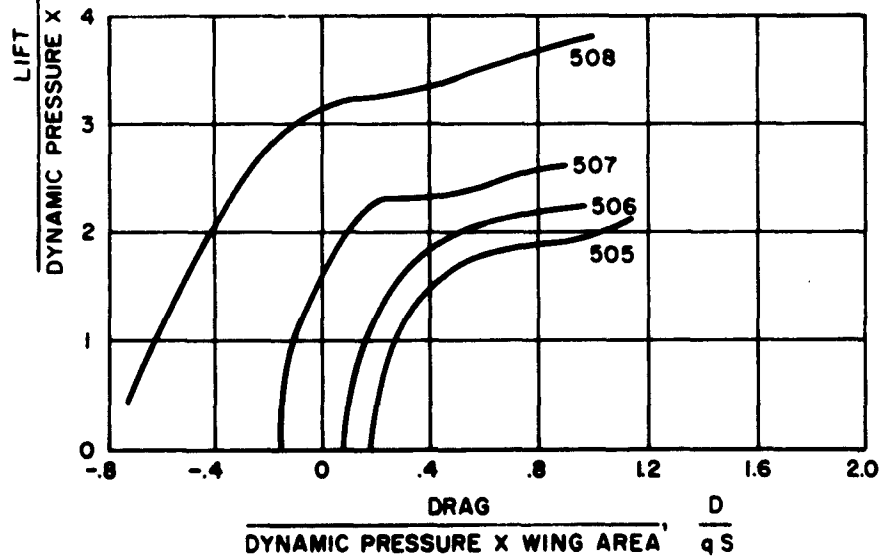
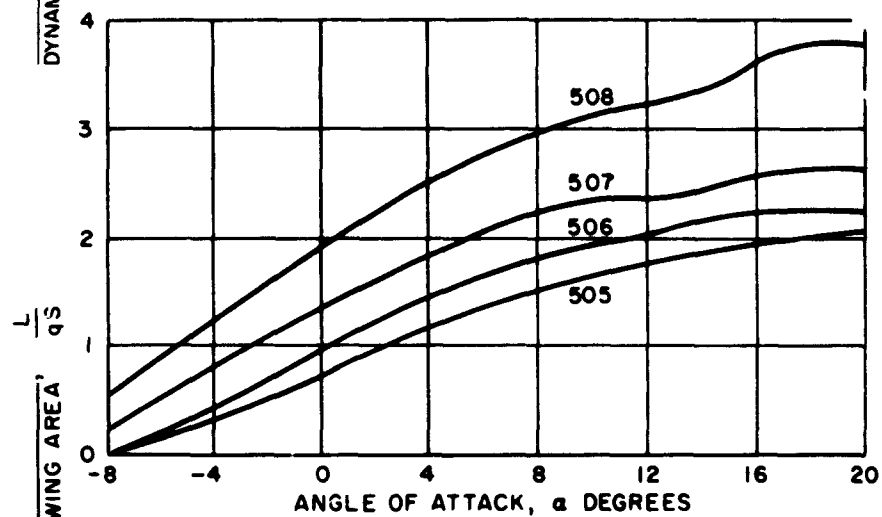
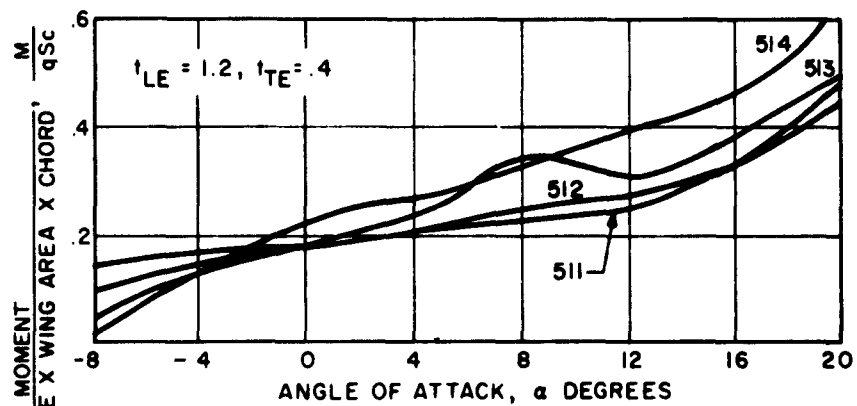


Figure 114. Configuration No. 51,  $\theta_F = -60^\circ$ ,  $\theta_R = +60^\circ$   
 $h/c = .20$ , (Runs 505 - 508)



CONFIGURATION NO. 6

RUN NO.	$J/qS$
511	.12
512	.26
513	.74
514	1.71

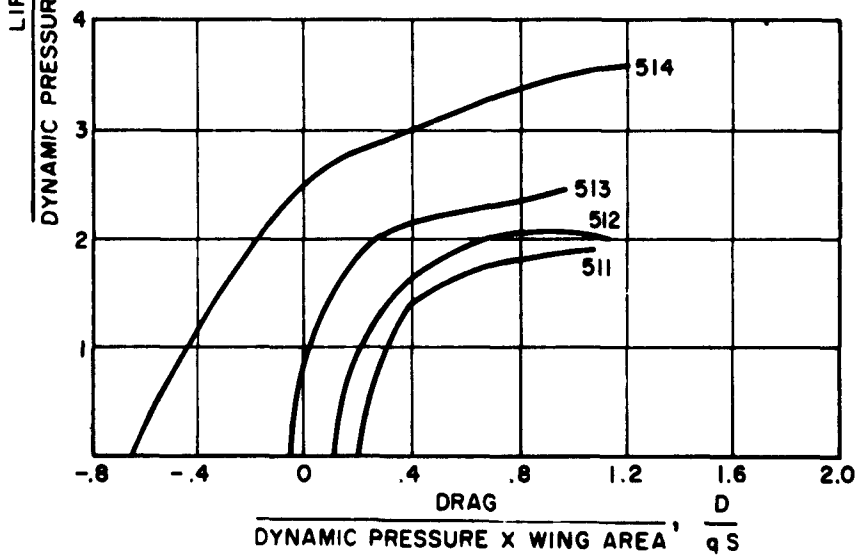
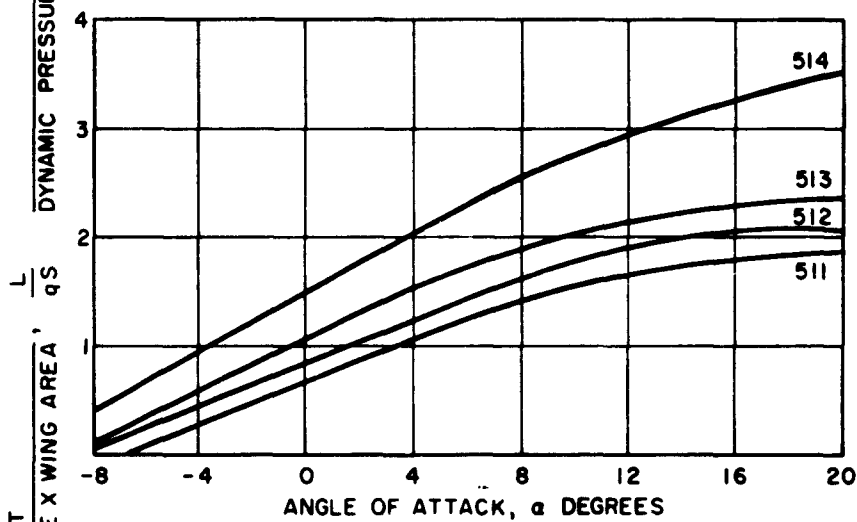
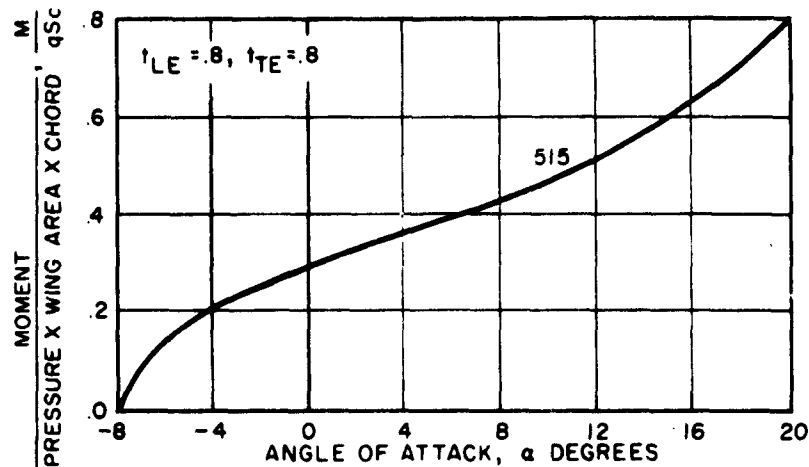


Figure 115. Configuration No. 6,  $\theta_F = -60^\circ, \theta_R = +60^\circ$   
 $h/c = .33$ , (Runs 511 - 514)



CONFIGURATION NO. 6

RUN NO.	J/qS
5.5	2.99

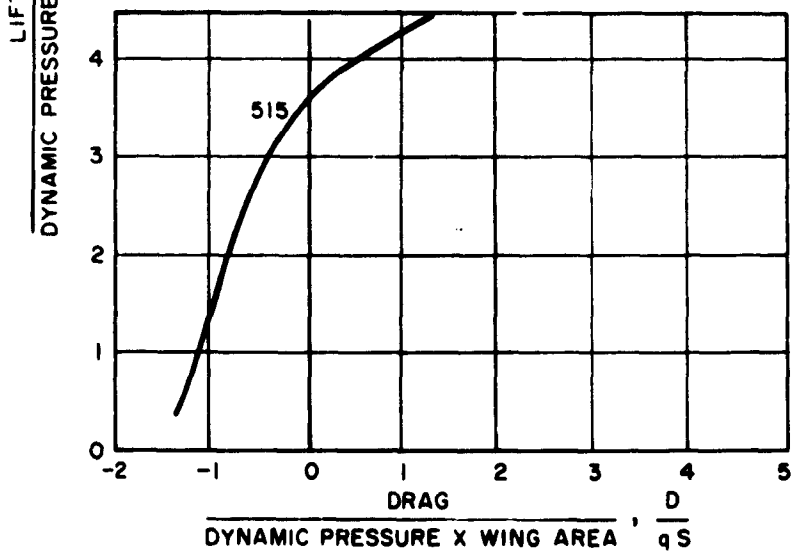
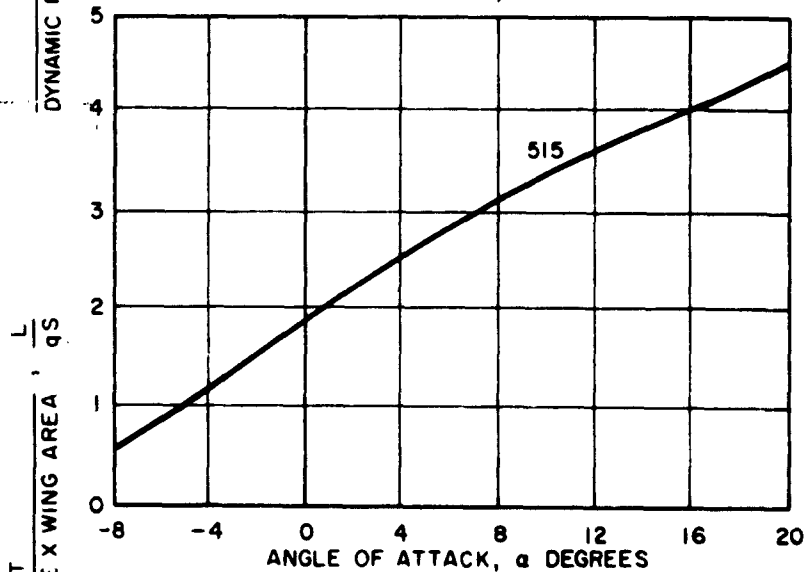
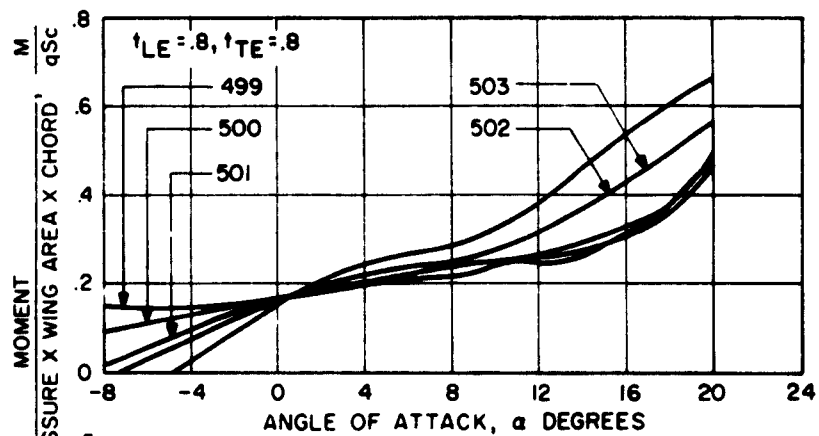


Figure 116. Configuration No. 6,  $\theta_F = -60^\circ$   $\theta_R = +60^\circ$   
 $h/c = .33$ , (Run 515)



CONFIGURATION NO. 50

RUN NO.	$J/qS$
499	.1058
500	.2723
501	.7518
502	1.7375
503	3.0084

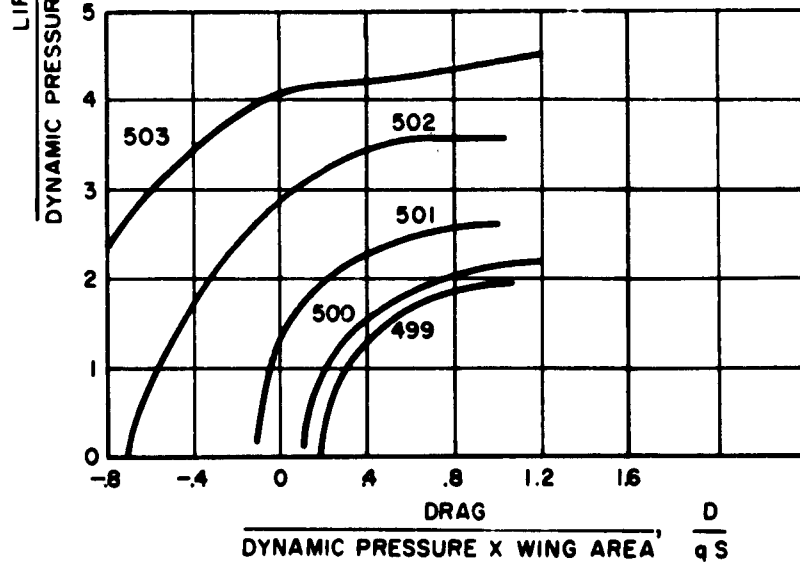
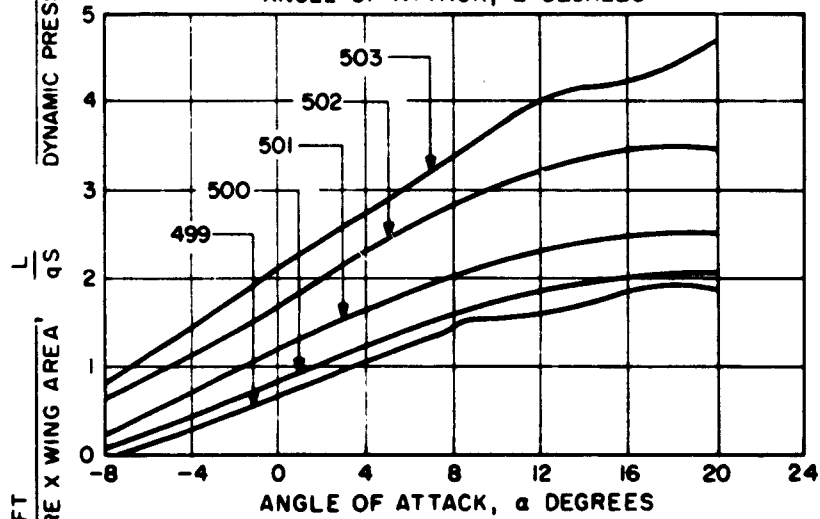
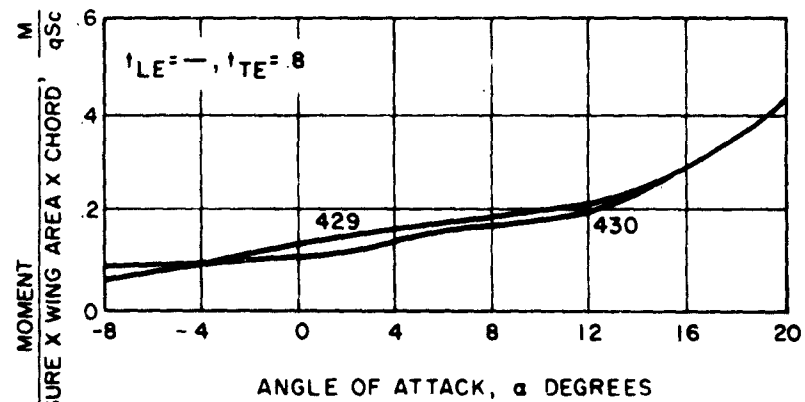


Figure 117. Configuration No. 50,  $\theta_F = -60^\circ$ ,  $\theta_R = +60^\circ$   
 $h/c = .33$ , (Runs 499 - 503)



CONFIGURATION NO.55

RUN NO.	J/qS
429	.631
430	.428

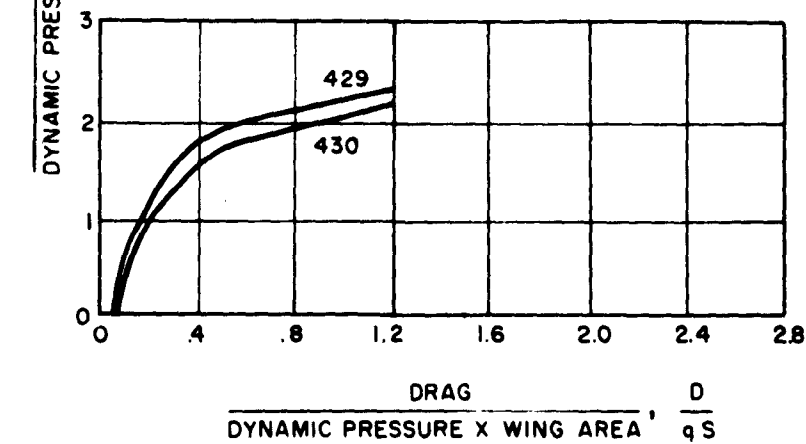
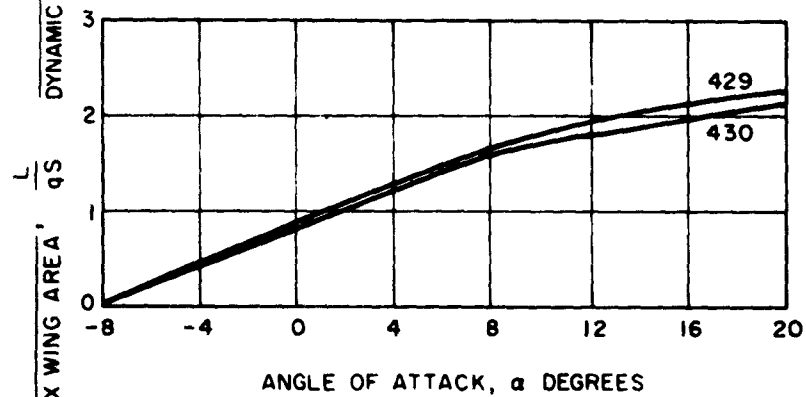
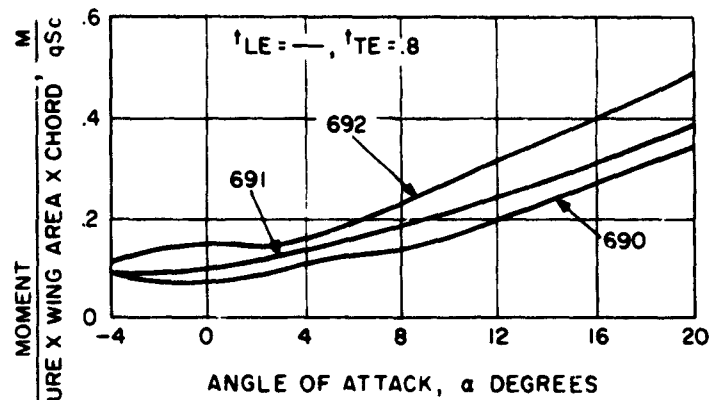


Figure 118. Configurations No. 55,  $\theta_F = -\theta_R = +60^\circ$   
 $h/c = .33$ , (Runs 429 - 430)



CONFIGURATION NO 20

RUN NO.	J/qS
690	.46
691	1.57
692	3.85

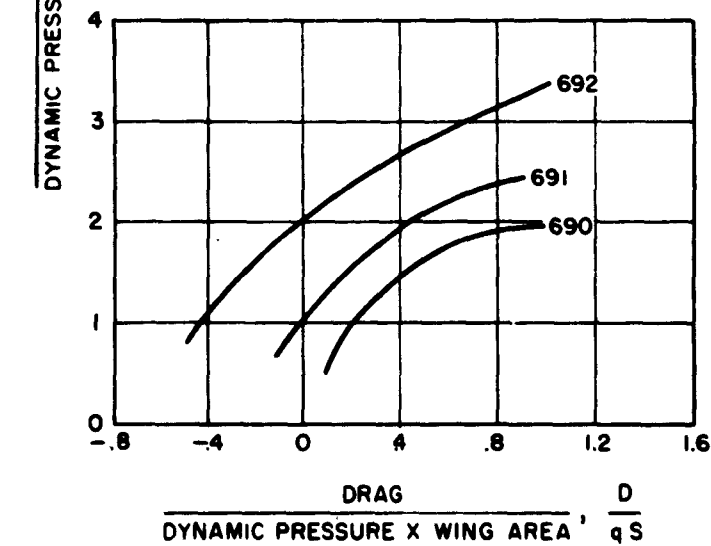
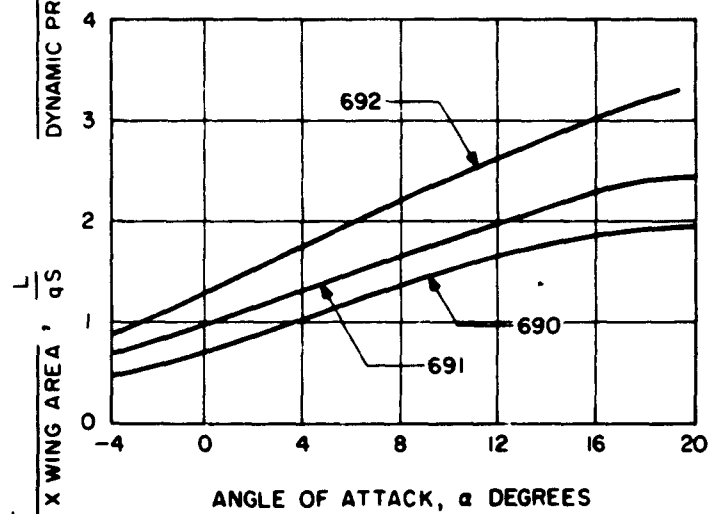
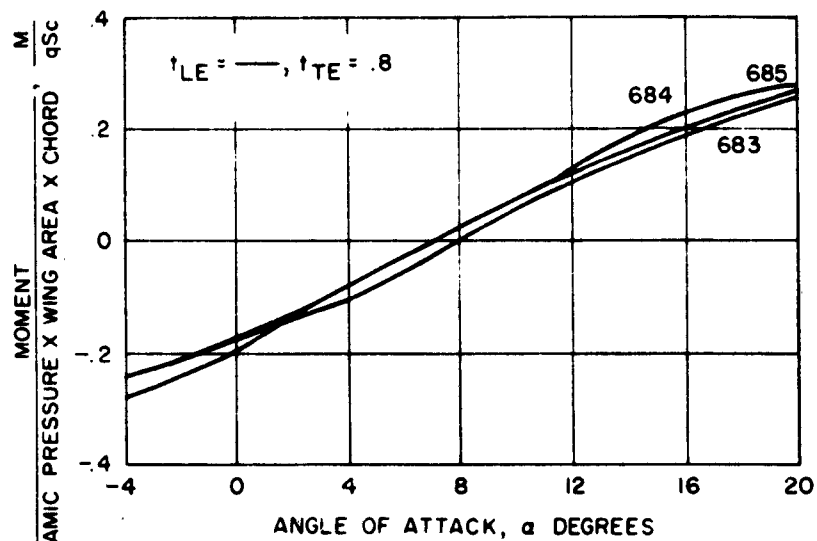


Figure 119. Configuration No. 26,  $\theta_F = -\theta_R = +60^\circ$   
 $h/c = \infty$ , (Runs 690 - 692)



CONFIGURATION NO 73

RUN NO.	J/qS
683	.152
684	.469
685	1.685

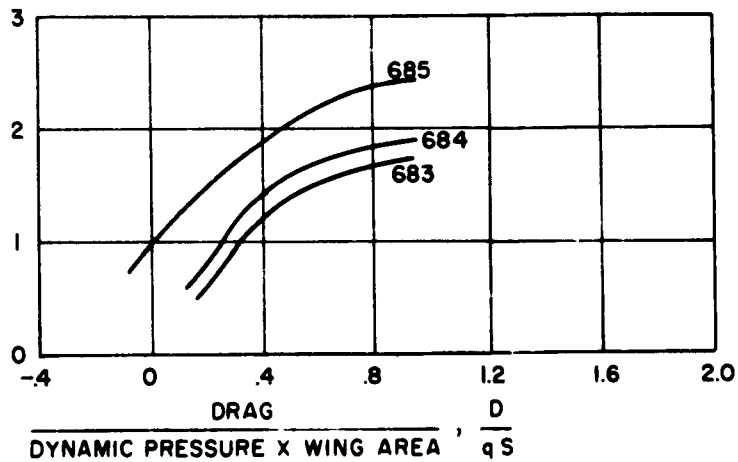
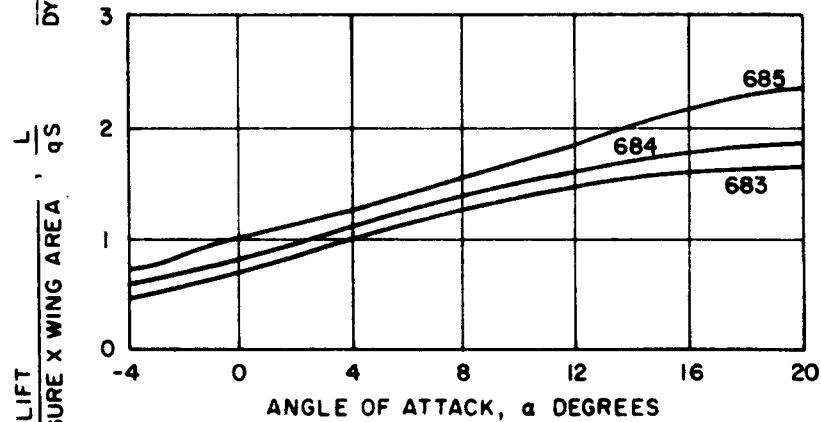


Figure 120. Configuration No. 73,  $\theta_F = -\theta_R = +60$   
 $h/c = \infty$ , (Runs 683 - 685)

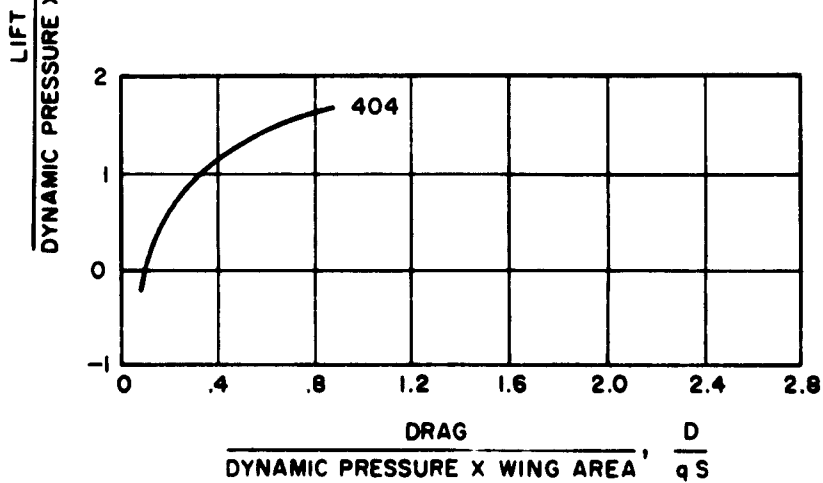
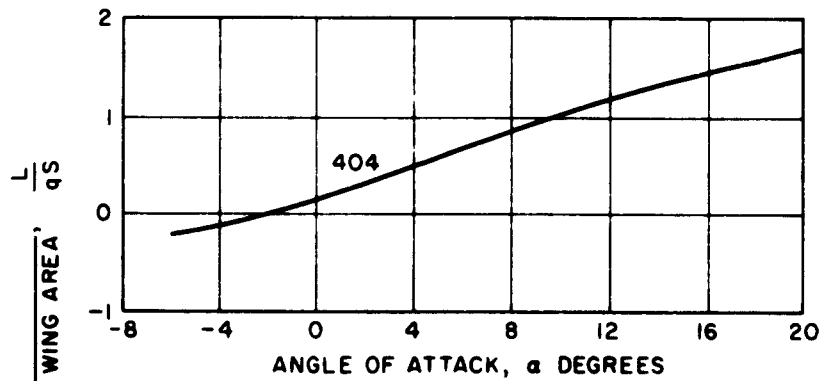
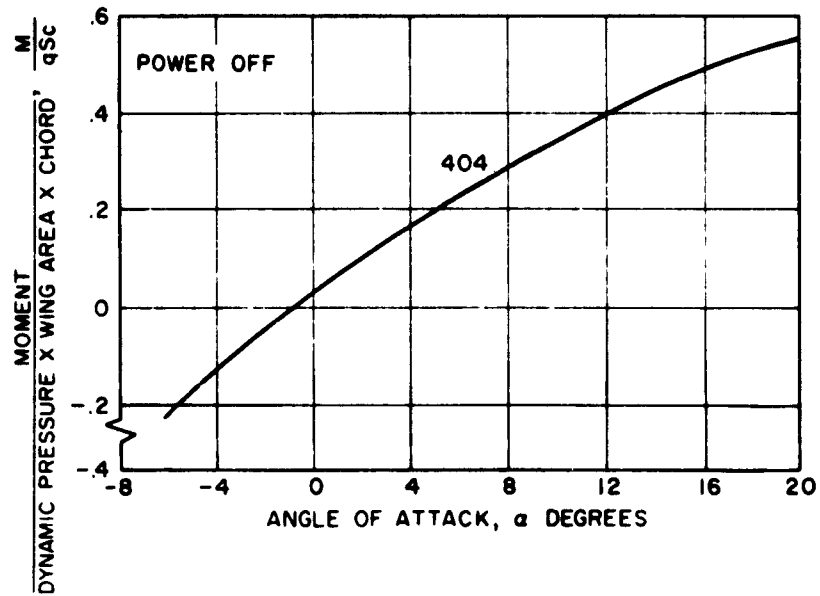
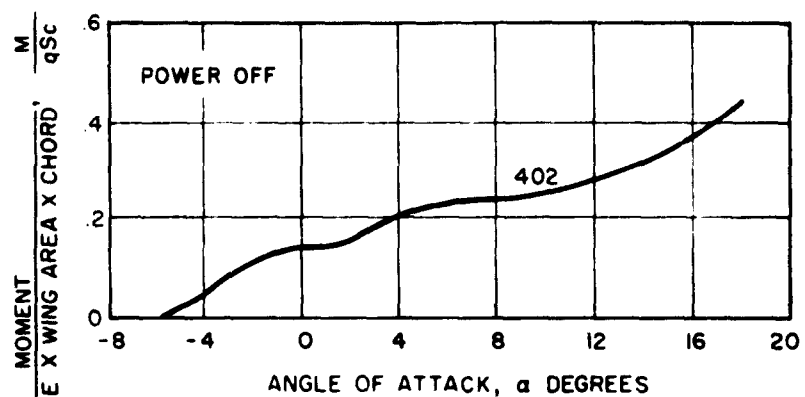


Figure 121. Configuration No. 81,  $\theta_F = -\theta_R = -h/c = .20$ , (Run 404)



CONFIGURATION NO.79

RUN NO.	J/qS
402	0

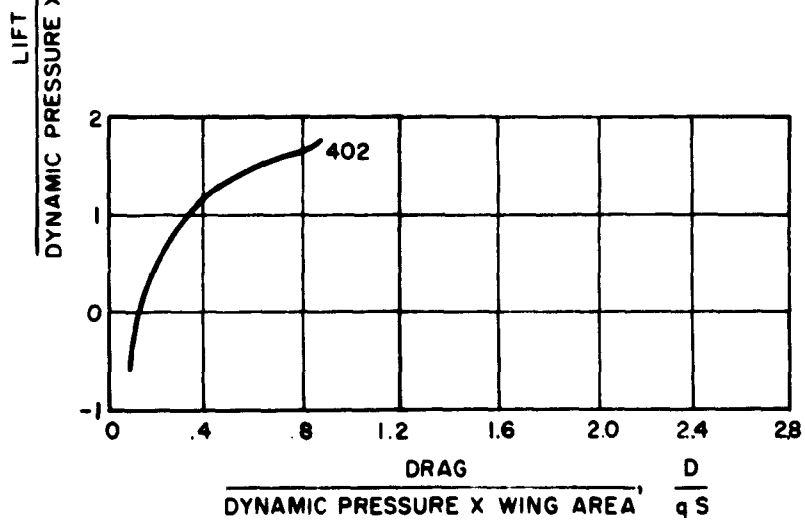
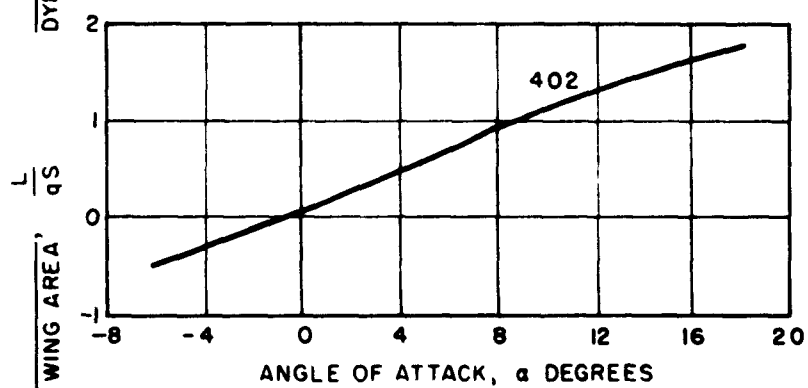


Figure 122. Configuration No. 79,  $\theta_F = -\theta_R = -h/c = .20$ , (Run 402)

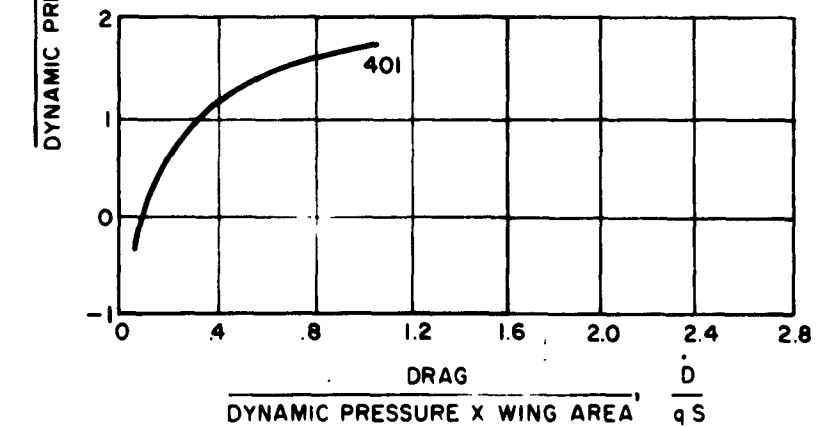
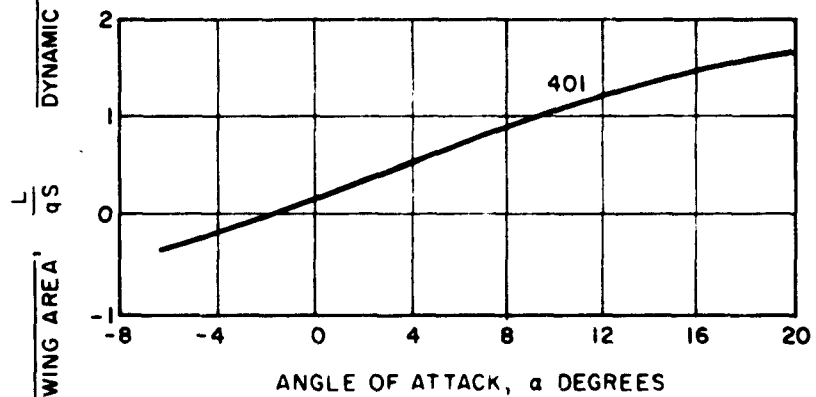
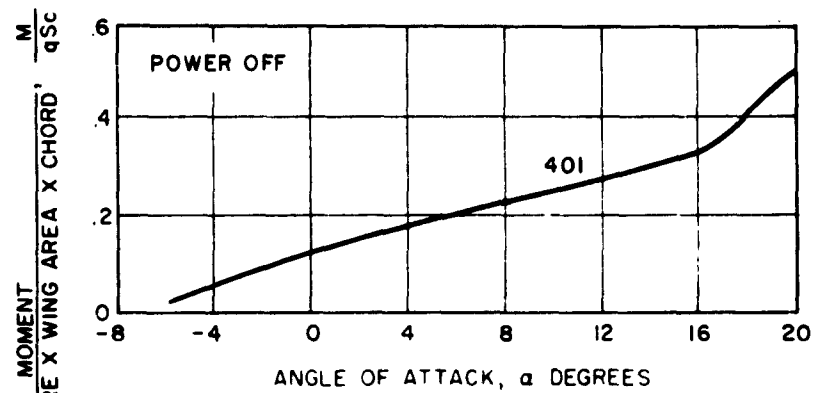
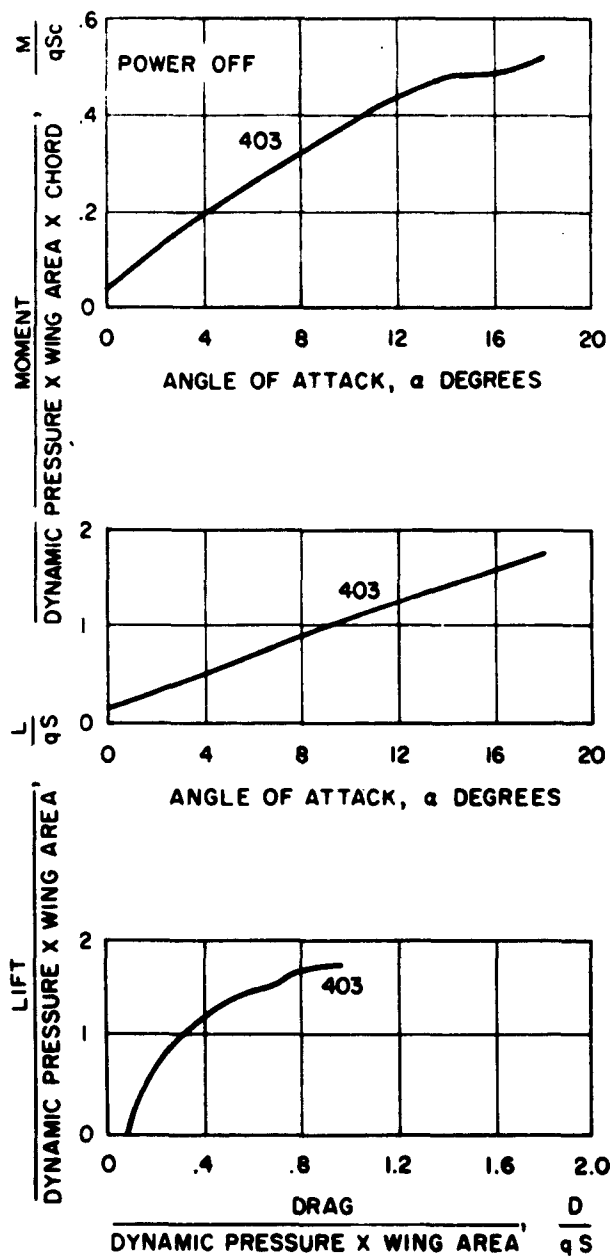


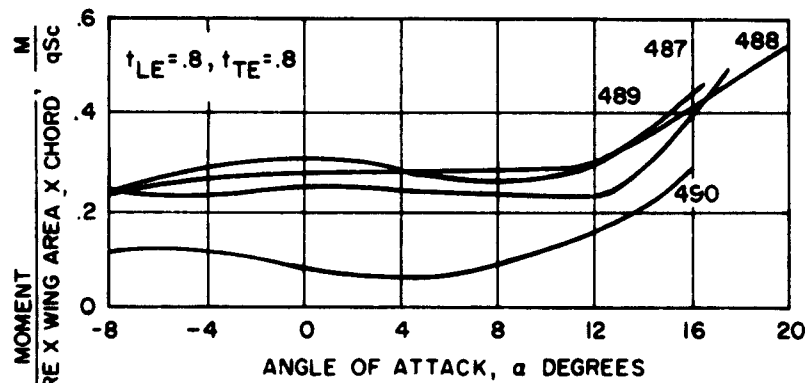
Figure 123. Configuration No. 78,  $\theta_F = -\theta_R = -h/c = .33$ , (Run 401)



CONFIGURATION NO. 80

RUN NO.	J/qS
403	0

Figure 124. Configuration No. 80,  $\theta_F = -\theta_R = -h/c = .33$ , (Run 403)



CONFIGURATION NO. 2

RUN NO.	J/qS
487	.07
488	.18
489	.53
490	1.19

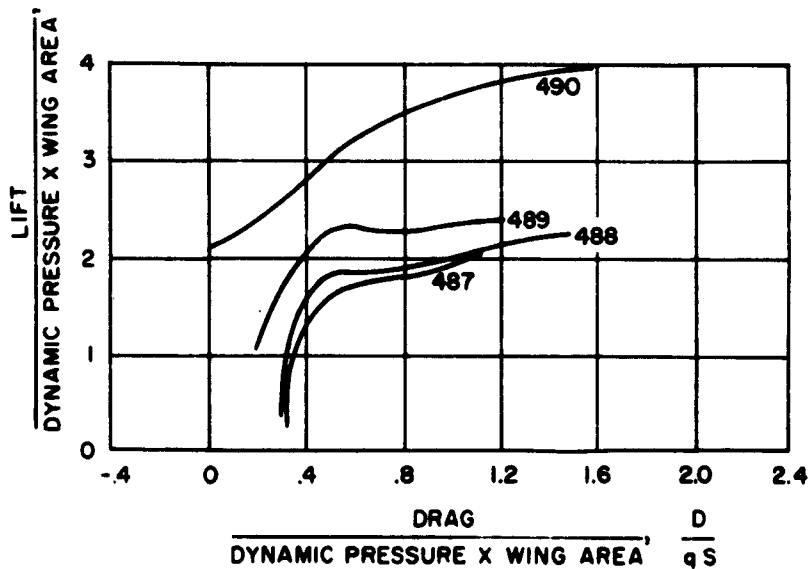
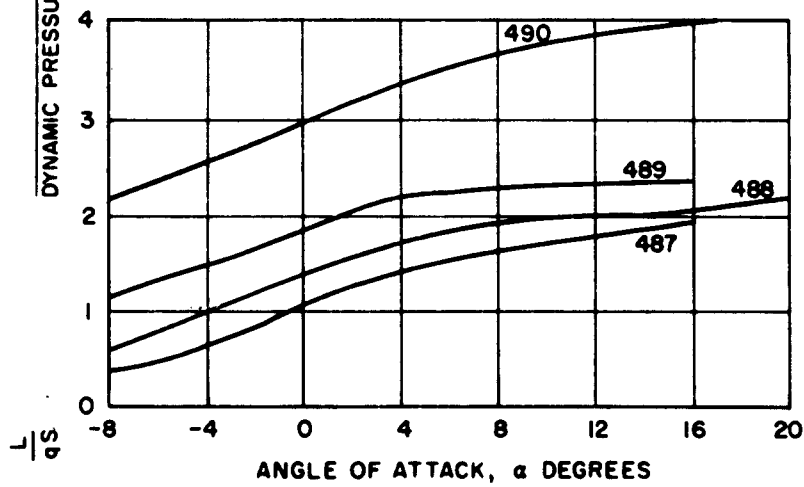
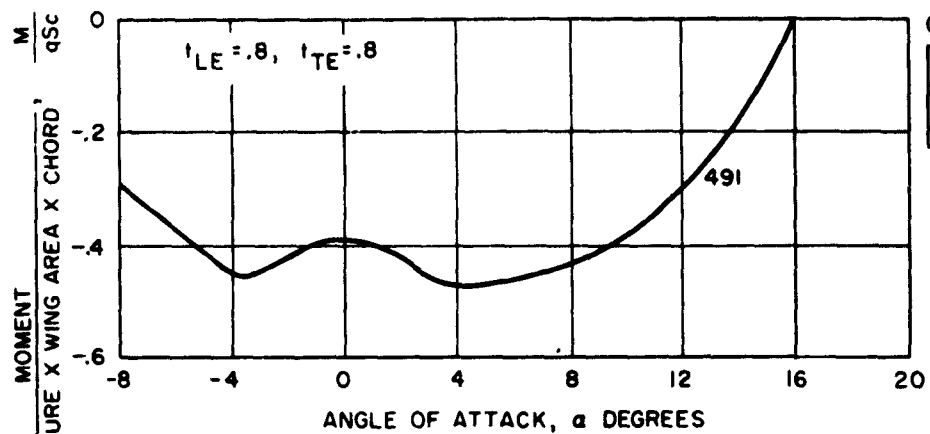


Figure 125. Configuration No. 2,  $\theta_F = -30^\circ$ ,  $\theta_R = -30^\circ$ ,  $h/c = .20$ ,  
(Runs 487 - 490)



CONFIGURATION NO.2

RUN NO.	J/qS
491	2.04

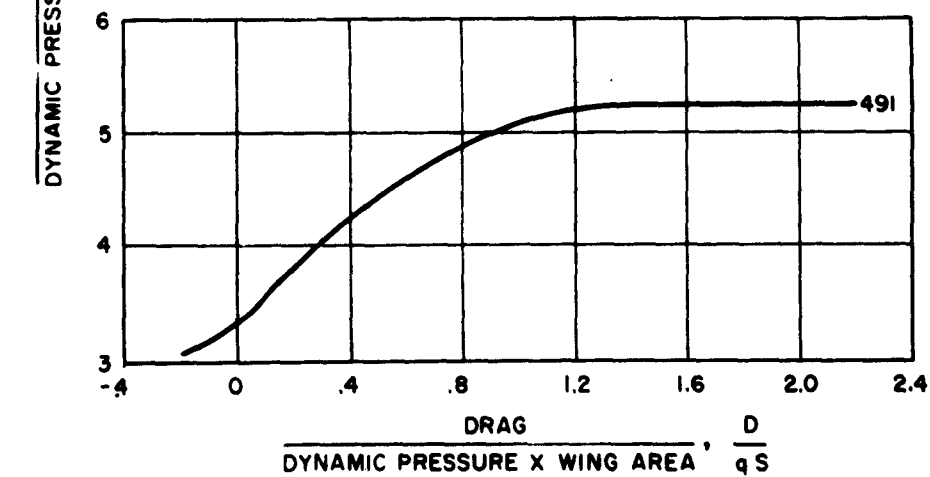
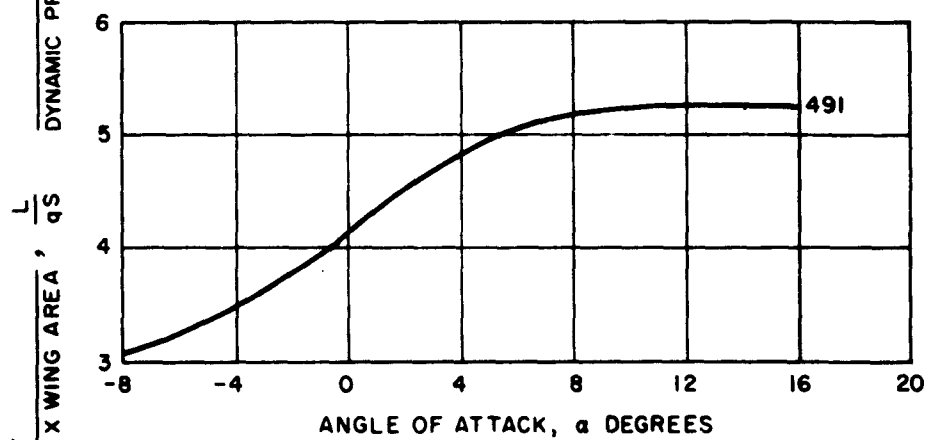
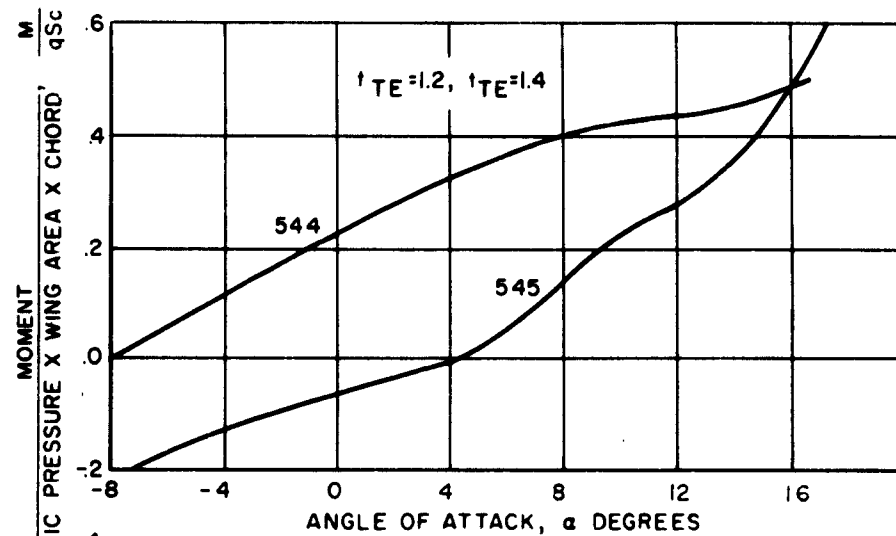


Figure 126. Configuration No. 2,  $\theta_F = -30 \times \theta_R = -30 \times h/c = .20$ , (Run 491)



CONFIGURATION  
NO. 15

RUN NO.	J/qS
544	.2148
545	1.315

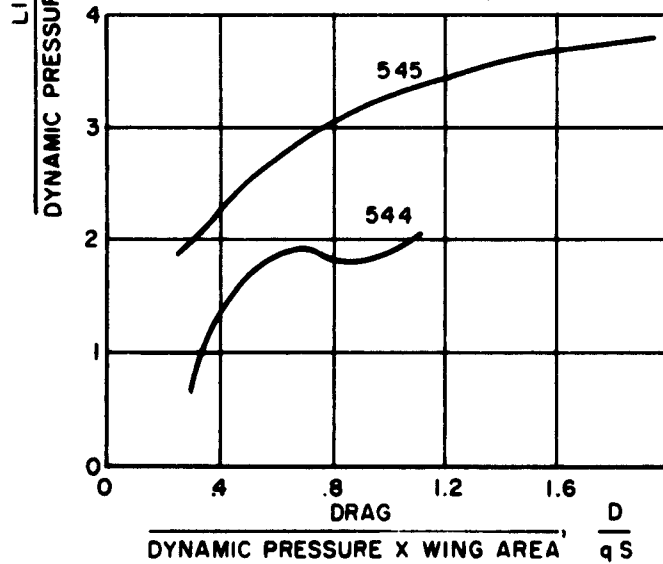
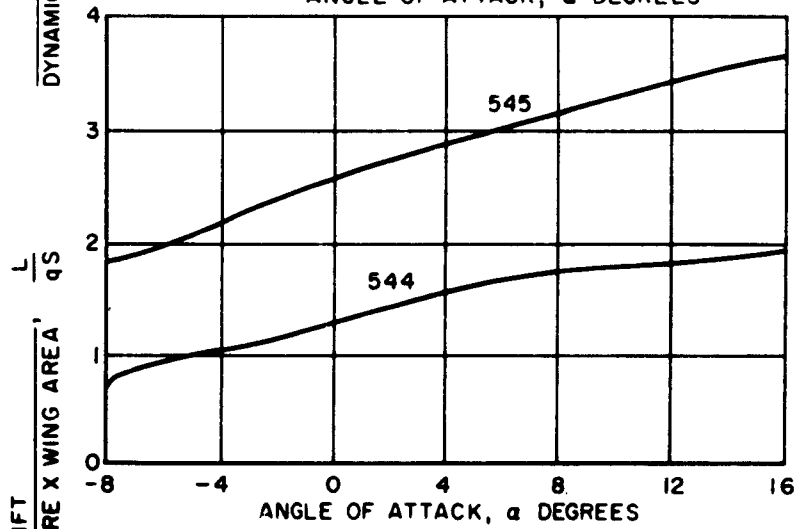


Figure 127. Configuration No. 15,  $\theta_F = -30^\circ$ ,  $\theta_R = -30^\circ$ ,  $h/c = .20$ ,  
(Runs 544 - 545)

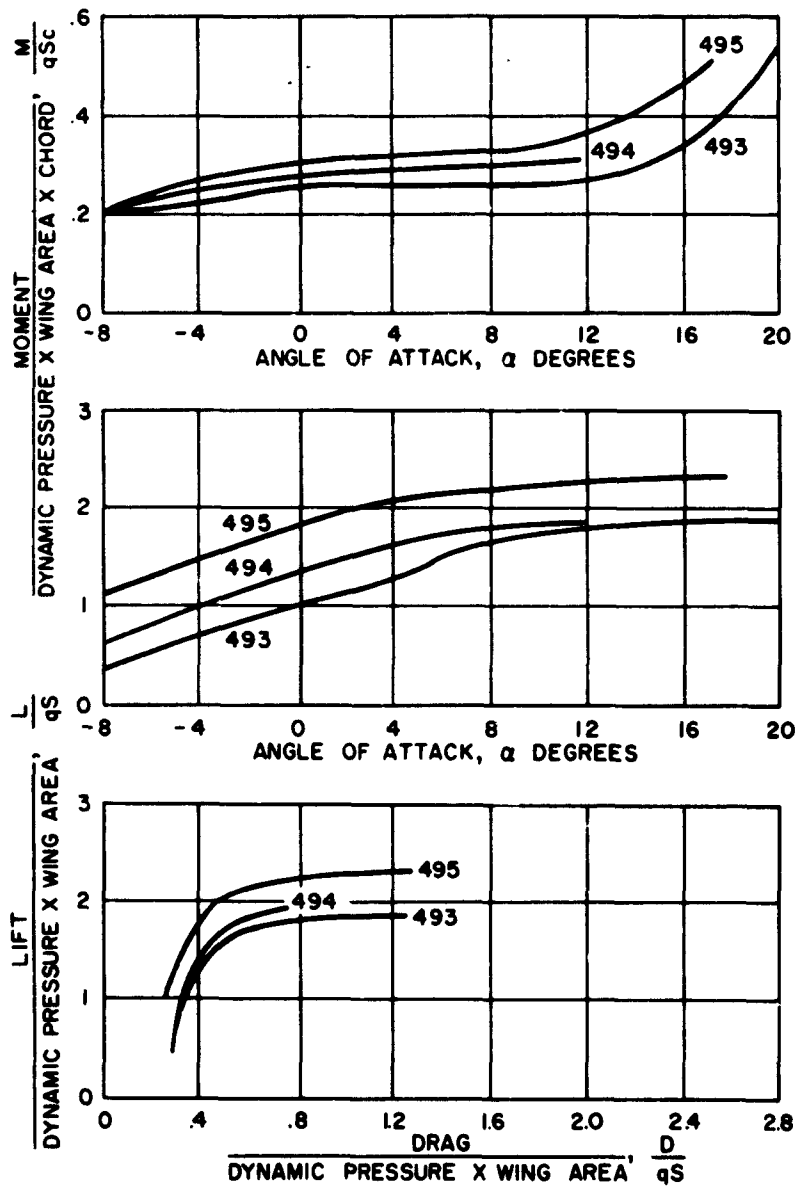
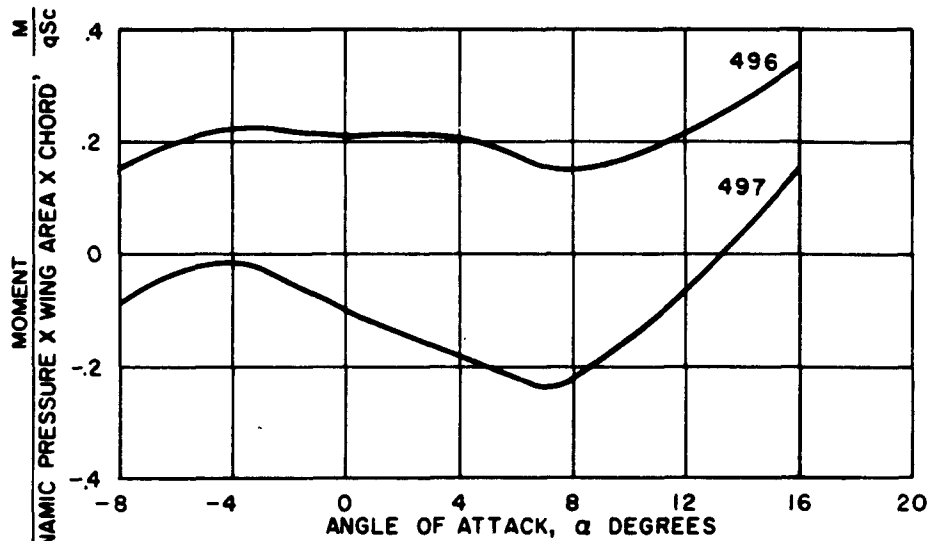


Figure 128. Configuration No. 1,  $\theta_F = -30^\circ$ ,  $\theta_R = -30^\circ$ ,  $h/c = .33$ ,  
(Runs 493 - 495)



CONFIGURATION NO. 1

RUN NO.	J/qS
496	1.228
497	2.125

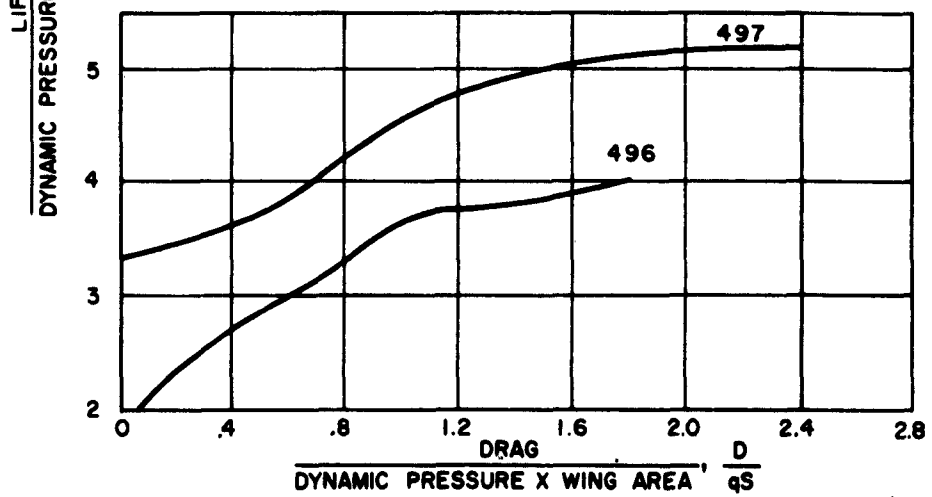
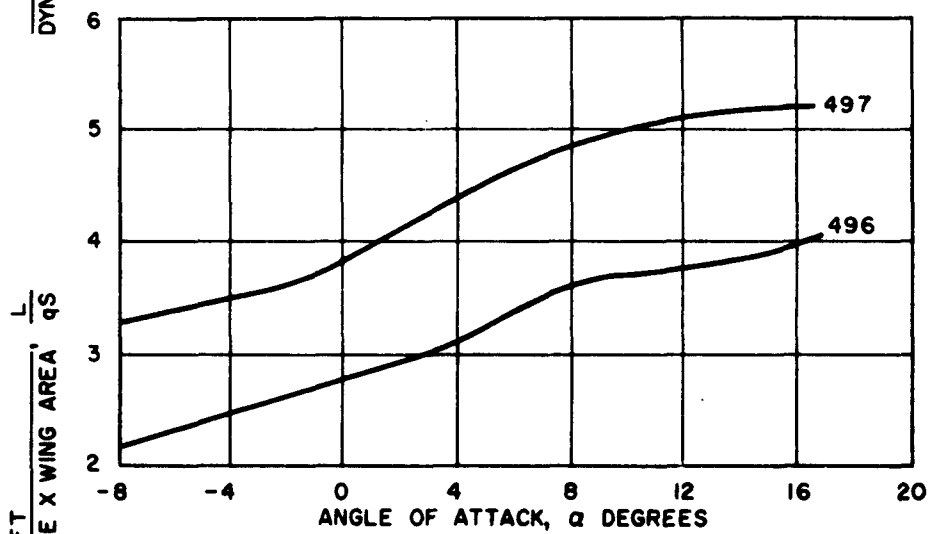
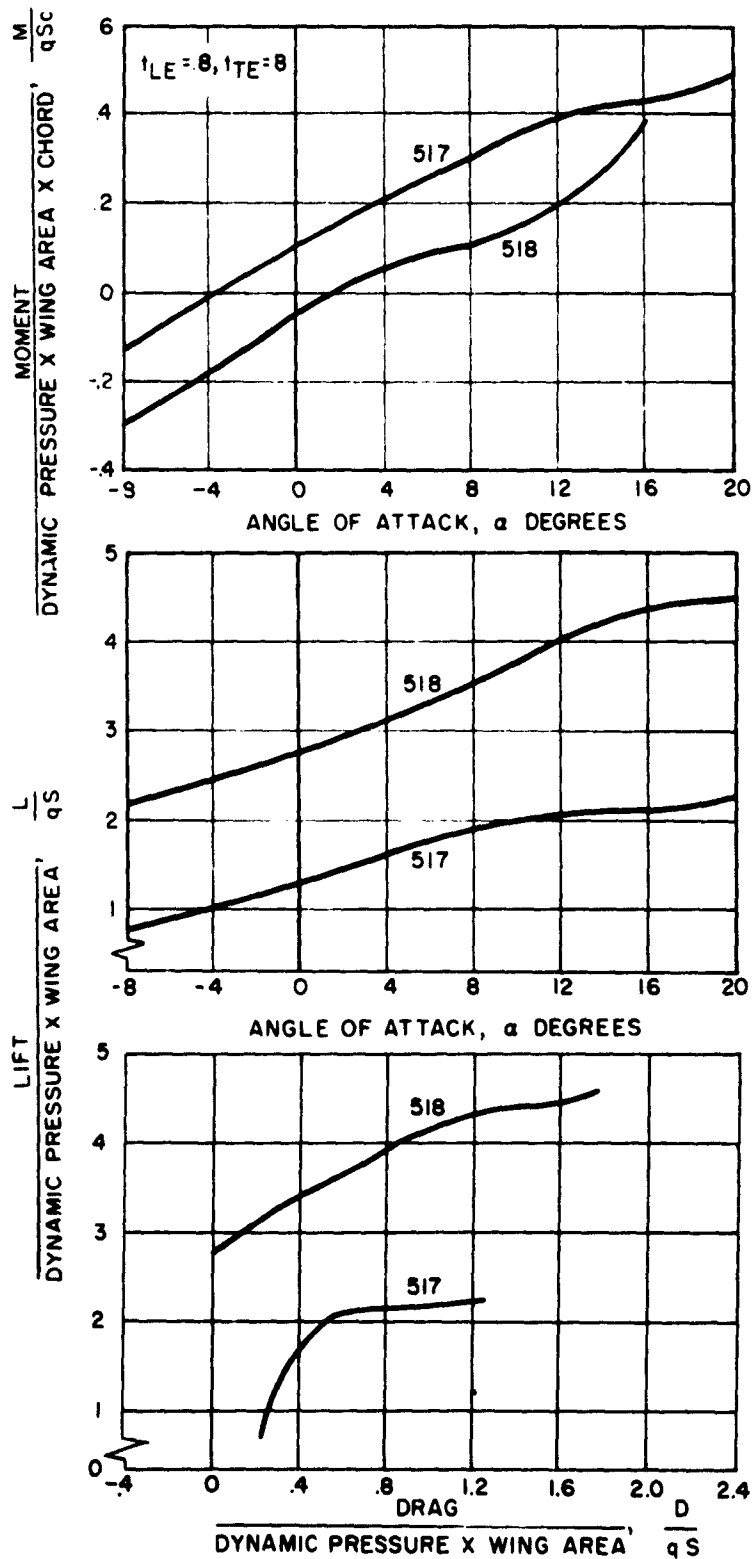


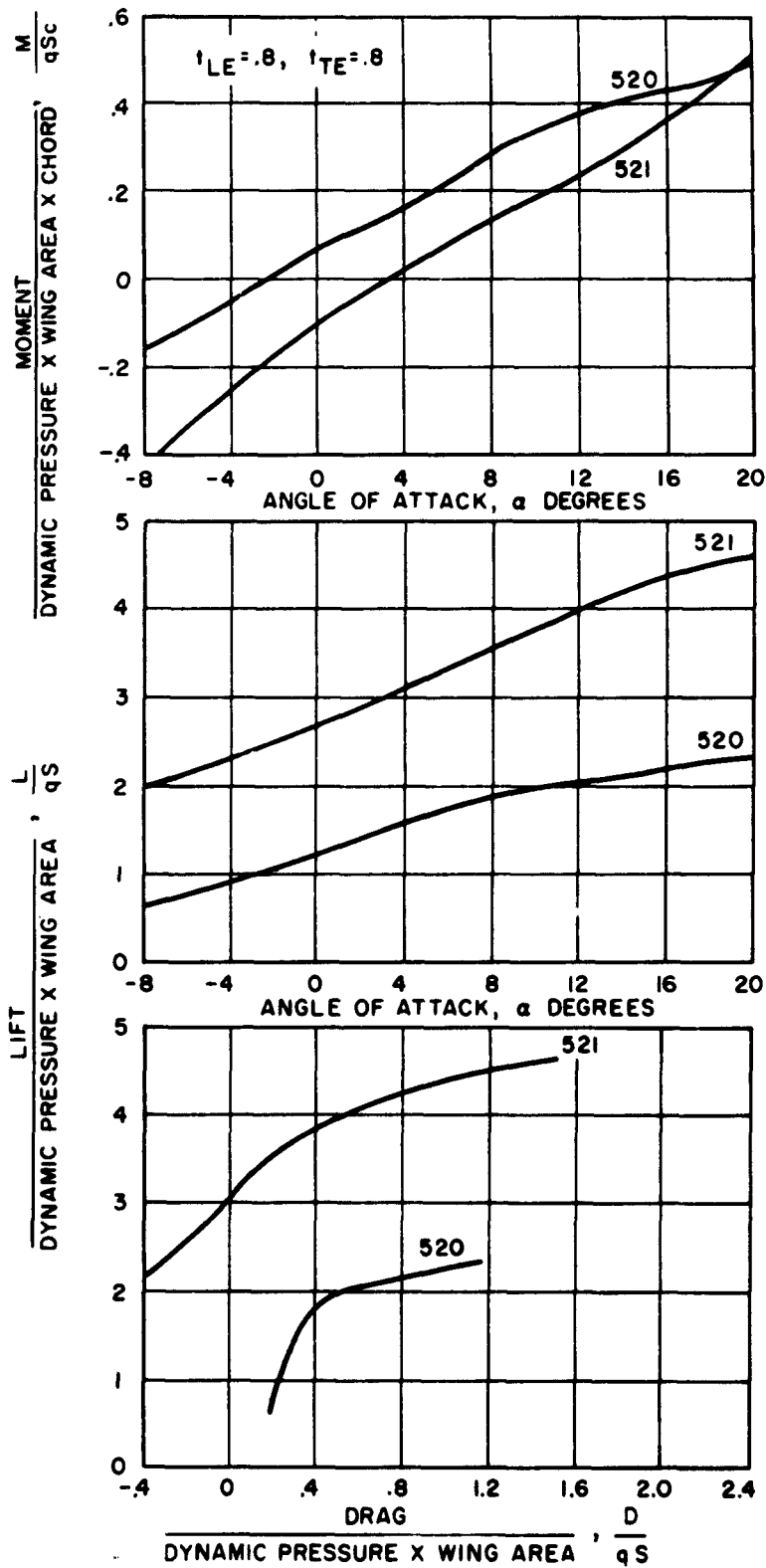
Figure 129. Configuration No. 1,  $\theta_F = -30^\circ$ ,  $\theta_R = -30^\circ$ ,  $h/c = .33$ ,  
(Runs 496 - 497)



CONFIGURATION NO. 4

RUN NO.	J/qS
517	.13
518	.84

Figure 130. Configuration No. 4,  $\theta_F = -30^\circ$ ,  $\theta_R = -30^\circ$ ,  $h/c = .33$ ,  
(Runs 517 - 518)



CONFIGURATION NO. 5

RUN NO.	J/qS
520	.10
521	.60

Figure 131. Configuration No. 5,  $\theta_F = -30^\circ$ ,  $\theta_R = -30^\circ$ ,  $h/c = .33$ ,  
(Runs 520 - 521)

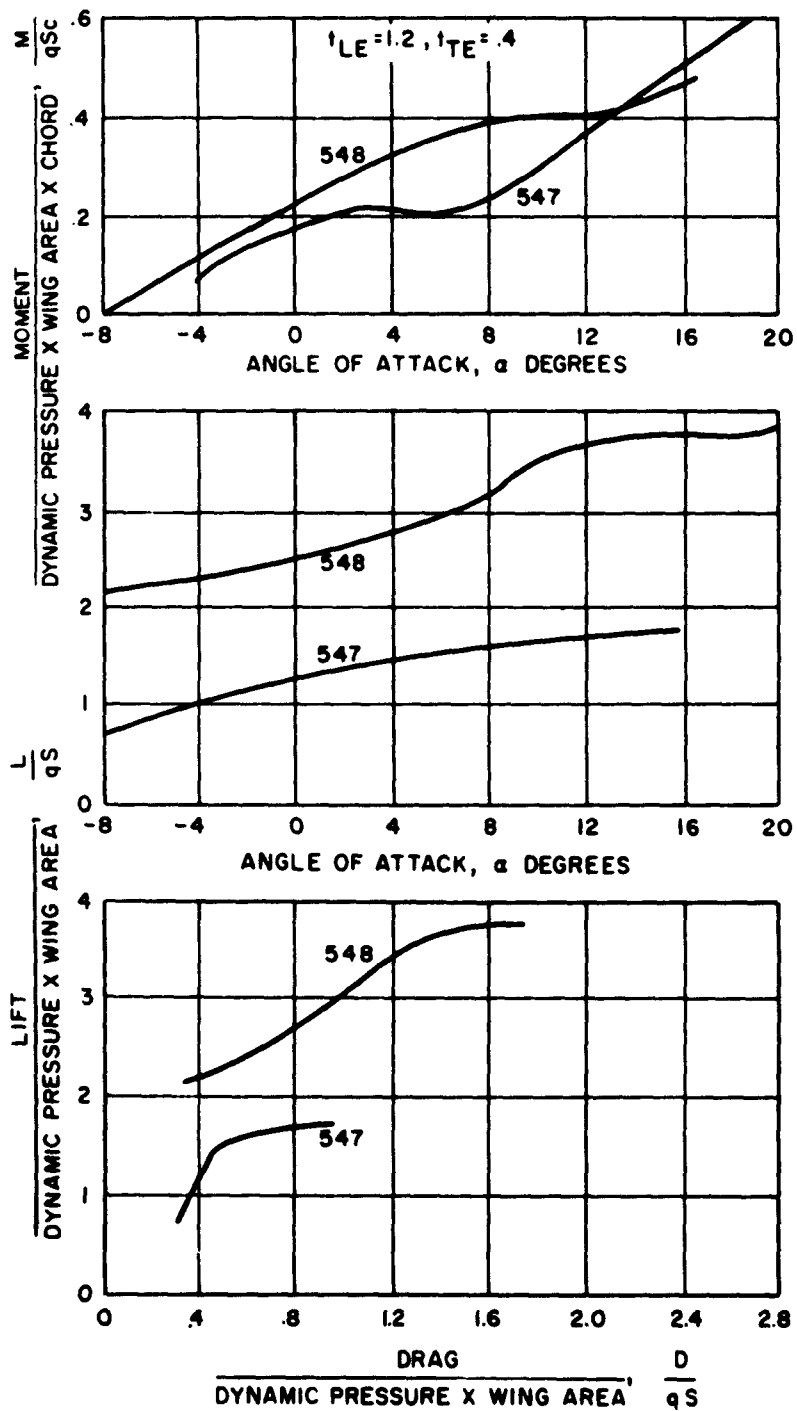
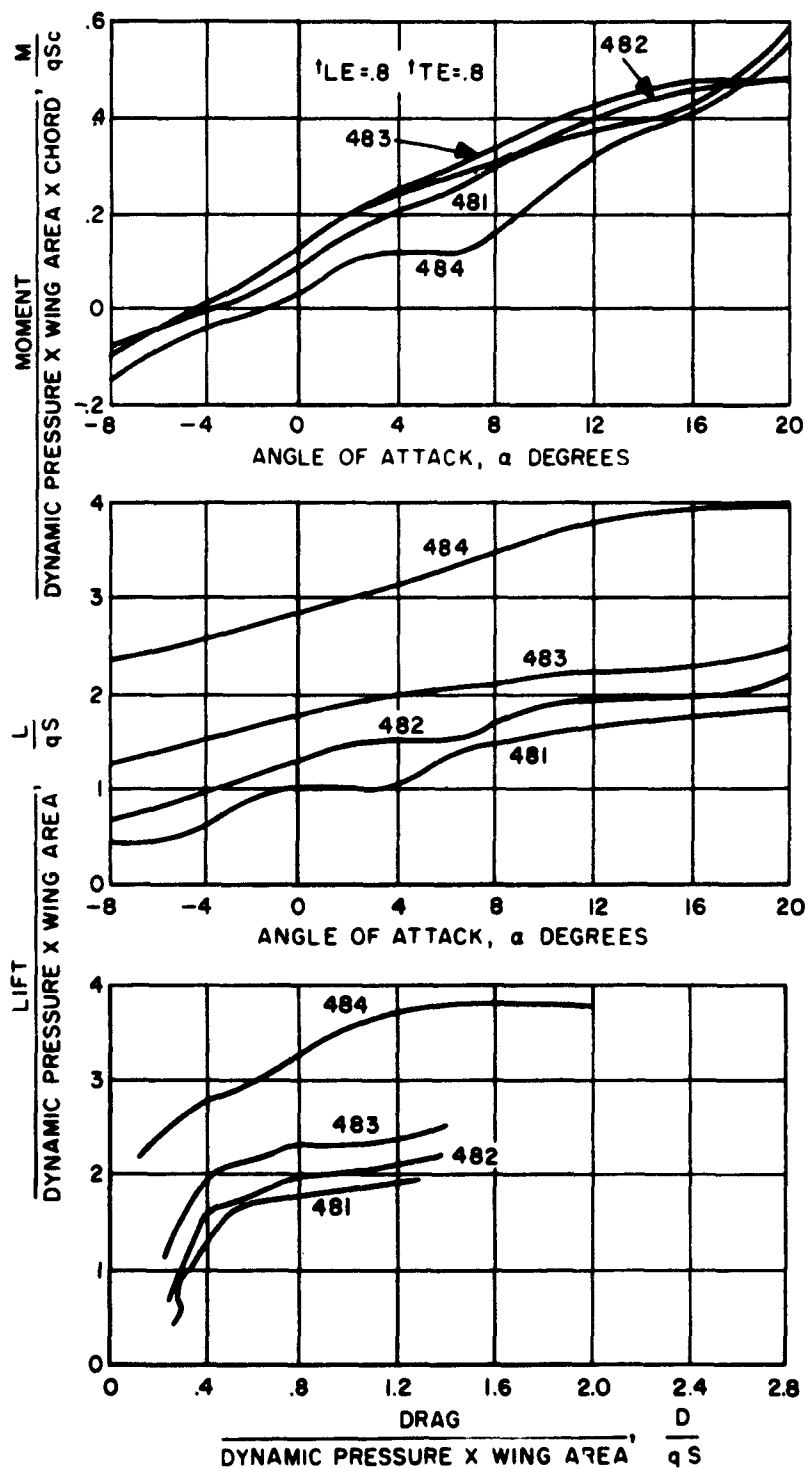


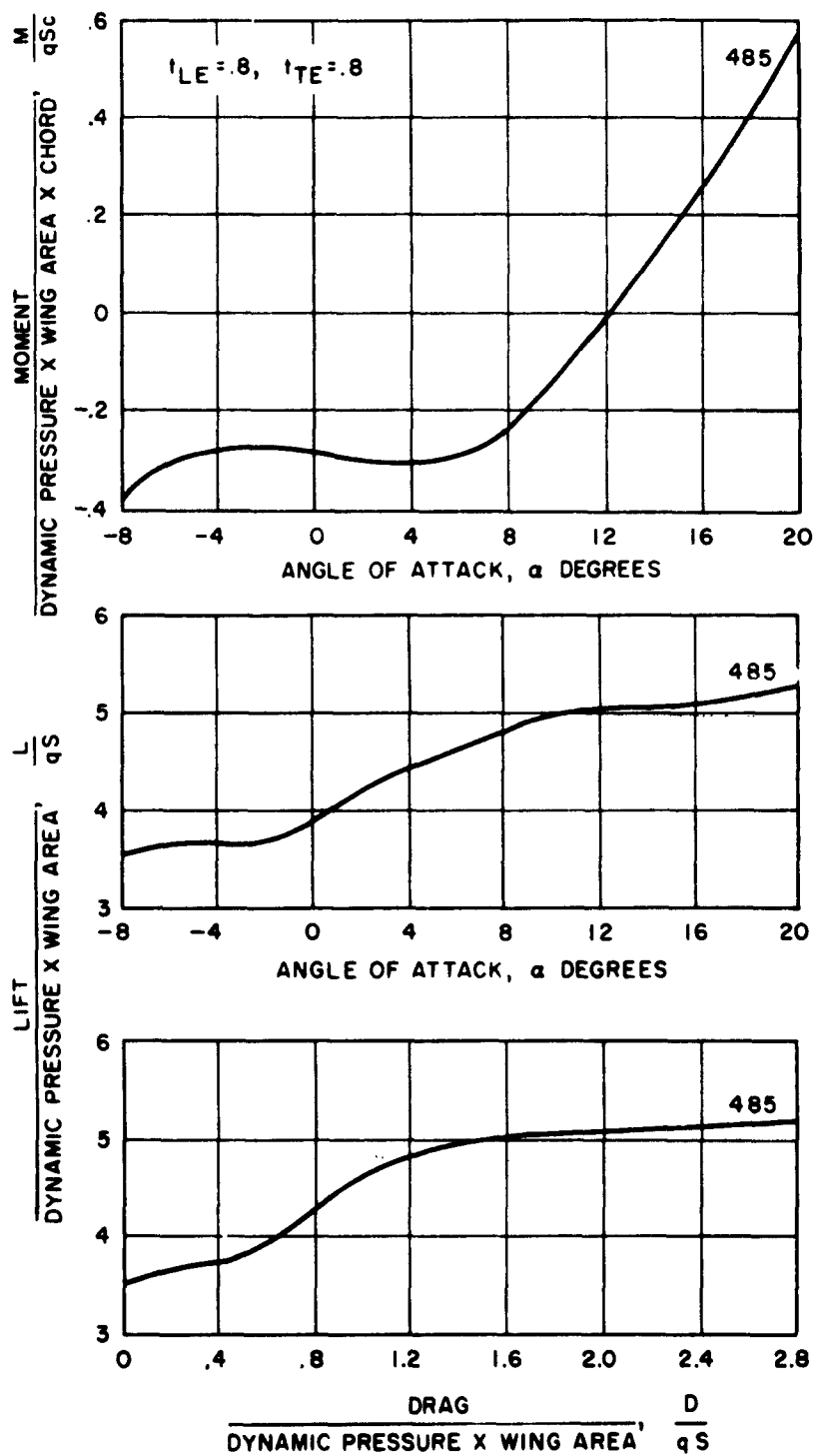
Figure 132. Configuration No. 13,  $\theta_F = -30^\circ$ ,  $\theta_R = -30^\circ$ ,  $h/c = .33$ ,  
 (Runs 547 - 548)



CONFIGURATION NO.28

RUN NO.	J/qS
481	.0763
482	.179
483	.5117
484	1.1877

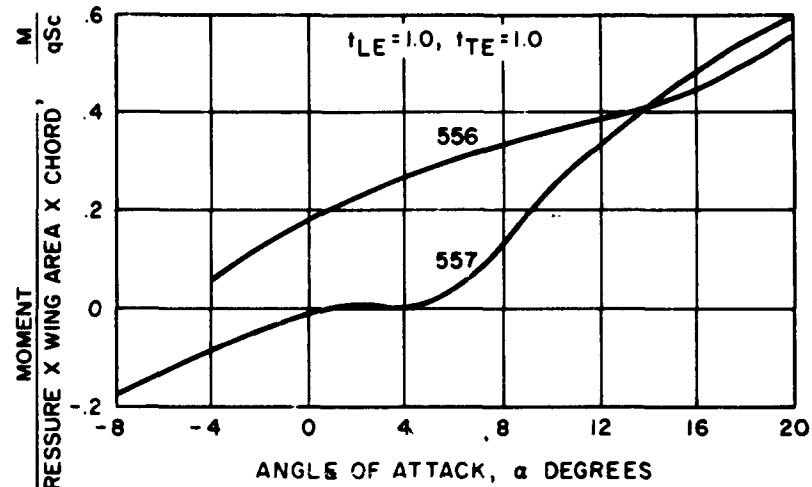
Figure 133. Configuration No. 28,  $\theta_F = -30^\circ$ ,  $\theta_R = -30^\circ$ ,  $h/c = .33$ ,  
(Runs 481 - 484)



CONFIGURATION NO. 28

RUN NO.	J/qS
485	2.0817

Figure 134. Configuration No. 28,  $\theta_F = -30^\circ$ ,  $\theta_R = -30^\circ$ ,  $h/c = .33$ , (Run 485)



CONFIGURATION NO.29

RUN NO.	J/qS
556	.1762
557	1.119

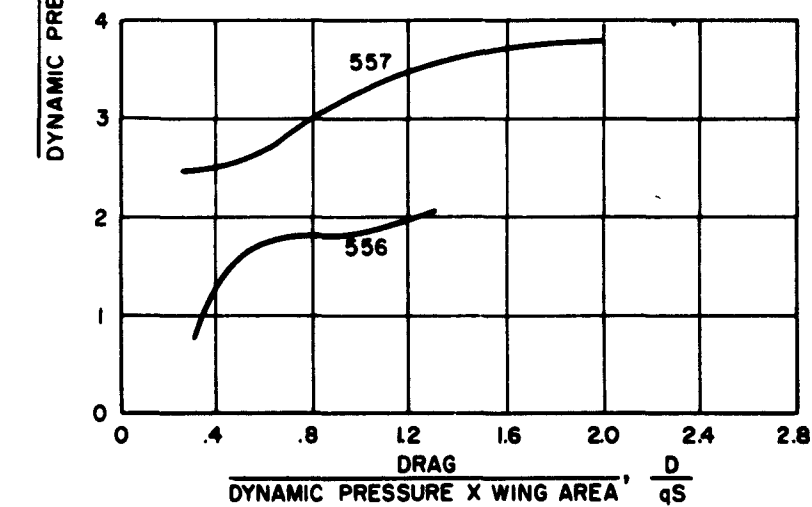
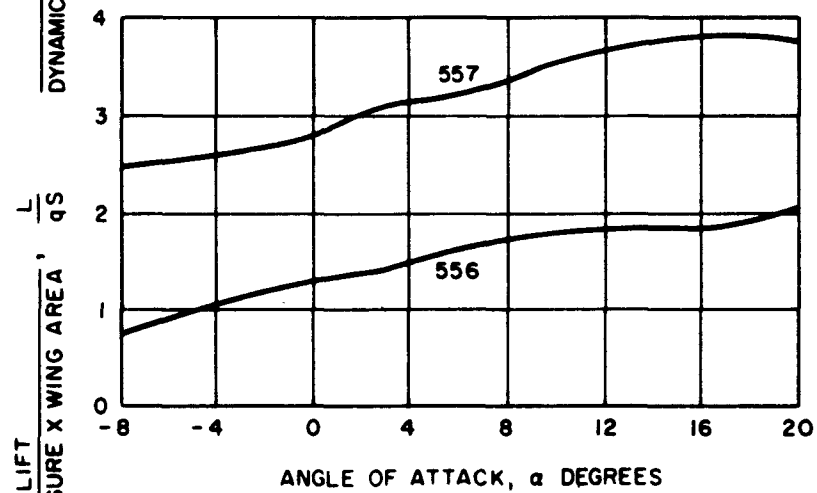
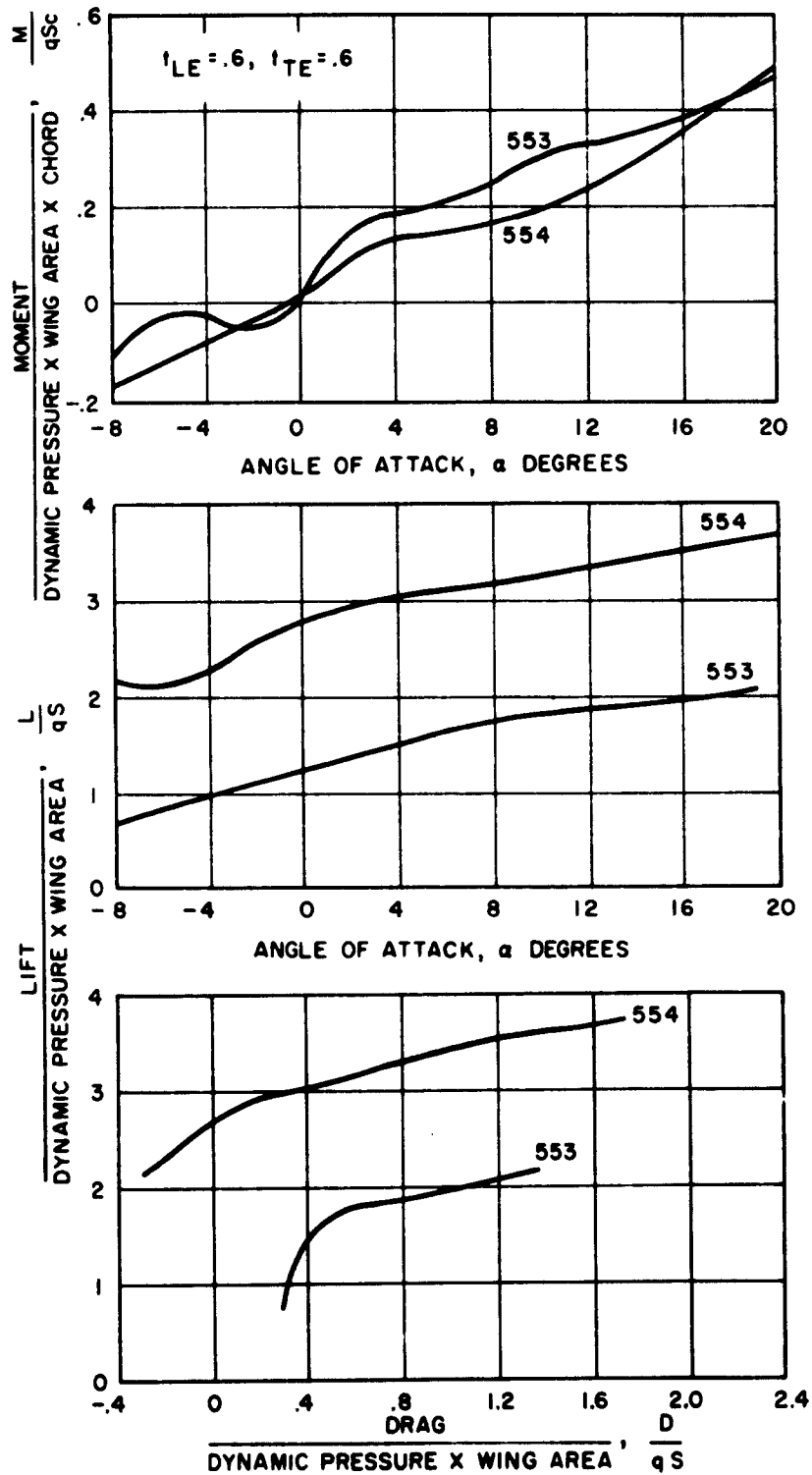


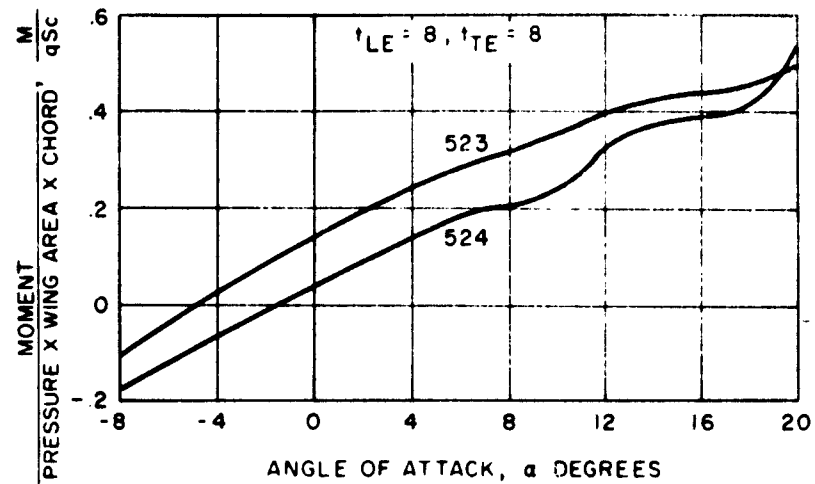
Figure 135. Configuration No. 29,  $\theta_F = -30^\circ$ ,  $\theta_R = -30^\circ$ ,  $h/c = .33$ ,  
(Runs 556 - 557)



CONFIGURATION NO.30

RUN NO.	J/qS
553	.0184
554	1.3277

Figure 136. Configuration No. 30,  $\theta_F = -30^\circ$ ,  $\theta_R = -30^\circ$ ,  $h/c = .33$ ,  
 (Runs 553 - 554)



CONFIGURATION NO. 48

RUN NO.	$J/qS$
523	.1882
524	1.1890

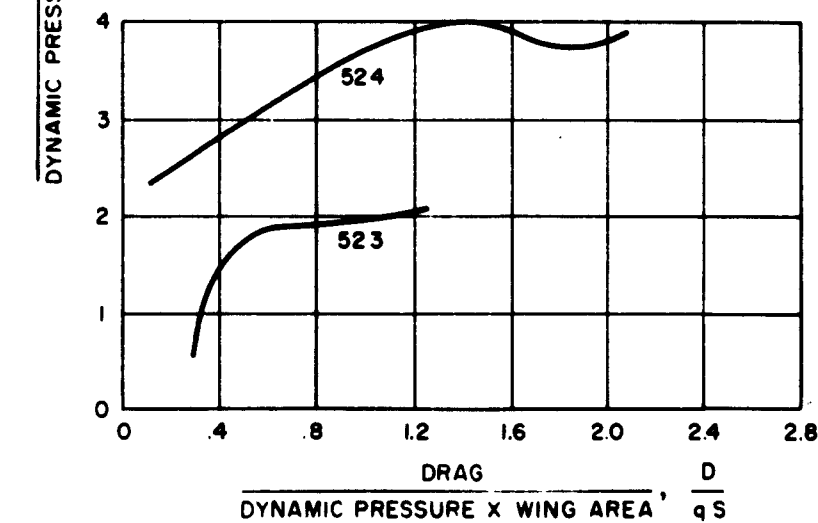
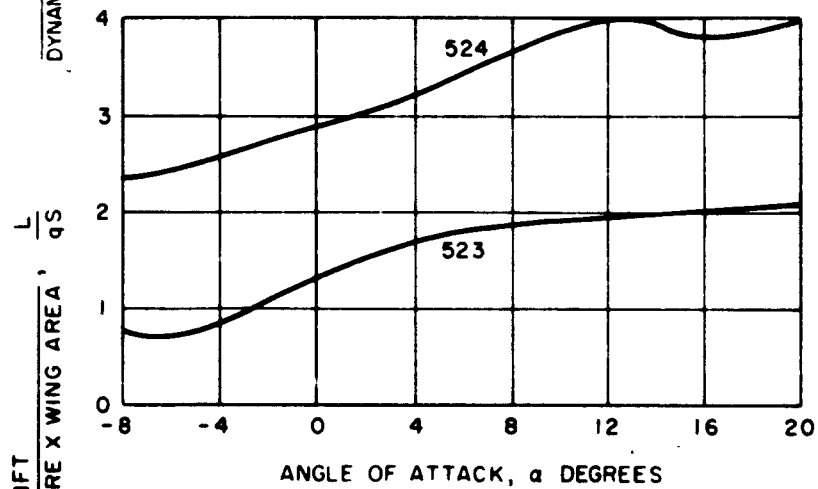
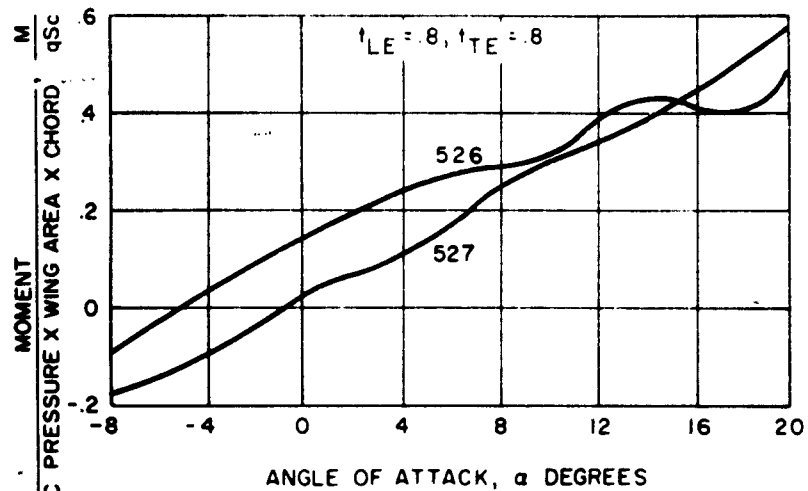


Figure 137. Configuration No. 48,  $\theta_F = -30^\circ$ ,  $\theta_R = -30^\circ$ ,  $h/c = .33$ ,  
(Runs 523 - 524)



CONFIGURATION NO. 49

RUN NO.	J/qS
526	.1797
527	1.2120

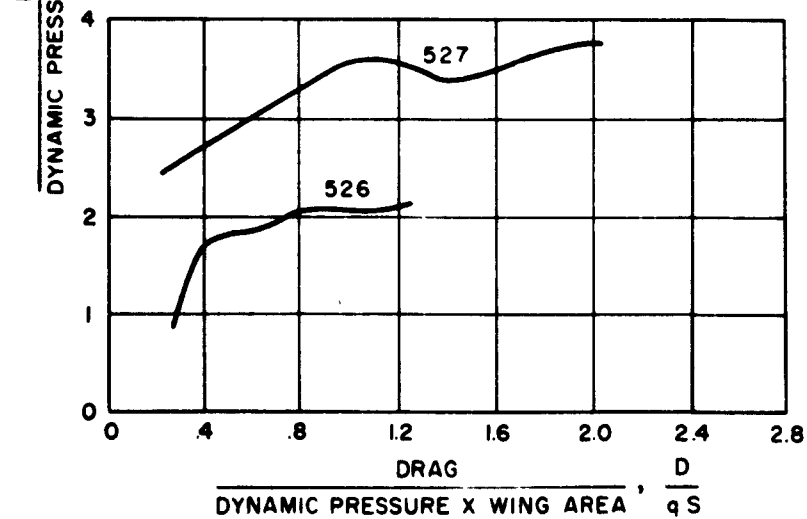
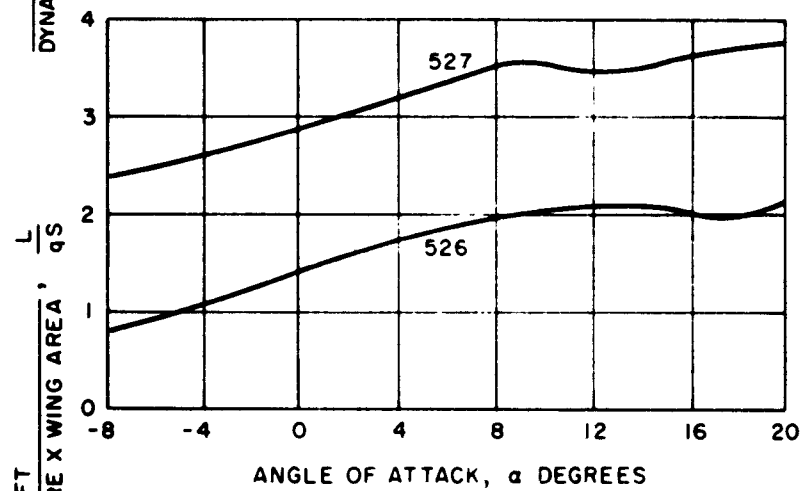
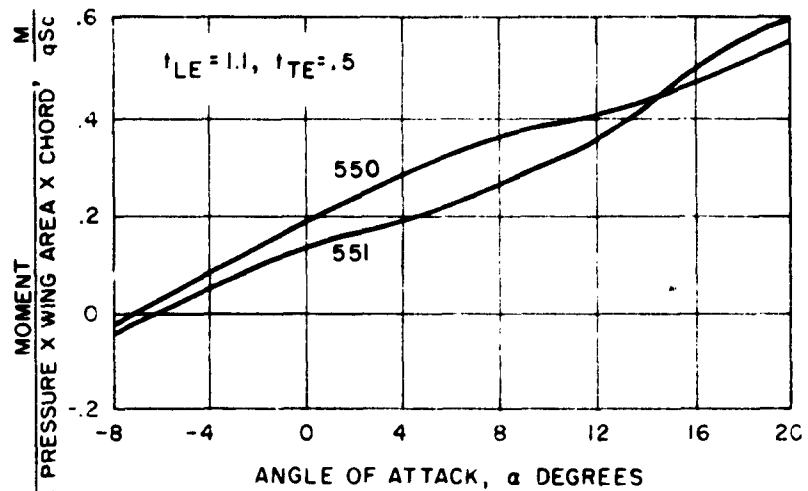


Figure 138. Configuration No. 49,  $\theta_F = -30^\circ$ ,  $\theta_R = -30^\circ$ ,  $h/c = .33$ ,  
(Runs 526 - 527)



CONFIGURATION NO. 52

RUN NO.	$J/qS$
550	.2
551	1.28

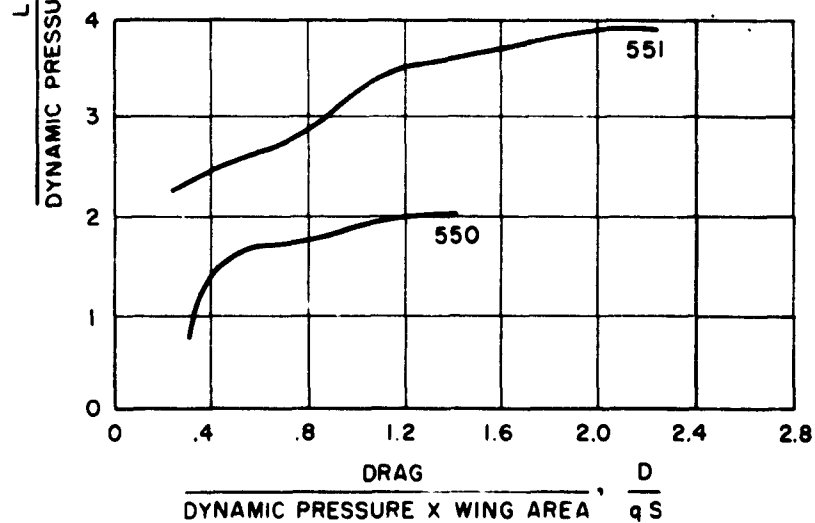
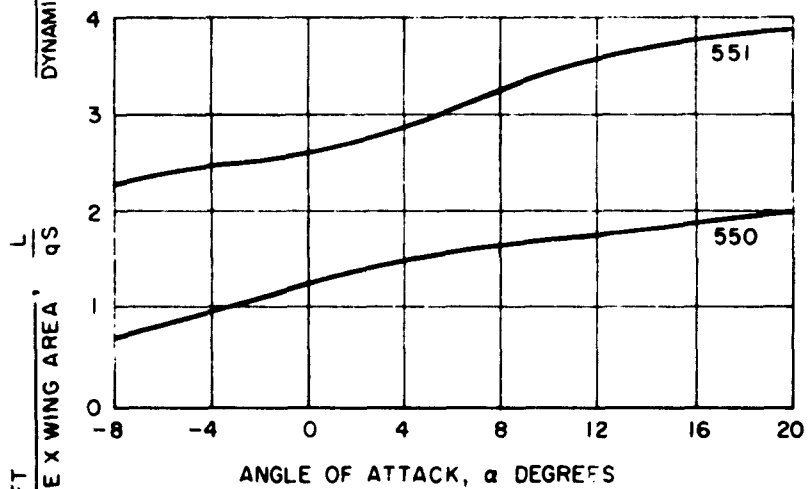
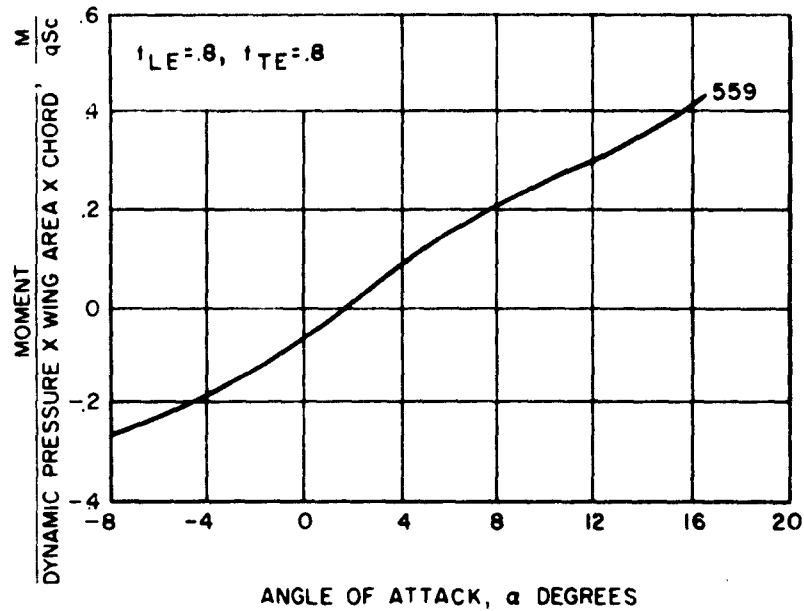


Figure 139. Configuration No. 52,  $\theta_F = -30^\circ$ ,  $\theta_R = -30^\circ$ ,  $h/c = .33$ ,  
(Runs 551 - 552)



CONFIGURATION NO. 57

RUN NO.	J/qS
559	.7316

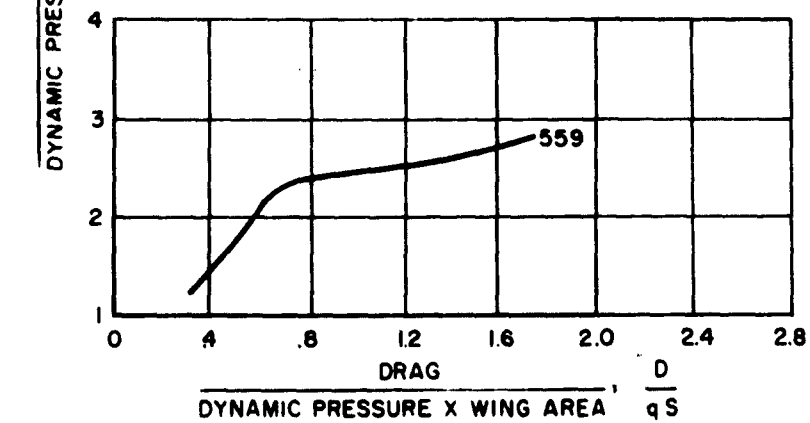
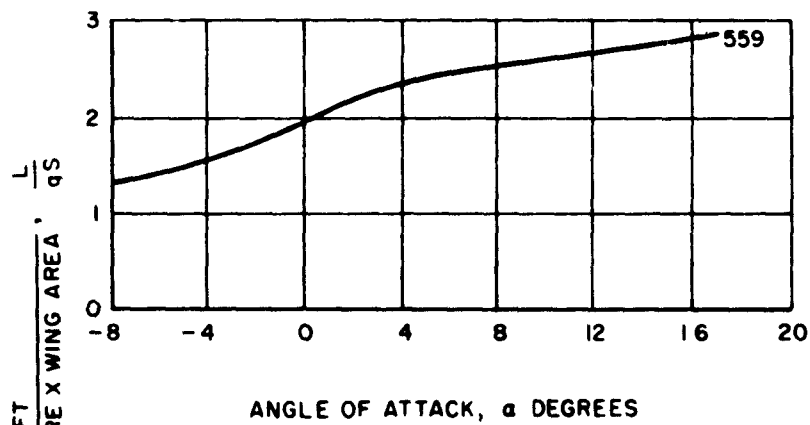


Figure 140. Configuration No. 57,  $\theta_F = -30^\circ$ ,  $\theta_R = -30^\circ$ ,  $h/c = .33$ , (Run 559)

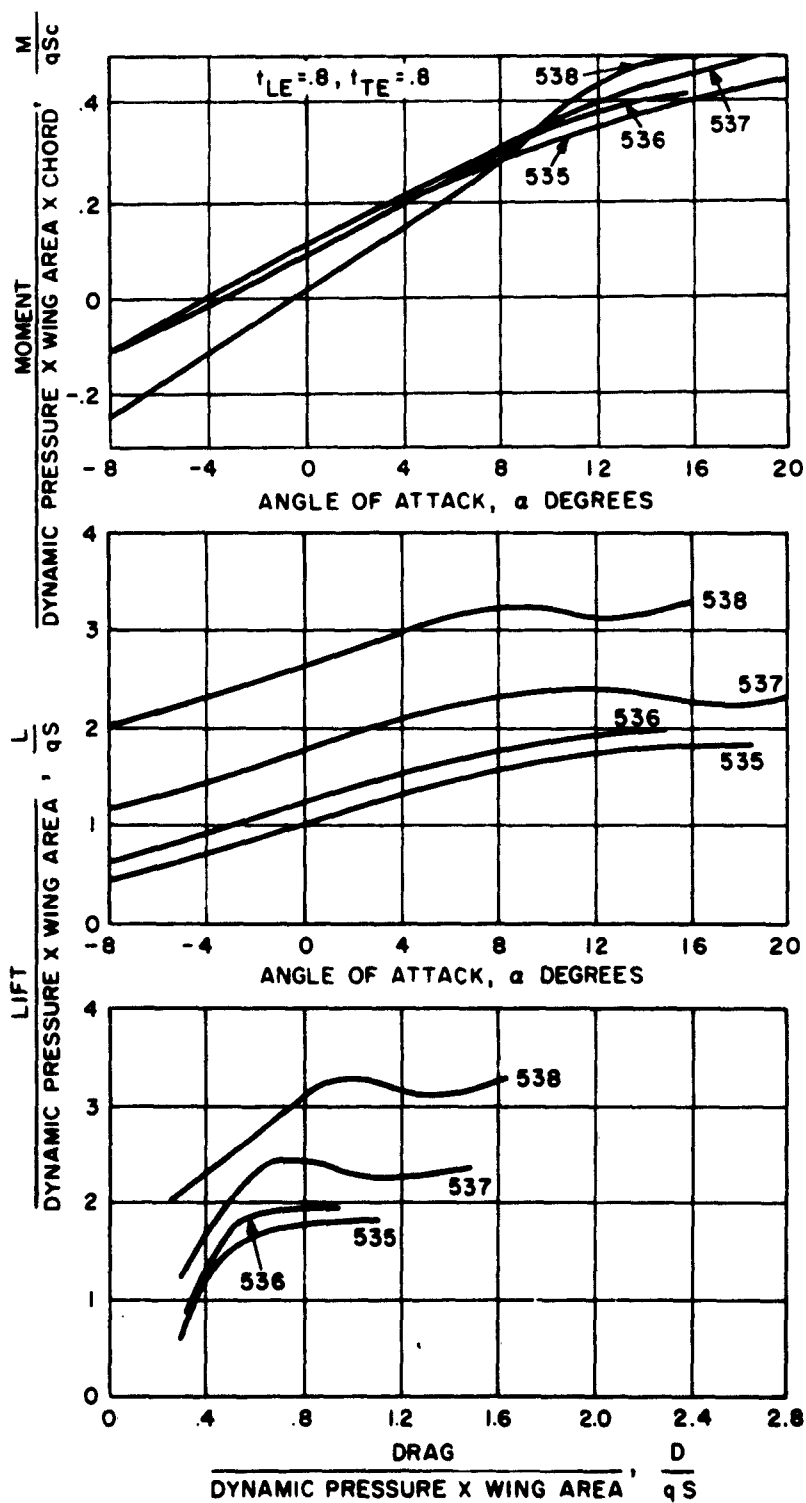
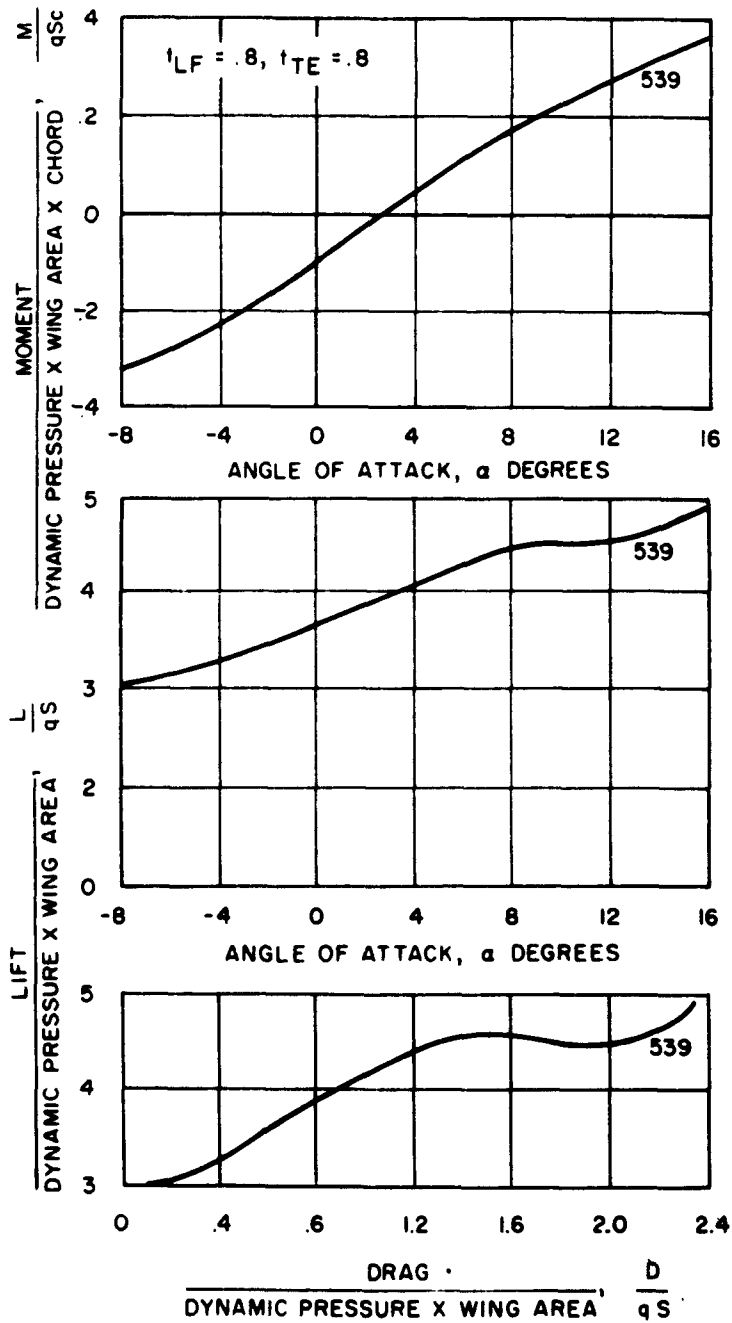


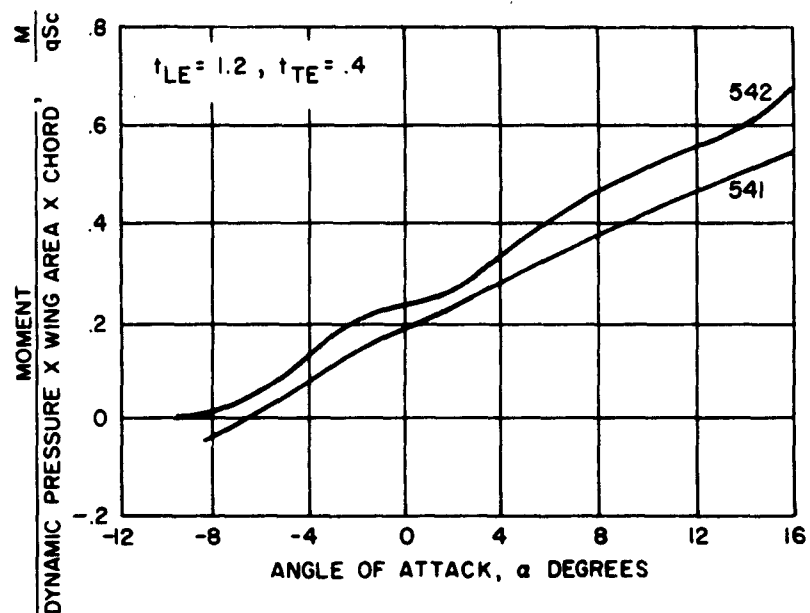
Figure 141. Configuration No. 3,  $\theta_F = -30^\circ$ ,  $\theta_R = -30^\circ$ ,  $h/c = .50$ ,  
 (Runs 535 - 538)



CONFIGURATION NO. 3

RUN NO.	J/qS
539	2.19

Figure 142. Configuration No. 3,  $\theta_F = -30^\circ$ ,  $\theta_R = -30^\circ$ ,  $h/c = .50$ , (Run 539)



CONFIGURATION NO.7

RUN NO.	J/qS
541	.2150
542	1.3426

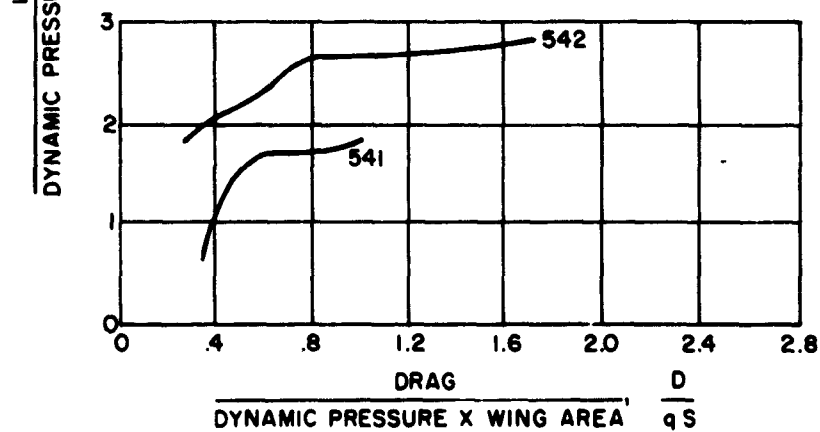
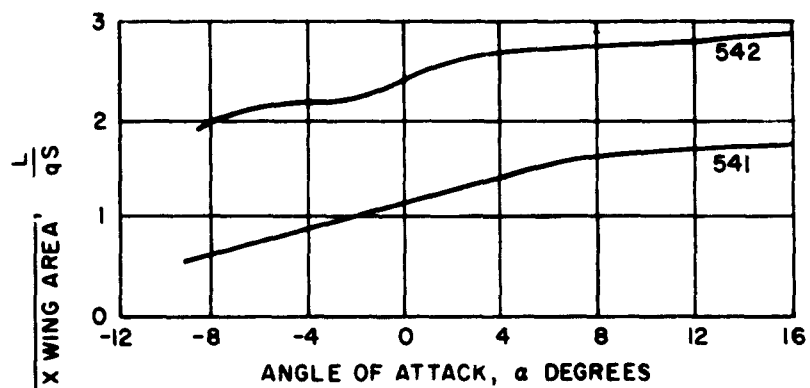
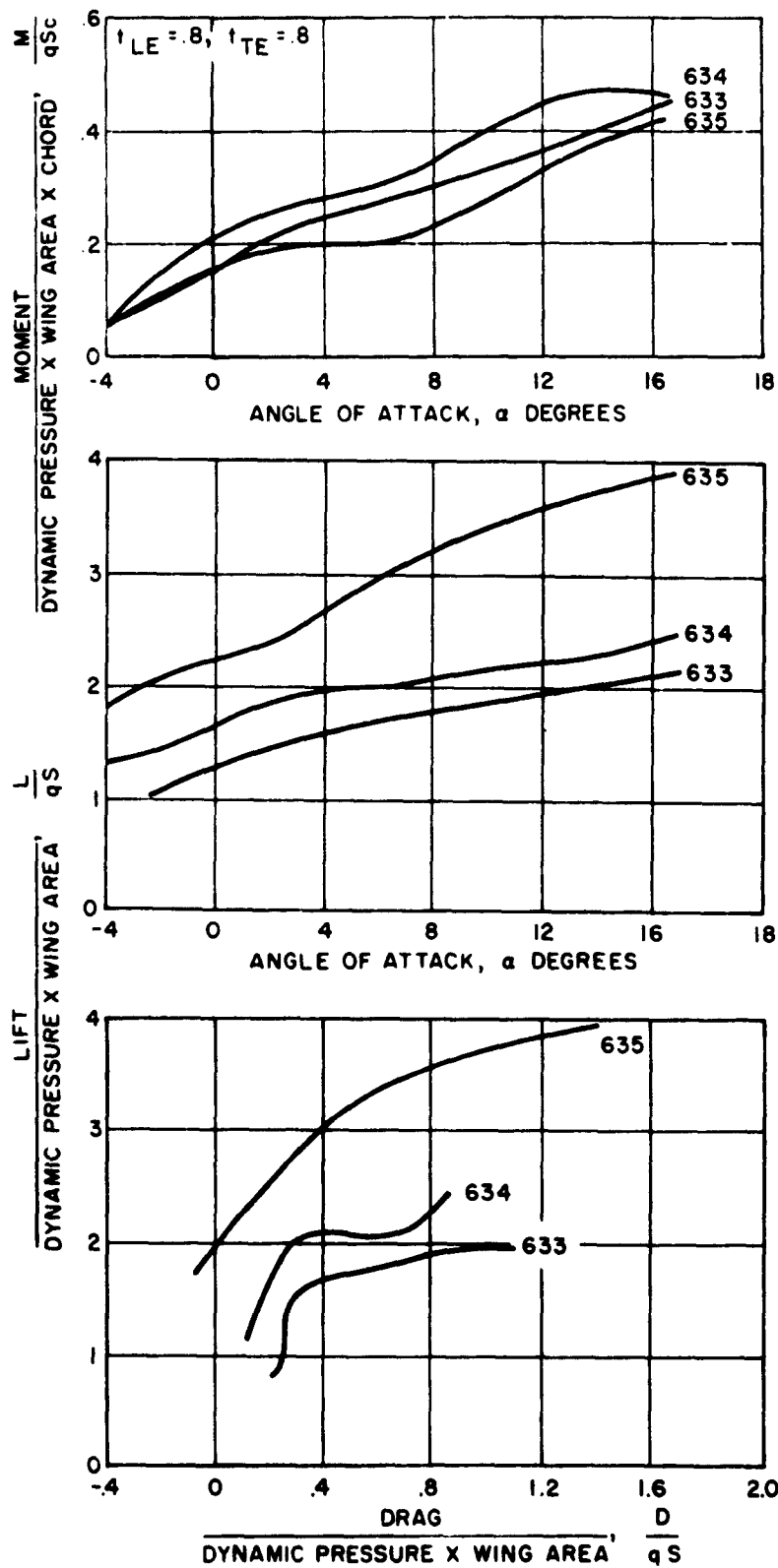


Figure 143. Configuration No. 7,  $\theta_F = -30^\circ$ ,  $\theta_R = -30^\circ$ ,  $h/c = .50$ ,  
(Runs 541 - 542)



CONFIGURATION NO. 42

RUN NO.	J/qS
633	.2031
634	.5681
635	1.3329

Figure 144. Configuration No. 42,  $\theta_F = -30 \times \theta_R = +30 \times h/c = .20$ ,  
(Runs 633-635)

CONFIGURATION NO. 68

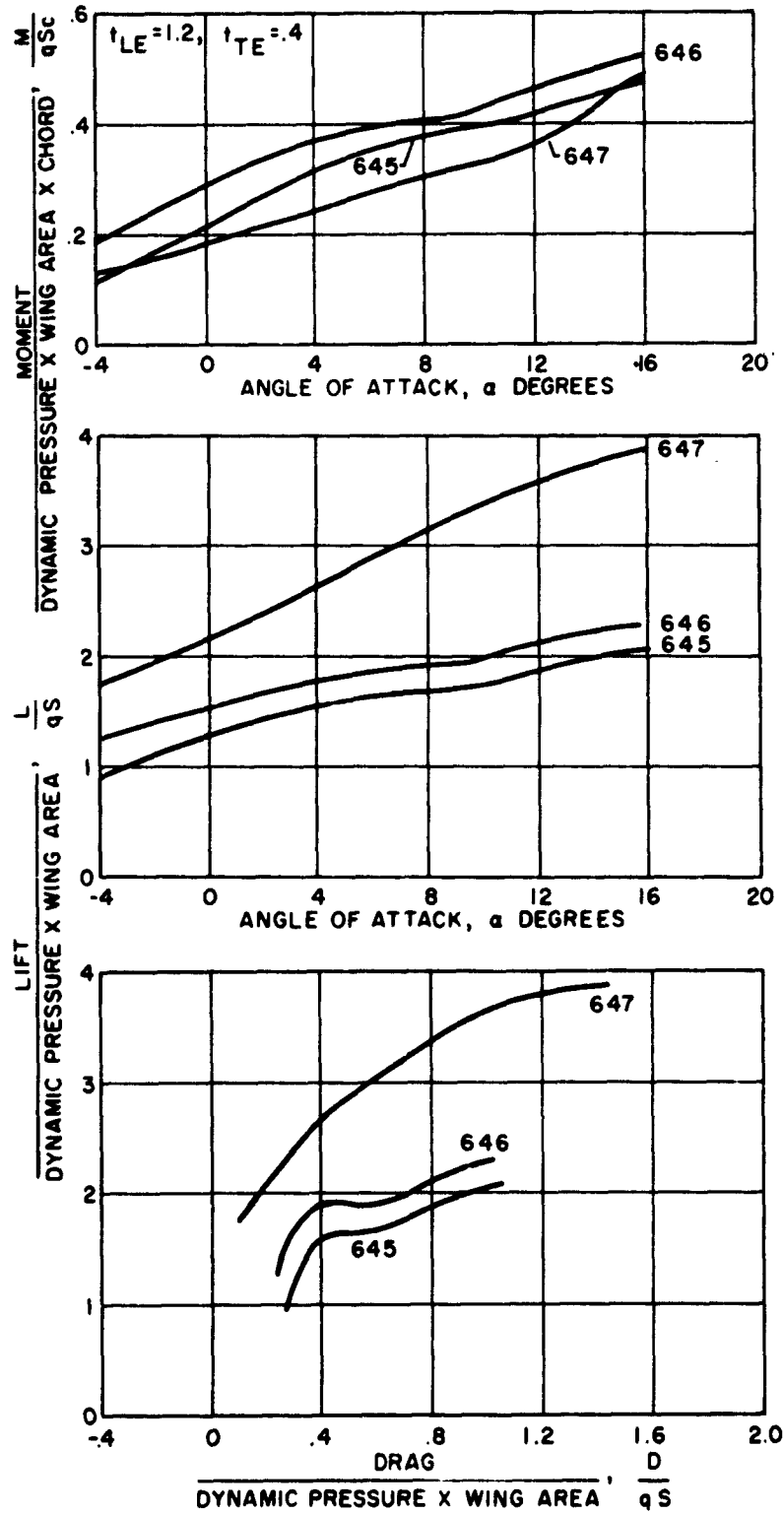
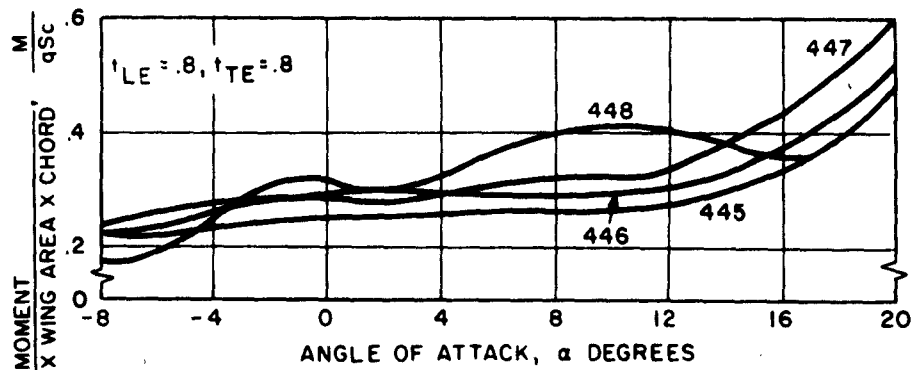


Figure 145. Configuration No. 68,  $\theta_F = -30^\circ$ ,  $\theta_R = +30^\circ$ ,  $h/c = .20$ ,  
(Runs 645-647)



CONFIGURATION NO. 8

RUN NO.	J/qS
445	.0775
446	.2182
447	.5895
448	1.3963

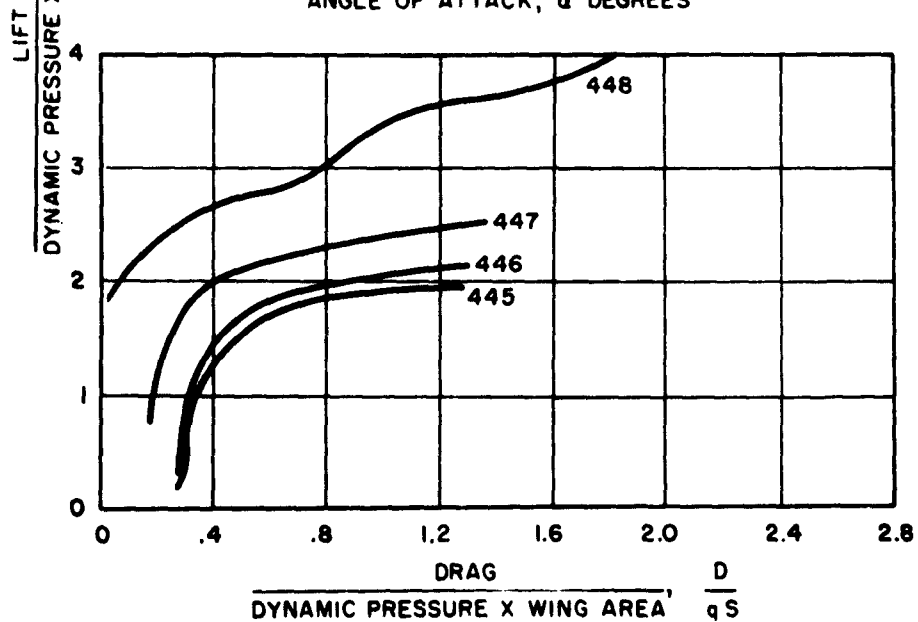
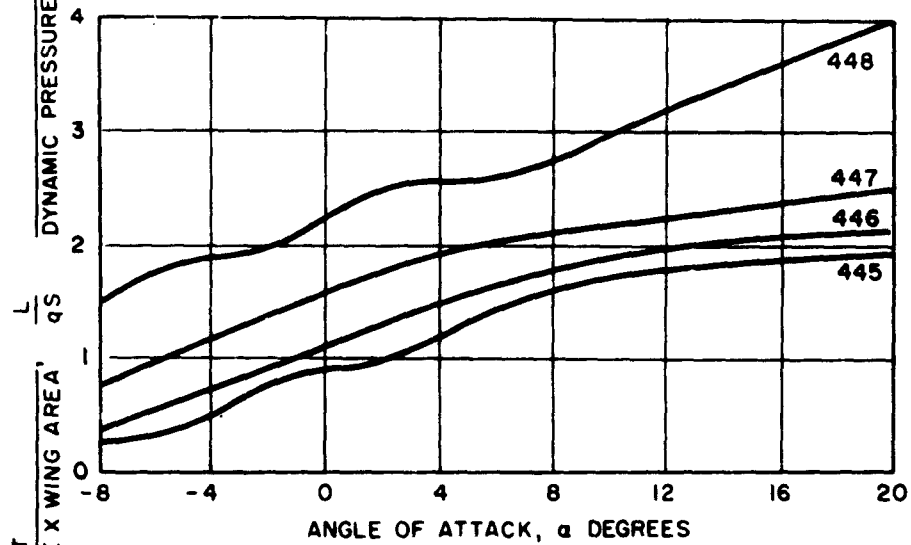
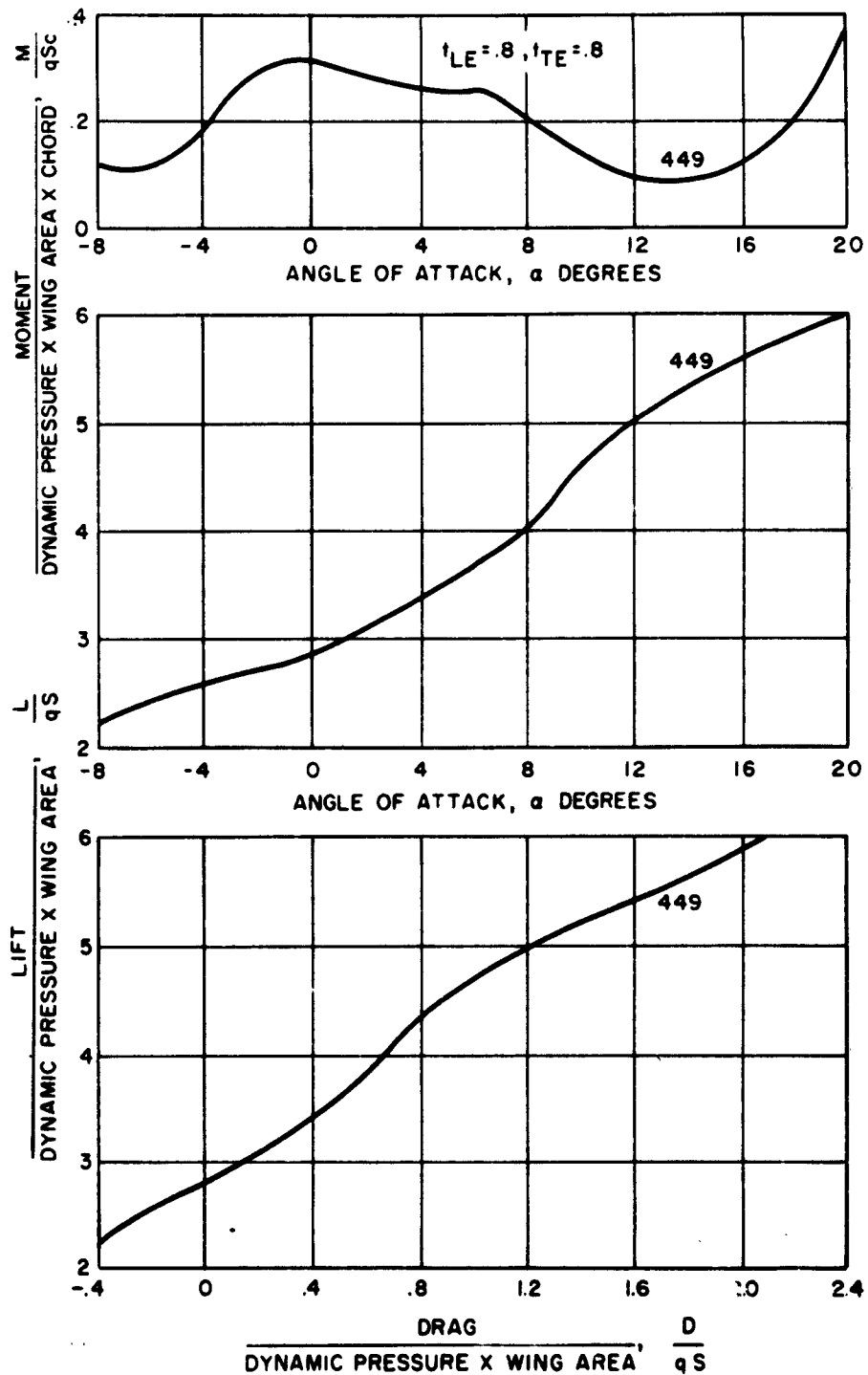


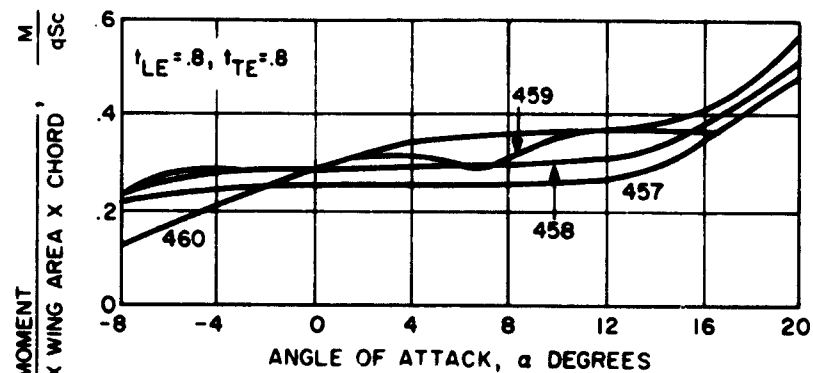
Figure 146. Configuration No. 8,  $\theta_F = -30^\circ$ ,  $\theta_R = +30^\circ$ ,  $h/c = .33$ ,  
(Runs 445-448)



CONFIGURATION NO. 8

RUN NO.	J/qS
449	2.4326

Figure 147. Configuration No. 8,  $\theta_F = -30^\circ$ ,  $\theta_R = 30^\circ$ ,  $h/c = .33$ ,  
(Run 449)



CONFIGURATION NO. 9

RUN NO.	J/qS
457	.0898
458	.1812
459	.5492
460	1.3075

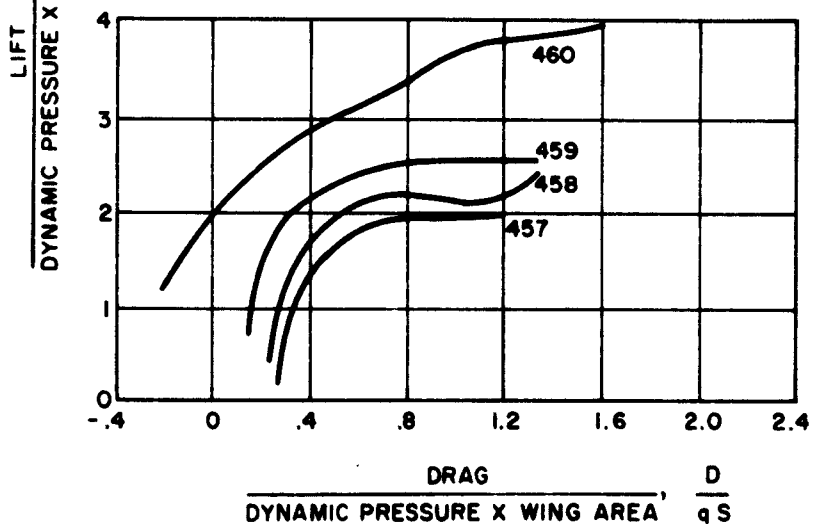
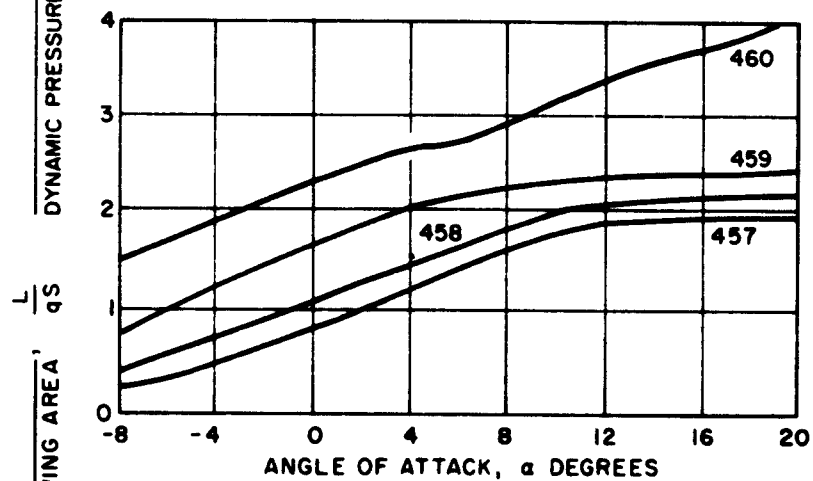
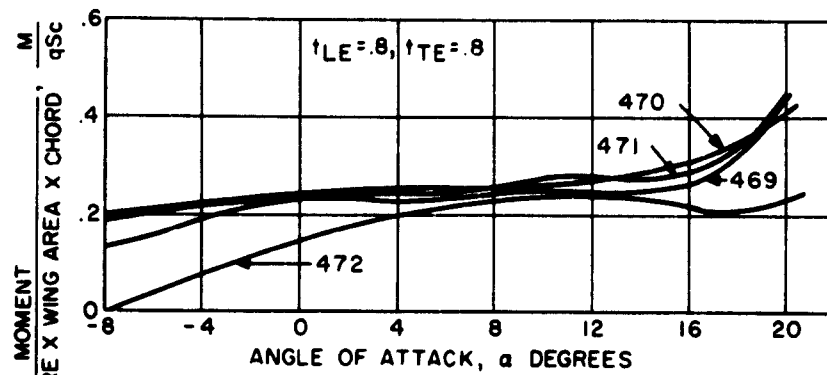


Figure 148. Configuration No. 9,  $\theta_F = -30^\circ$ ,  $\theta_R = +30^\circ$ ,  $h/c = .33$ ,  
(Runs 457-460)



CONFIGURATION NO. 10

RUN NO.	J/qS
469	.0729
470	.1555
471	.4105
472	.9404

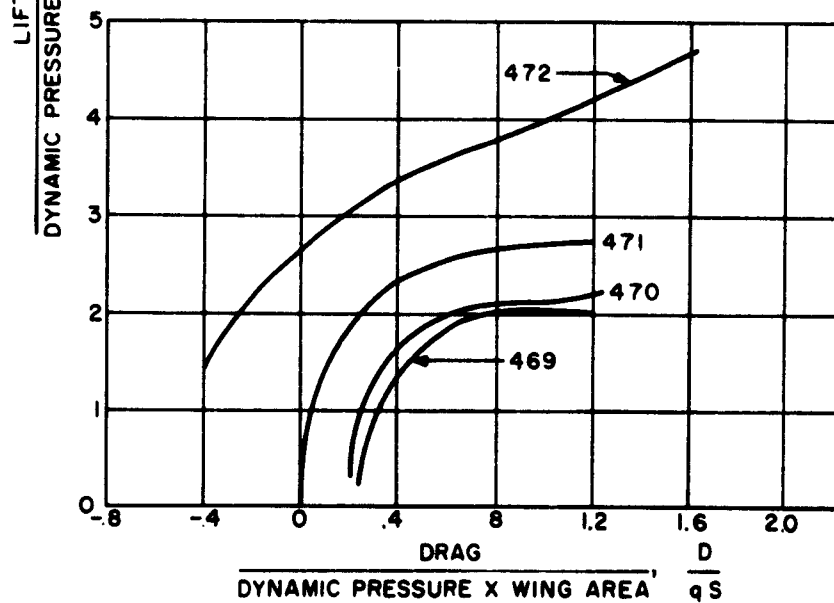
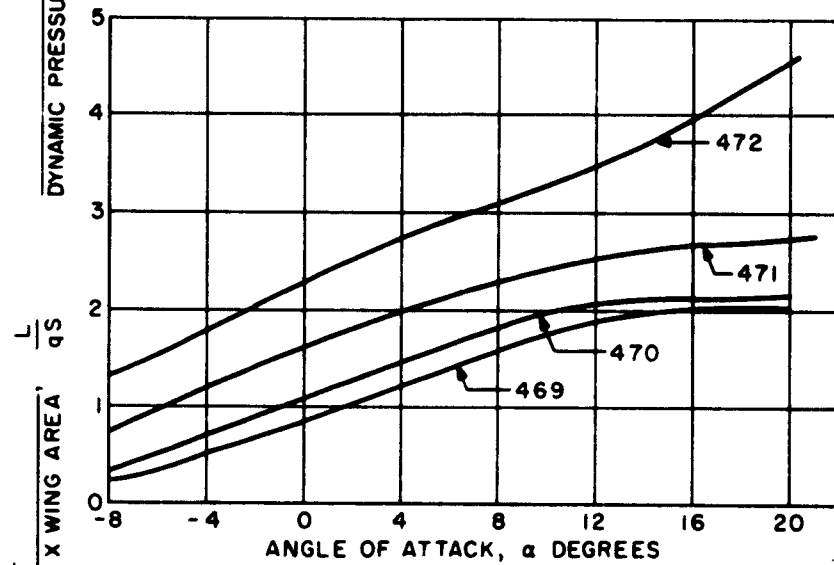
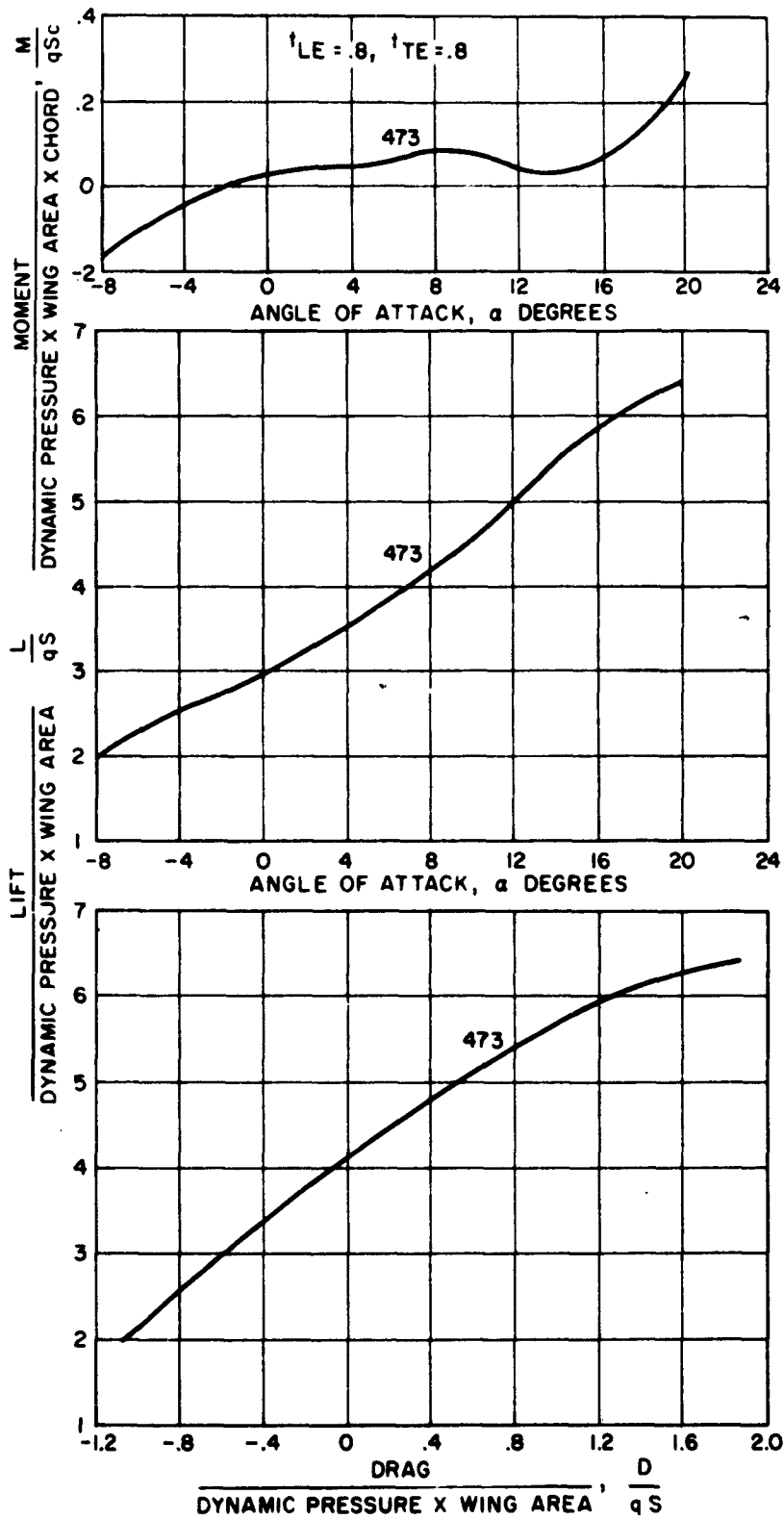


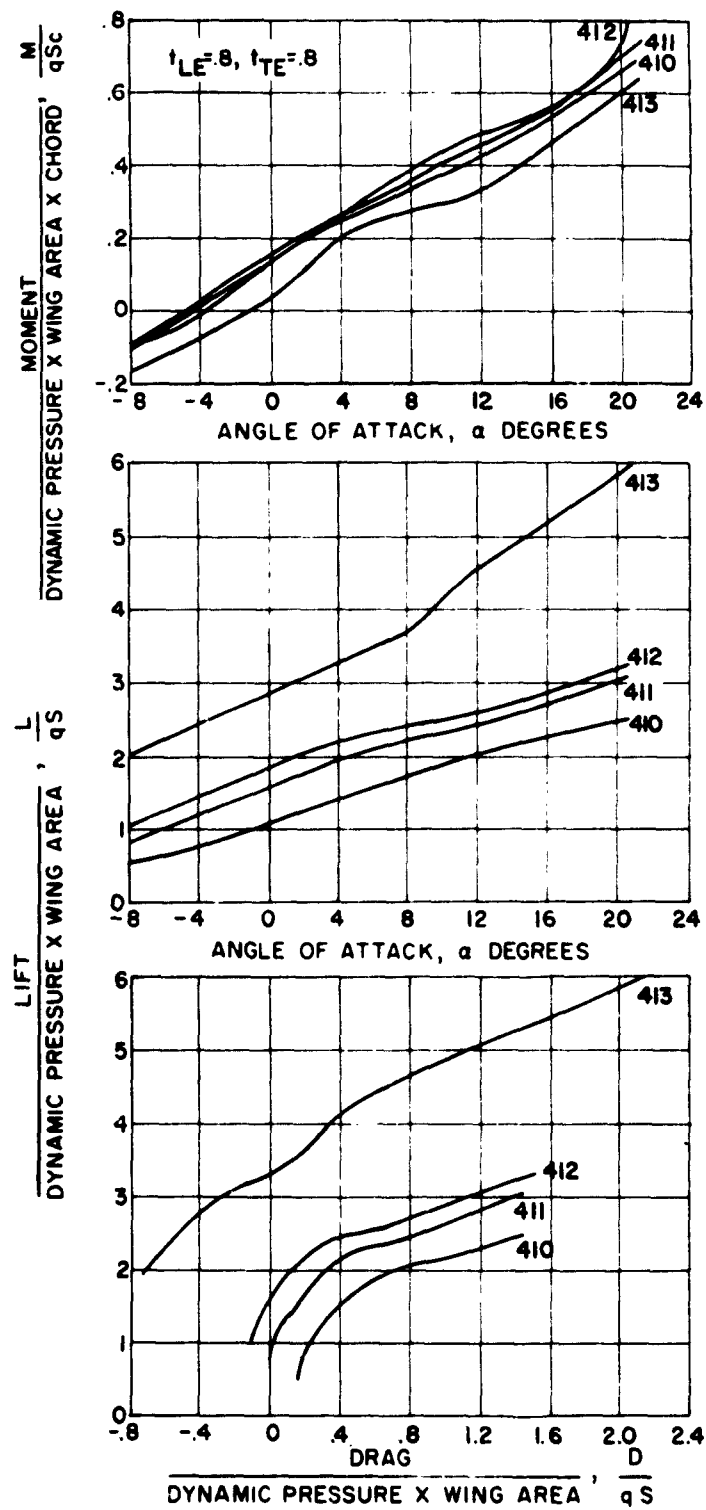
Figure 149. Configuration No. 10,  $\theta_F = -30^\circ$ ,  $\theta_R = +30^\circ$ ,  $h/c = .33$ ,  
(Runs 469-472)



CONFIGURATION NO. 10

RUN NO.	J/qS
473	1.6323

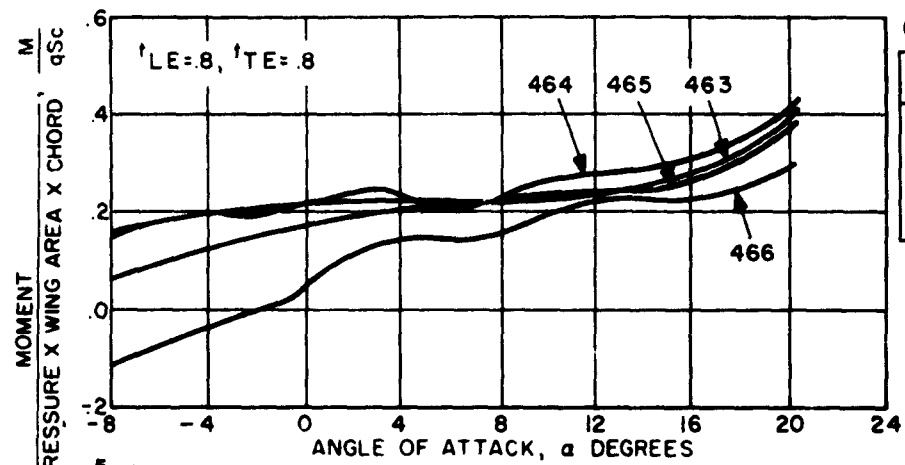
Figure 150. Configuration No. 10,  $\theta_F = -30^\circ$ ,  $\theta_R = +30^\circ$ ,  $h/c = .33$ ,  
(Run 473)



CONFIGURATION NO. 82

RUN NO.	J/qS
410	.243
411	.696
412	1.013
413	2.50

Figure 151. Configuration No. 82,  $\theta_F = -30^\circ$ ,  $\theta_R = +30^\circ$ ,  $h/c = .33$ ,  
(Runs 410-413)



CONFIGURATION NO. 11

RUN NO.	J/qS
463	.0645
464	.1243
465	.3103
466	.6885

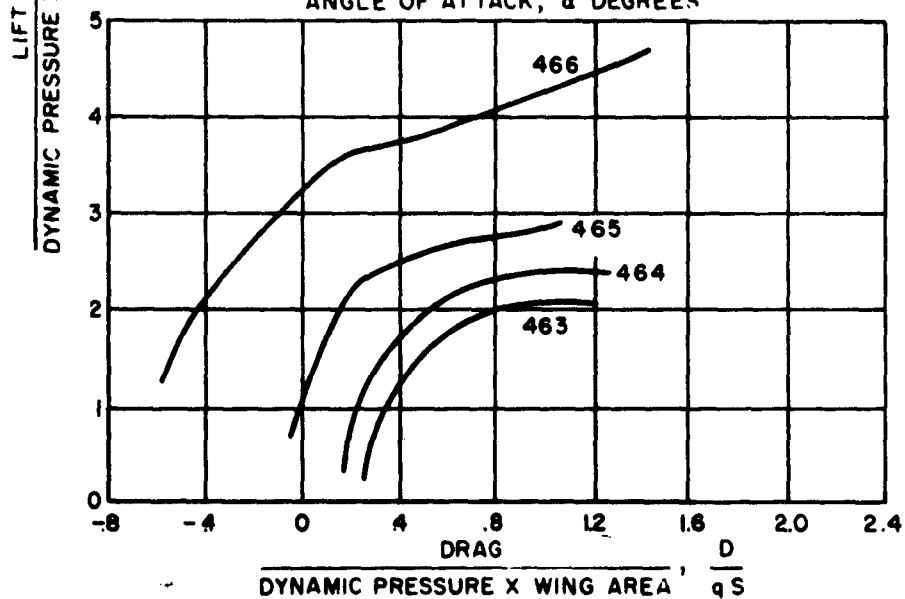
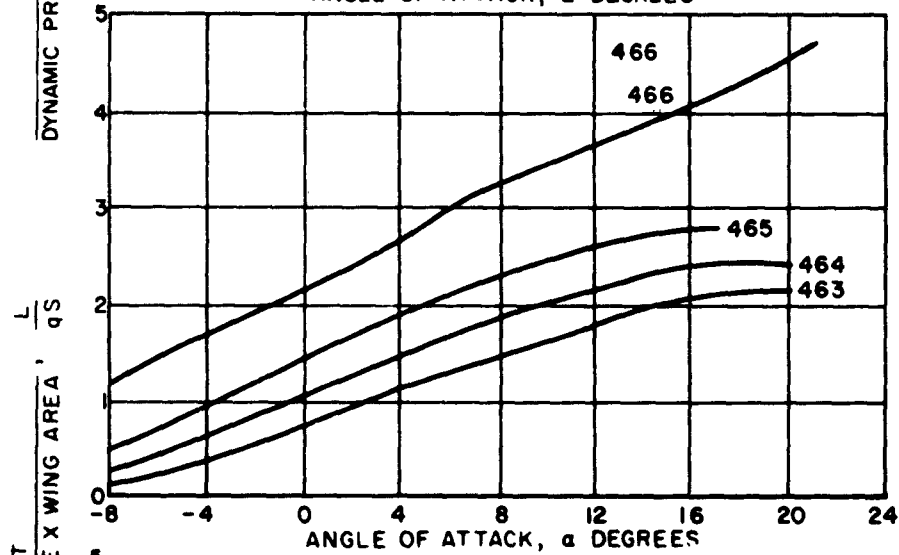
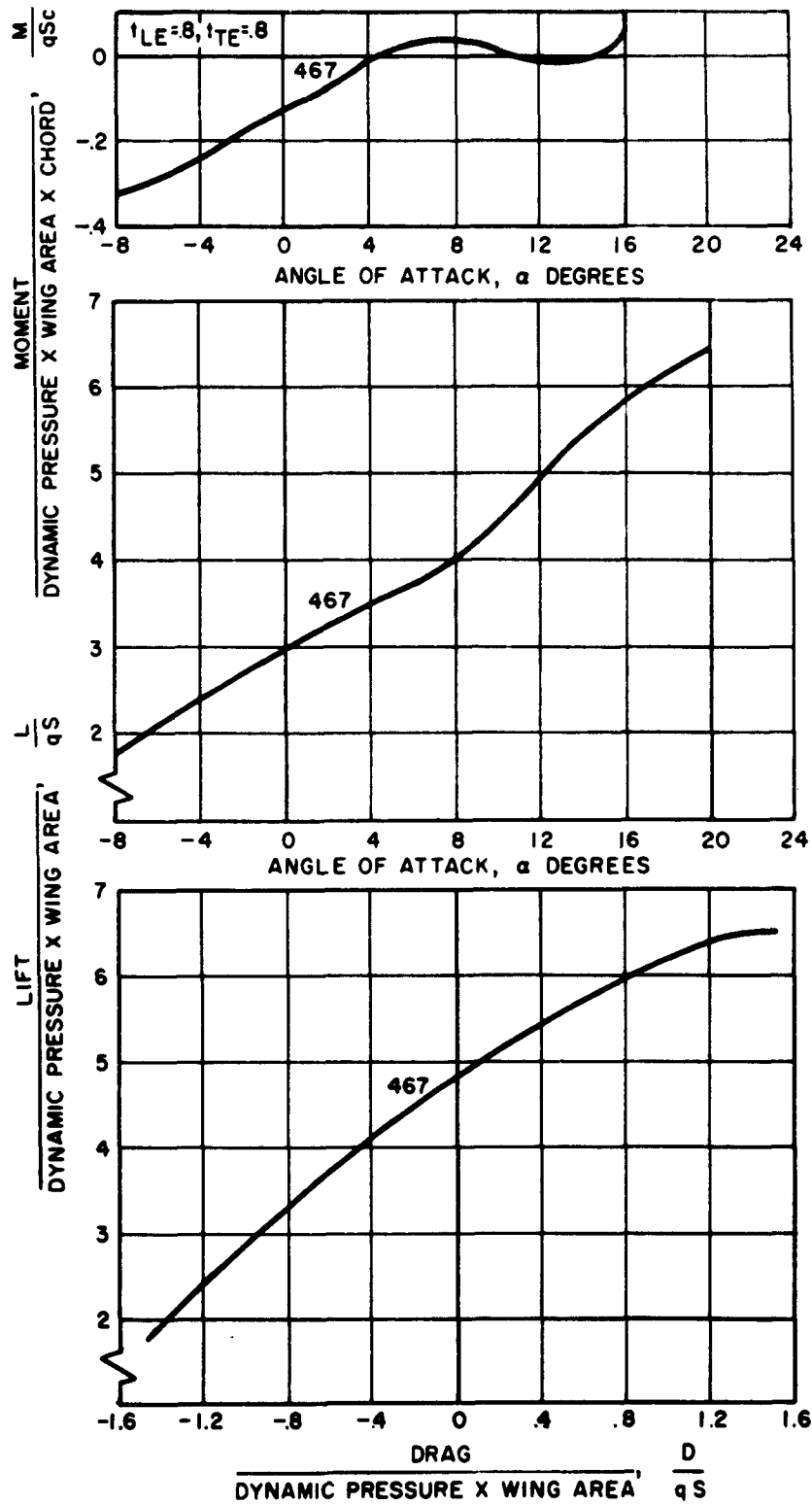


Figure 152. Configuration No. 11,  $\theta_F = -30^\circ$ ,  $\theta_R = +30^\circ$ ,  $h/c = .33$ ,  
(Runs 463-466)



CONFIGURATION NO. 11

RUN NO.	J/qS
467	1.1789

Figure 153. Configuration No. 11,  $\theta_F = -30^\circ$ ,  $\theta_R = +30^\circ$ ,  $h/c = .33$ ,  
(Run 467)

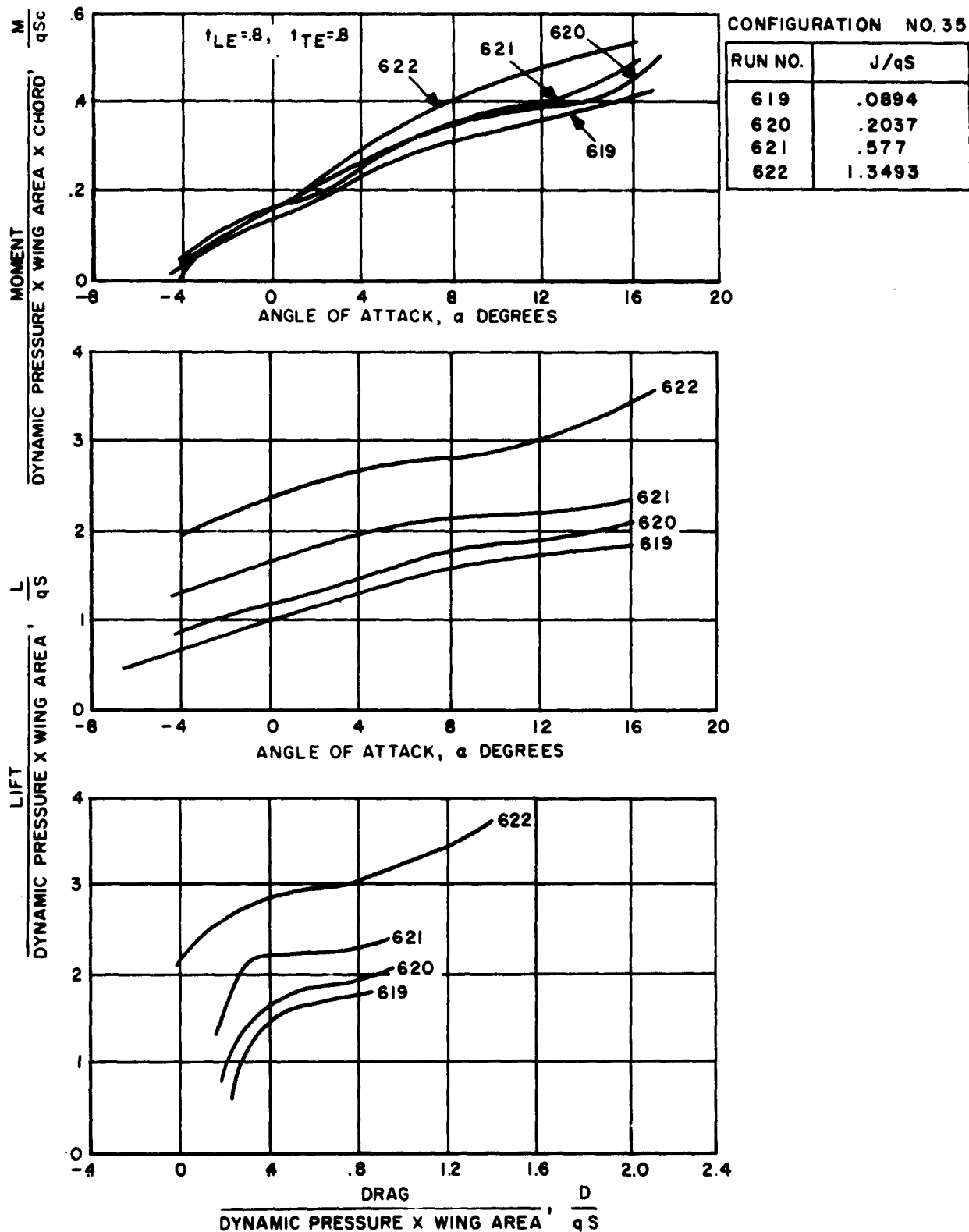
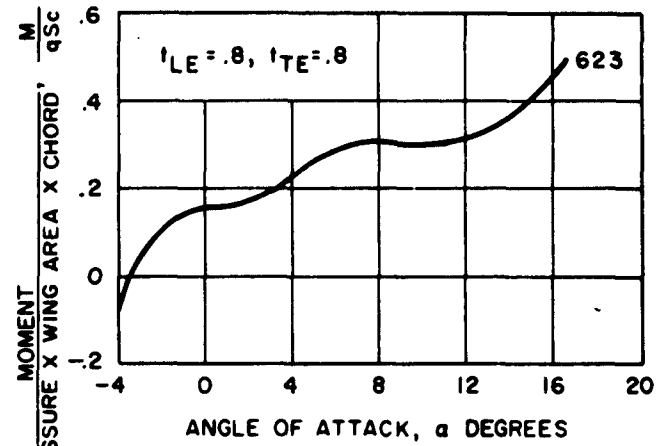


Figure 154. Configuration No. 35,  $\theta_F = -30^\circ$ ,  $\theta_R = +30^\circ$ ,  $h/c = .33$ ,  
 (Runs 619-622)



CONFIGURATION NO.35

RUN NO.	J/qS
623	2.3464

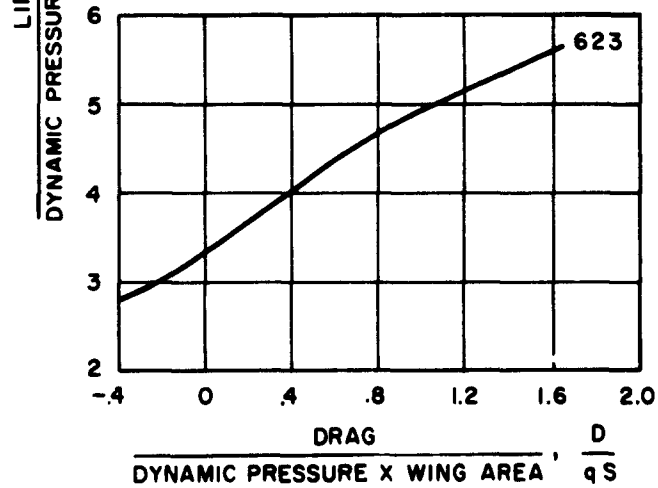
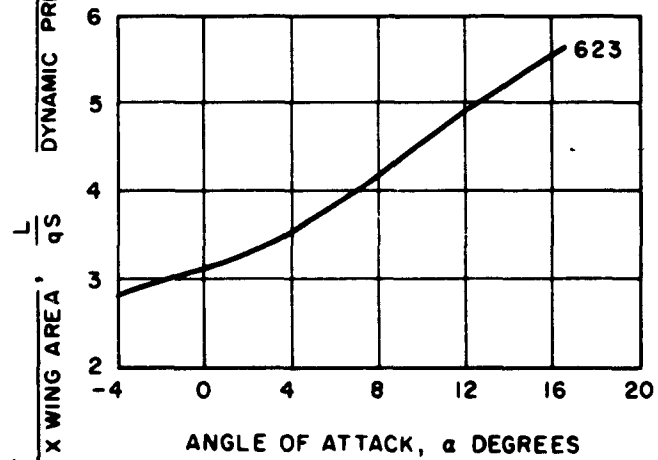
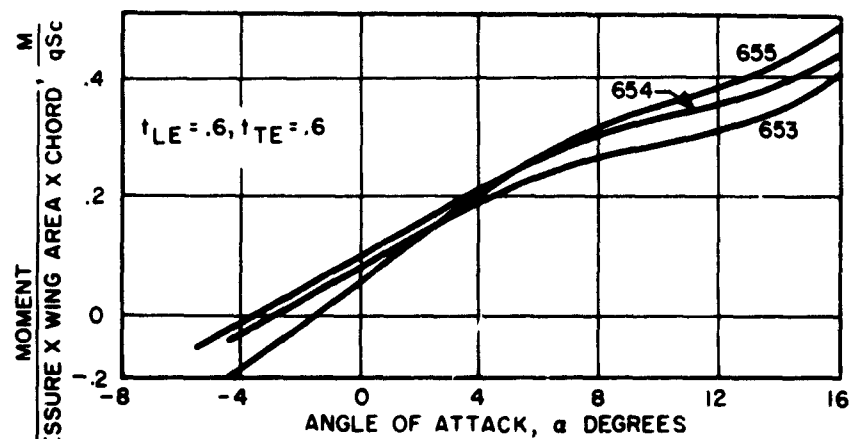


Figure 155. Configuration No. 35,  $\theta_F = -30^\circ$ ,  $\theta_R = +30^\circ$ ,  $h/c = .33$ ,  
(Run 623)



RUN NO.	J/qS
653	.22
654	.62
655	1.45

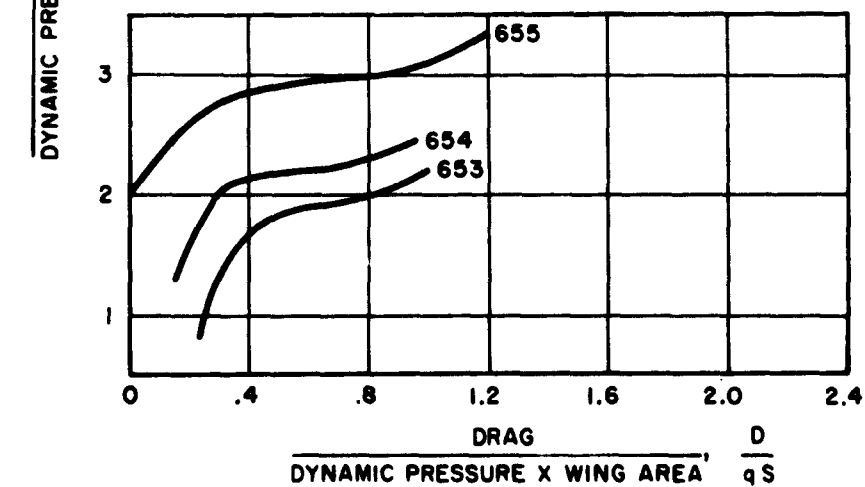
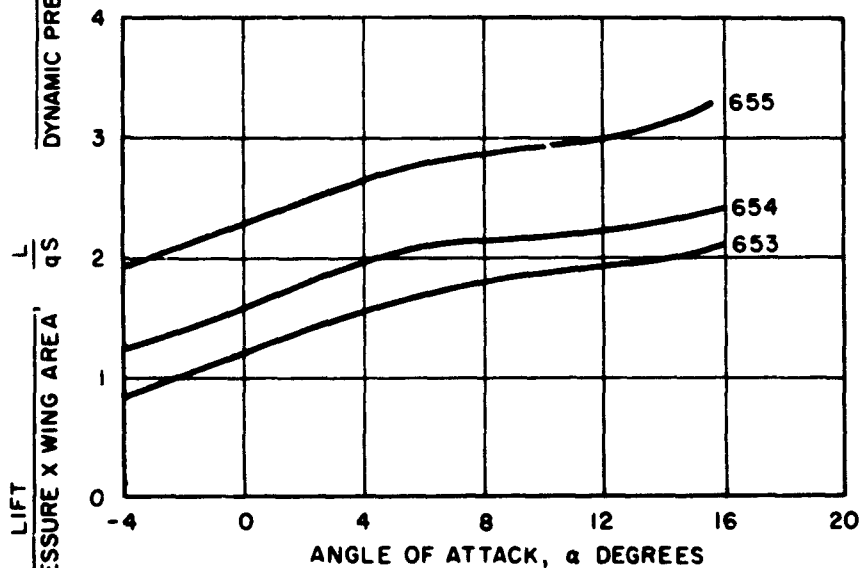
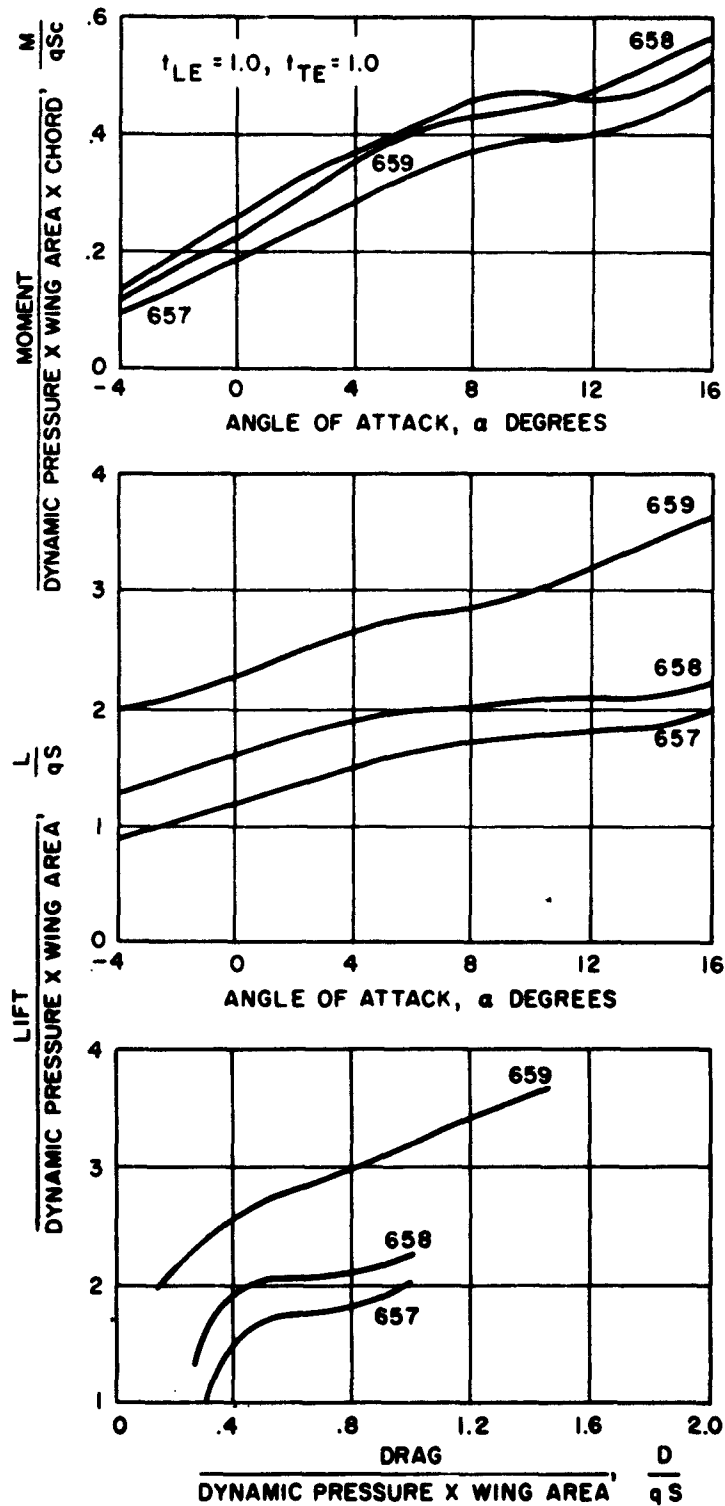


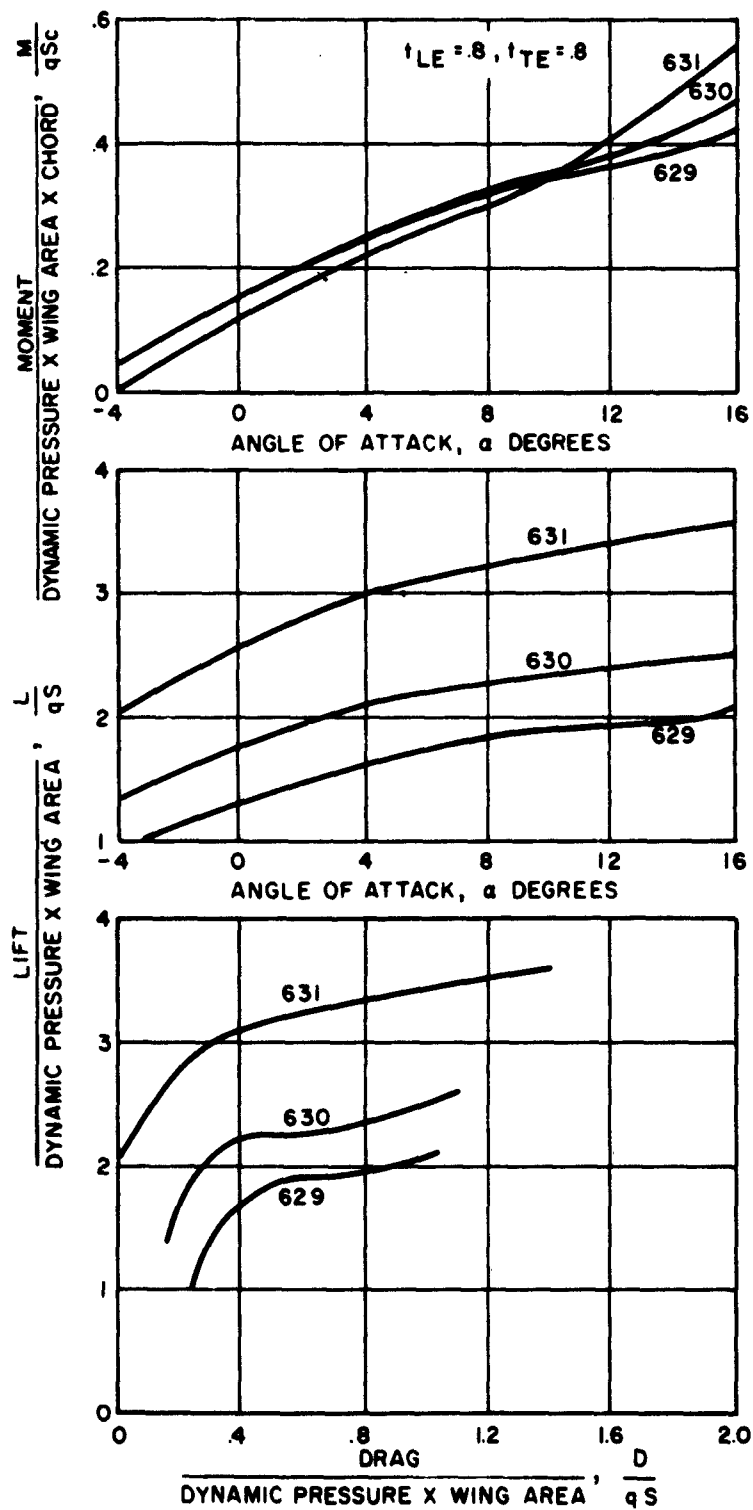
Figure 156. Configuration No. 46,  $\theta_F = -30^\circ$ ,  $\theta_R = +30^\circ$ ,  $h/c = .33$ ,  
(Runs 653-655)



CONFIGURATION NO. 47

RUN NO.	J/qS
657	.191
658	.530
659	1.240

Figure 157. Configuration No. 47,  $\theta_F = -30 \times \theta_R = +30 \times h/c = .33$ ,  
(Runs 657-659)



CONFIGURATION NO. 66

RUN NO.	J/qS
629	.200
630	.573
631	1.343

Figure 158. Configuration No. 66,  $\theta_F = -30 \times \theta_R = +30 \times h/c = .33$ ,  
(Runs 629-631)

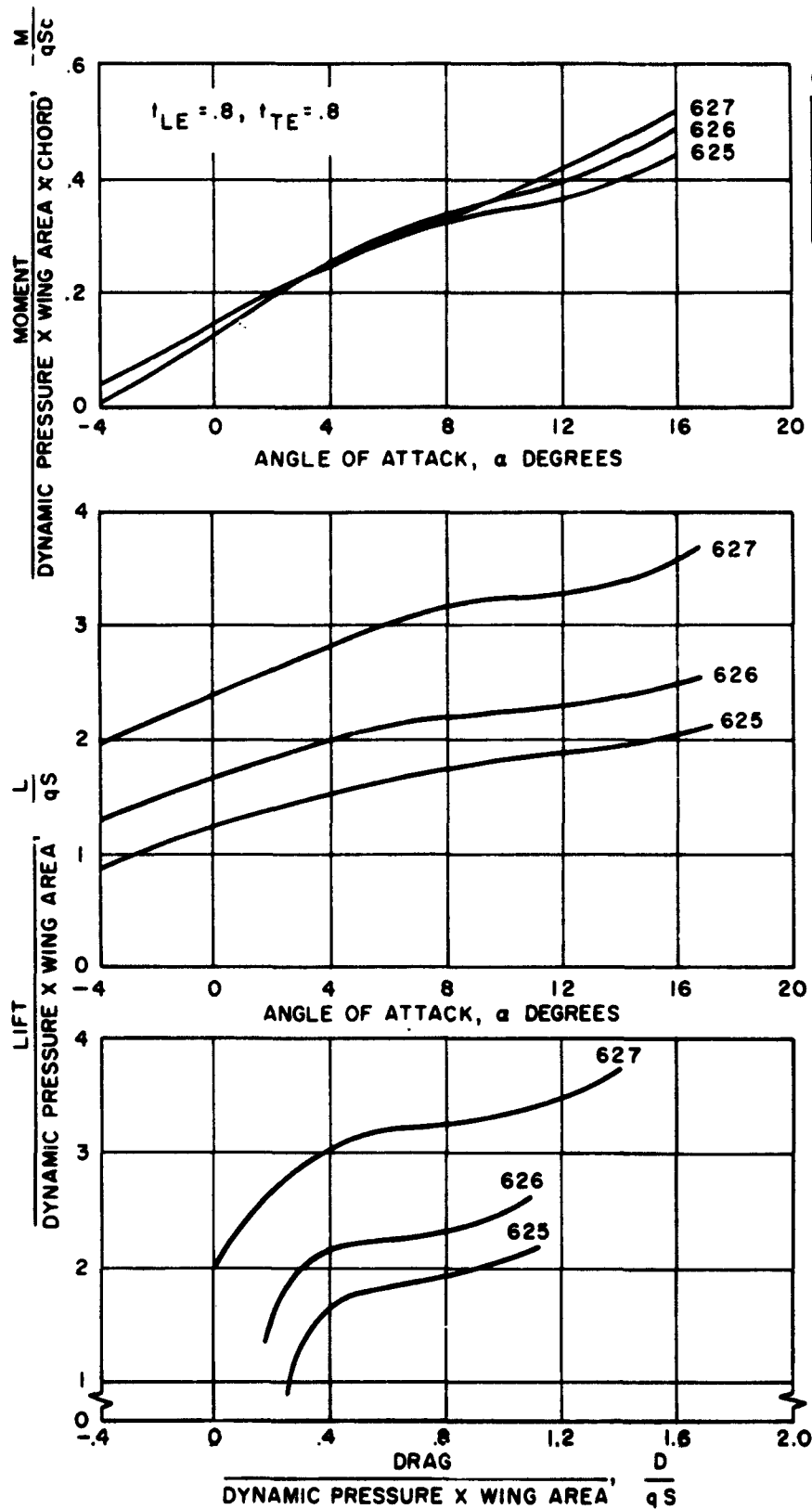
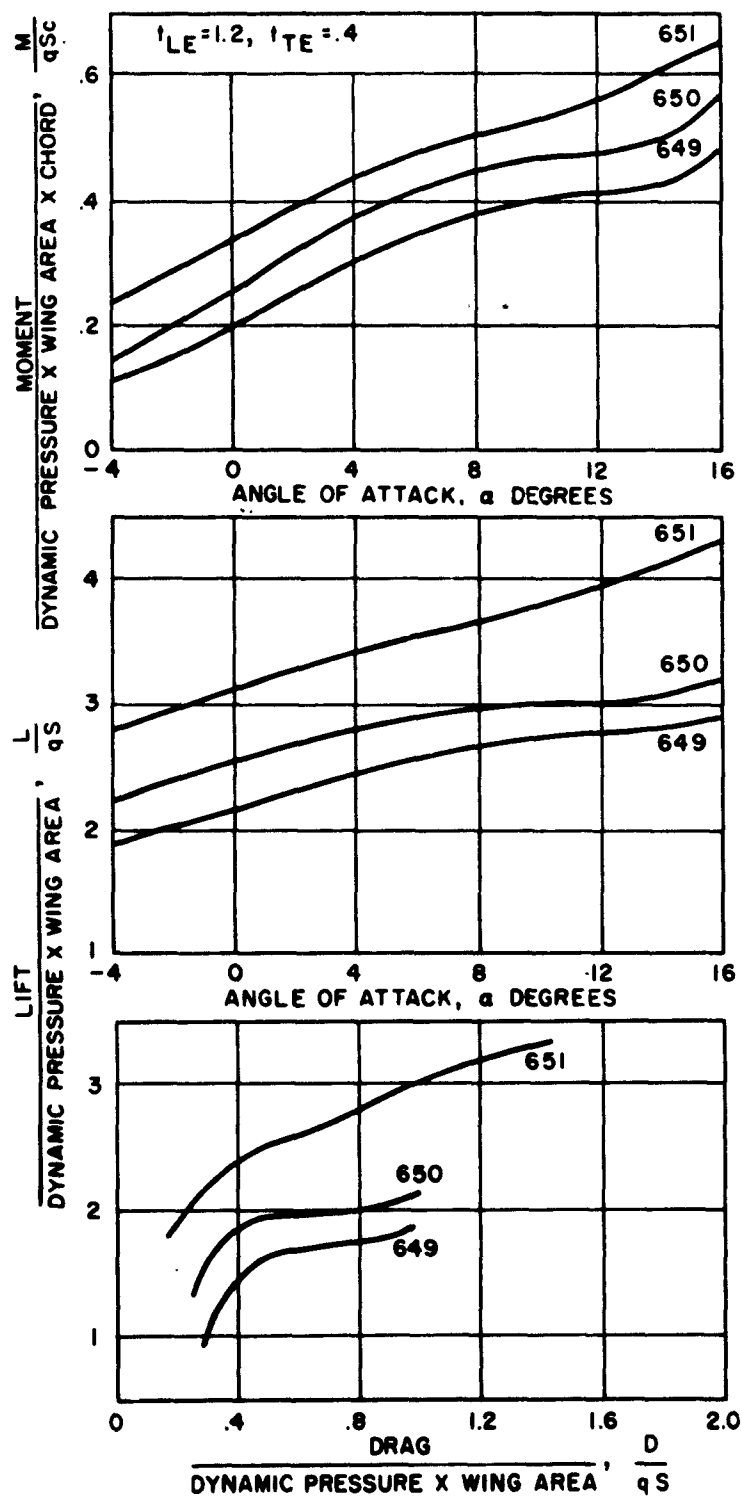


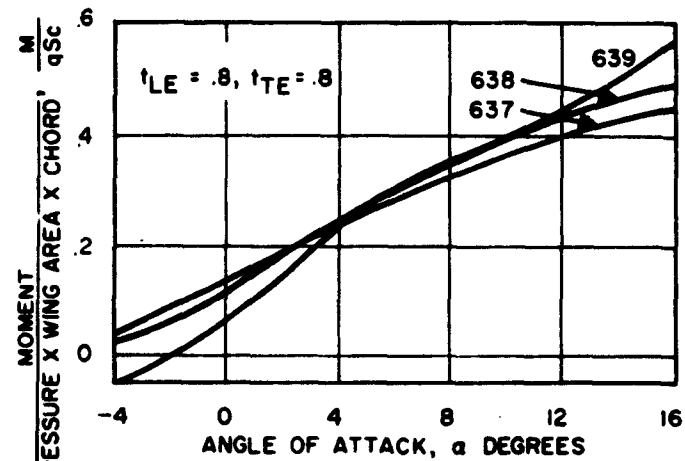
Figure 159. Configuration No. 65,  $\theta_F = -30 \times \theta_R = +30 \times h/c = .33$ ,  
(Runs 625-627)



CONFIGURATION NO. 69

RUN NO.	J/qS
649	.225
650	.618
651	1.444

Figure 160. Configuration No. 69,  $\theta_F = -30^\circ$ ,  $\theta_R = +30^\circ$ ,  $h/c = .33$ ,  
(Runs 649-651)



CONFIGURATION NO. 43

RUN NO.	J/qS
637	.2135
638	.5837
639	1.3609

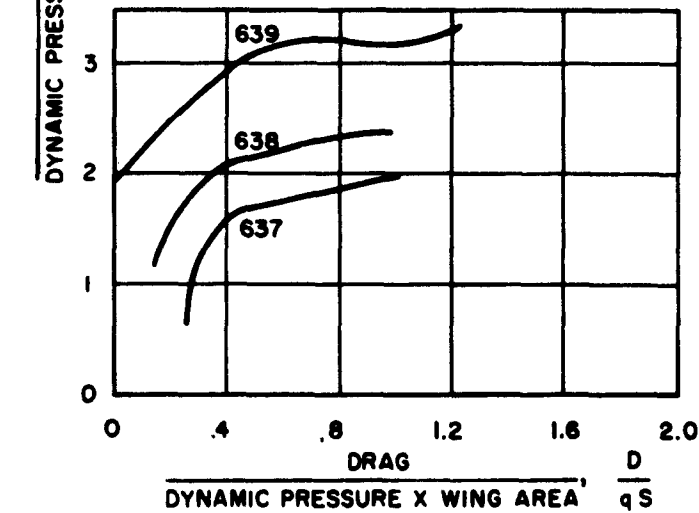
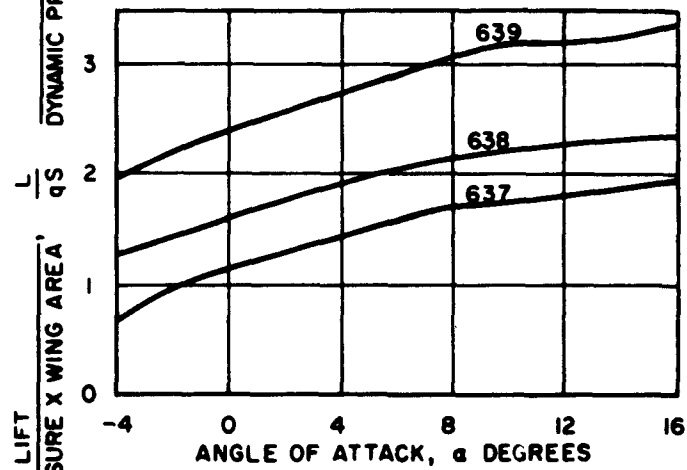
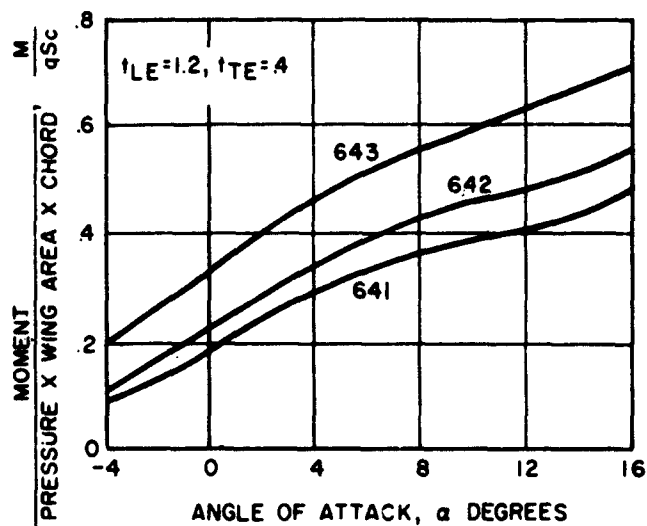


Figure 161. Configuration No. 43,  $\theta_F = -30^\circ$ ,  $\theta_R = +30^\circ$ ,  $h/c = .50$ ,  
(Runs 637-639)



CONFIGURATION NO. 67

RUN NO.	J/qS
641	.216
642	.616
643	1.413

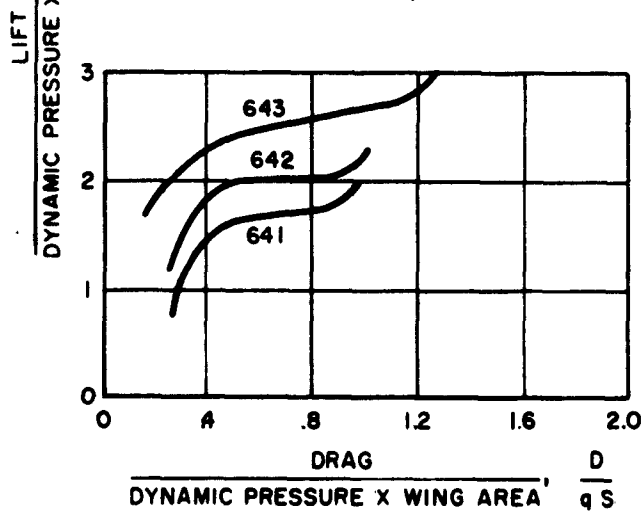
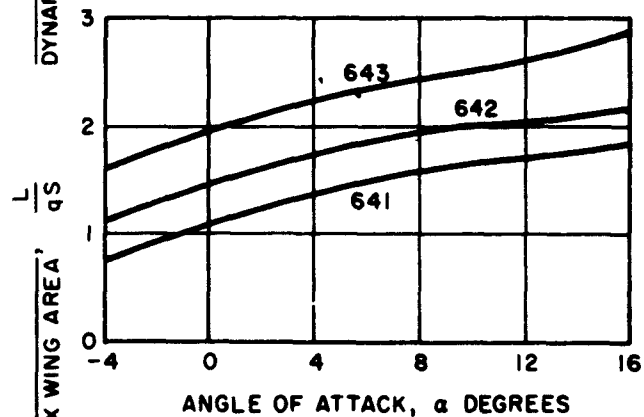
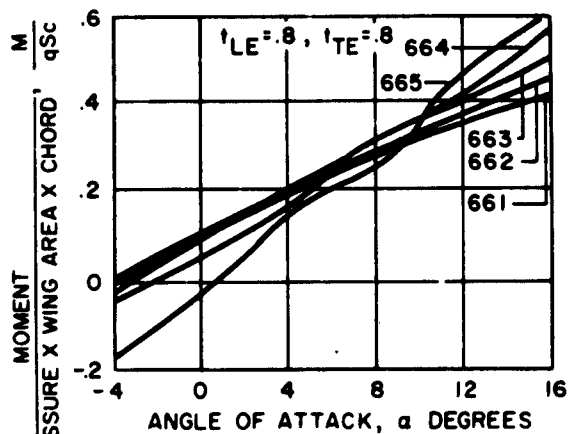


Figure 162. Configuration No. 67,  $\theta_F = -30^\circ$ ,  $\theta_R = +30^\circ$ ,  $h/c = .50$ ,  
(Runs 641-643)



CONFIGURATION NO.70

RUN NO.	J/qS
661	.094
662	.214
663	.590
664	1.369
665	2.407

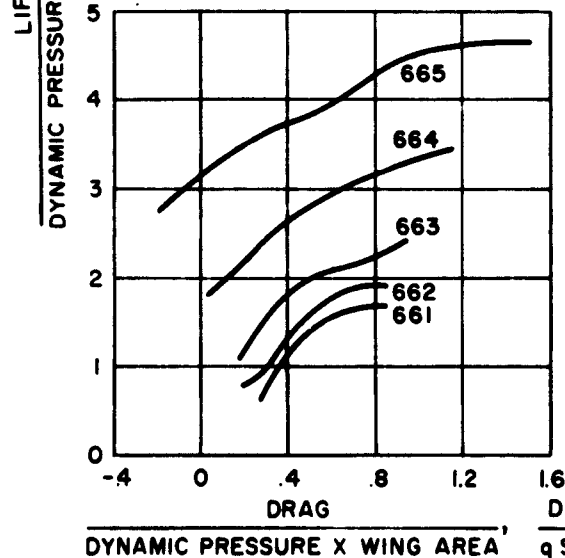
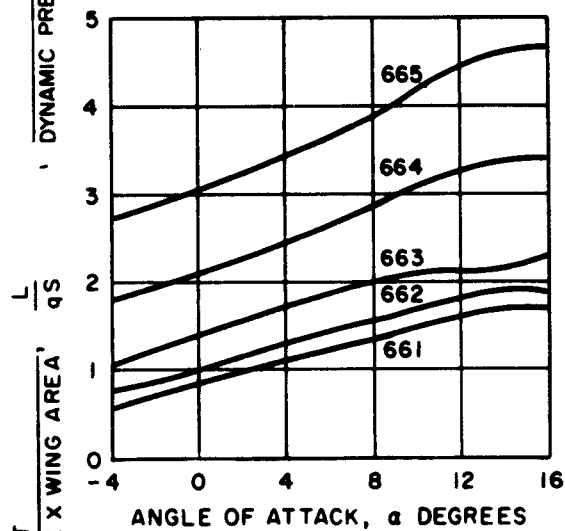
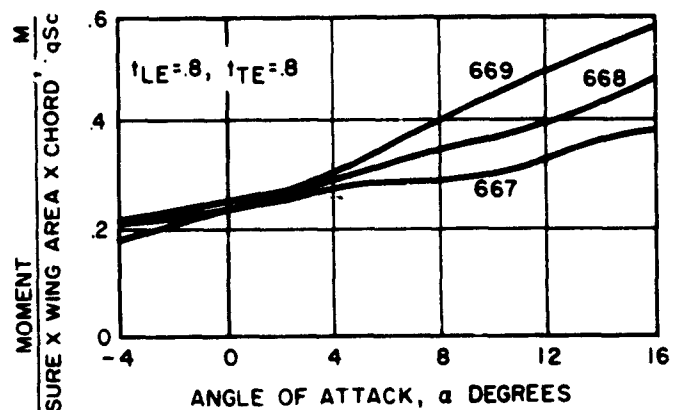


Figure 163. Configuration No. 70,  $\theta_F = -30^\circ$ ,  $\theta_R = +30^\circ$ ,  $h/c = \infty$ ,  
(Runs 661-665)



CONFIGURATION NO. 71

RUN NO.	J/qS
667	.208
668	.586
669	1.358

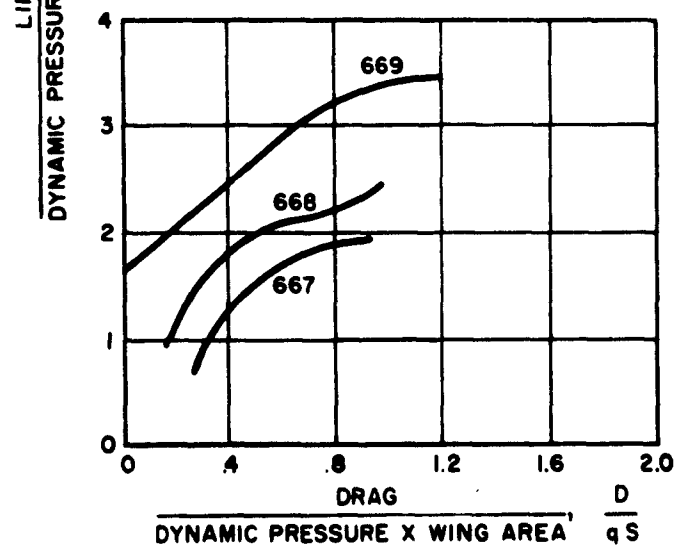
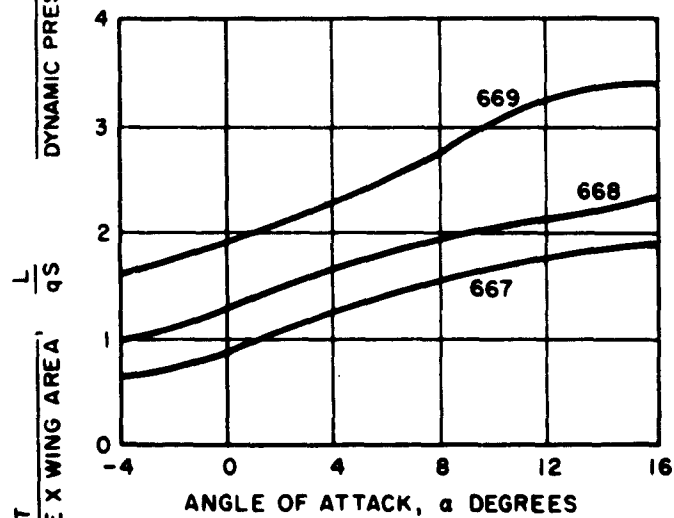
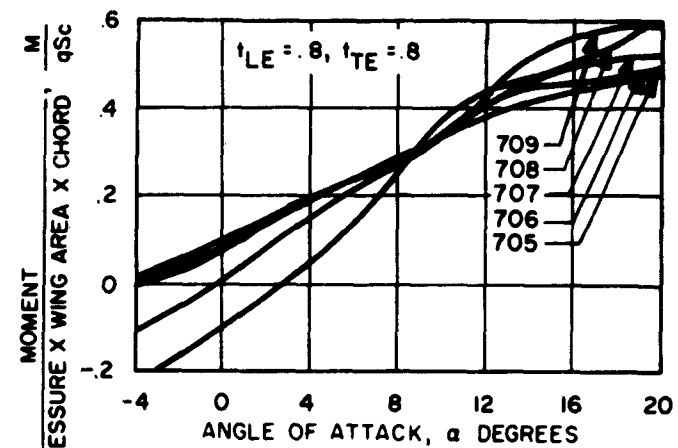


Figure 164. Configuration No. 71,  $\theta_F = -30^\circ$ ,  $\theta_R = +30^\circ$ ,  $h/c = \infty$ ,  
(Runs 667-669)



CONFIGURATION NO. 76

RUN NO.	J/qS
705	.068
706	.215
707	.611
708	1.459
709	2.486

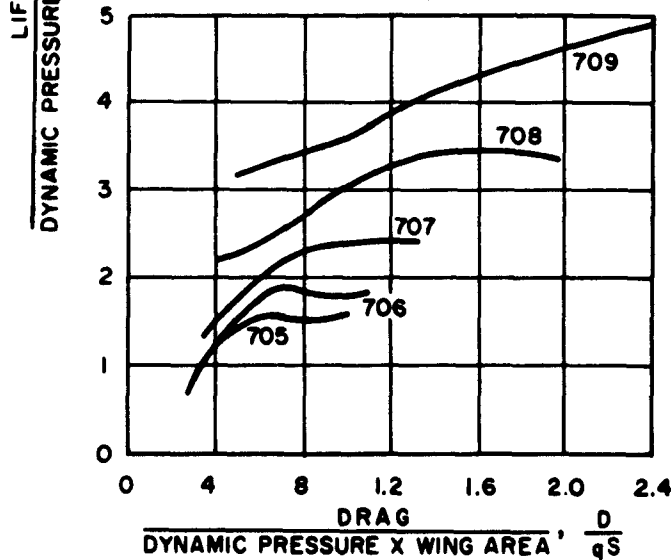
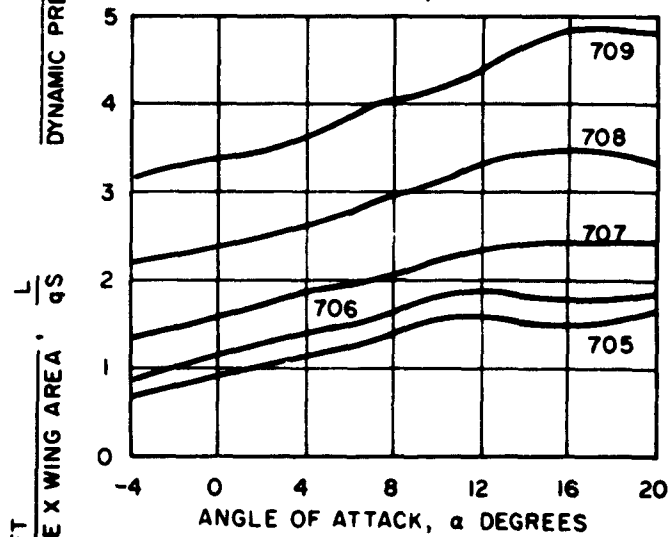
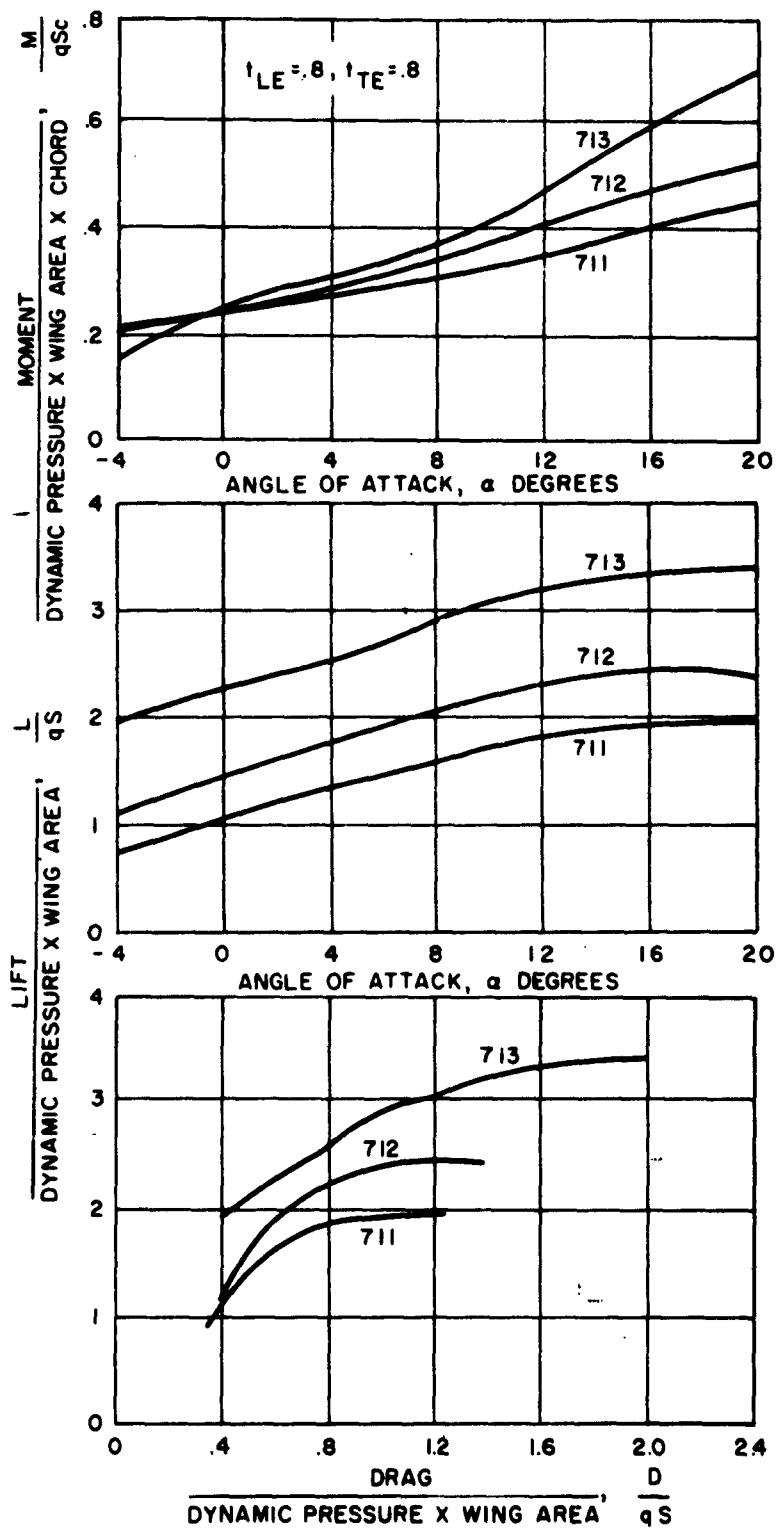


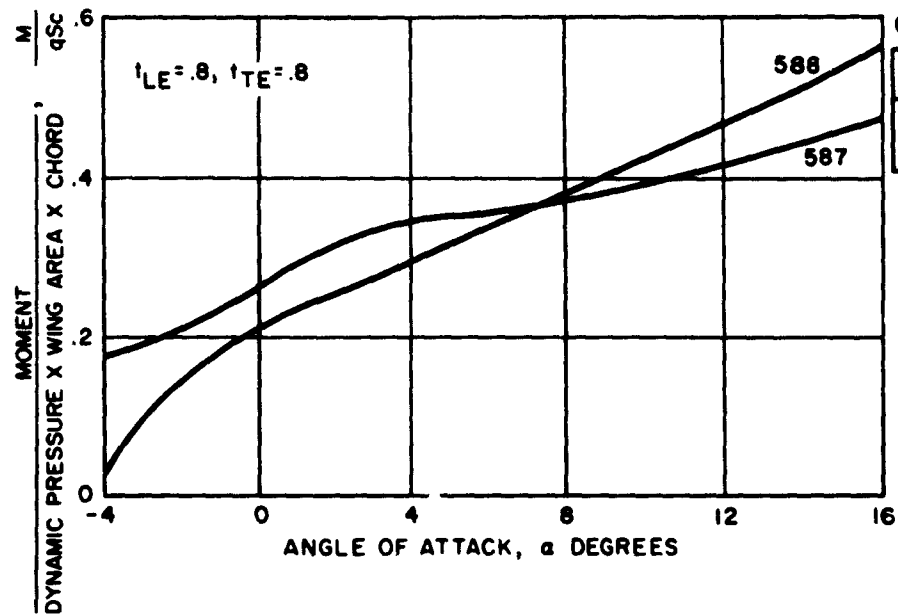
Figure 165. Configuration No. 76,  $\theta_F = -30^\circ$ ,  $\theta_R = +30^\circ$ ,  $h/c = \infty$ ,  
(Runs 705-709)



CONFIGURATION NO. 77

RUN NO.	J/qS
711	.227
712	.604
713	1.407

Figure 166. Configuration No. 77,  $\theta_F = -30^\circ$ ,  $\theta_R = +30^\circ$ ,  $h/c = \infty$ ,  
(Runs 711-713)



CONFIGURATION NO. 18

RUN NO.	J/qS
587	.3608
588	.9669

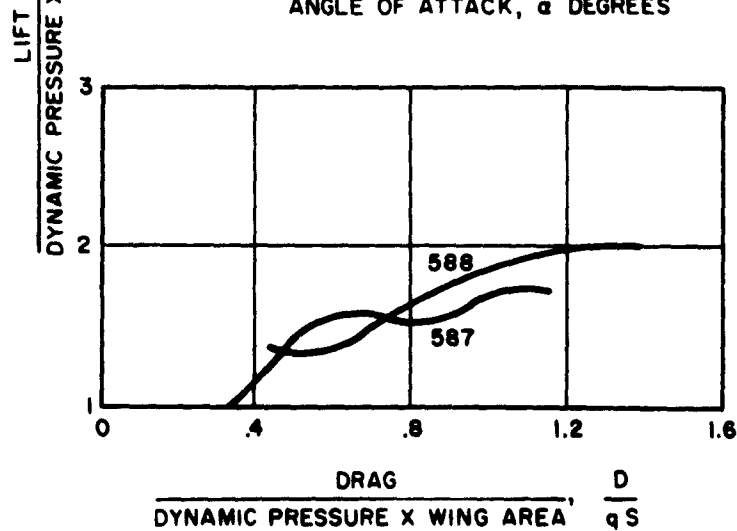
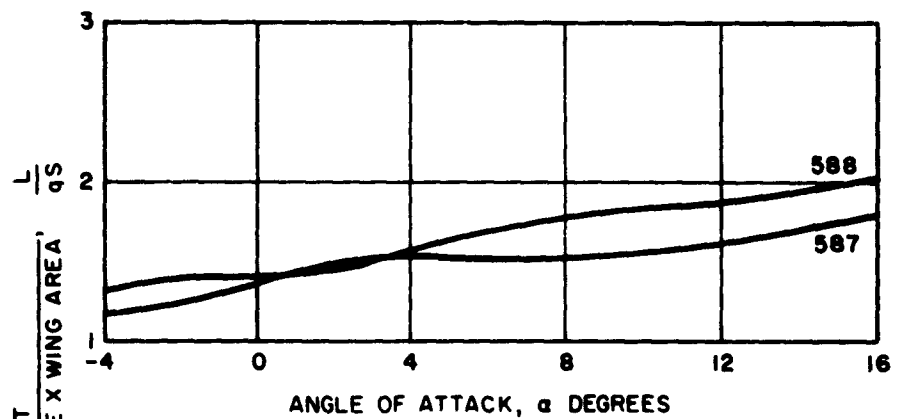


Figure 167. Configuration No. 18,  $\theta_F = +30^\circ$ ,  $\theta_R = -30^\circ$ ,  $h/c = .20$ ,  
(Runs 587-588)

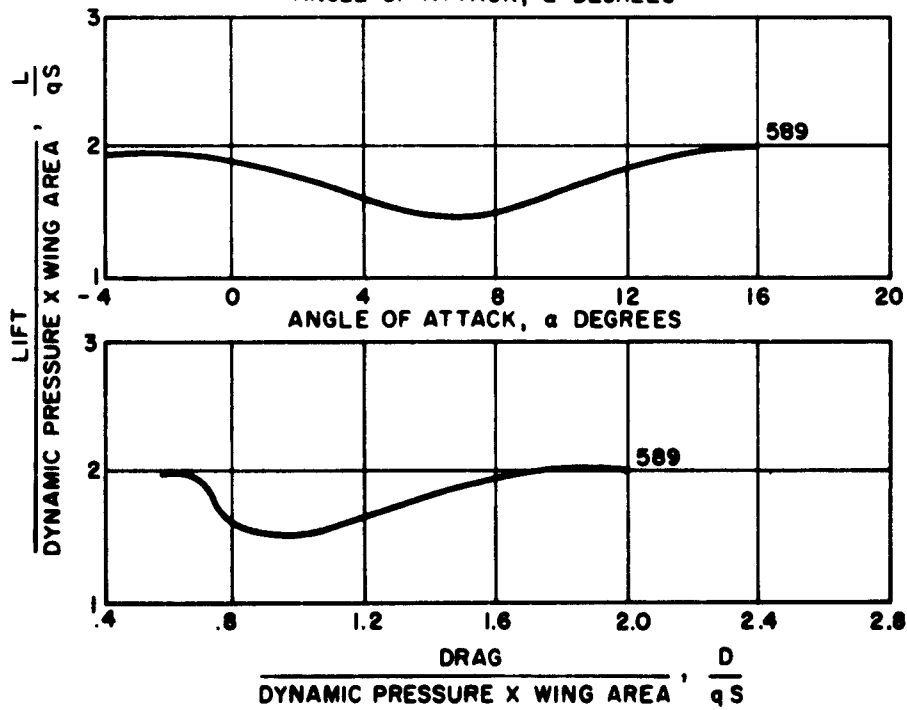
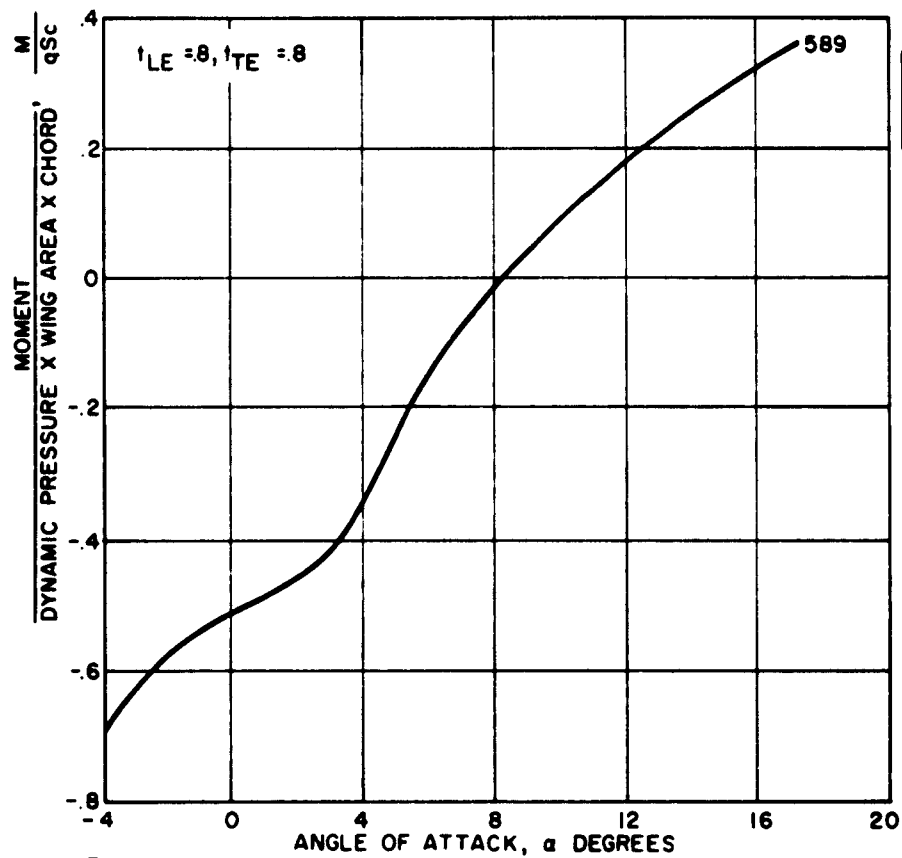
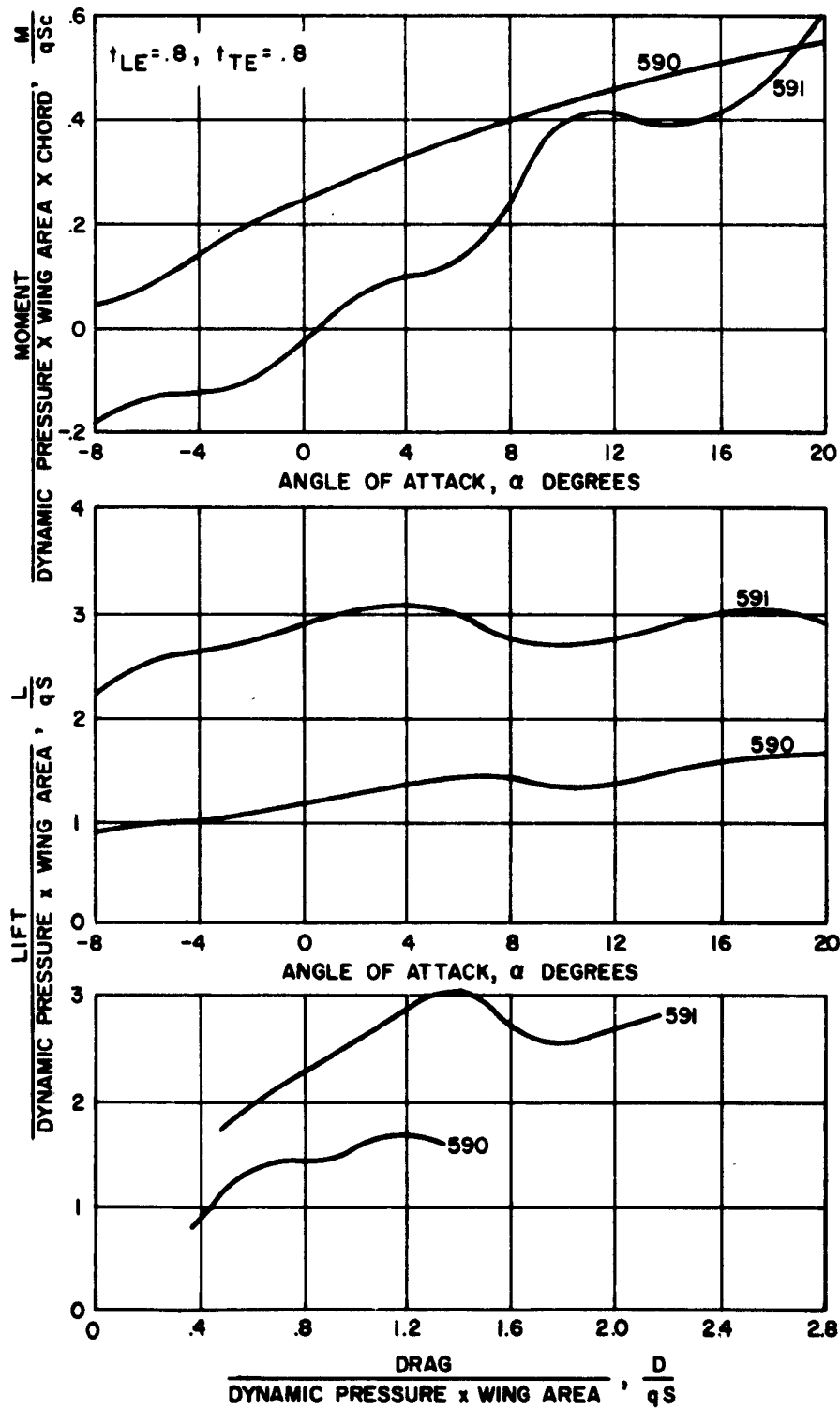


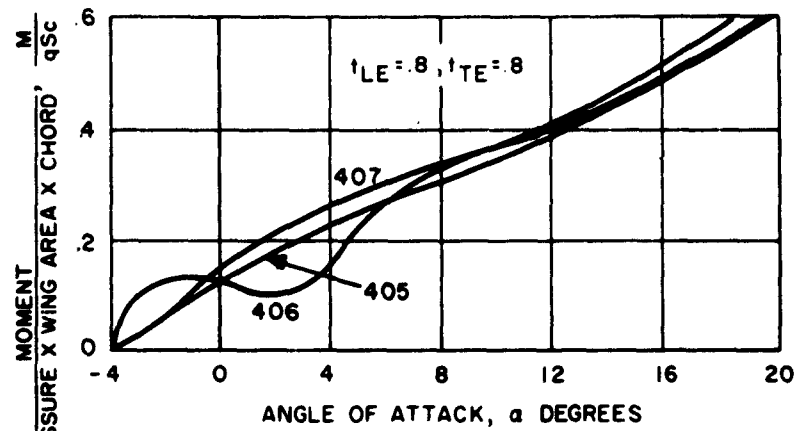
Figure 168. Configuration No. 18,  $\theta_F = -30^\circ$ ,  $\theta_R = +30^\circ$ ,  $h/c = .20$ ,  
(Run 589)



CONFIGURATION NO.16

RUN NO.	J/qS
590	.3640
591	2.2339

Figure 169. Configuration No. 16,  $\theta_F = +30^\circ$ ,  $\theta_R = -30^\circ$ ,  $h/c = .50$ ,  
(Runs 590-591)



CONFIGURATION NO. 31

RUN NO.	J/qS
405	.2333
406	.7225
407	.9651

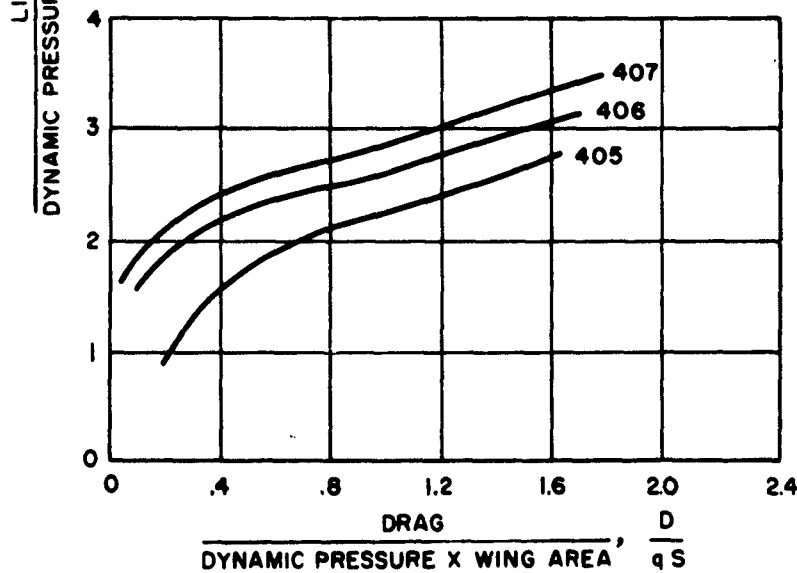
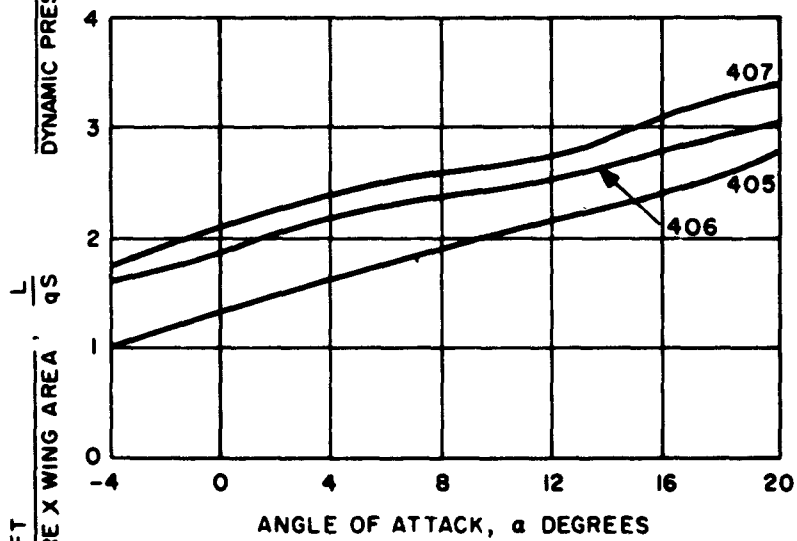
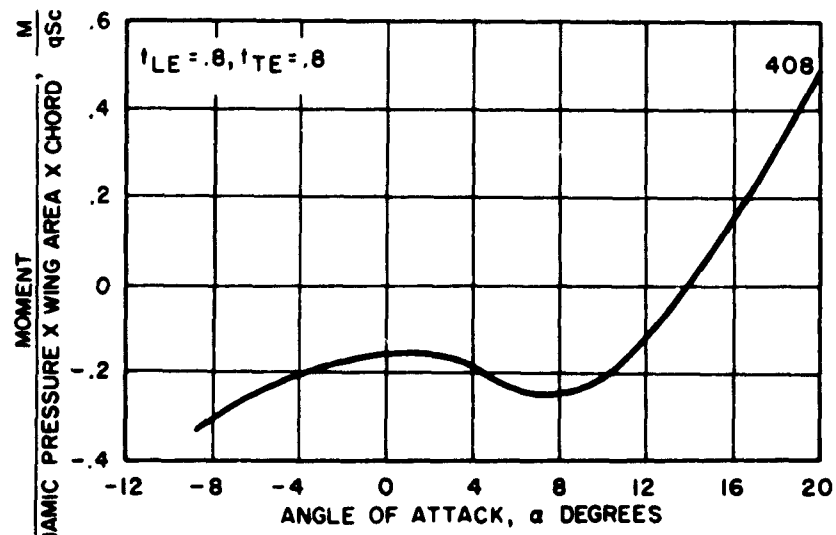


Figure 170. Configuration No. 31,  $\theta_F = -30$   $\theta_R = -30$   $h/c = .33$ ,  
(Runs 405-407)



CONFIGURATION NO. 31

RUN NO.	J/qS
408	2.5328

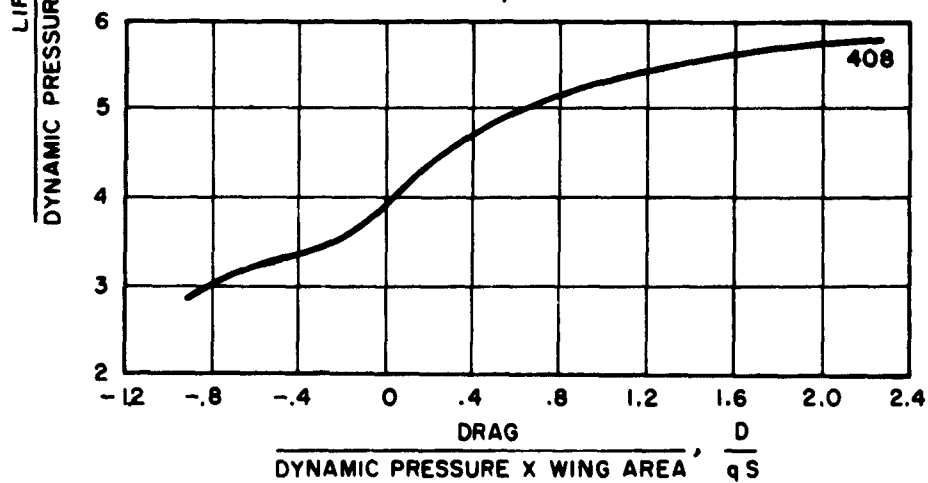
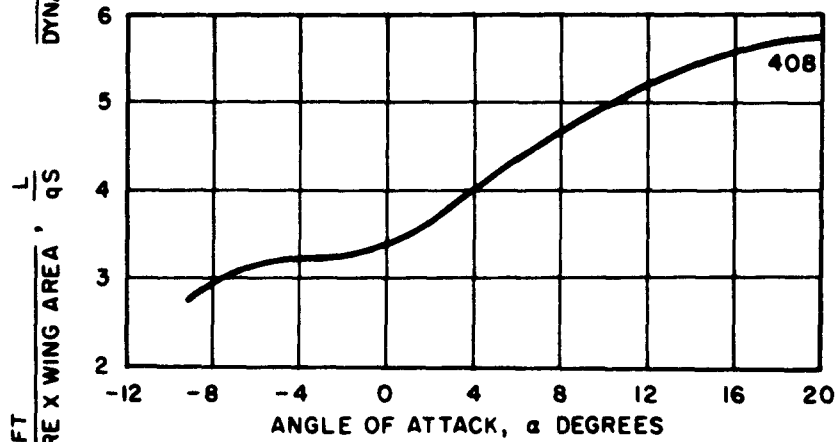
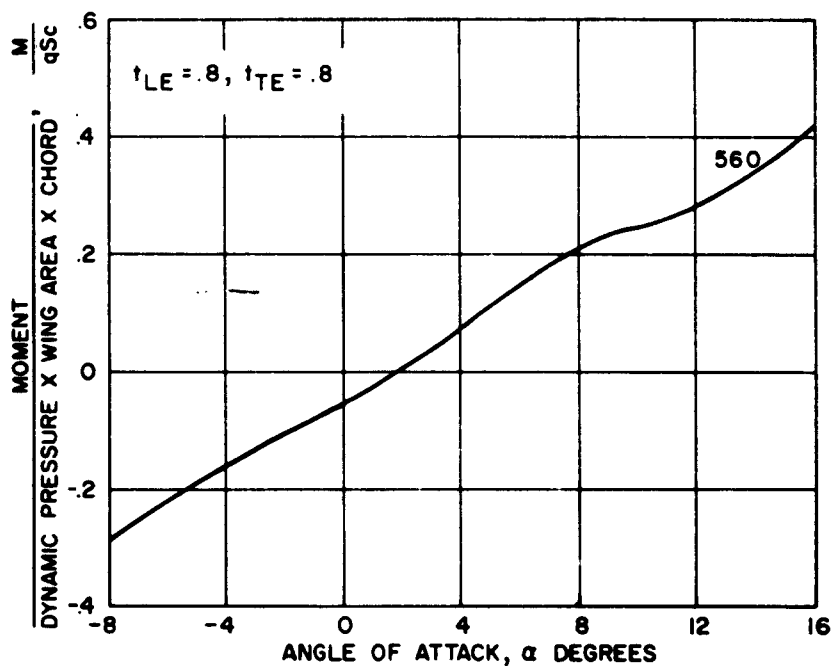


Figure 171. Configuration No. 31,  $\theta_F = -30$   $\theta_R = -30$   $h/c = .33$ ,  
(Run 408)



CONFIGURATION NO. 58

RUN NO.	J/qS
560	.523

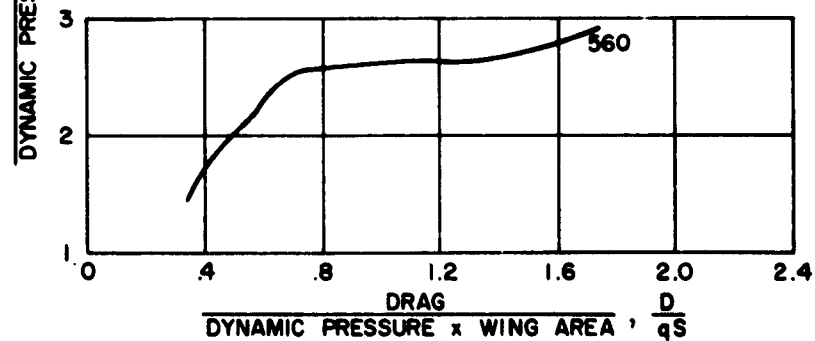
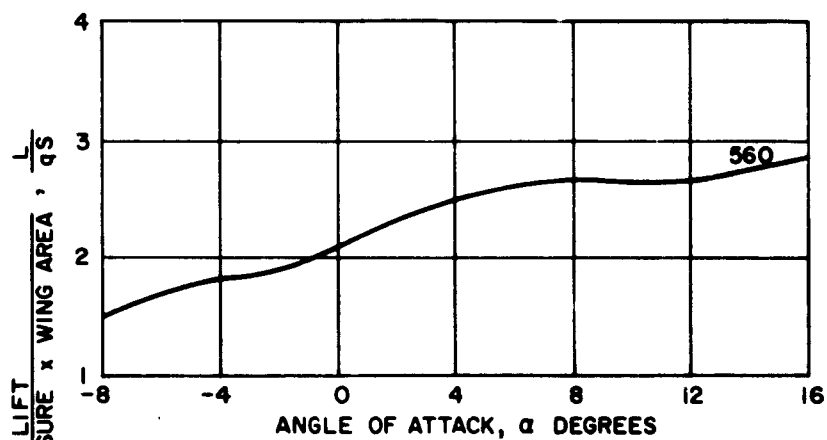
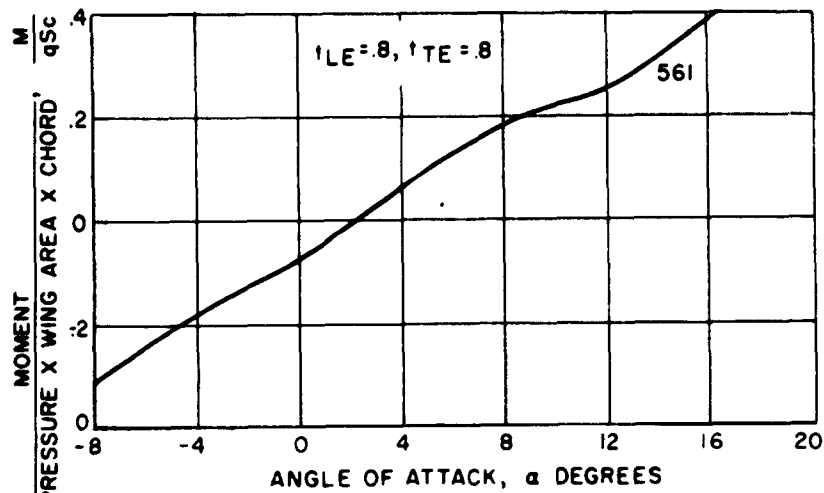


Figure 172. Configuration No. 58,  $\theta_F = -30 \times \theta_R = -30 \times h/c = .33$ ,  
(Run 560)



CONFIGURATION NO. 59

RUN NO.	J/qS
561	.913

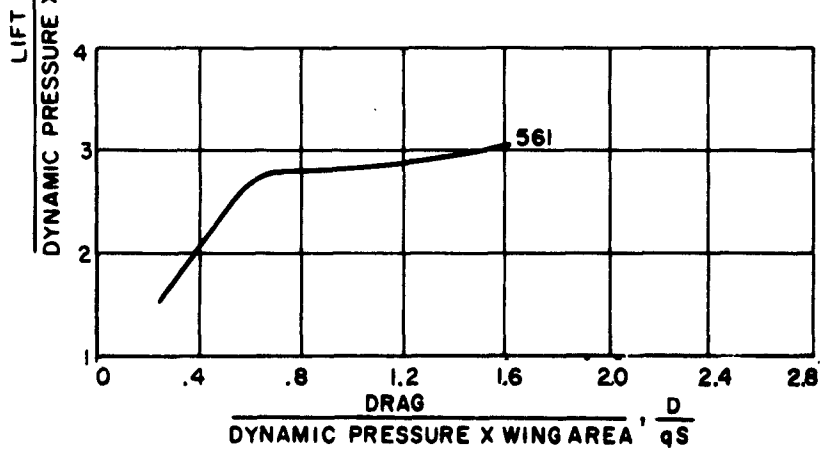
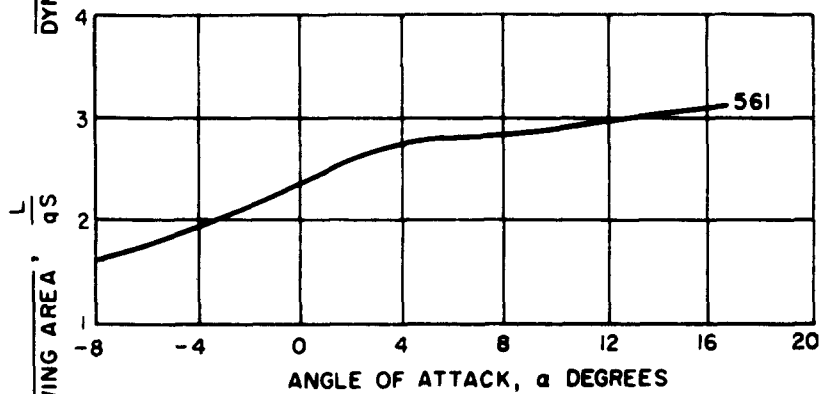


Figure 173. Configuration No. 59,  $\theta_F = -30^\circ$ ,  $\theta_R = -30^\circ$ ,  $h/c = .33$ ,  
(Run 561)

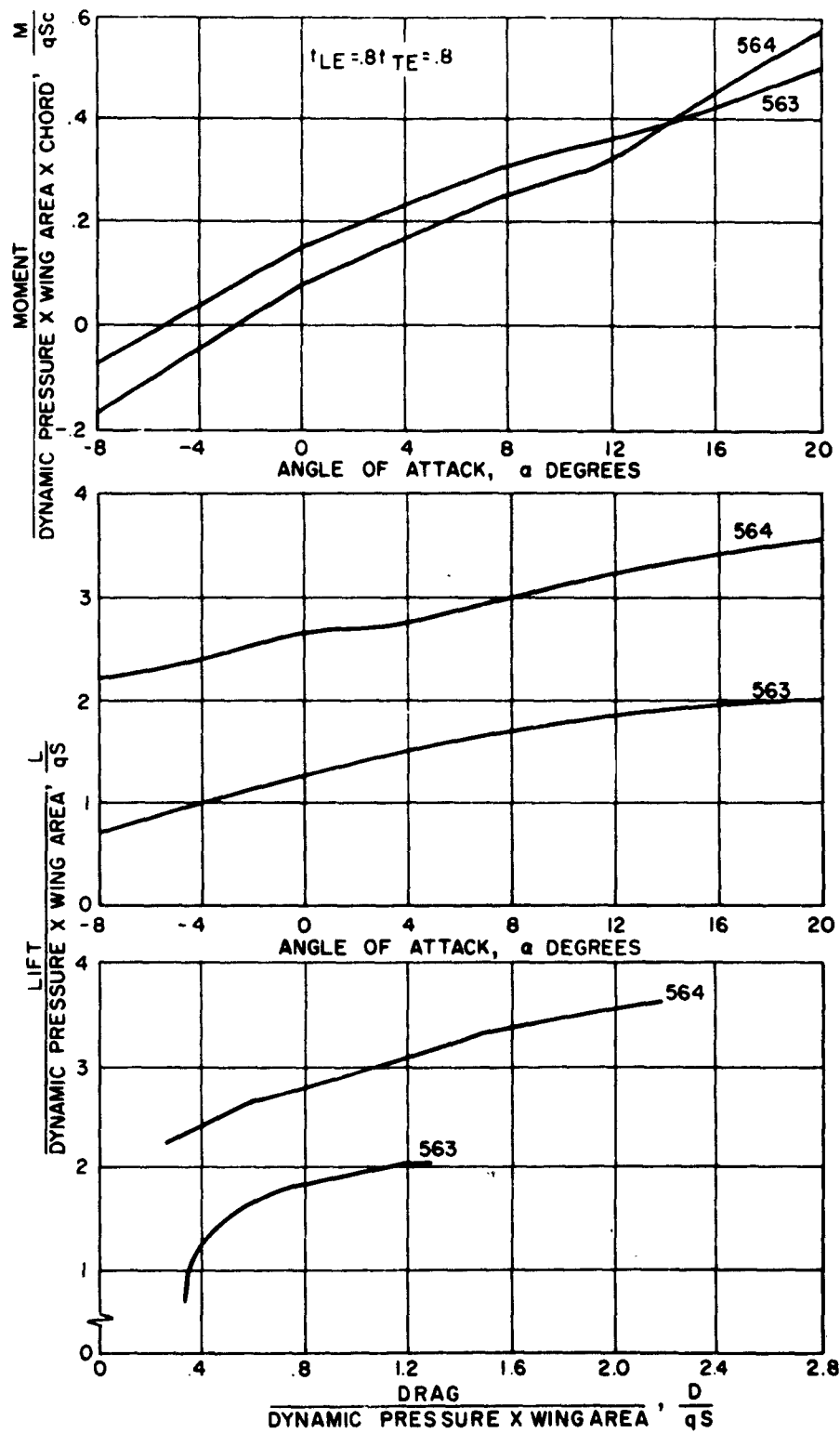


Figure 174. Configuration No. 60,  $\theta_F = -30^\circ$ ,  $\theta_R = -30^\circ$ ,  $h/c = .33$ ,  
(Runs 563-564)

CONFIGURATION NO. 44

RUN NO.	J/qS
575	.20

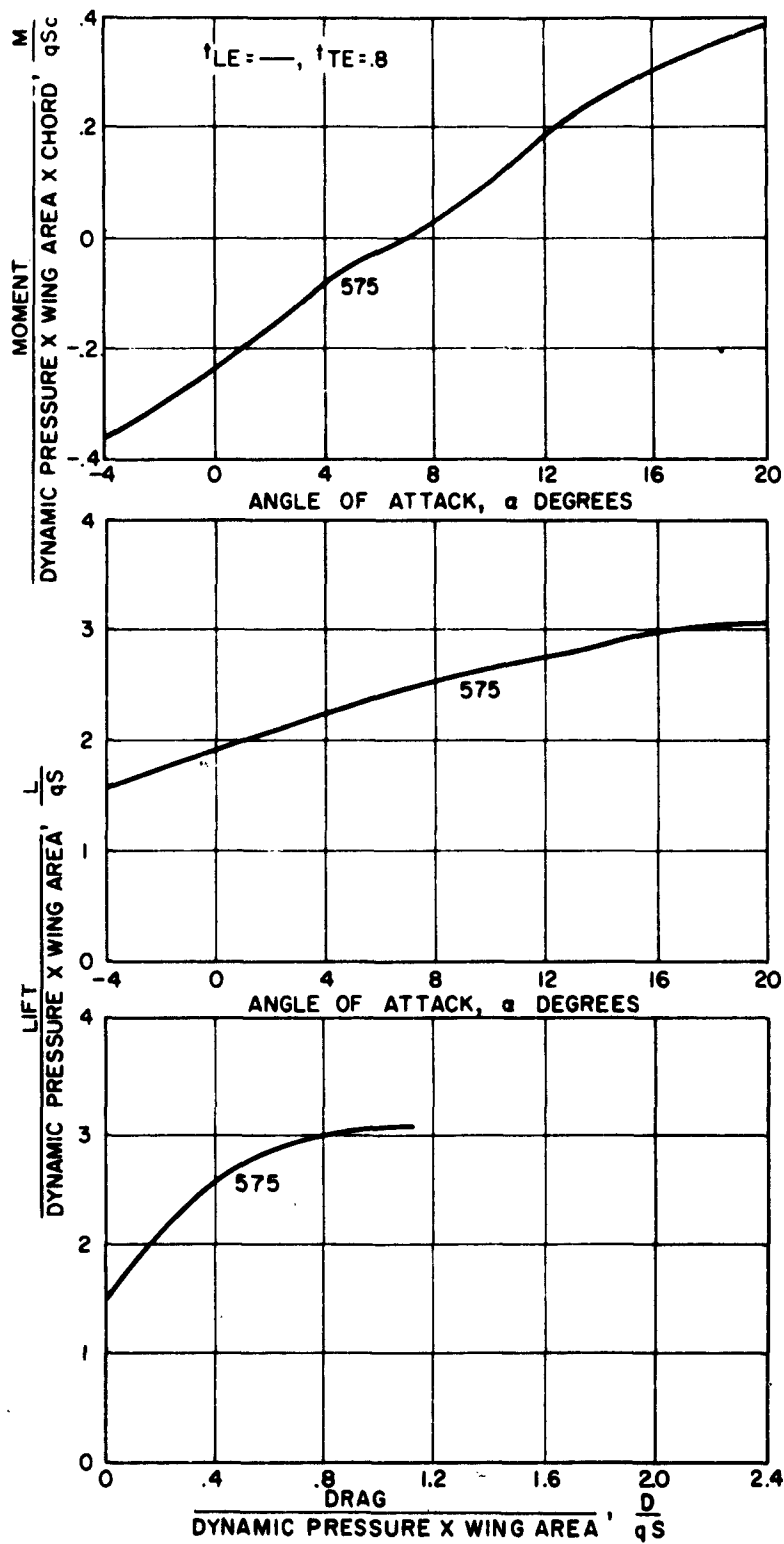


Figure 175. Configuration No. 44,  $\theta_F = -\theta_R = -30^\circ$ ,  $h/c = .33$ ,  
(Run 575)

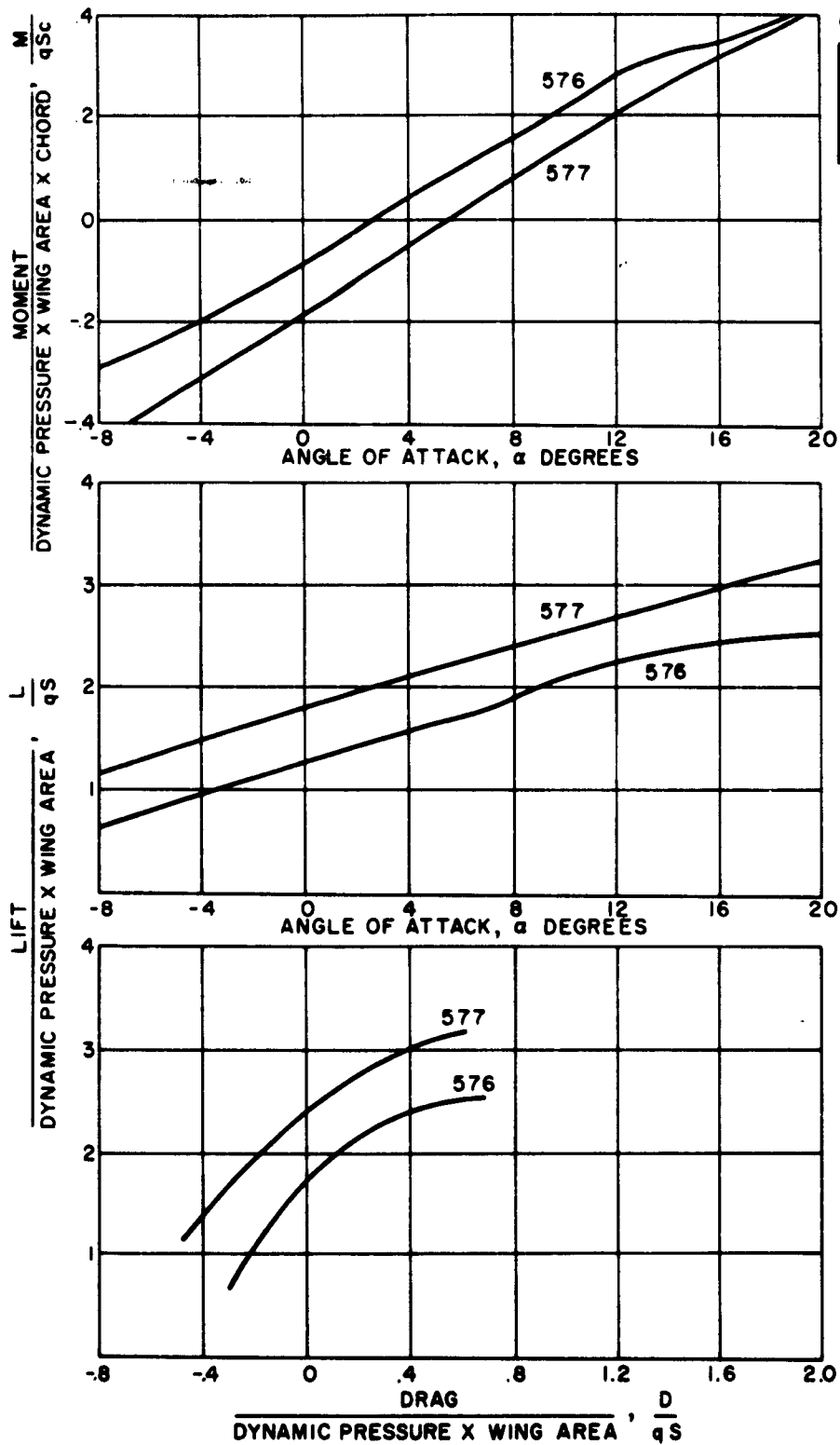


Figure 176. Configuration No. 45,  $\theta_F = -\theta_R = -30^\circ$ ,  $h/c = .50$ ,  
(Run 576-577)

CONFIGURATION NO. 32

RUN NO.	J/qS
694	.5317
695	1.8190
696	4.2295

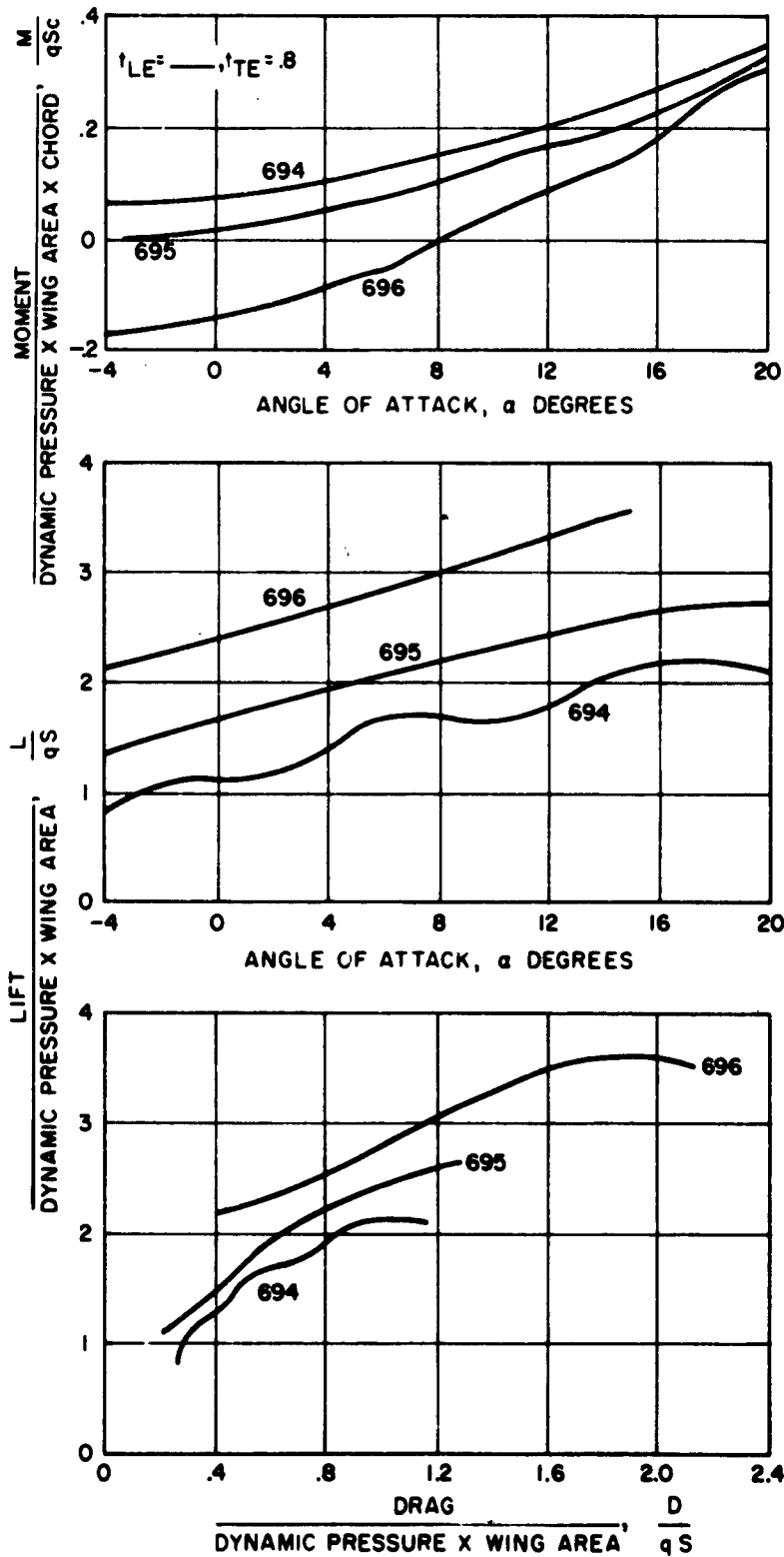


Figure 177. Configuration No. 32,  $\theta_F = -\theta_R = -30 \times h/c = \infty$ ,  
(Runs 694-696)

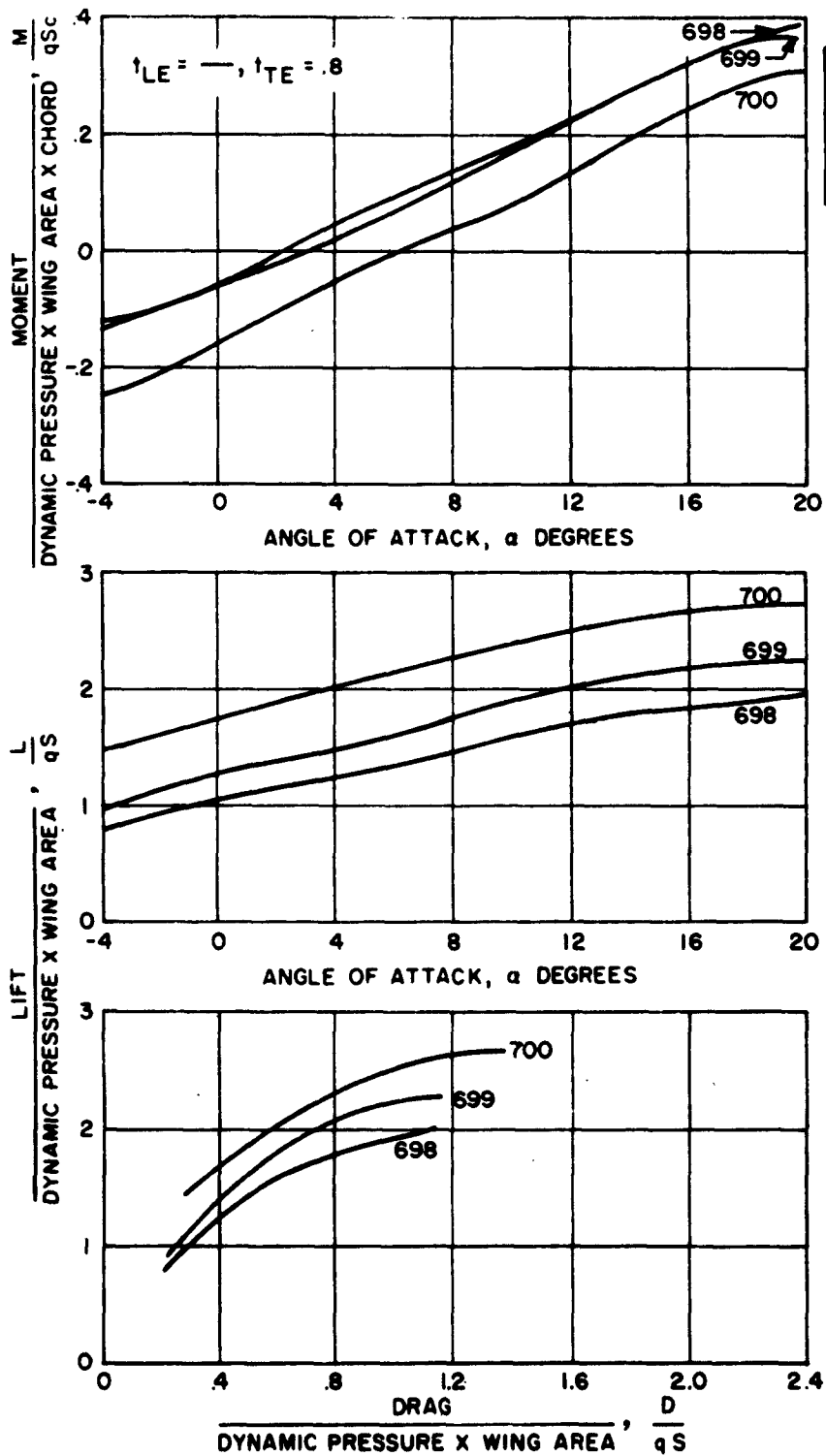
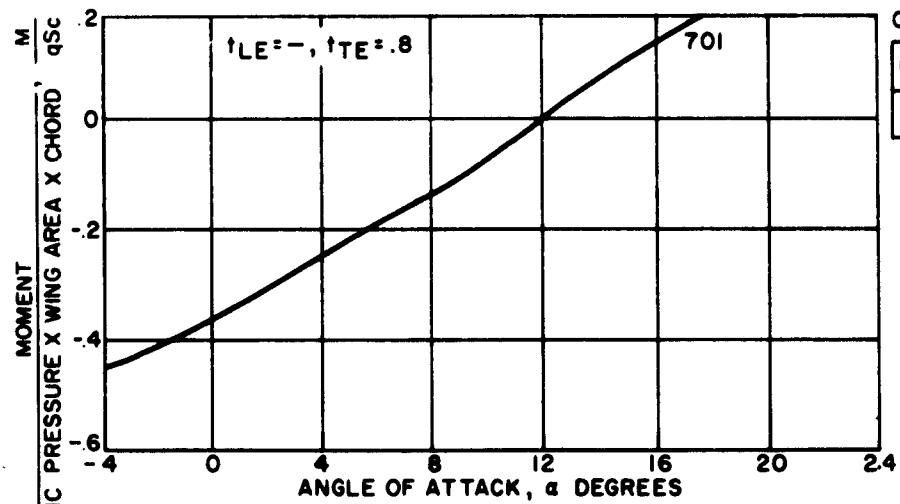


Figure 178. Configuration No. 33,  $\theta_F = -\theta_R = -30^\circ$ ,  $h/c = \infty$ ,  
 (Runs 698-700)



CONFIGURATION NO. 33

RUN NO.	J/qS
701	2.4900

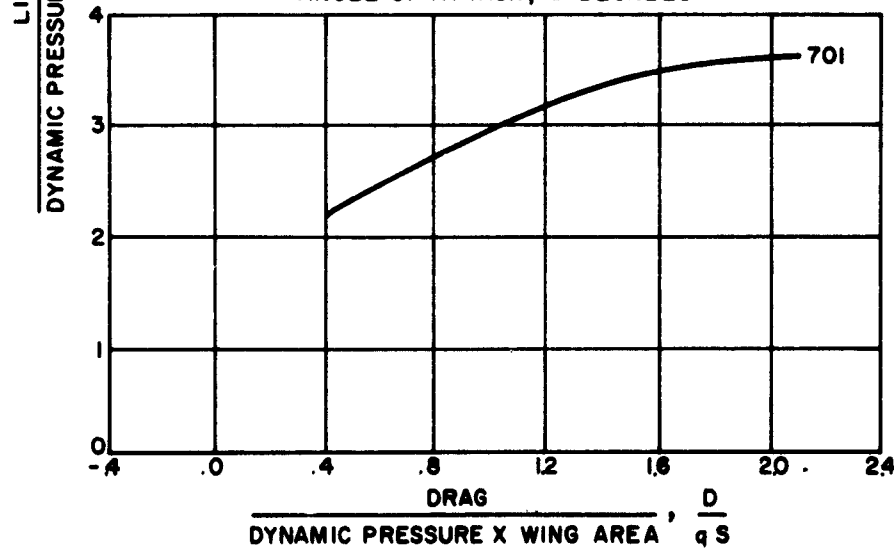
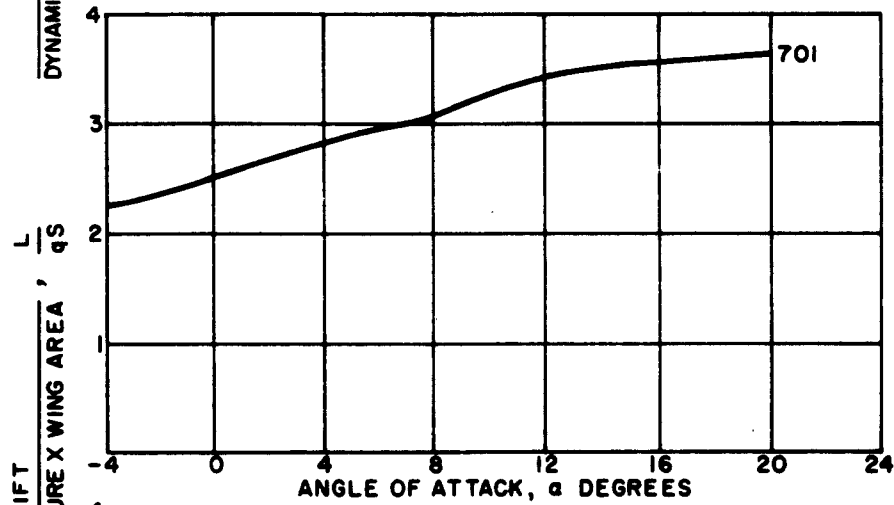
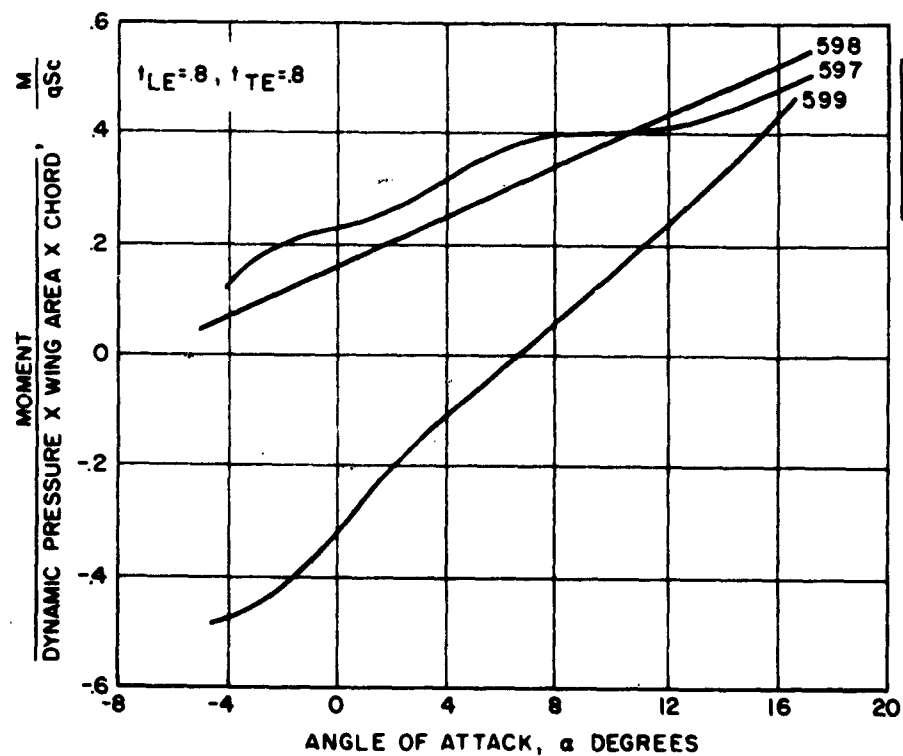


Figure 179. Configuration No. 33,  $\theta_F = -\theta_R = -30^\circ$ ,  $h/c = \infty$ ,  
(Run 701)



CONFIGURATION NO. 21

RUN NO.	J/qS
597	.1994
598	.5478
599	1.2174

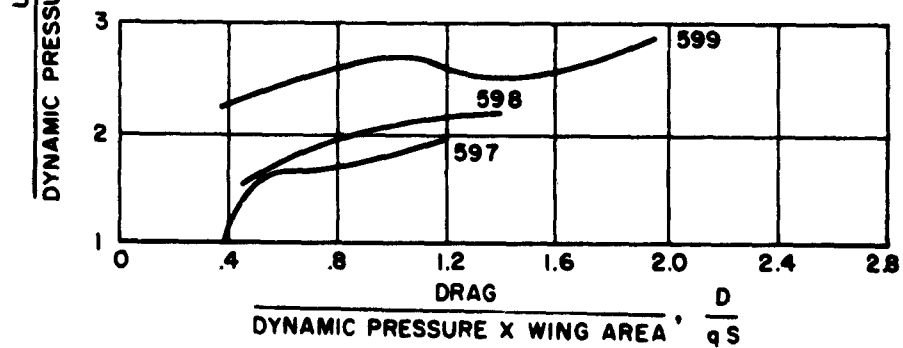
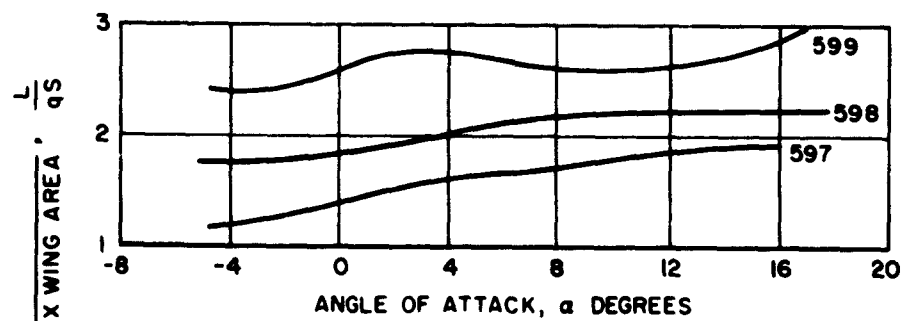
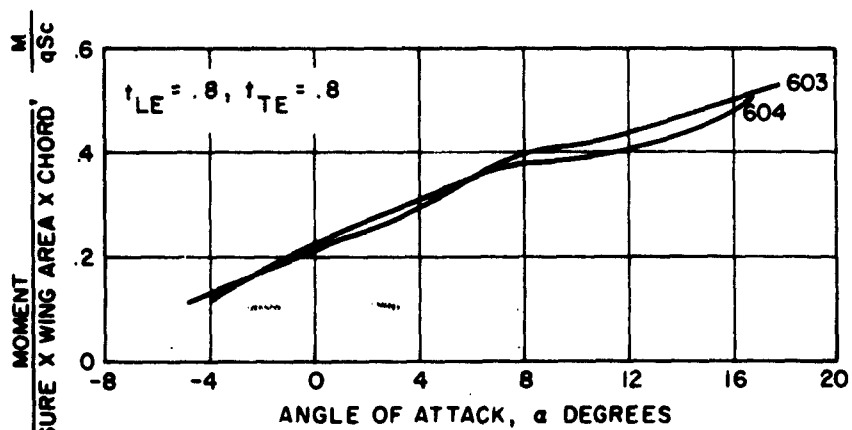


Figure 180. Configuration No. 21,  $\theta_F = 0^\circ$   $\theta_R = -30^\circ$   $h/c = .20$ ,  
(Runs 597-599)



CONFIGURATION NO. 20

RUN NO.	J/qS
603	.20
604	.56

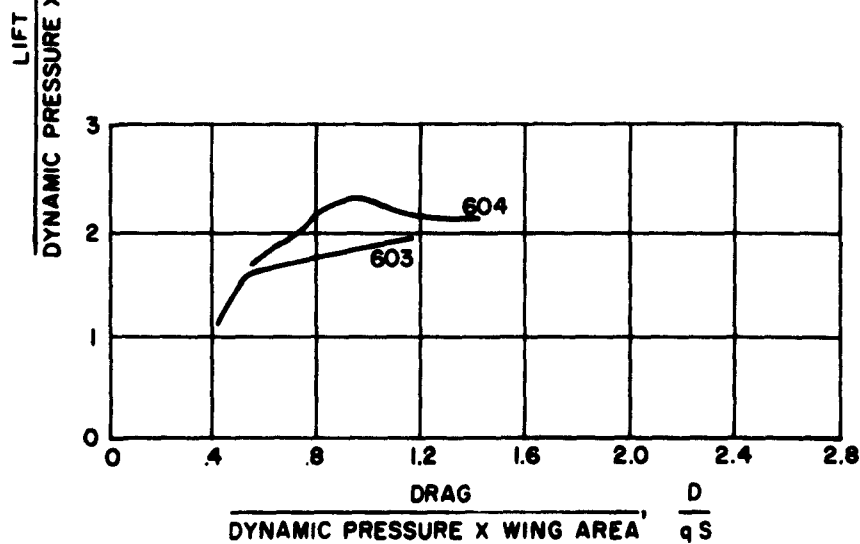
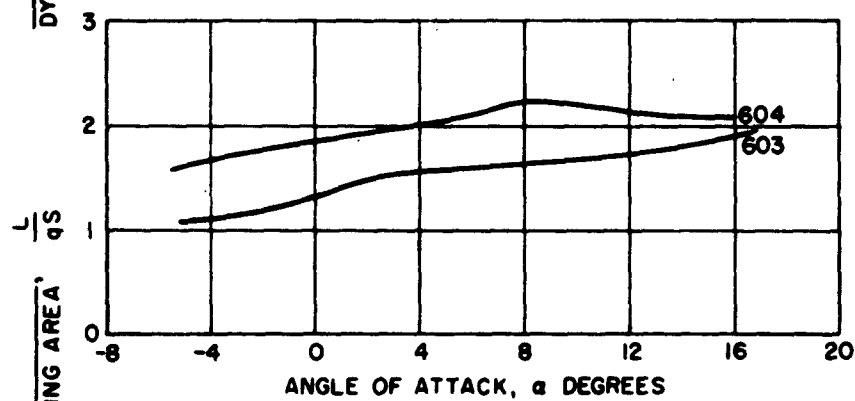
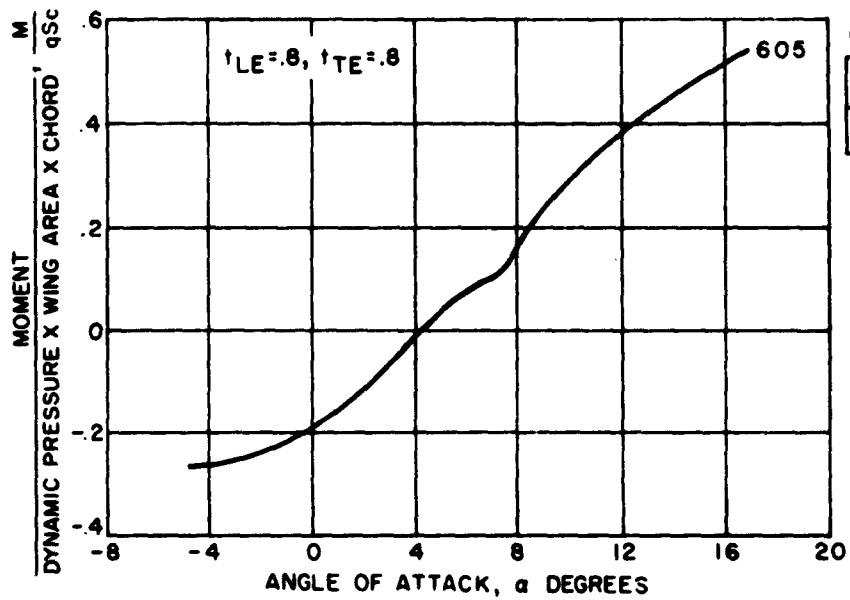


Figure 181. Configuration No. 20,  $\theta_F = 0^\circ$   $\theta_R = -30^\circ$   $h/c = .33$ ,  
(Runs 603-604)



CONFIGURATION NO. 20

RUN NO.	J/qS
605	1.27

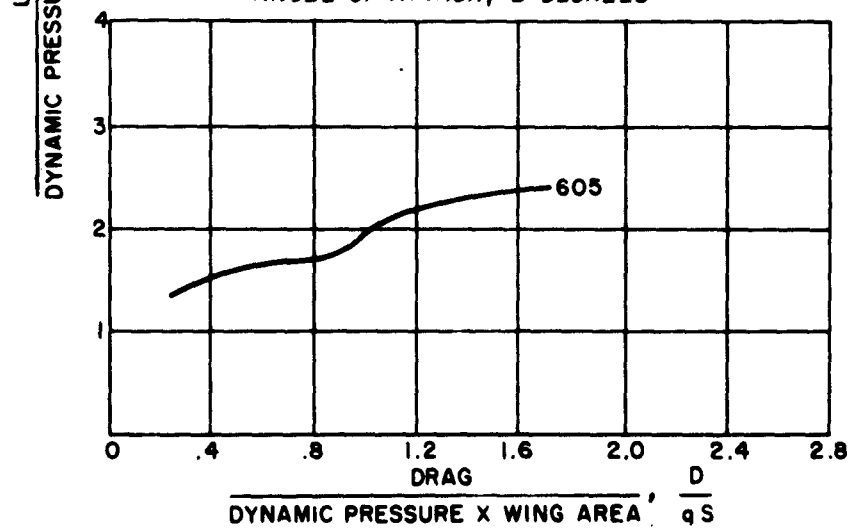
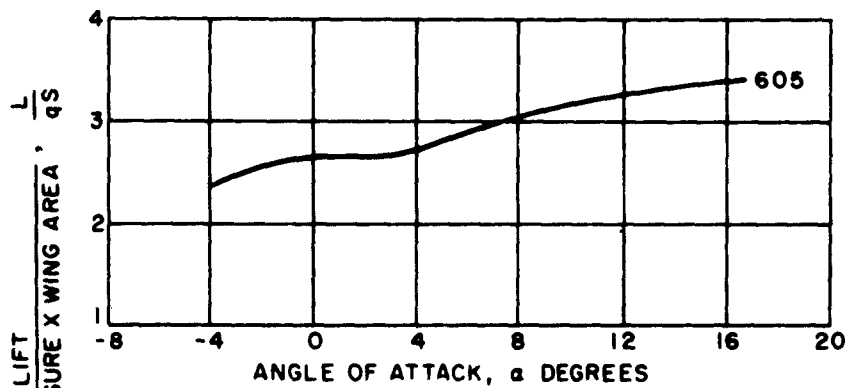
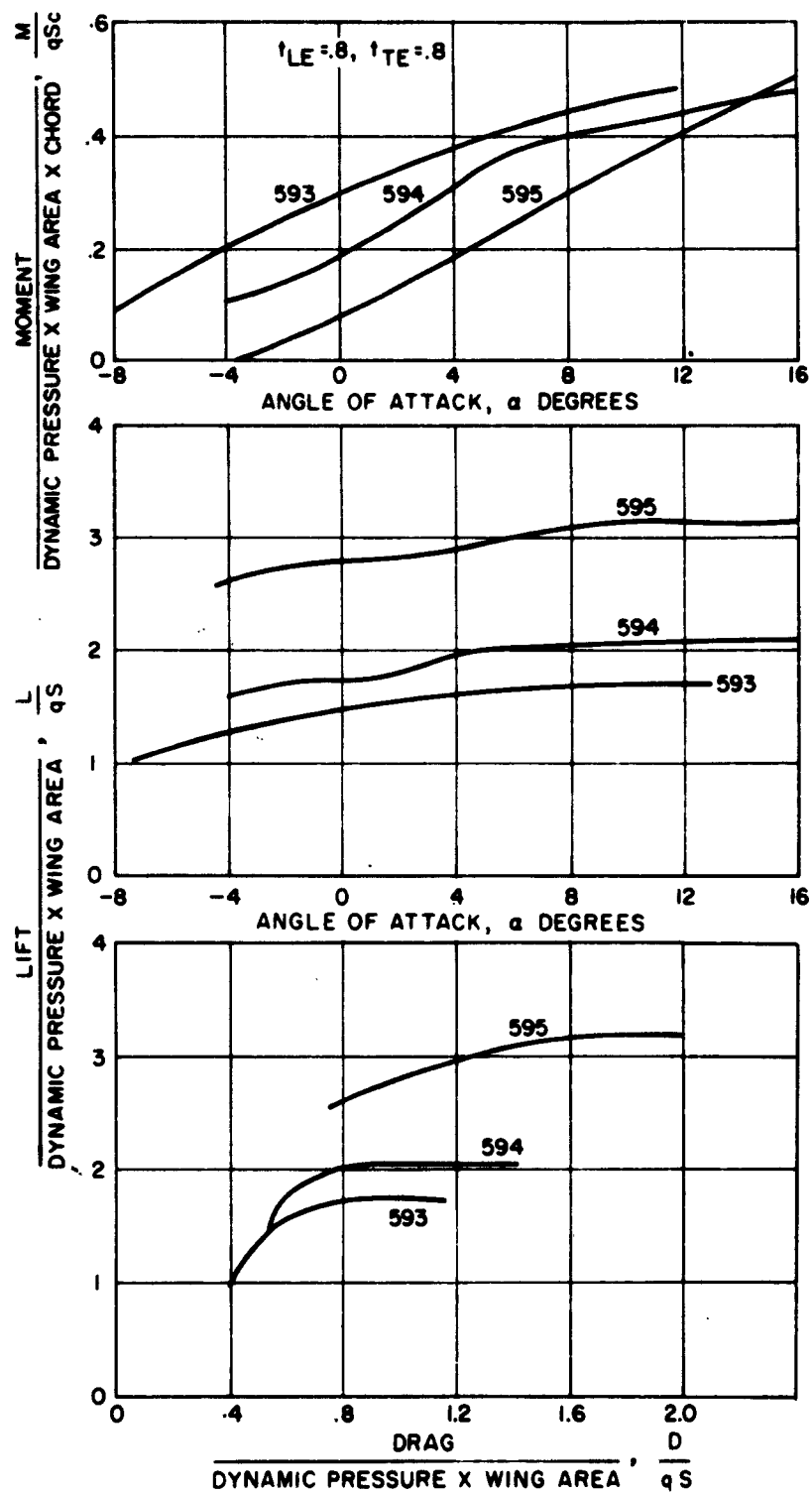


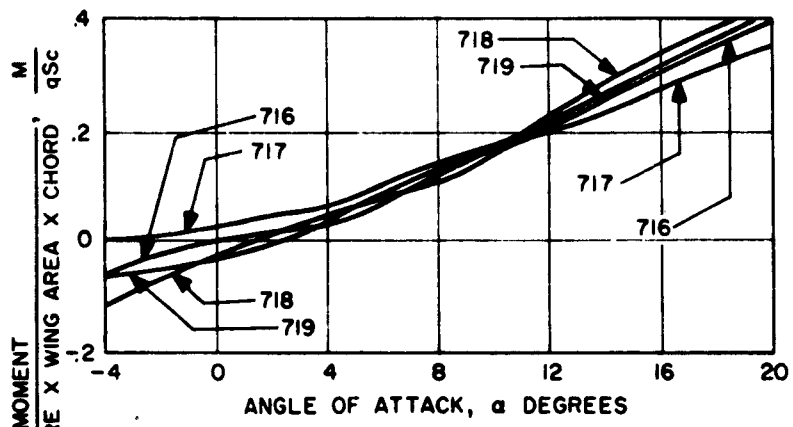
Figure 182. Configuration No. 20,  $\theta_F = 0^\circ$   $\theta_R = -30^\circ$   $h/c = .33$ ,  
(Run 605)



CONFIGURATION NO. 19

RUN NO.	J/qS
593	.20
594	.55
595	1.29

Figure 183. Configuration No. 19,  $\theta_F = 0^\circ$   $\theta_R = -30^\circ$   $h/c = .50$ ,  
 (Runs 593-595)



CONFIGURATION NO.14

RUN NO.	J/qS
716	.034
717	.128
718	.054
719	.0295

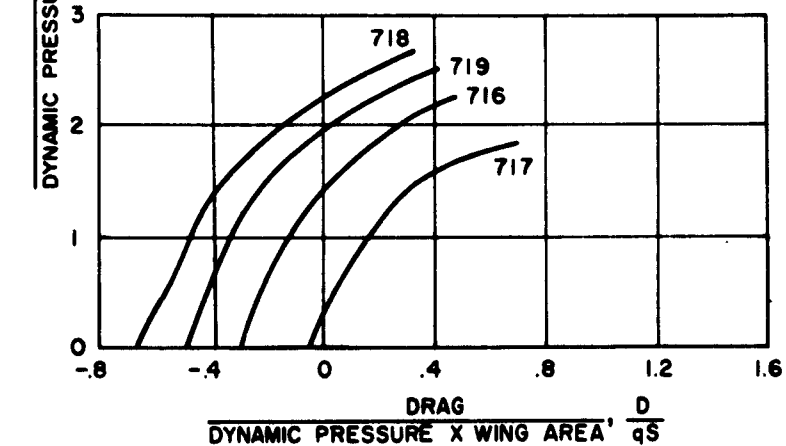
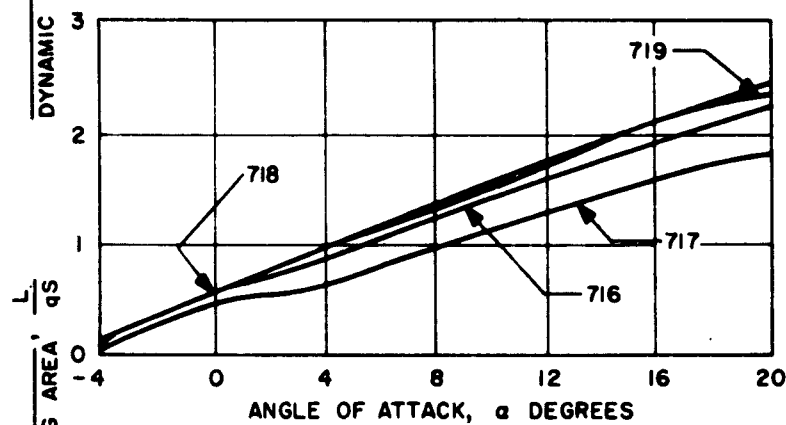


Figure 184. Configuration No. 14,  $\theta_F = -\theta_R = -h/c = \infty$ ,  
(Runs 716-719)

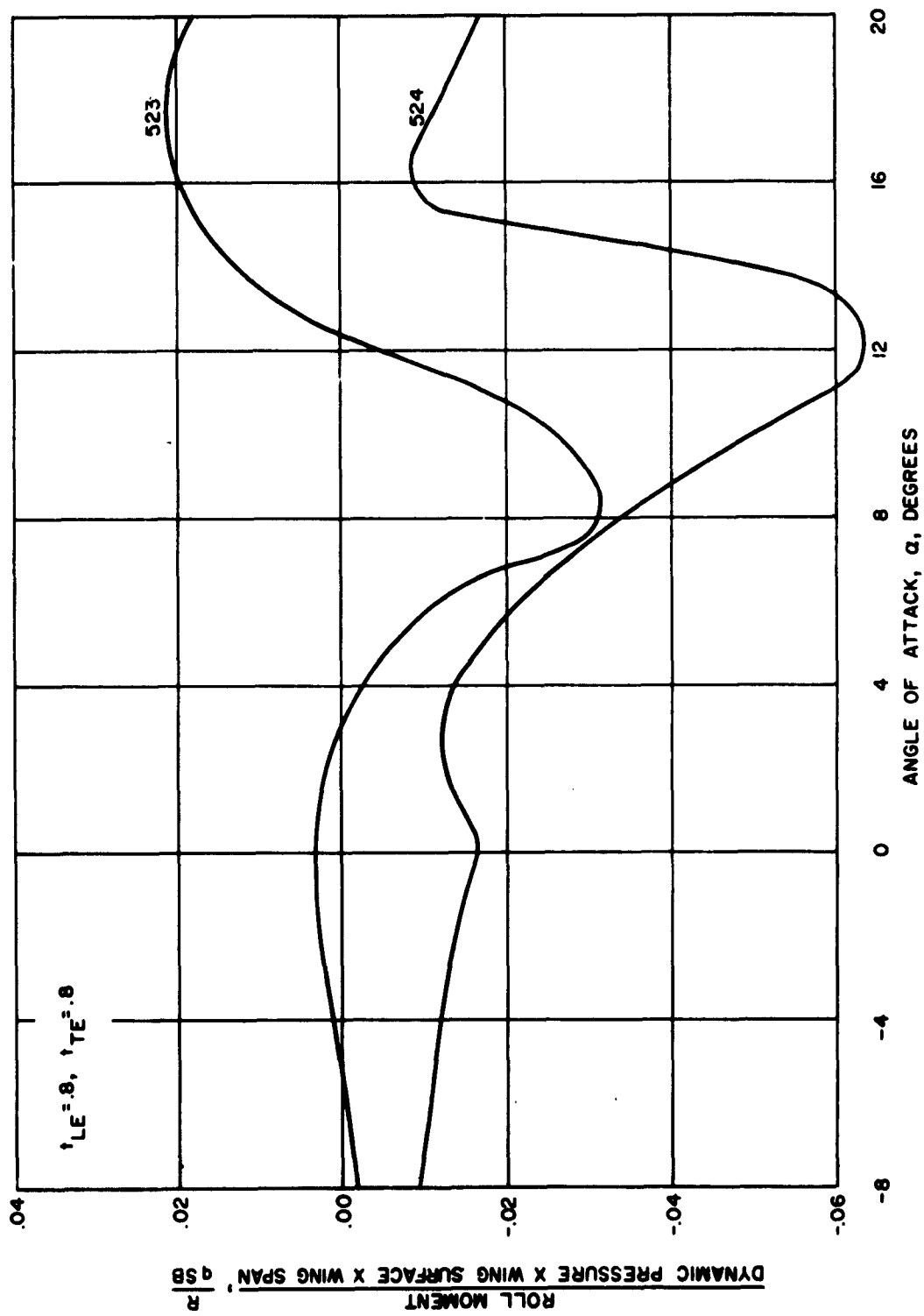


Figure 185. Configuration No. 48,  $\theta_F = -30^\circ$ ,  $\theta_R = -30^\circ$ ,  $h/c = .33$ ,  
(Runs 523-524, Roll Angle =  $5^\circ$ )

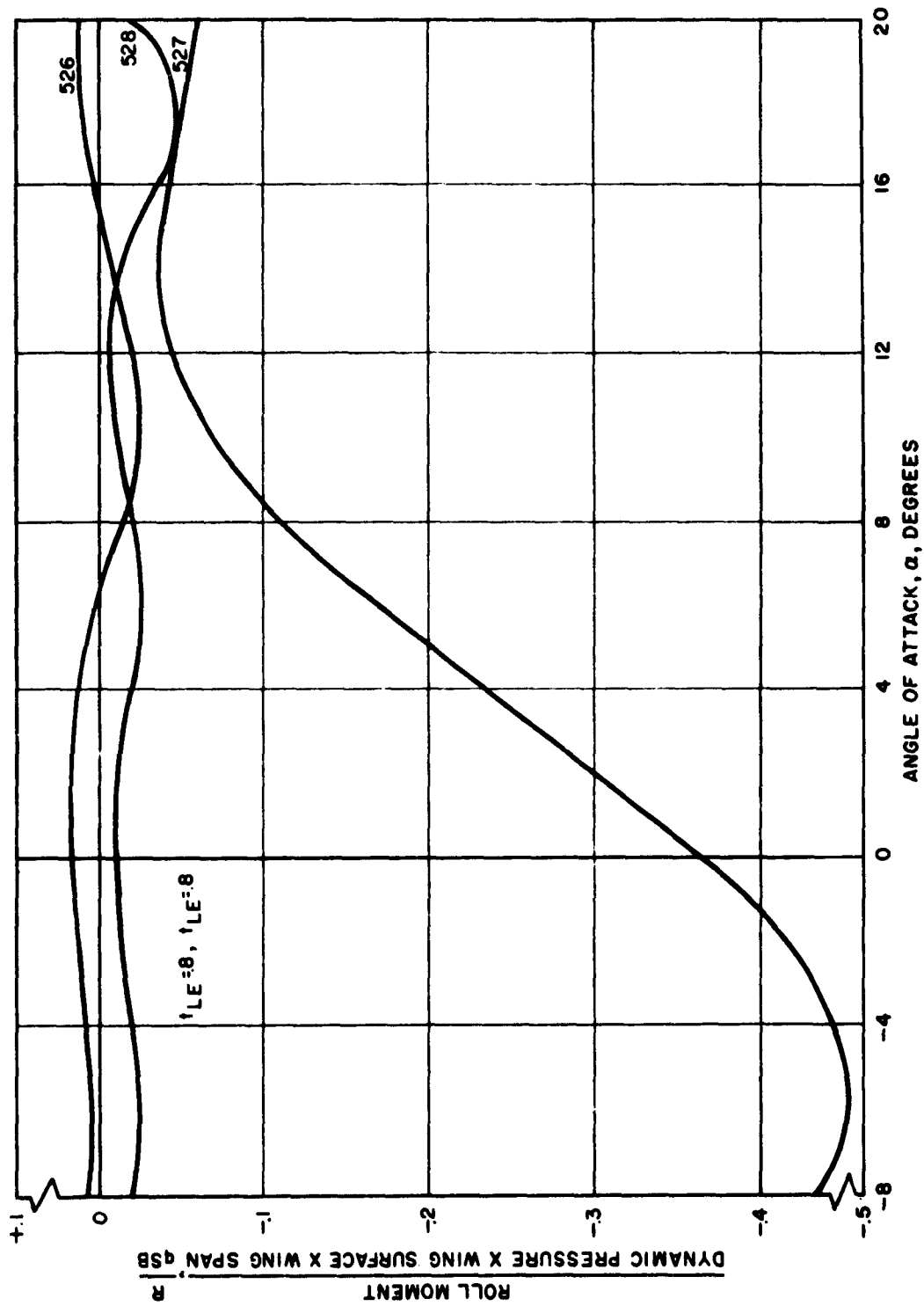


Figure 186. Configuration No. 49,  $\theta_F = -30^\circ$ ,  $\theta_R = -30^\circ$ ,  $h/c = .33$ ,  
 (Runs 526-528, Roll Angle =  $10^\circ$ )

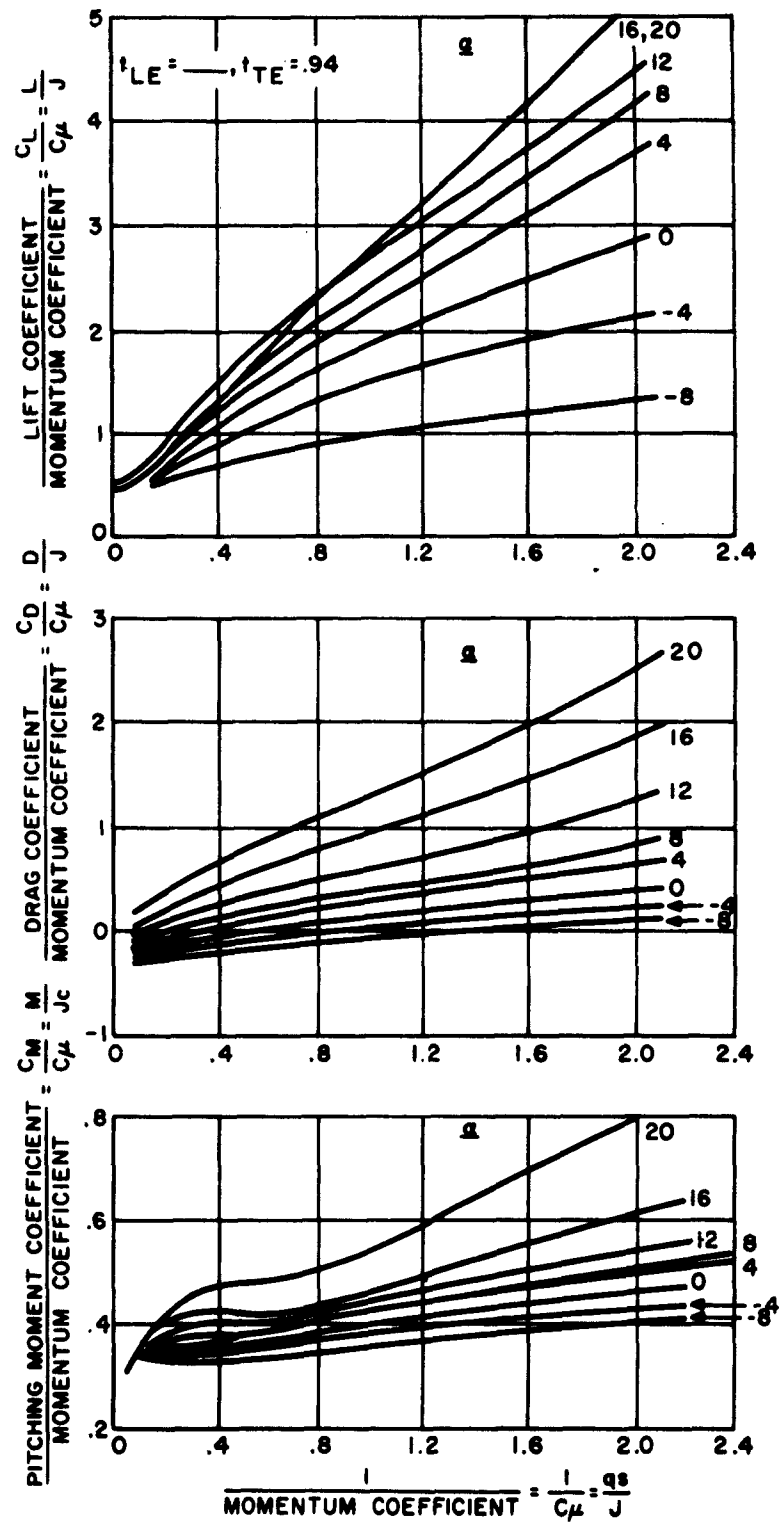


Figure 187. Configuration No. 12,  $\theta_F = -\theta_R = +30$ ,  $h/c = .33$

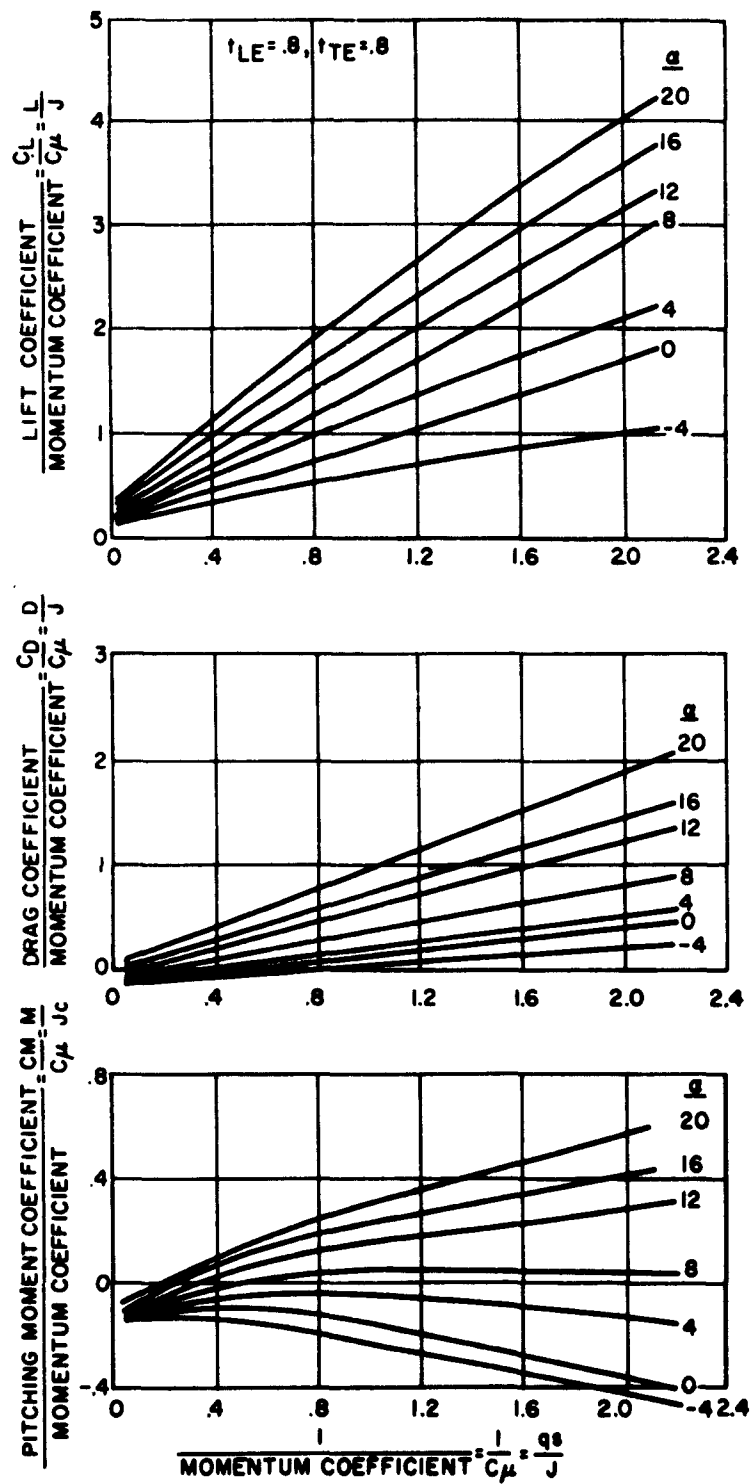


Figure 188. Configuration No. 73,  $\theta_F = -\theta_R = +60^\circ$ ,  $h/c = \infty$

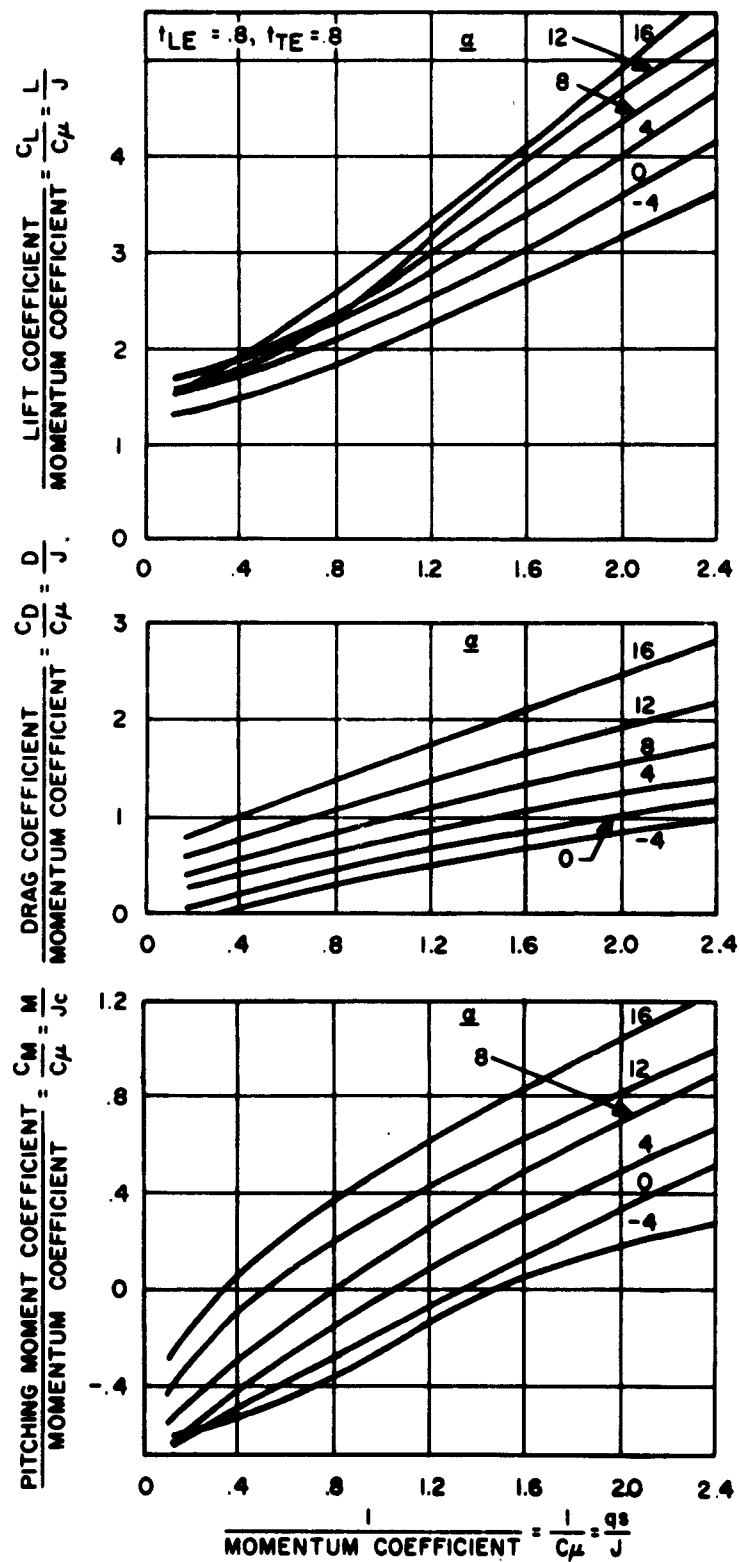


Figure 189. Configuration No. 64,  $\theta_F = 0^\circ$ ,  $\theta_R = 0^\circ$ ,  $h/c = .2$

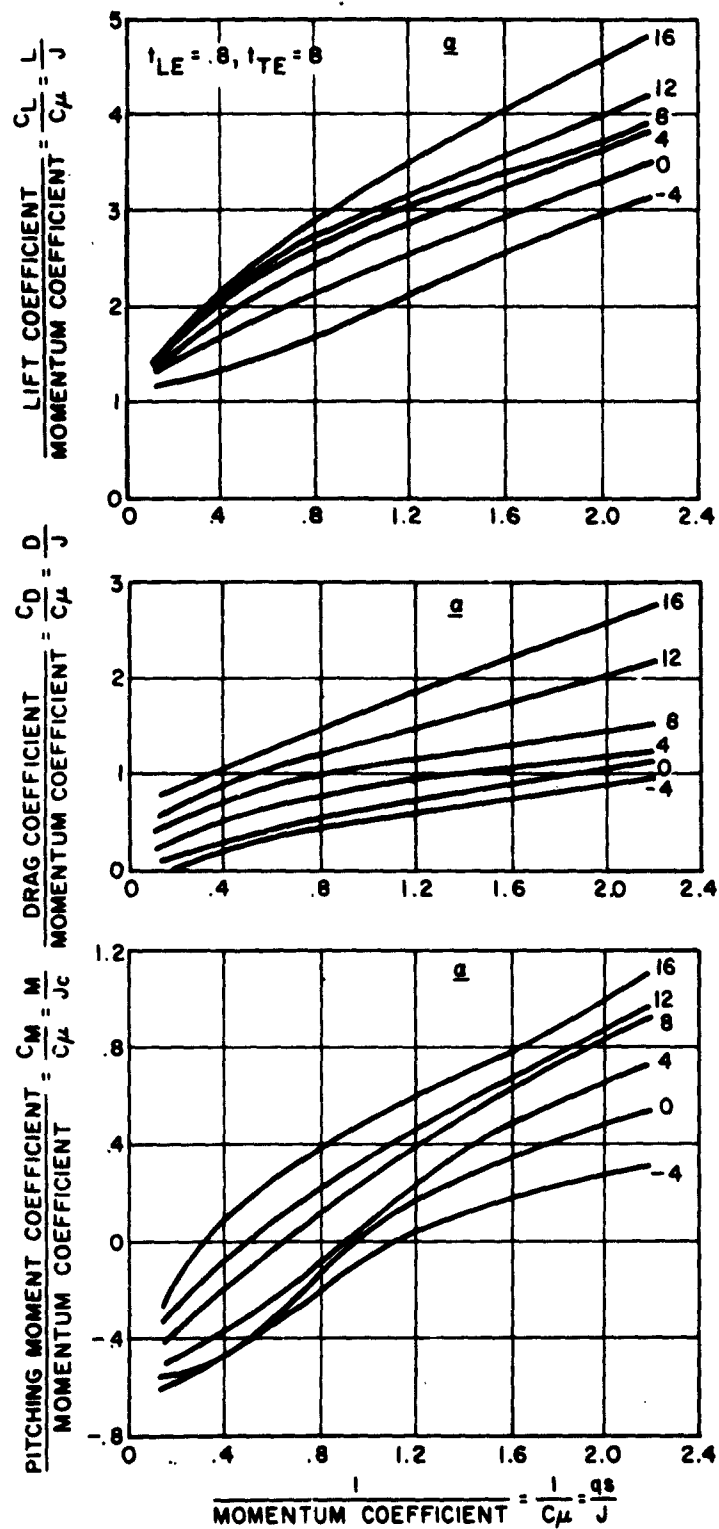


Figure 190. Configuration No. 63,  $\theta_F = 0^\circ$ ,  $\theta_R = 0^\circ$ ,  $h/c = .33$

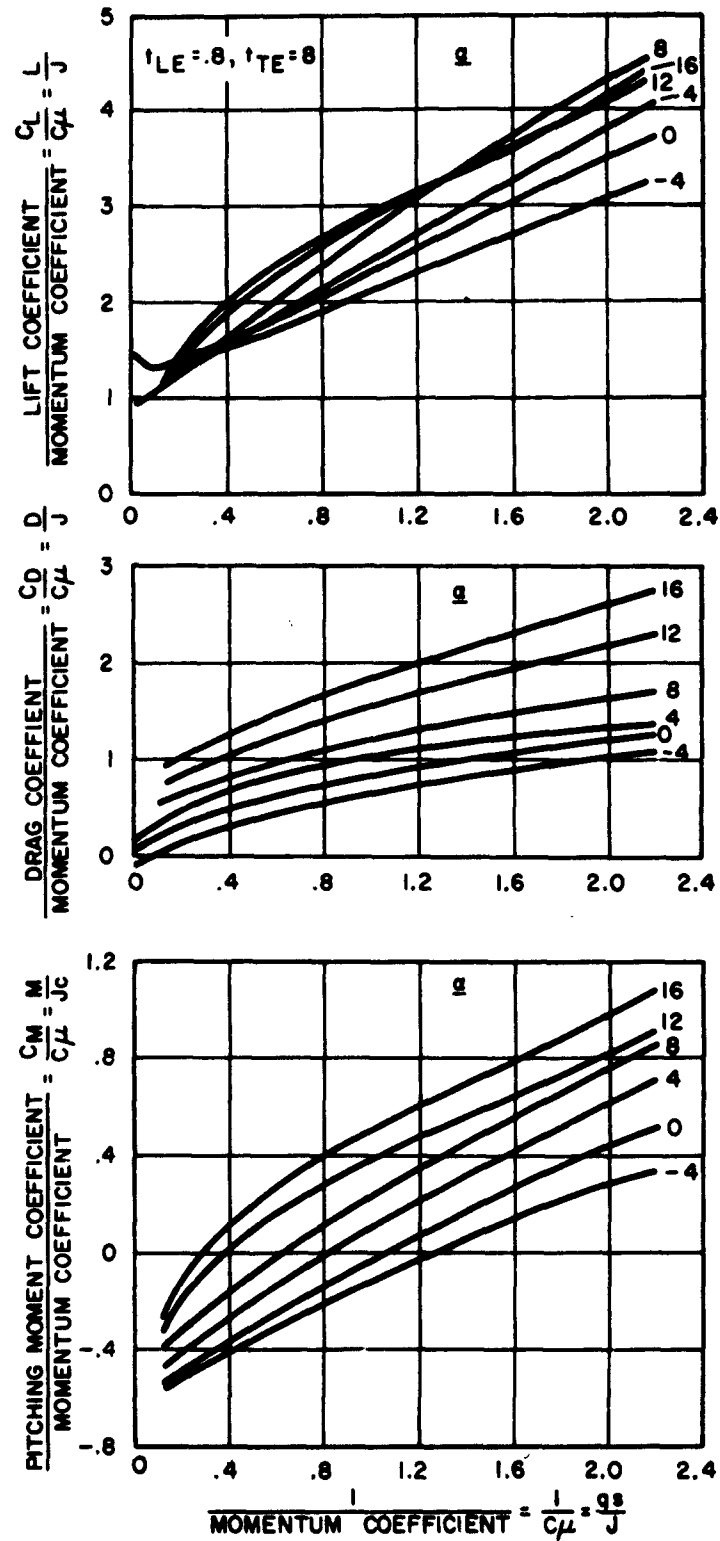


Figure 191. Configuration No. 20,  $\theta_F = 0^\circ$ ,  $\theta_R = -30^\circ$ ,  $h/c = .33$

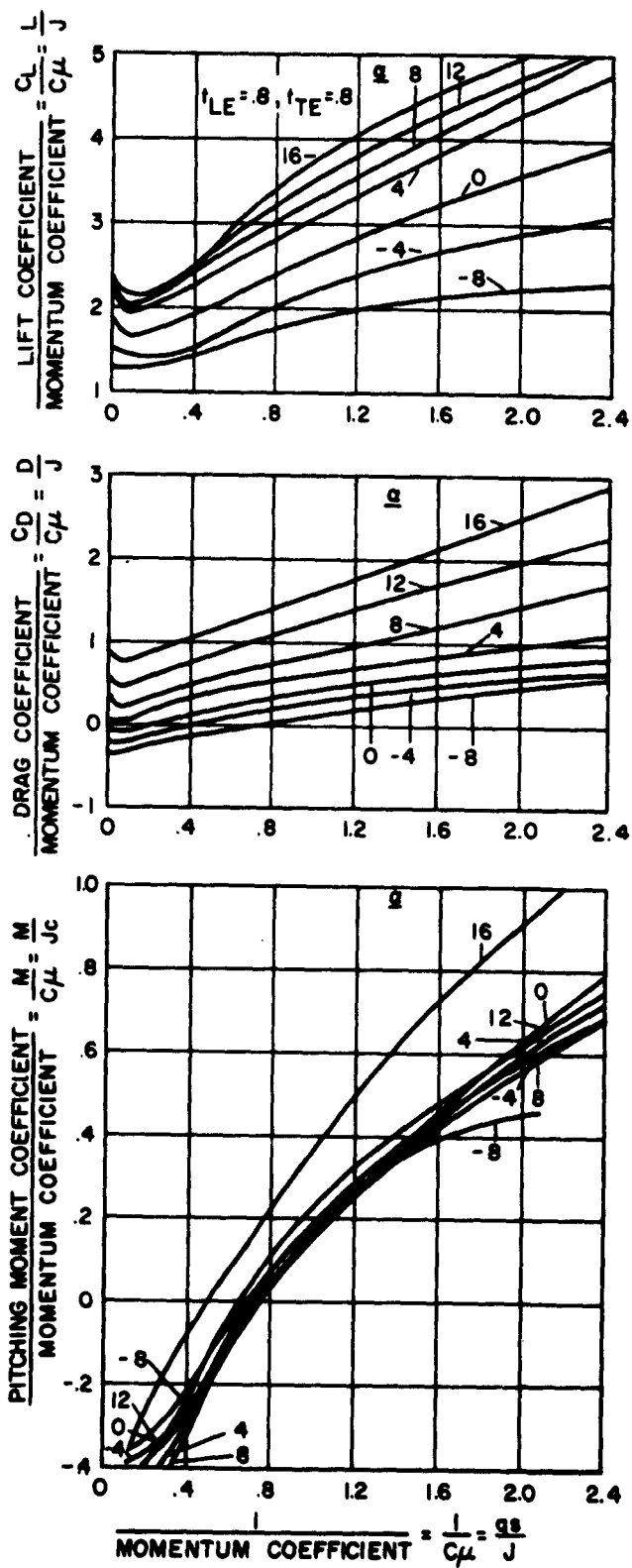


Figure 192. Configuration No. 2,  $\theta_F = -30^\circ$ ,  $\theta_R = -30^\circ$ ,  $h/c = .20$

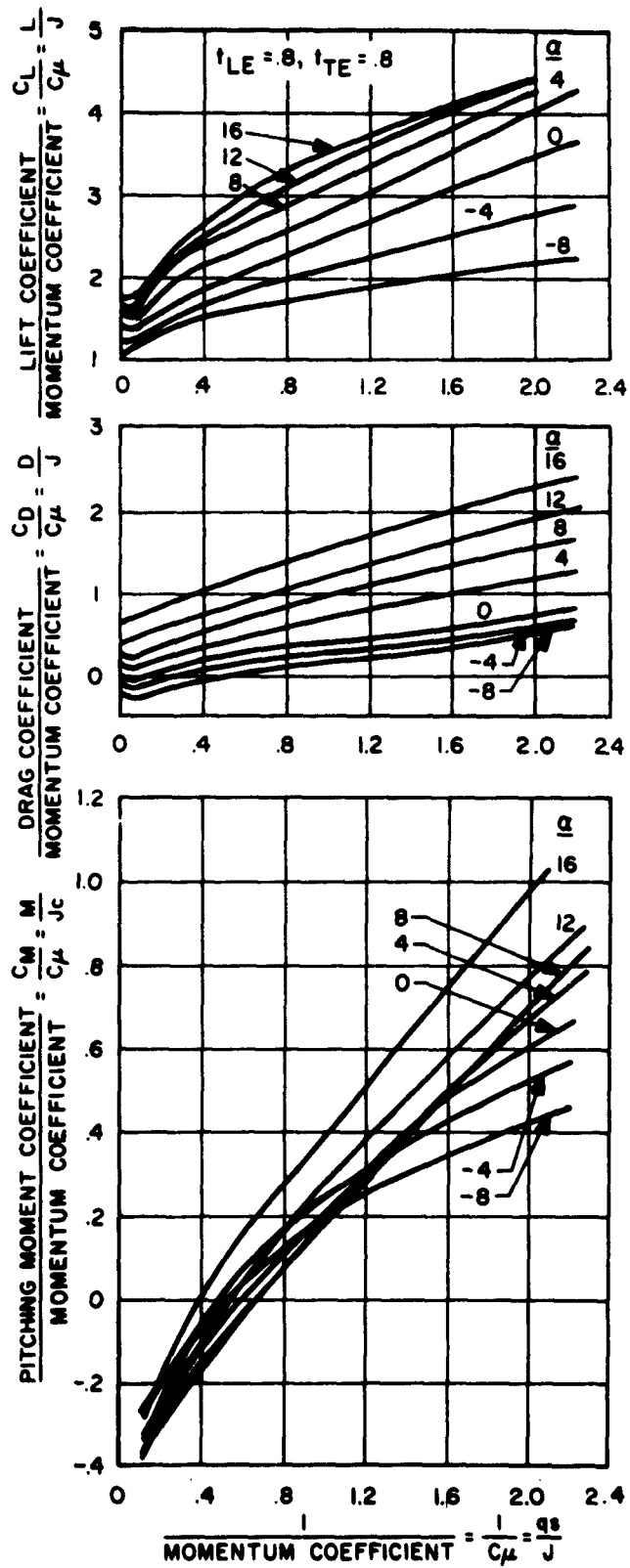


Figure 193. Configuration No. 1,  $\theta_F = -30^\circ$ ,  $\theta_R = -30^\circ$ ,  $h/c = .33$

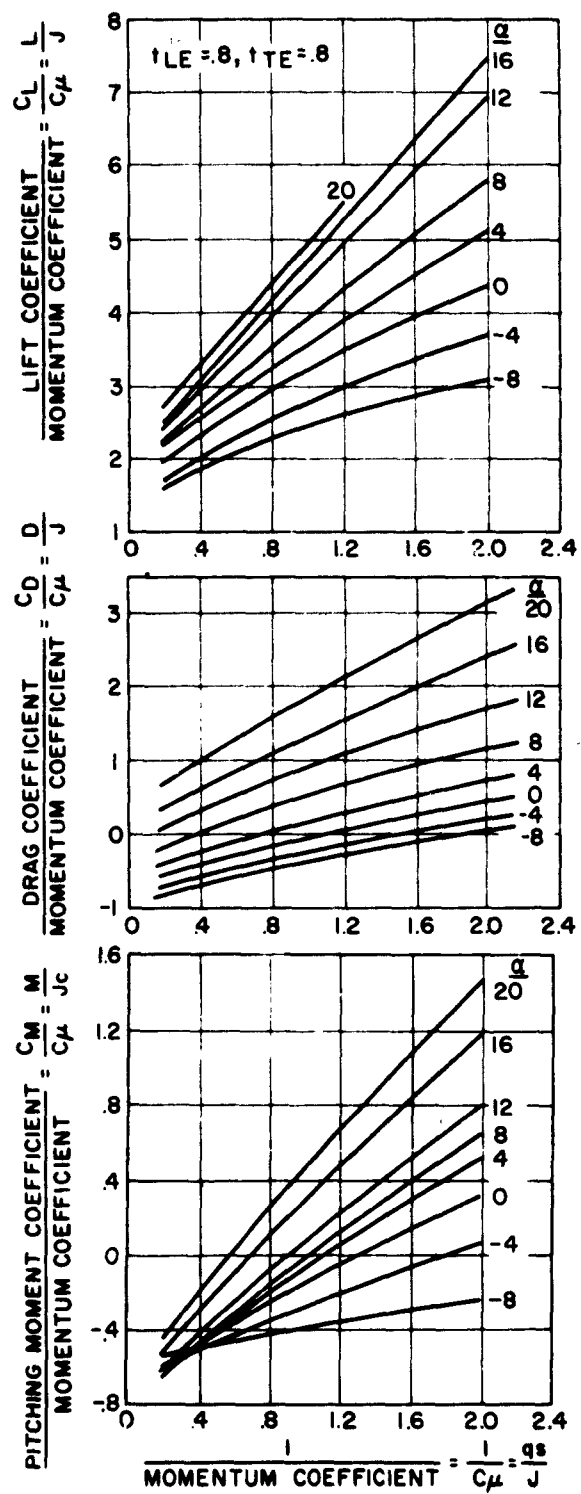


Figure 194. Configuration No. 4,  $\theta_F = -30^\circ$ ,  $\theta_R = -30^\circ$ ,  $h/c = .33$

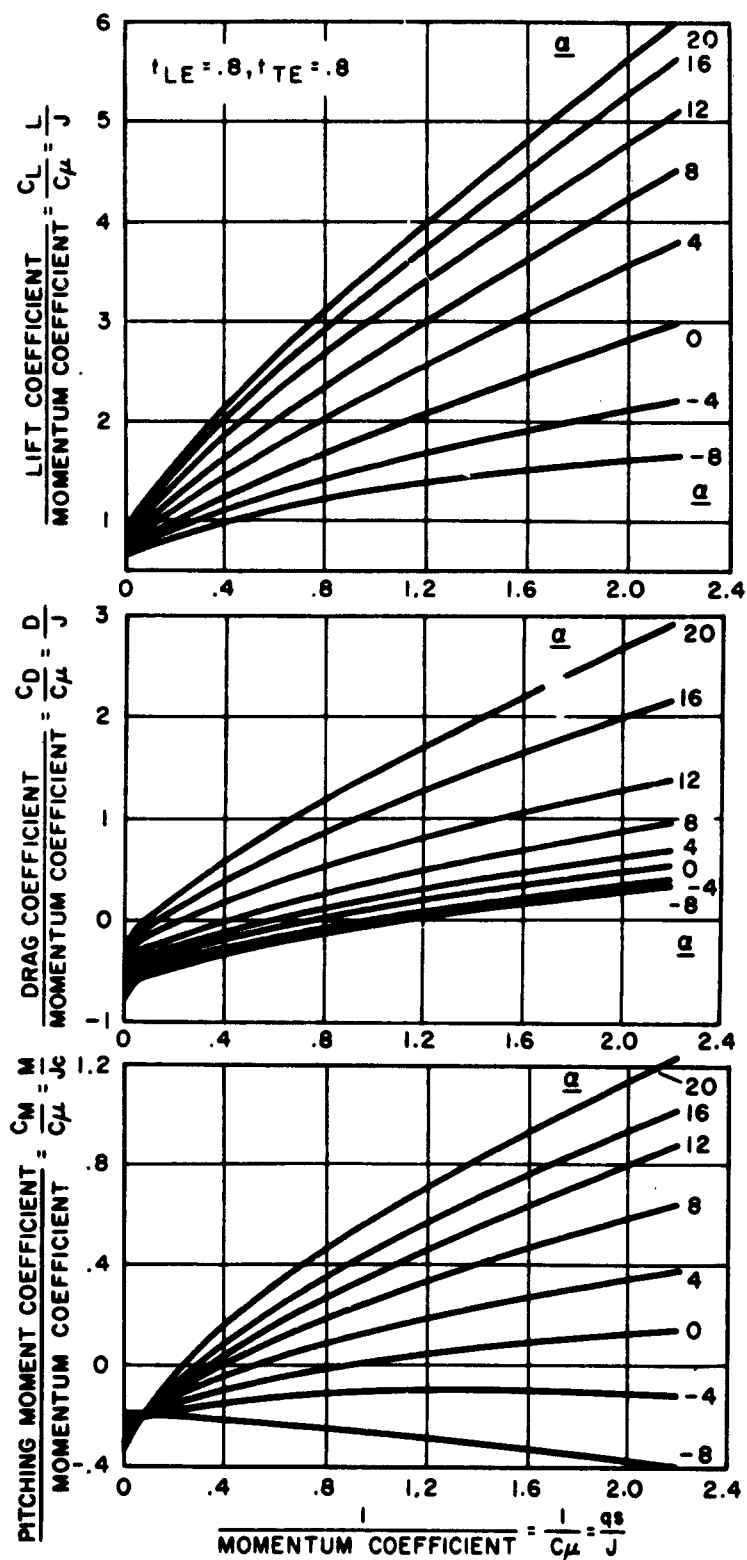


Figure 195. Configuration No. 5,  $\theta_F = -30^\circ$ ,  $\theta_R = -30^\circ$ ,  $h/c = .33$

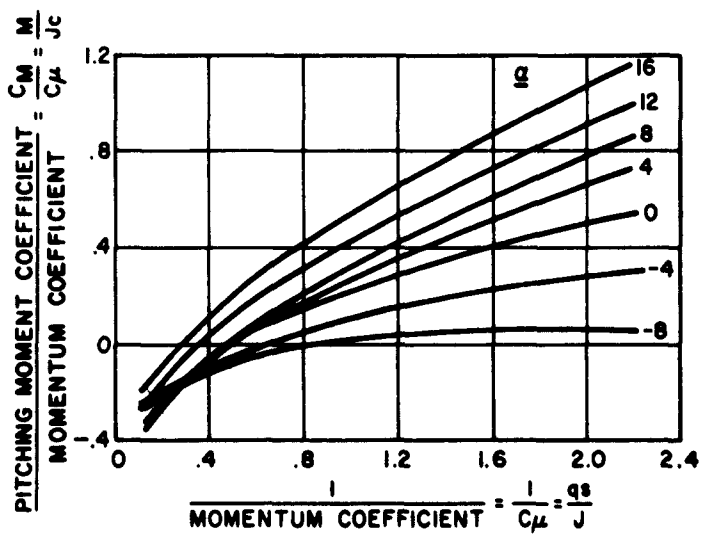
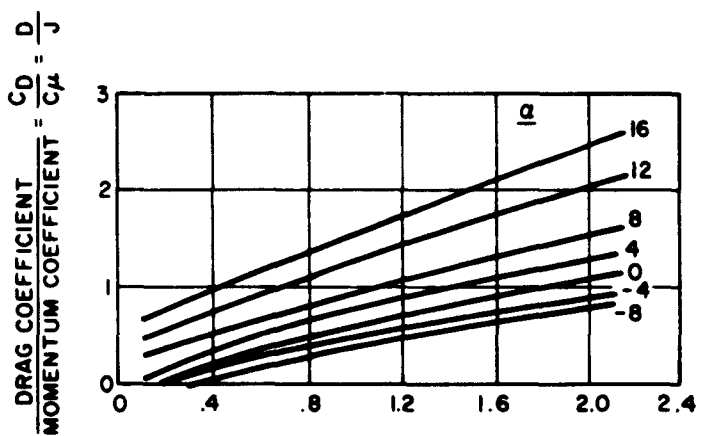
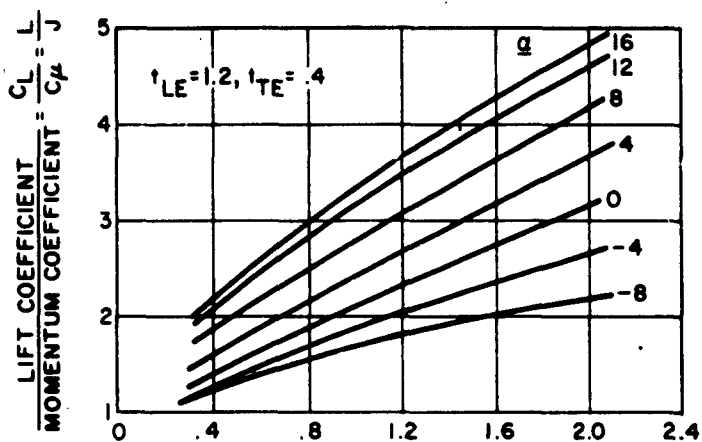


Figure 196. Configuration No. 13,  $\theta_F = -30^\circ$ ,  $\theta_R = -30^\circ$ ,  $h/c = .33$

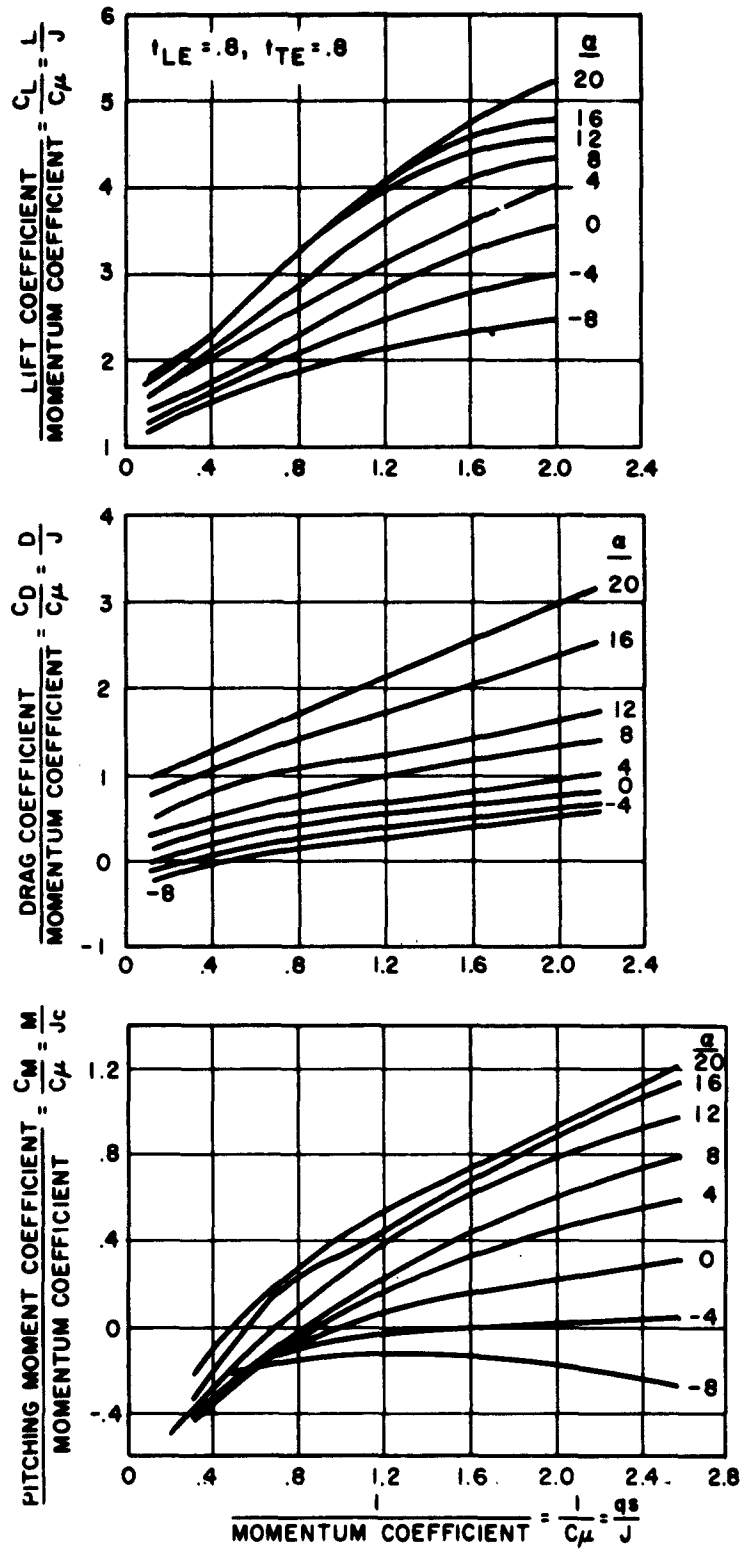


Figure 197. Configuration No. 28,  $\theta_F = -30^\circ$ ,  $\theta_R = -30^\circ$ ,  $h/c = .33$

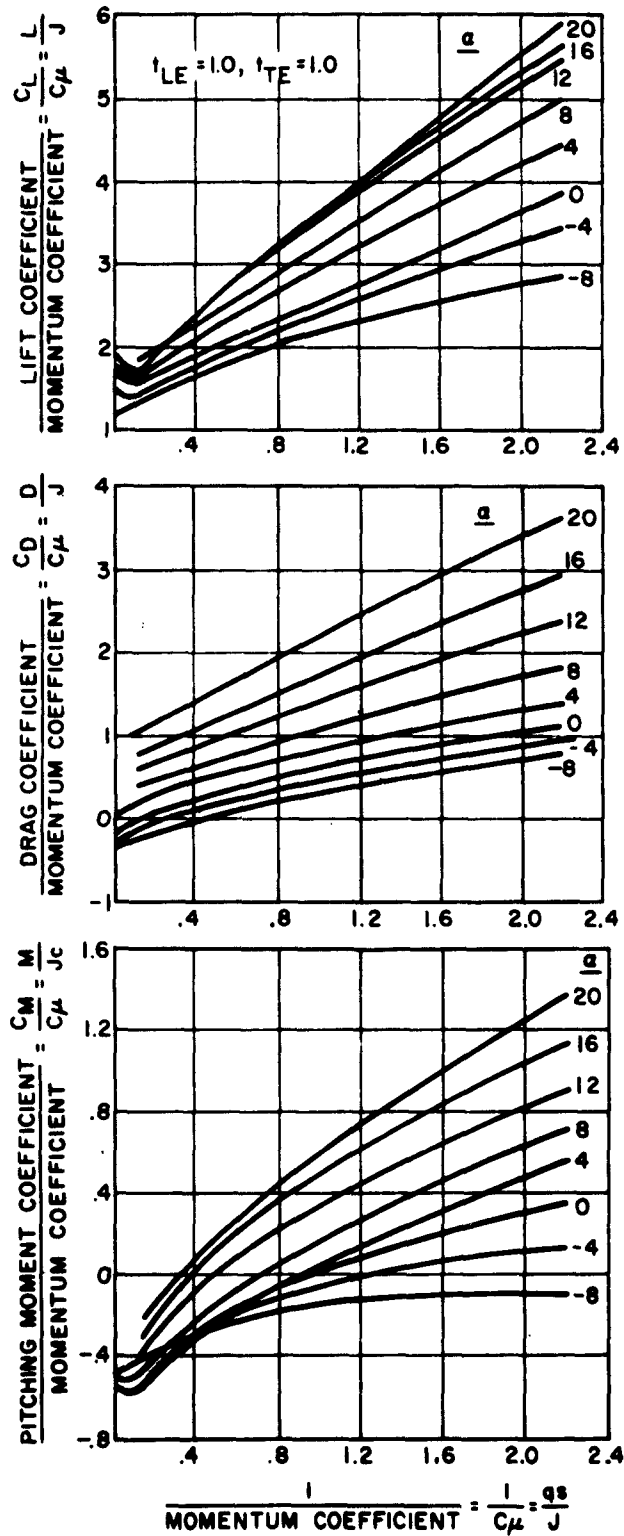
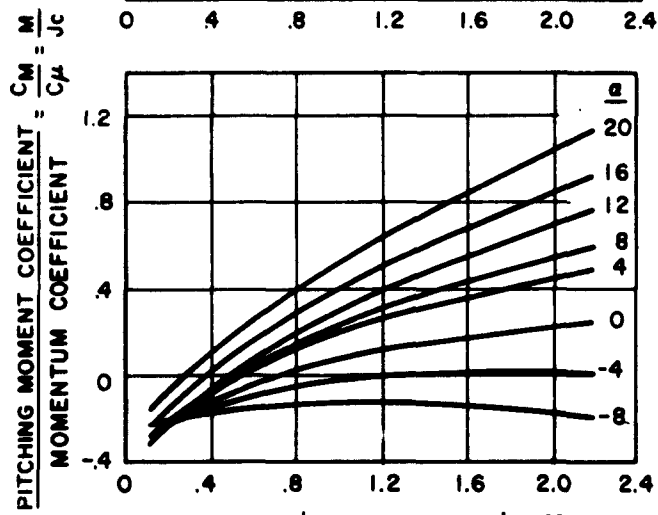
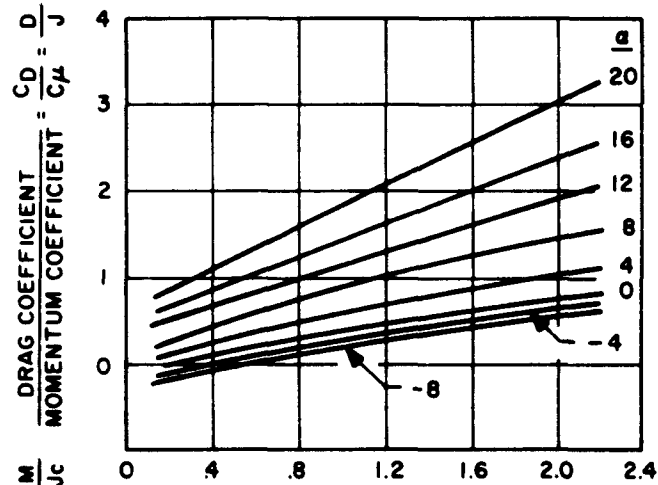
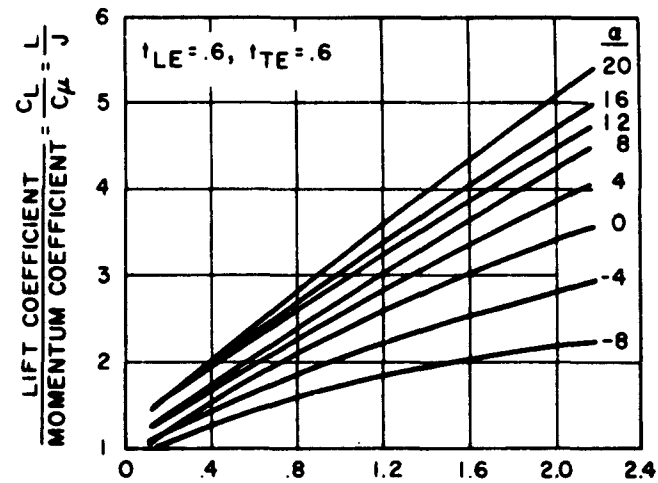


Figure 198. Configuration No. 29,  $\theta_F = -30^\circ$ ,  $\theta_R = -30^\circ$ ,  $h/c = .33$



$$\frac{1}{\text{MOMENTUM COEFFICIENT}} = \frac{1}{C_\mu} = \frac{qs}{J}$$

Figure 199. Configuration No. 30,  $\theta_F = -30^\circ$ ,  $\theta_R = -30^\circ$ ,  $h/c = .33$

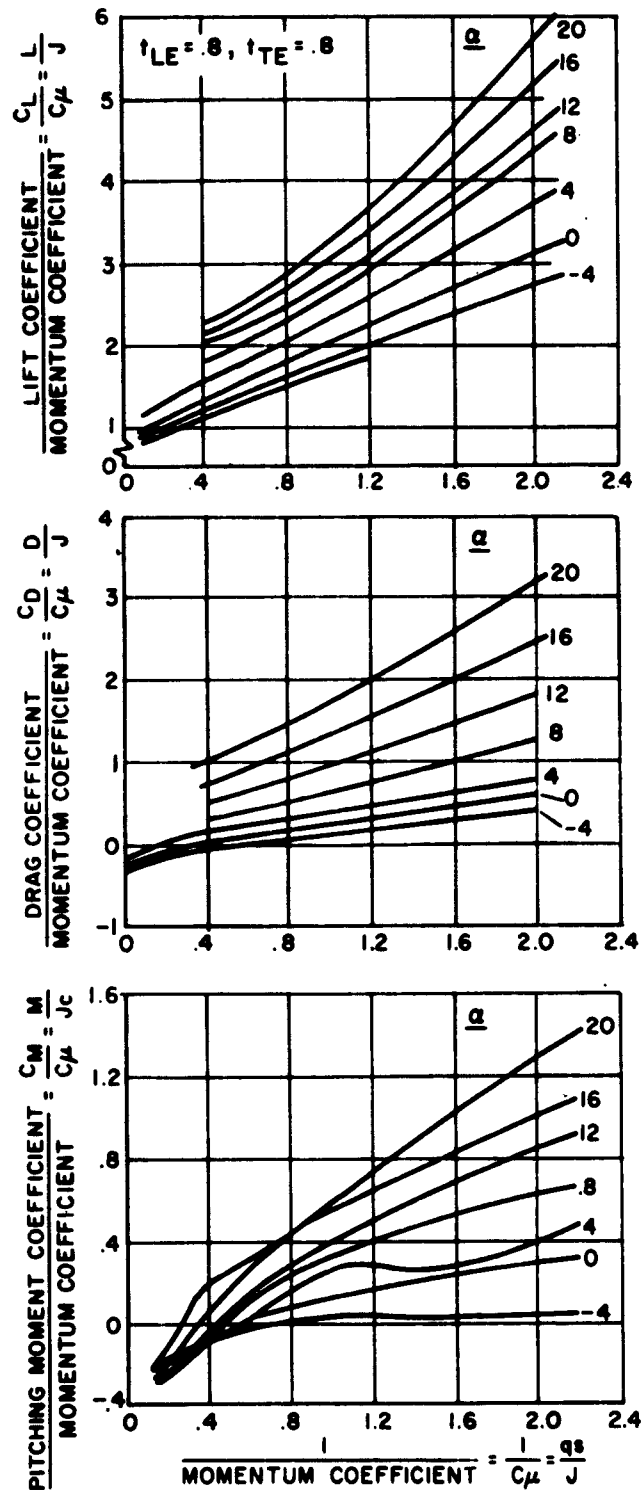


Figure 200. Configuration No. 31,  $\theta_F = -30$   $\theta_R = -30$ ,  $h/c = .33$

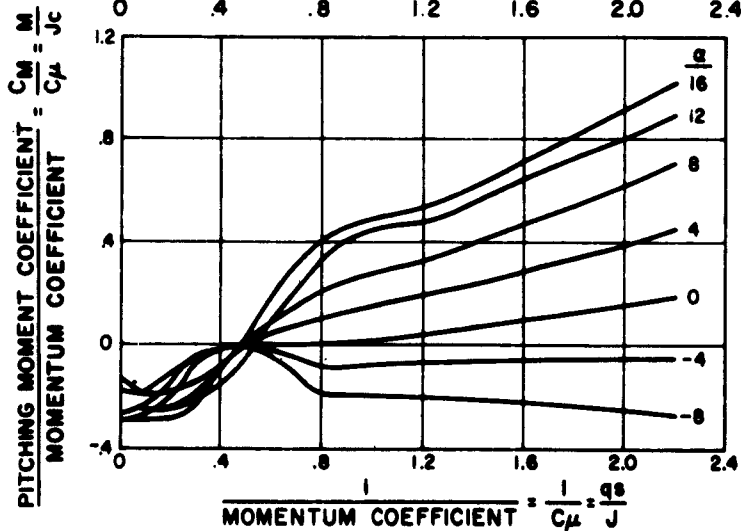
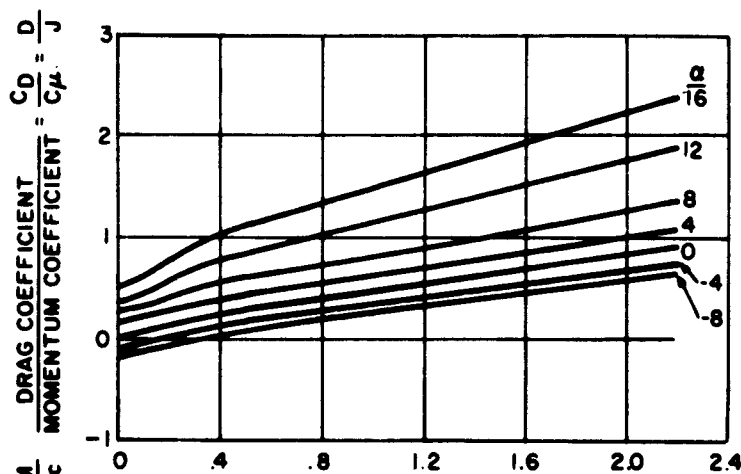
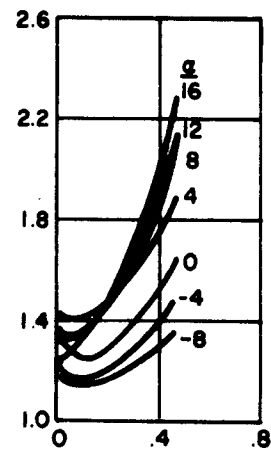
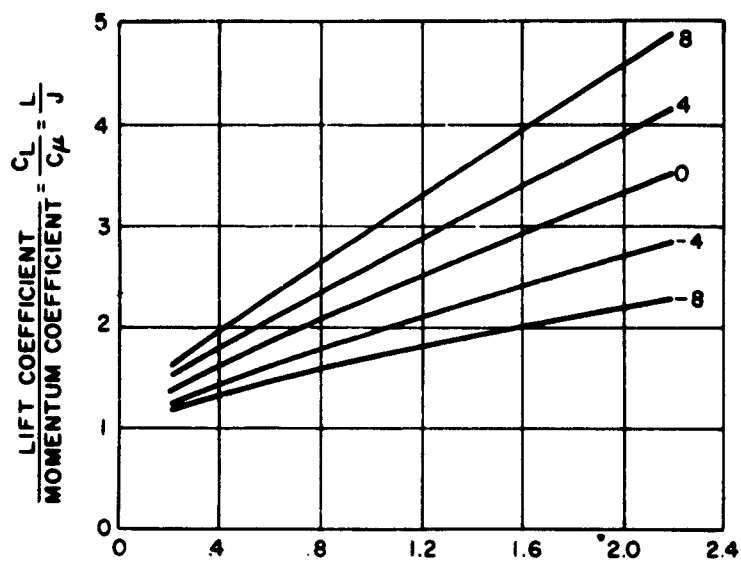


Figure 201. Configuration No. 3,  $\theta_F = -30^\circ$ ,  $\theta_R = -30^\circ$ ,  $h/c = .50$



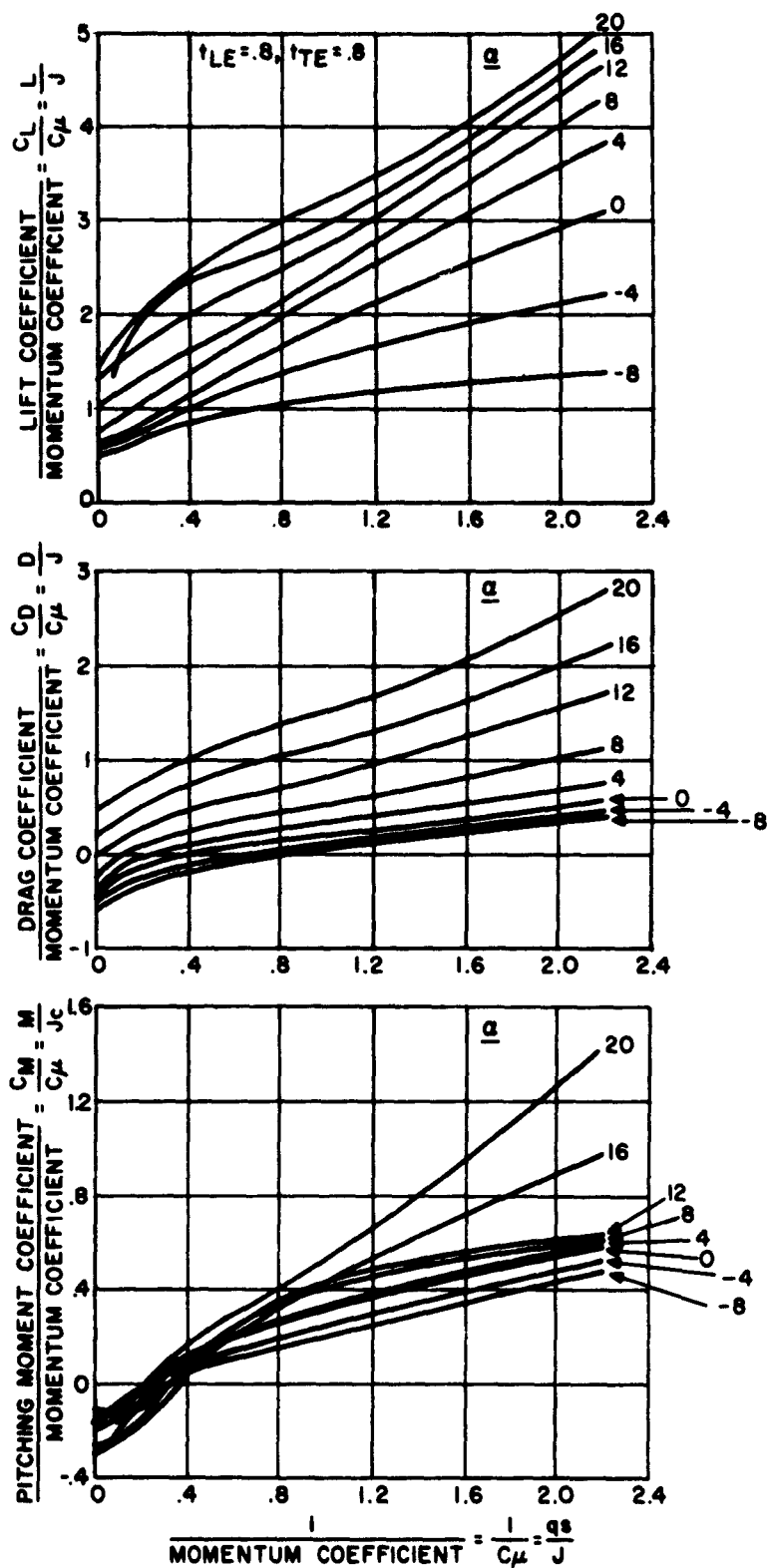


Figure 203. Configuration No. 8,  $\theta_F = -30^\circ$ ,  $\theta_R = +30^\circ$ ,  $h/c = .33$

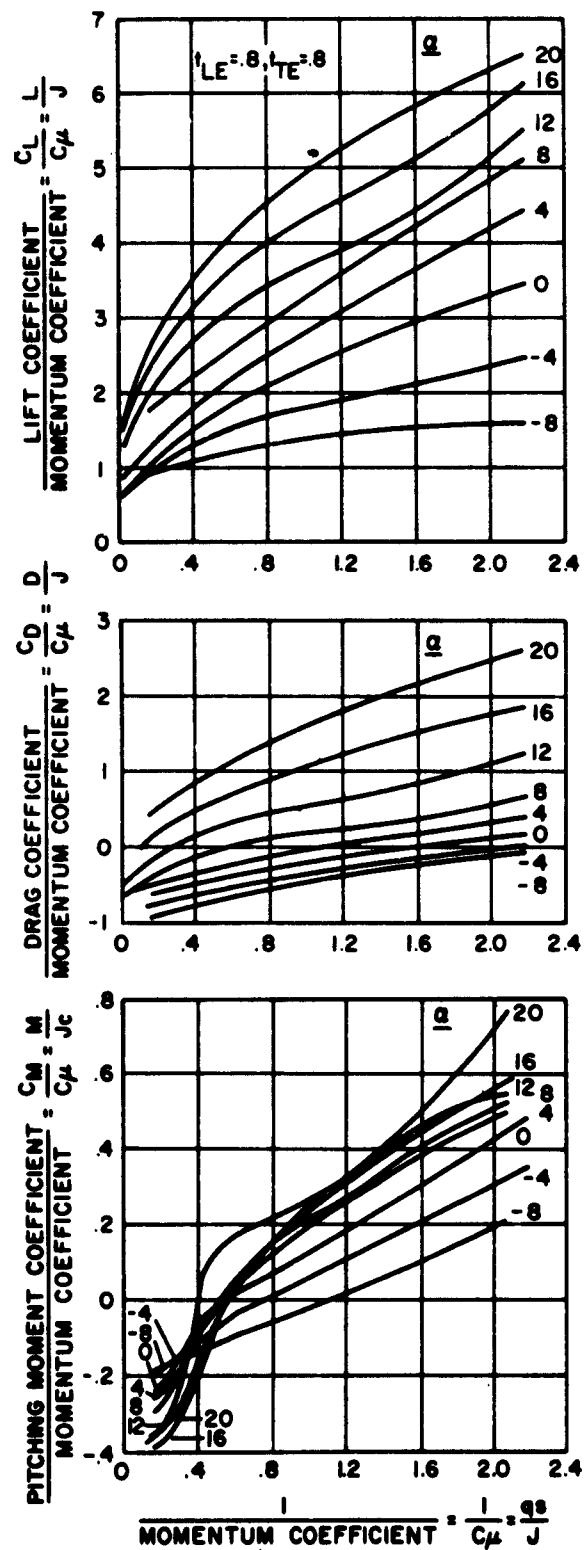


Figure 204. Configuration No. 10,  $\theta_F = -30^\circ$ ,  $\theta_R = +30^\circ$ ,  $h/c = .33$

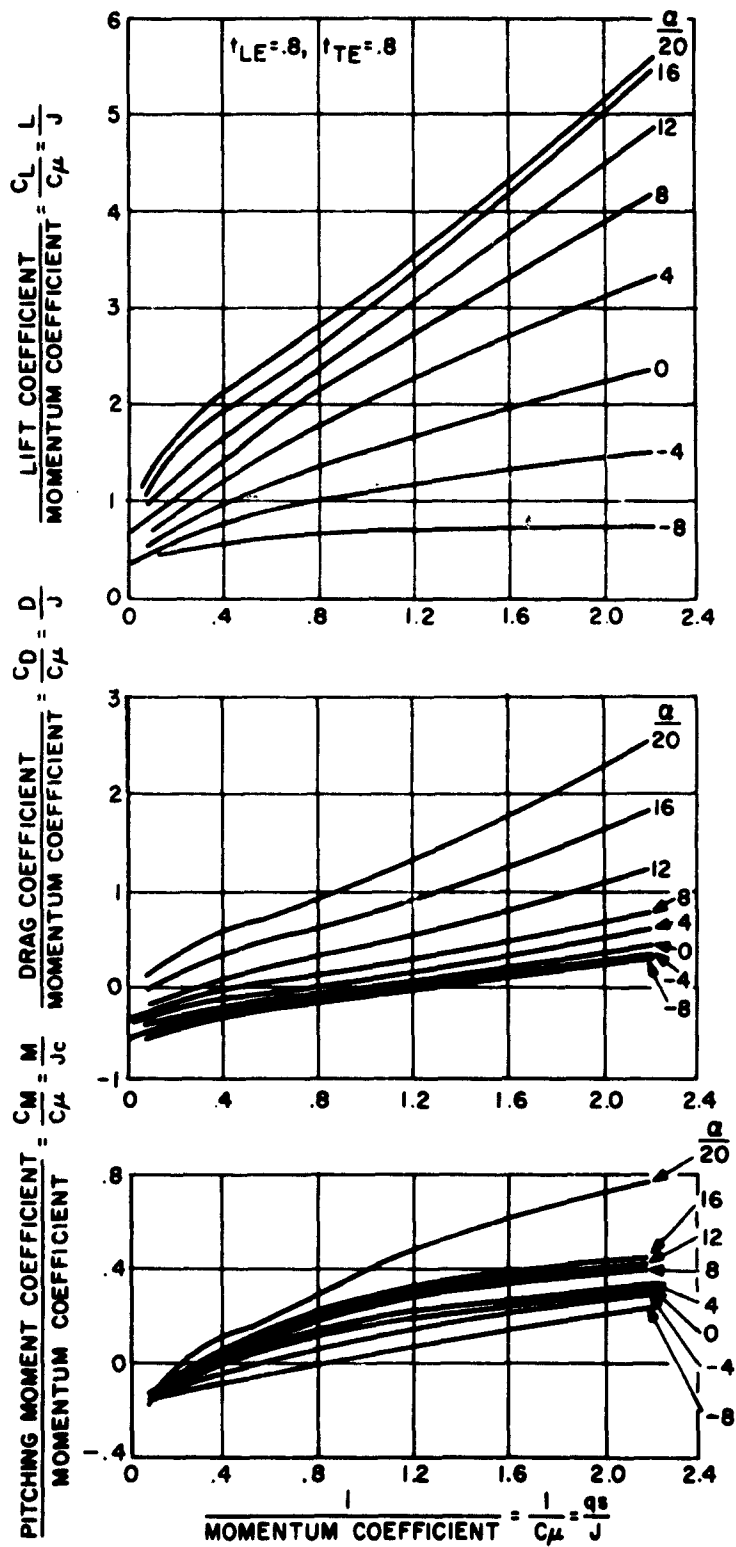


Figure 205. Configuration No. 11,  $\theta_F = -30^\circ$ ,  $\theta_R = +30^\circ$ ,  $h/c = .33$

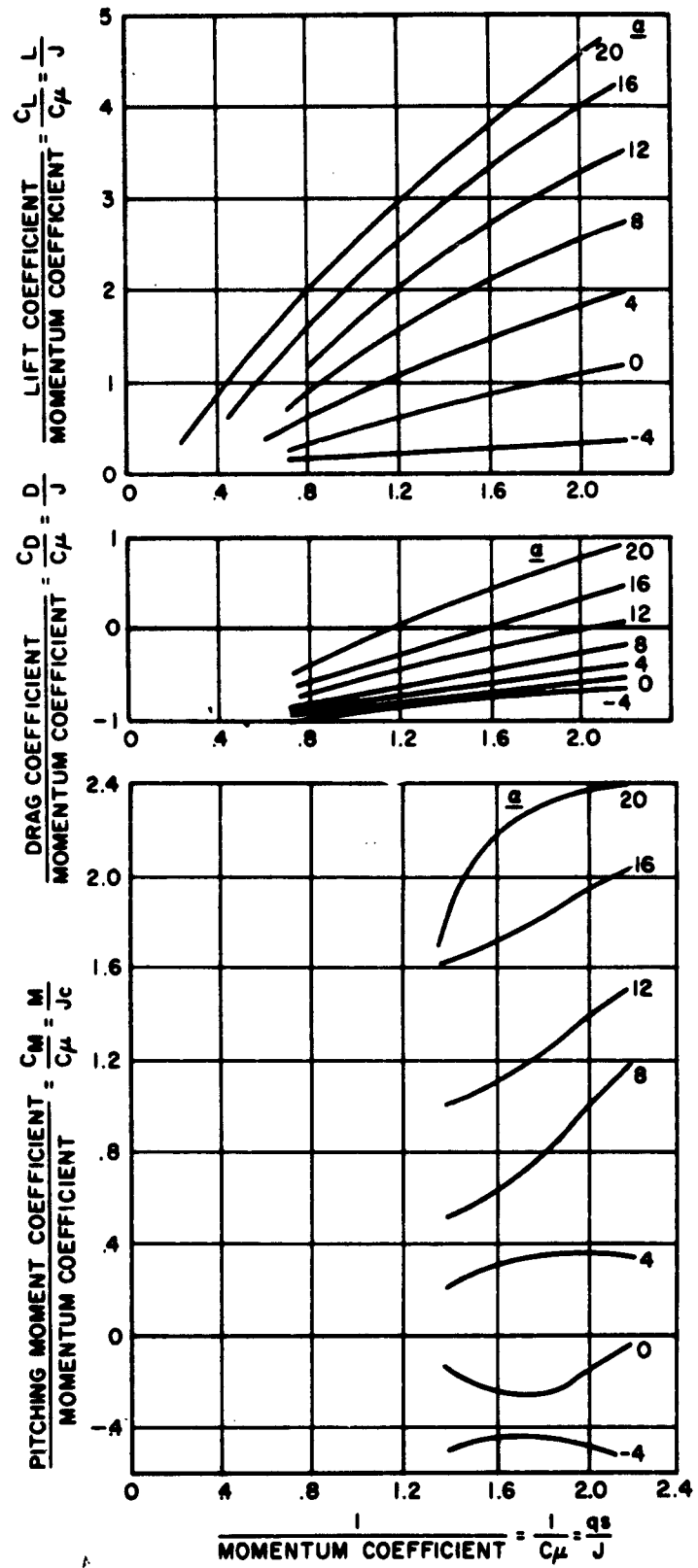


Figure 206. Configuration No. 14,  $\theta_F = -\theta_R = -$ ,  $h/c = \infty$

## APPENDIX D

### MOVING MODEL TEST RESULTS (NASA TRACK DATA)

Appendix D includes the data obtained from development testing performed at the NASA track facility (See Volume I, Page 74). The method of presentation used in Figures 207 to 211 of Appendix D consists of plotting the variation of the conventional aerodynamic coefficients divided by the momentum coefficient for specific angles of attack.

This development testing was performed without the honeycomb flow straighteners behind the fan. As a result, this altered the flow distribution within the model which in turn rendered the resultant data questionable. Specifically, there was a disparity between the flow distribution across the measuring station and the basic distribution obtained in the static room. This factor prevented a simple integration of the flow.

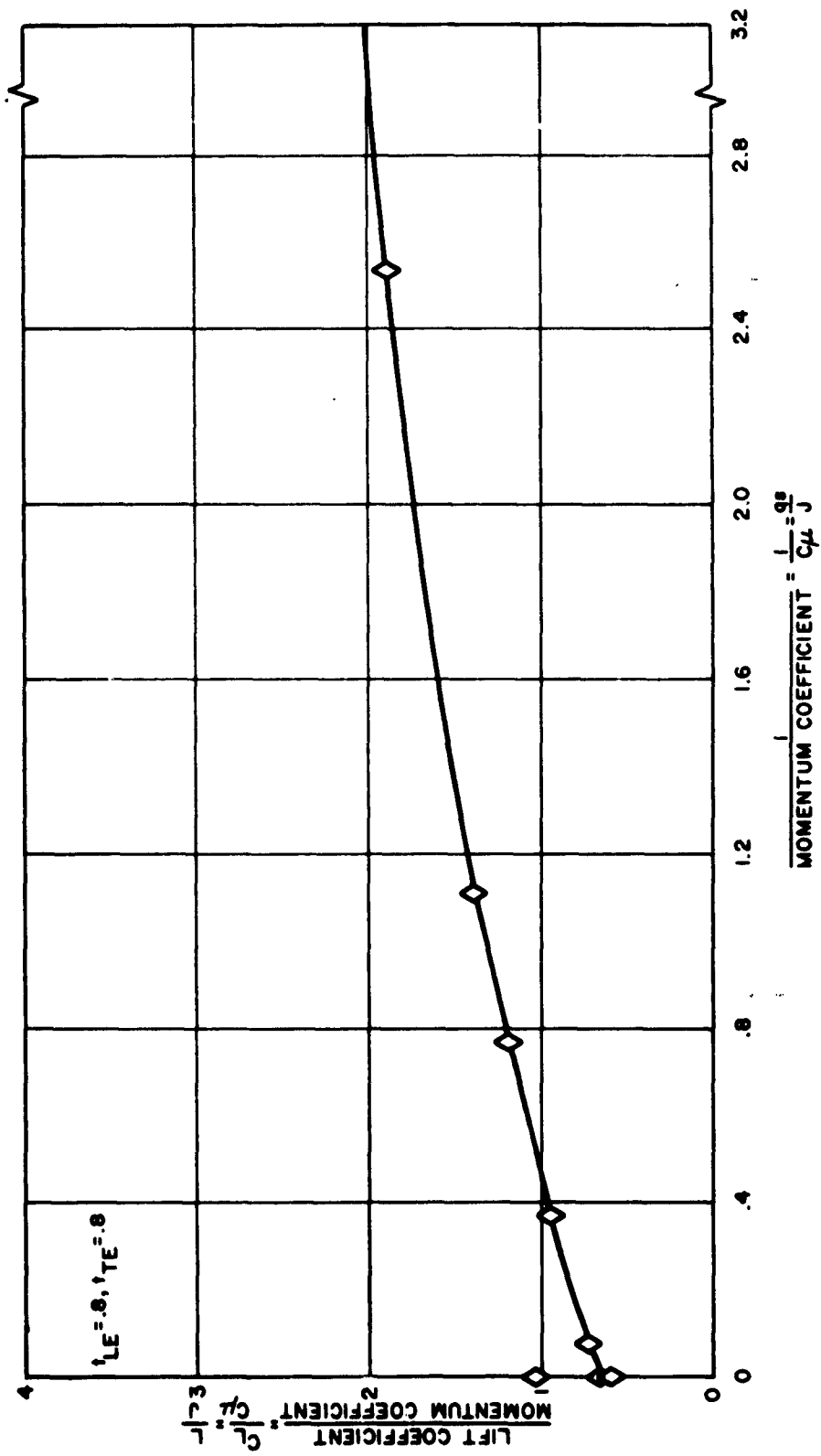


Figure 207. Configuration No. 70,  $\theta_F = -30$ ,  $\theta_R = +30$ ,  $h/c = \infty$

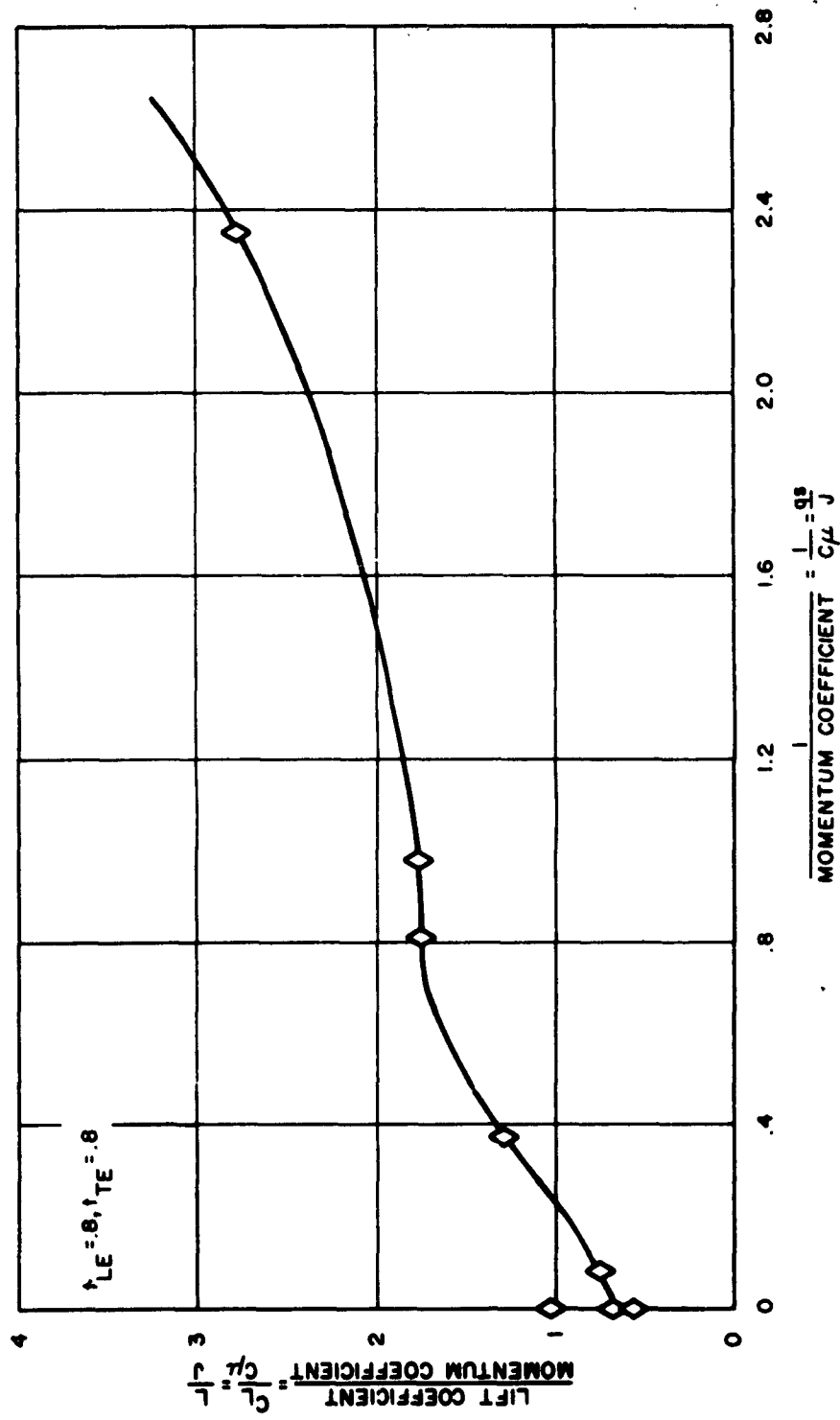


Figure 208. Configuration No. 35,  $\theta_F = -30$ ,  $\theta_R = +30$ ,  $h/c = .33$

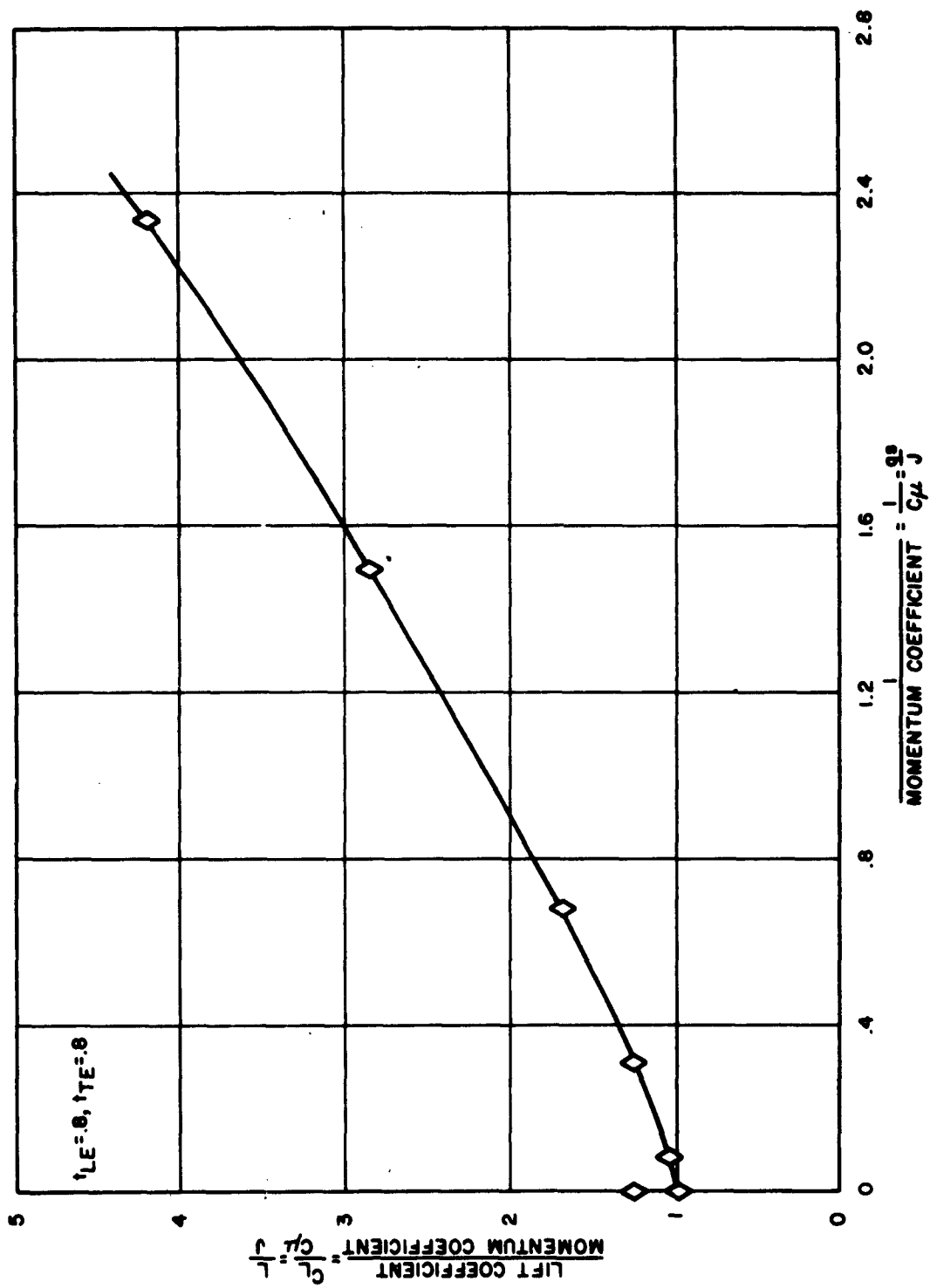


Figure 209. Configuration No. 28,  $\theta_F = -30^\circ$ ,  $\theta_R = -30^\circ$ ,  $h/c = .33$

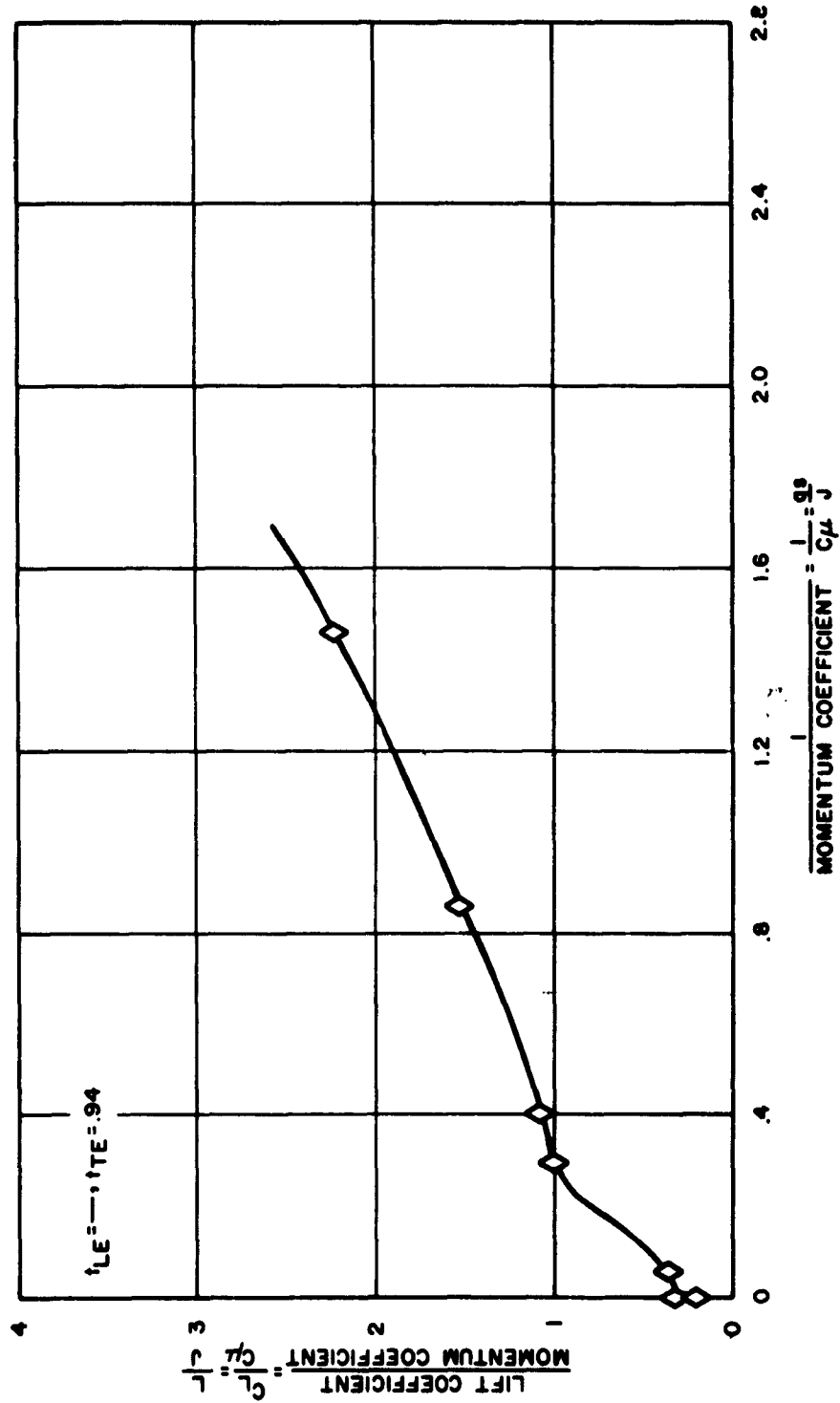


Figure 210. Configuration No. 37,  $\theta_F = \theta_R = +30$ ,  $h/c = .33$

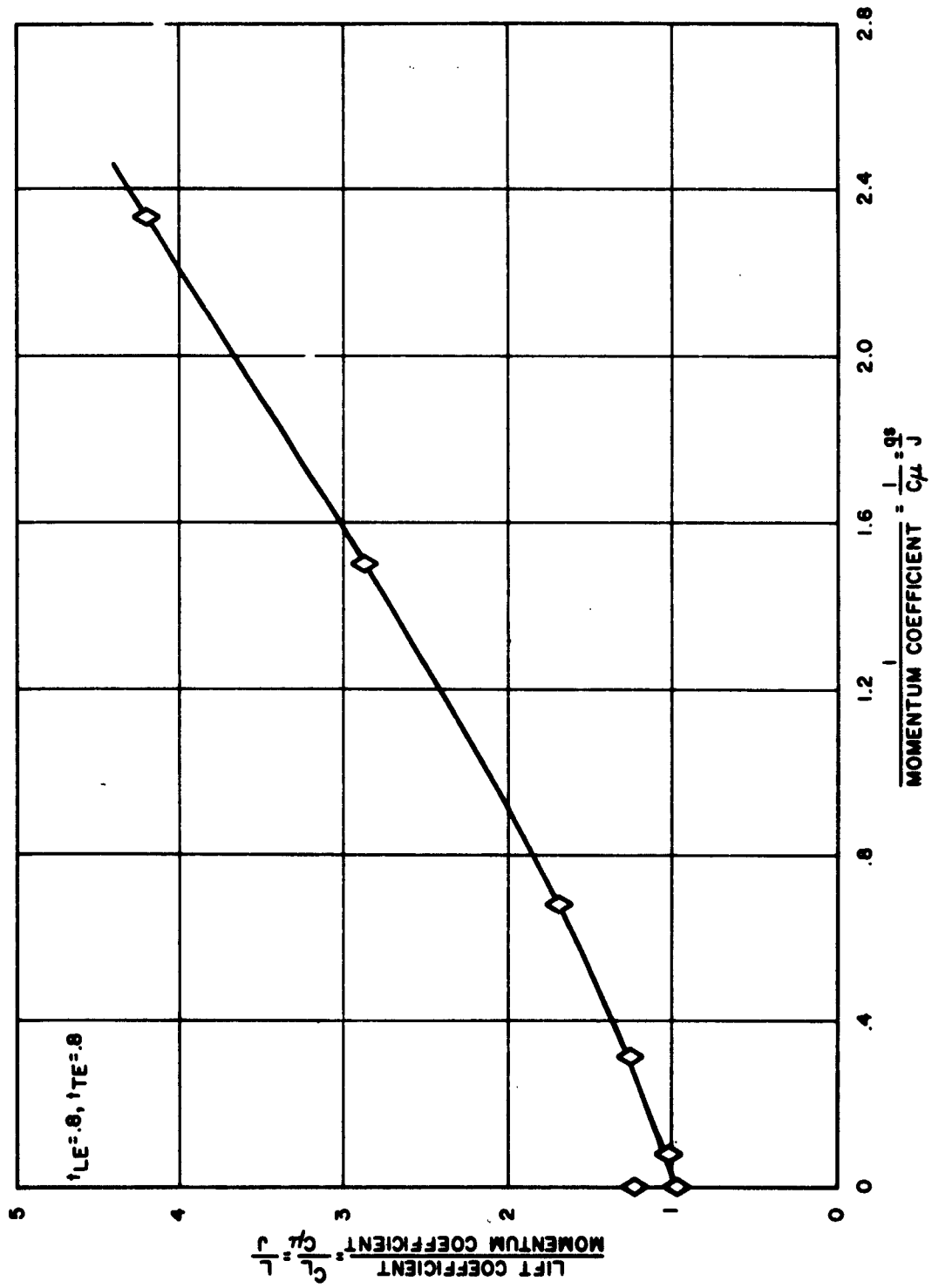


Figure 211. Configuration No. 31,  $\theta_F = -30$ ,  $\theta_R = -30$ ,  $h/c = .33$

APPENDIX E

UNIVERSITY OF TORONTO DYNAMIC MODEL DATA

PART I

Research on the Dynamics of an Airplane Flying  
in the "Ground Cushion"

by

G. Kurylowich

R. C. Radford

B. Etkin

PREFACE

In response to a proposal entitled "Proposal for Research on the Dynamics of an Airplane Flying in the Ground Cushion" by B. Etkin, dated Jan. 11, 1961, the Vertol Division of the Boeing Airplane Company made available the sum of \$5000 to the University of Toronto for research in the indicated area. (Order No. 96-54391.)

This report, together with Ref. 1, are submitted in compliance with the terms of the contract, as the final report required.

## I. INTRODUCTION

A self-propelled GETOL model similar in concept to the Vertol drawings supplied was constructed and flown over the UTIA 20 ft. diameter track to determine the feasibility of this means of testing, and to obtain any results possible. The tests proved successful and are described in detail in Ref. 1. Some of the data obtained is reproduced from that report in Section III herein.

In addition to the work reported in Ref. 1, a program of static tests was undertaken to determine the velocity distribution of the air issuing from the peripheral jet slots of the model. This was accomplished by mounting the model in a test rig while a total pressure traverse of the slots was made. These results are presented in Section II. Additional related information derived from wind-tunnel tests of a rectangular wing of aspect ratio 4 is in process of publication (Ref. 2).

## II. VELOCITY DISTRIBUTION OF THE ANNULAR JET

The annular jet of the Vertol model was investigated with pressure probes to obtain the distribution of flow. In addition, the model was held over a ground board coated with lamp black and kerosene to obtain a visual picture of jet behaviour. This last test was conducted at a height of 1/8" above the ground board and is shown in Figure 213. The following is a summary of the test data obtained.

The pressure probing system used is shown in Figure 214. The model was attached to two Dexion sections which acted as tracks when the model-Dexion combination was placed on the guide rails. 18 shrouded pressure probes were attached, by means of plasticene, to the Dexion stand D such that these probes were approximately 1/32" below the undersurface of the model's wing. By moving the Dexion track-model combination over the guide rails, a pressure traverse was made at the positions shown in Figure 212. By this means, all traverses through the annular jet could be made within one minute of model running time. The pressure probes were connected to a manometer board, inclined at a 45° angle, which was photographed to produce the records.

The pressure readings are presented in Table I, while Figure 215 to Figure 219 inclusive are the graphical presentation of  $V^2$  through the annular jet. Figures 220 and 221 is a cross-plot of Figures 215 to 219 and shows the span-wise variation of  $V^2$  (proportional to jet momentum flux) at  $d/G = .2, .4, .6, \text{ and } .8$ . A graphical integration of these curves then produced the total jet momentum flux and average velocity (see Appendix A).

## III. TEST FLIGHTS

The feasibility study of the track facility was accomplished by the analysis of 6 flights. Two of these were runs over a level track while the other four were for flights over ramps having 1/8", 1/4", and 1/2" maximum heights.

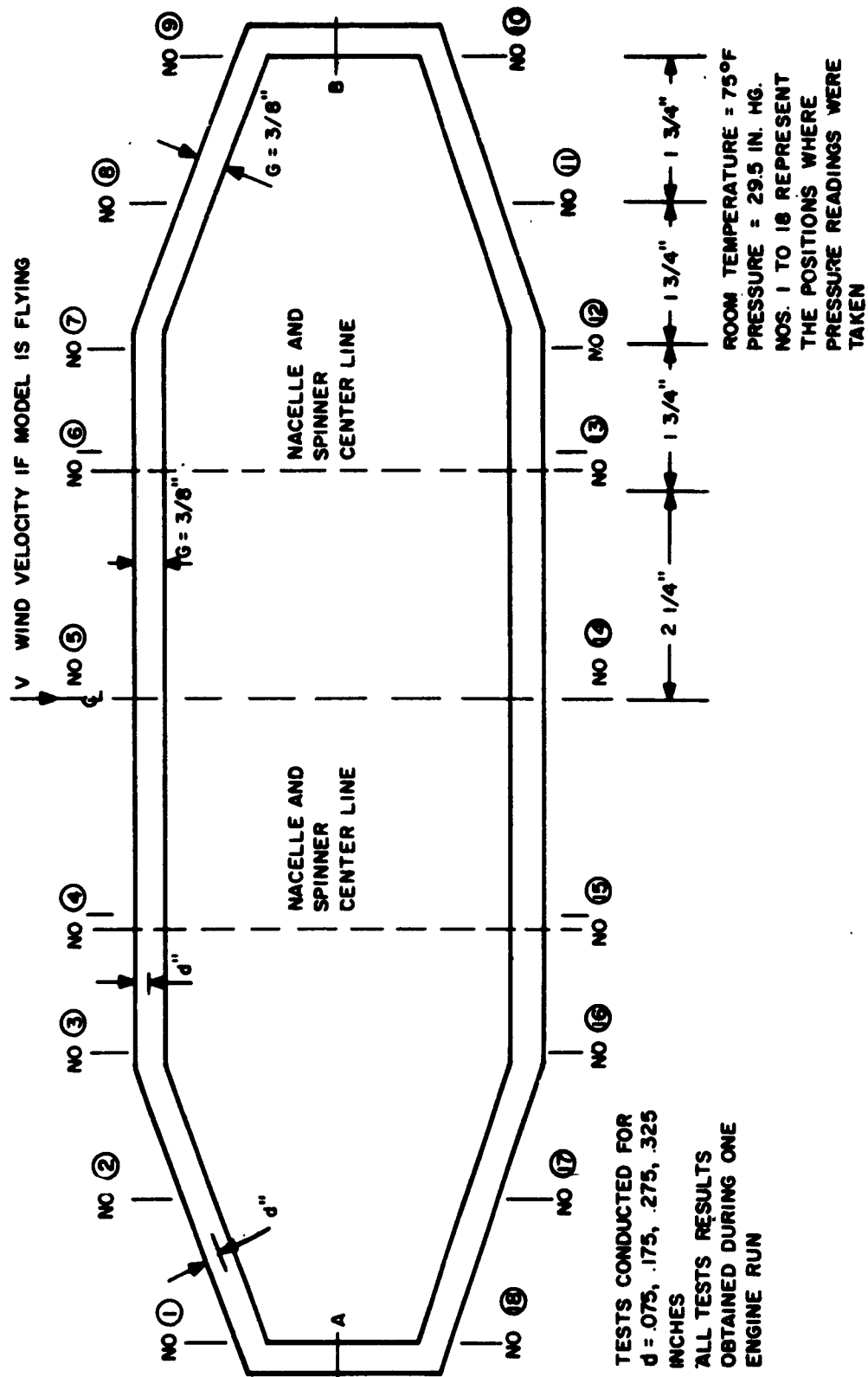


Figure 212. Probe Layout for Measuring Pressures

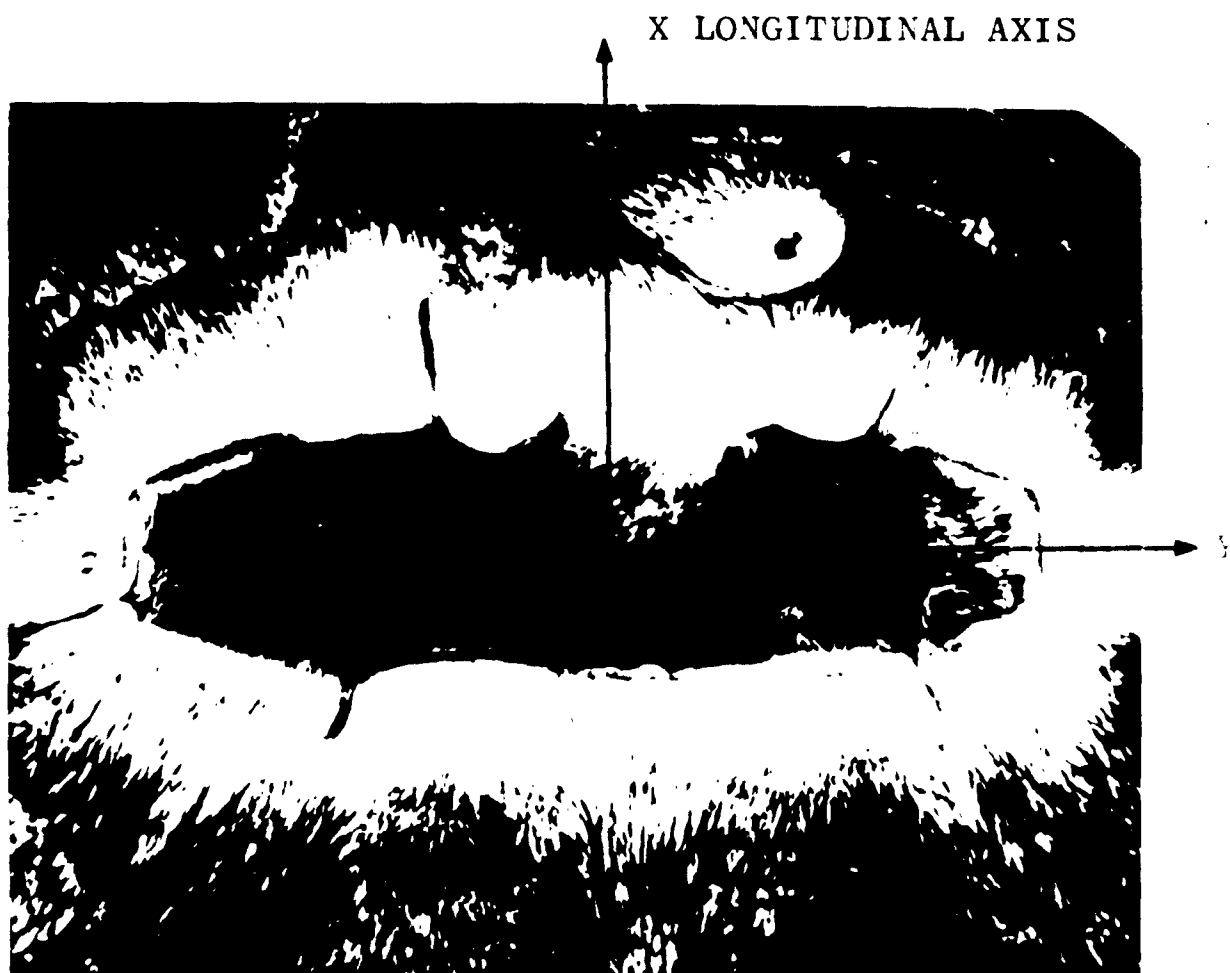


Figure 213. Flow Visualization Study (Height = 1/8 inch)

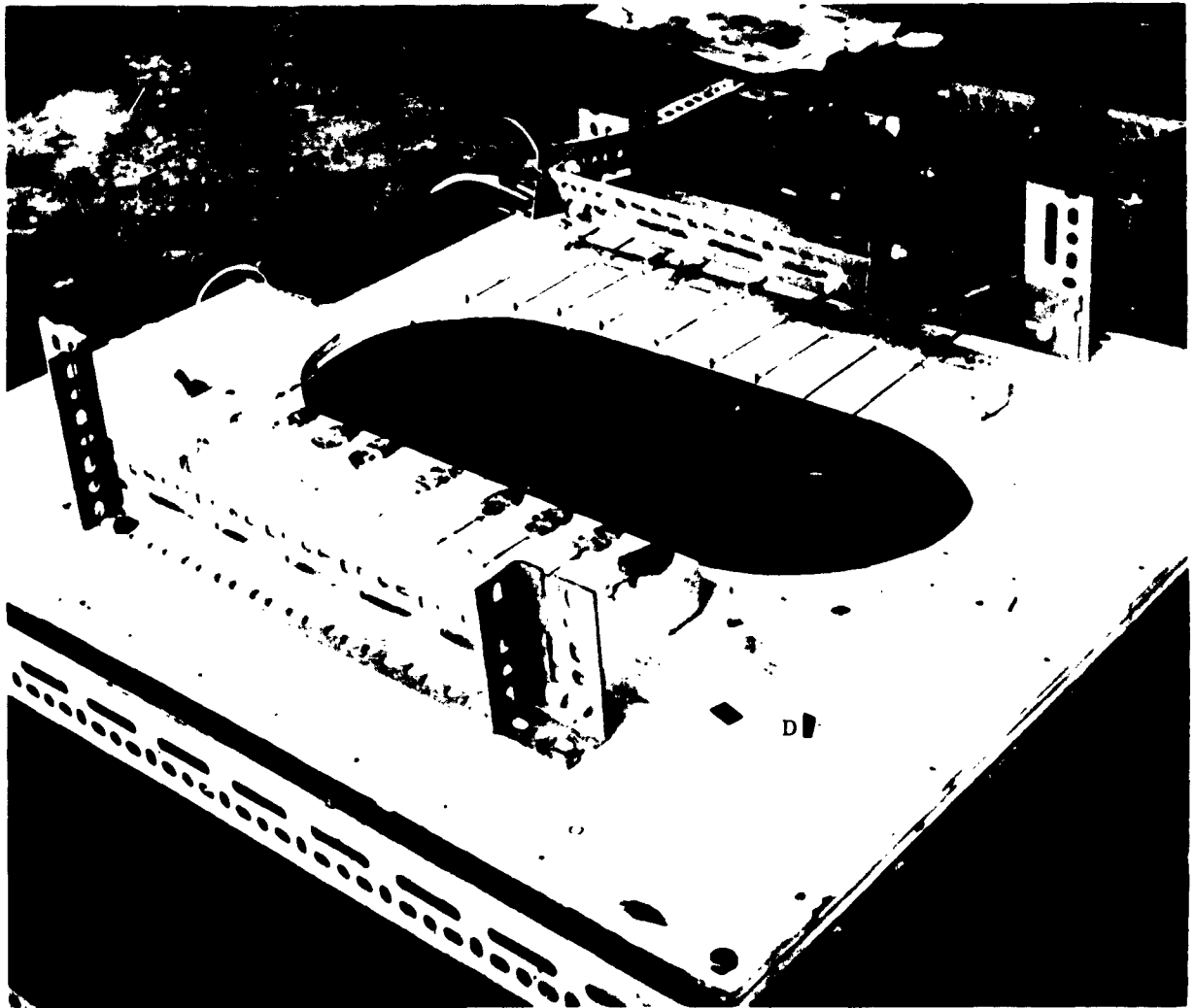


Figure 214. Static Test Rig

TABLE I  
PRESSURE READING DATA

$$\sqrt{2} \Delta p = \frac{(P_o - p)^2}{\sqrt{2}}$$

$$V^2 \text{ (ft/sec)}^2$$

TAP NO	.075''	.175''	.275''	.325''	.075''	.175''	.275''	.325''
1	.80	.90	1.00	2.05	2470	2680	3094	6350
2	0	.30	.70	1.75	0	927	2160	5410
3	0	.55	1.15	1.75	0	1700	3560	5410
4	0	.60	1.45	2.40	0	1850	4480	7420
5	0	.25	.70	1.70	0	772	2160	5260
6	1.05	1.70	1.90	2.60	3250	5250	5880	8040
7	.10	1.40	1.40	1.05	309.4	4330	4330	3250
8	0	.15	.30	.60	0	464	928	1860
9	.2	0	.70	2.00	618.0	0	2160	6180
10	.9	.9	.20	0	2780	2780	619	0
11	1.10	1.15	.70	0	3400	3560	2160	0
12	1.65	1.80	1.85	1.65	5100	5560	5720	5100
13	.70	1.25	1.25	2.15	2160	3870	3870	6650
14	.60	.50	.60	.70	1860	1545	1860	2160
15	1.40	1.95	1.90	.80	4325	6020	5880	2470
16	1.30	1.40	1.20	1.00	4020	4320	3720	3094
17	.80	1.00	1.00	0	2470	3094	3094	0
18	.75	1.00	.70	0	2320	3094	2160	0
19	reference							
20	taps							

BY NUMERICAL INTEGRATION

$$J = .68 \text{ lbs}$$

$$V_{av} = 77.5' / \text{sec. (r.m.s.)}$$

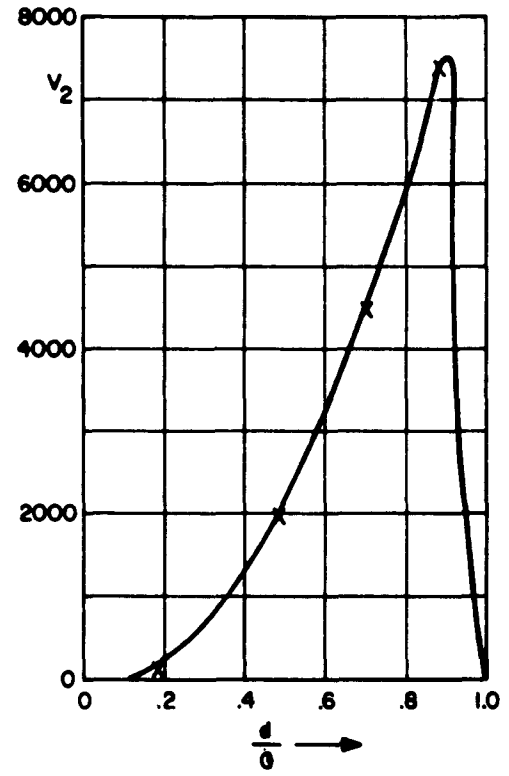
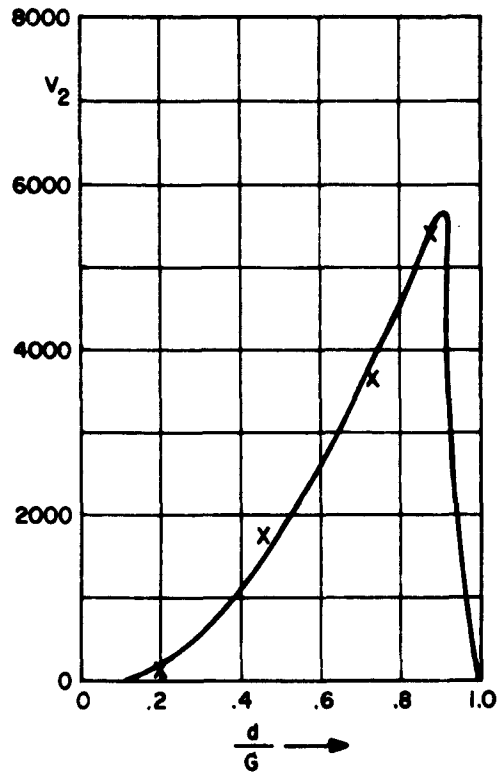
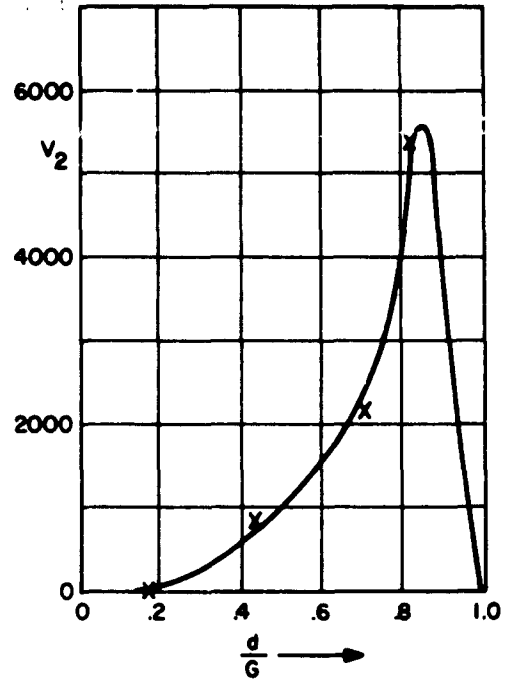
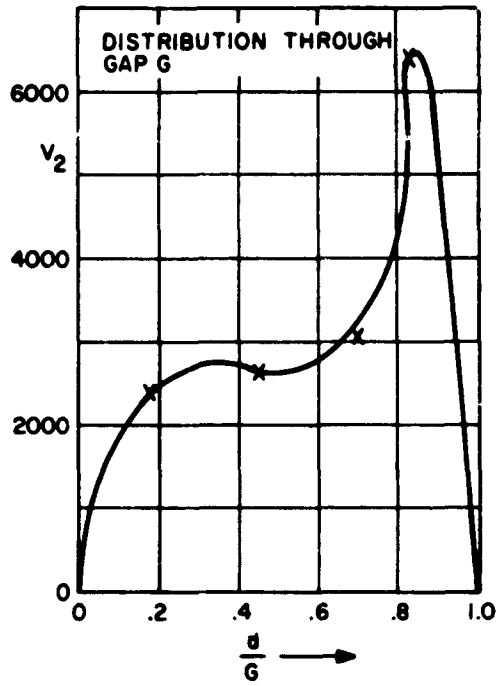


Figure 215. Presentation of  $V^2$  through the Annular Jet  
(Graphs No. 1, 2, 3 and 4)

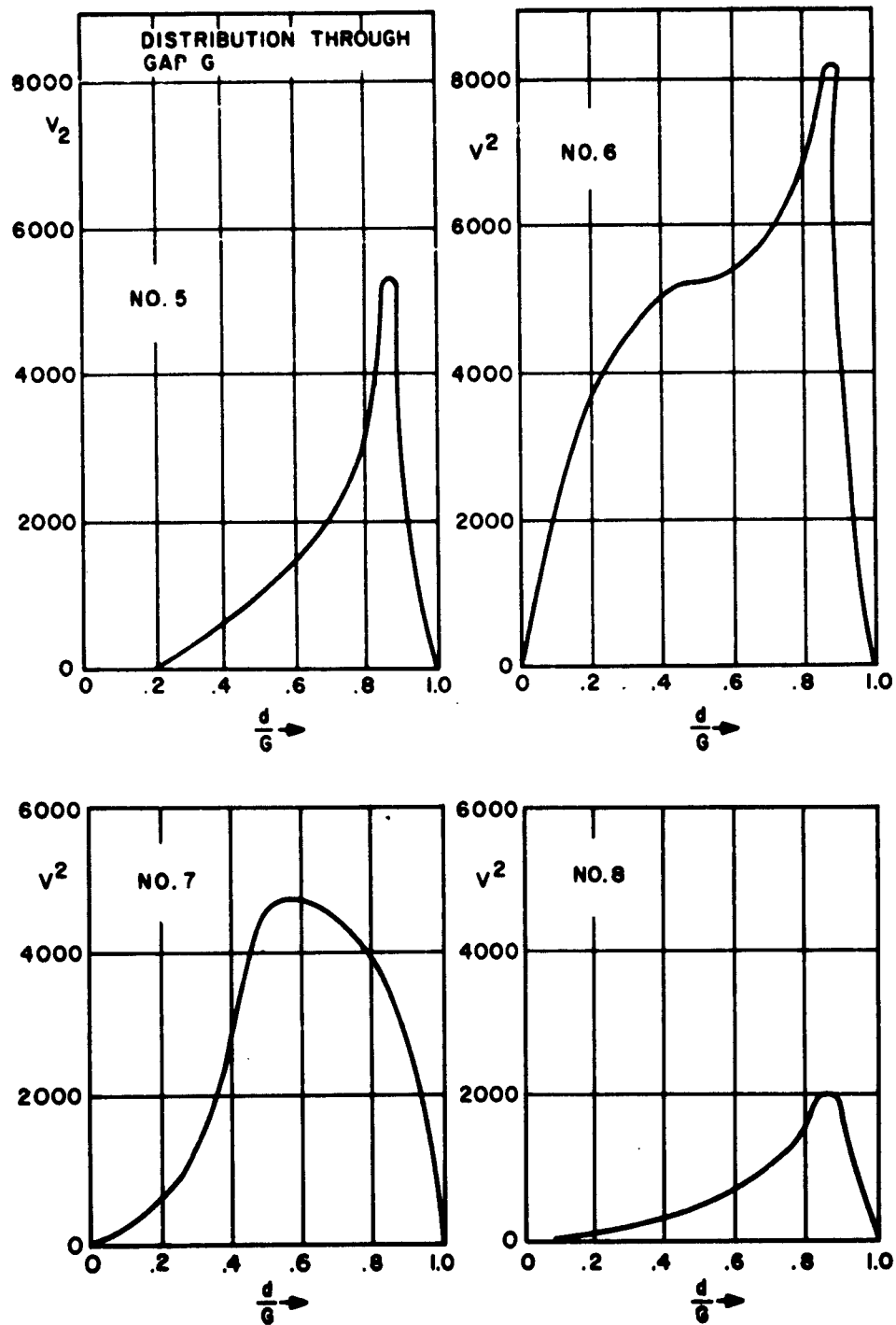


Figure 216. Presentation of  $V^2$  through the Annular Jet  
(Graphs No. 5, 6, 7 and 8)

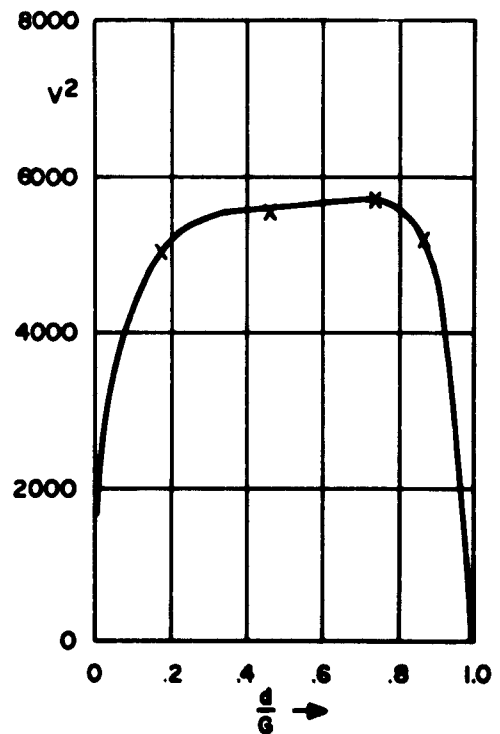
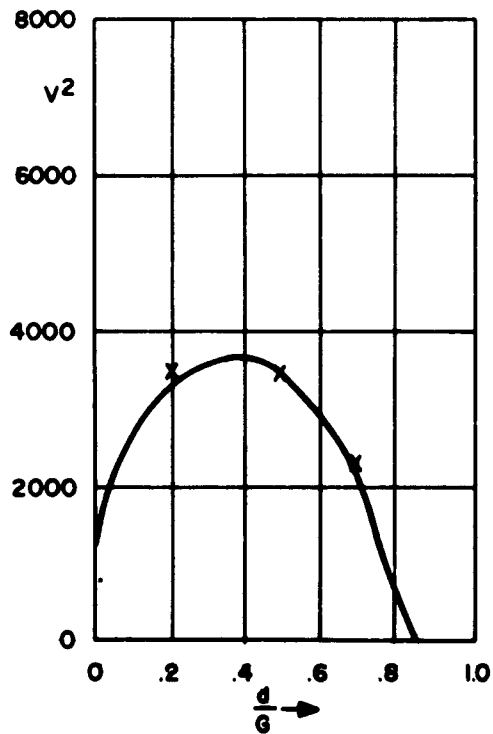
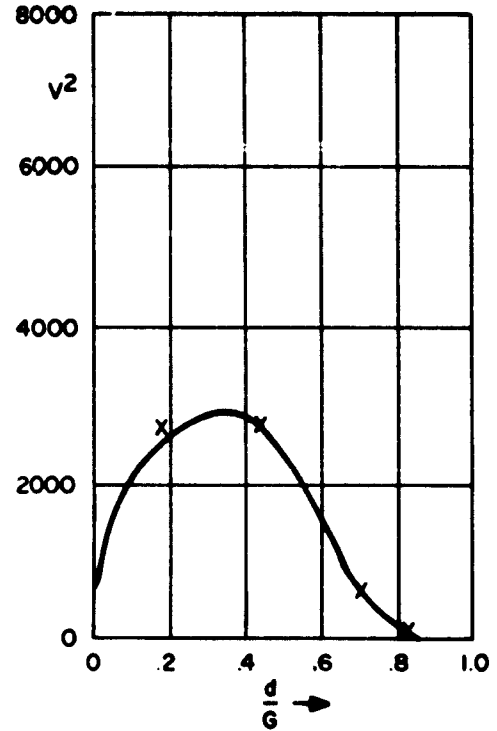
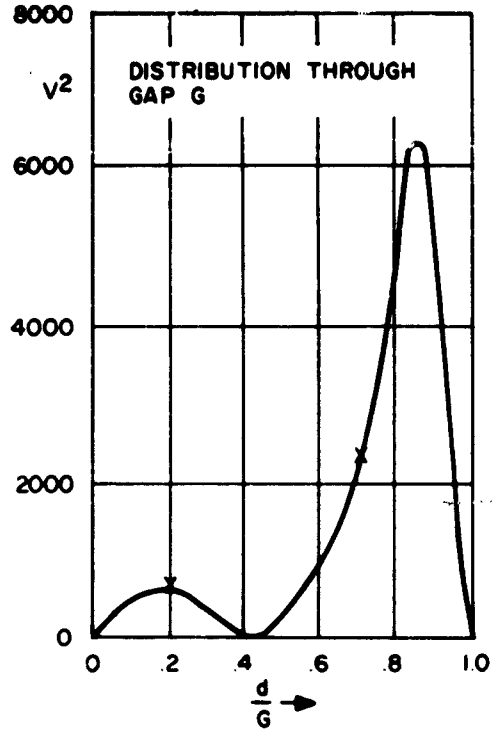


Figure 217. Presentation of  $V^2$  through the Annular Jet (Graphs No. 9, 10, 11 and 12)

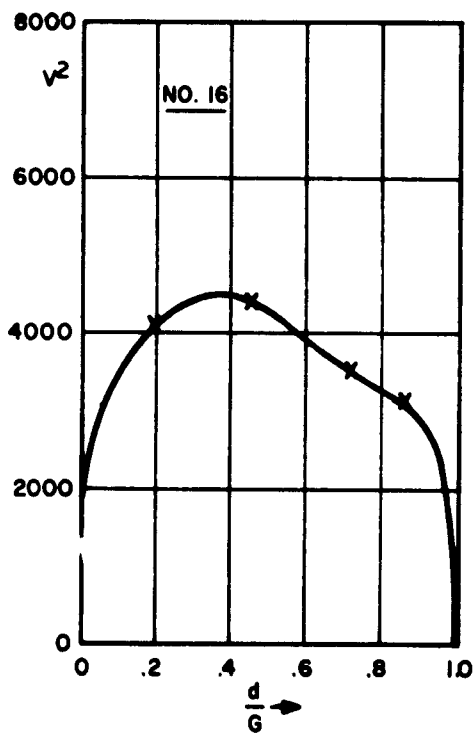
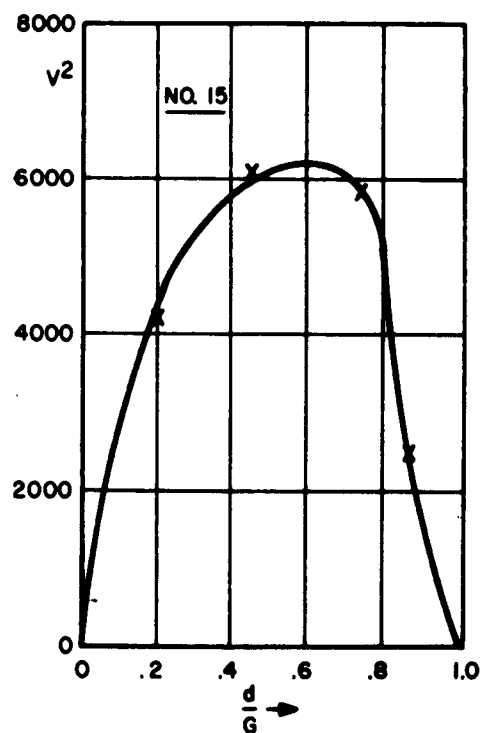
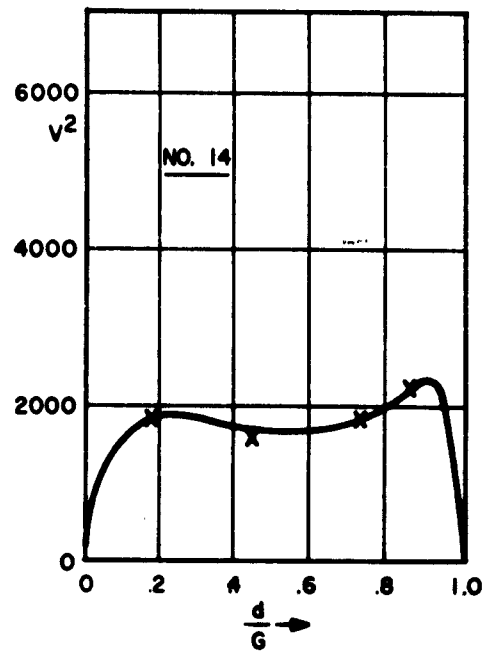
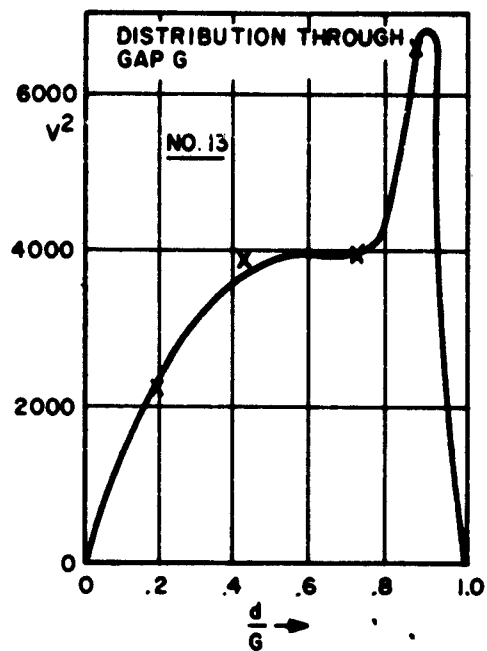


Figure 218. Presentation of  $V^2$  through the Annular Jet  
(Graphs No. 13, 14, 15 and 16)

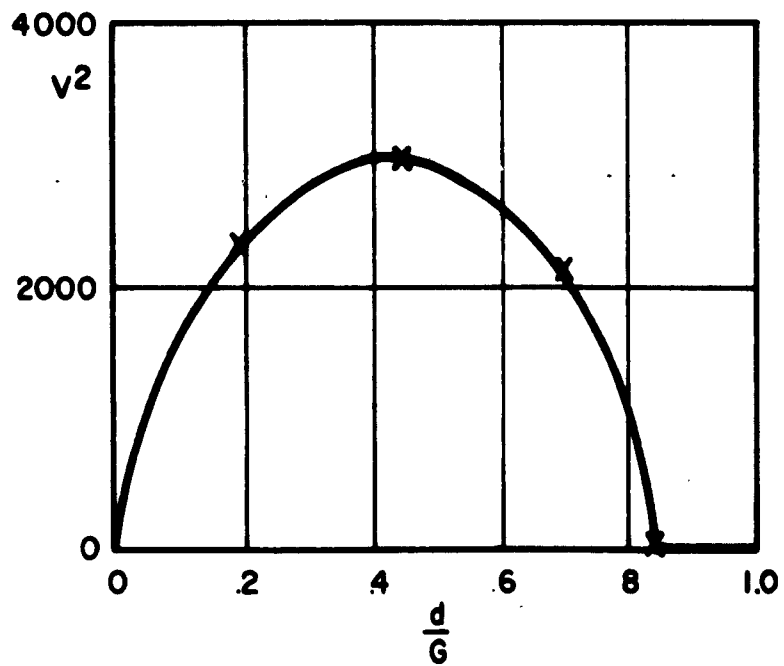
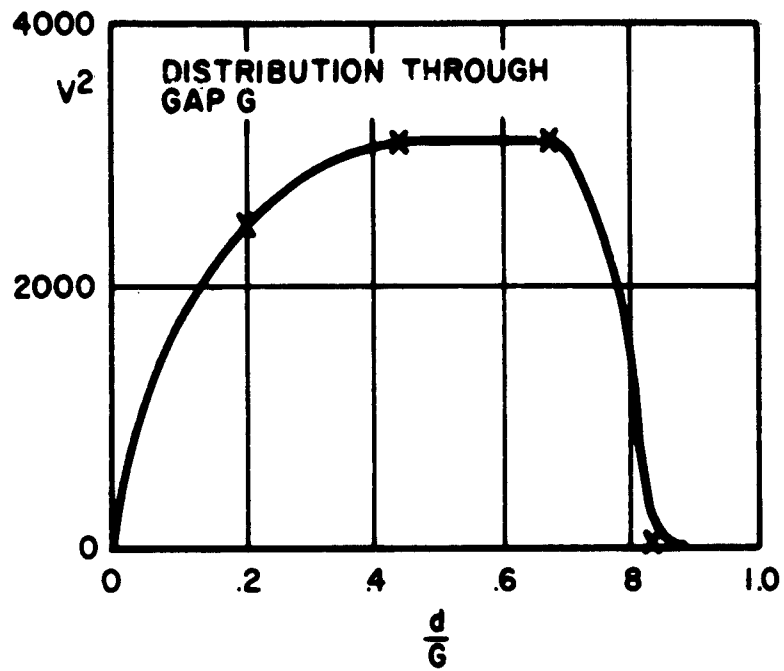


Figure 219. Presentation of  $v^2$  through the Annular Jet (Graphs No. 17 and 18)

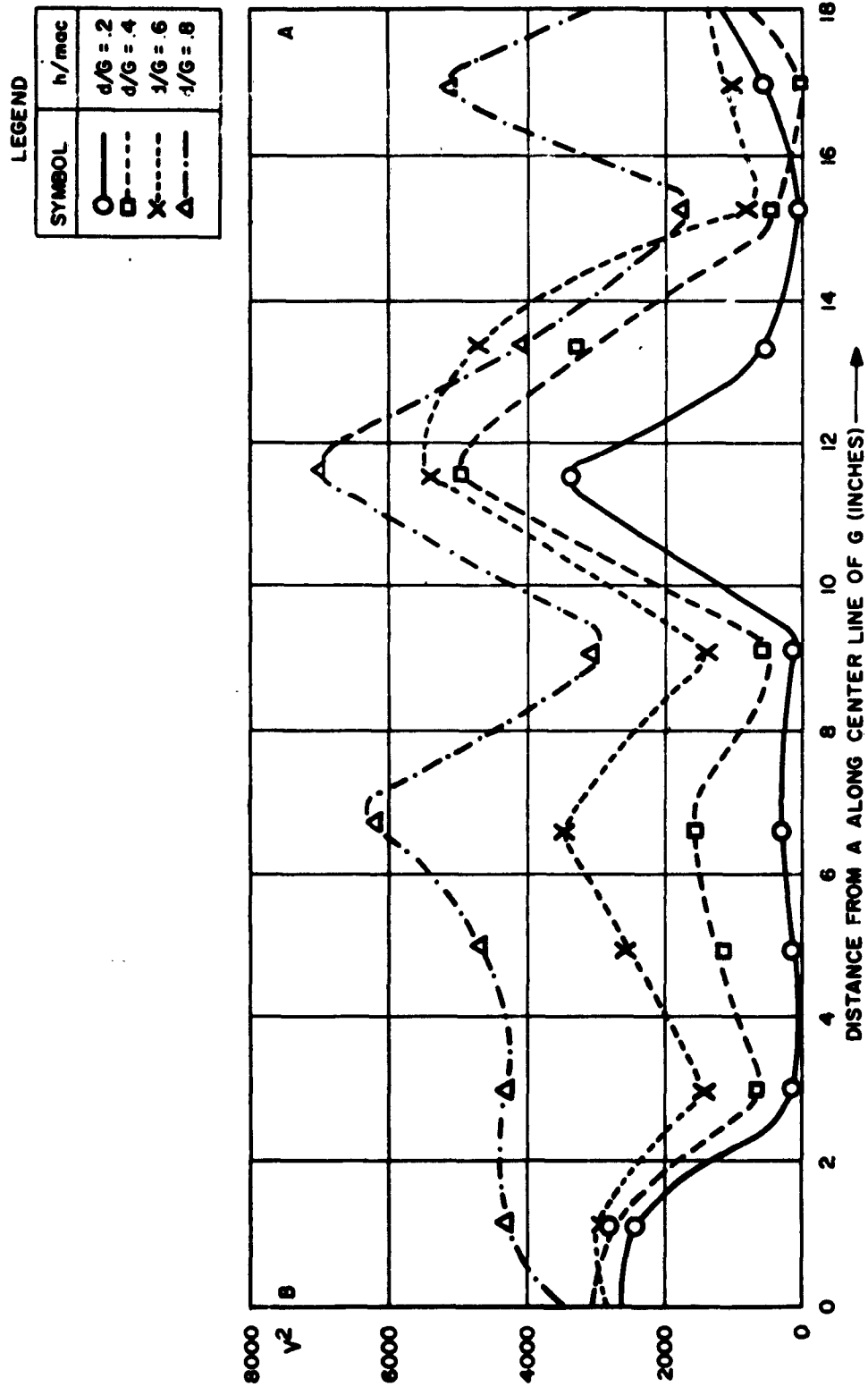


Figure 220. Spanwise Flux Distribution from A to B along Leading Edge of the Model

LEGEND

SYMBOL	$h/m\phi c$
○	$d/G = .2$
□	$d/G = .4$
X	$d/G = .6$
△	$d/G = .8$

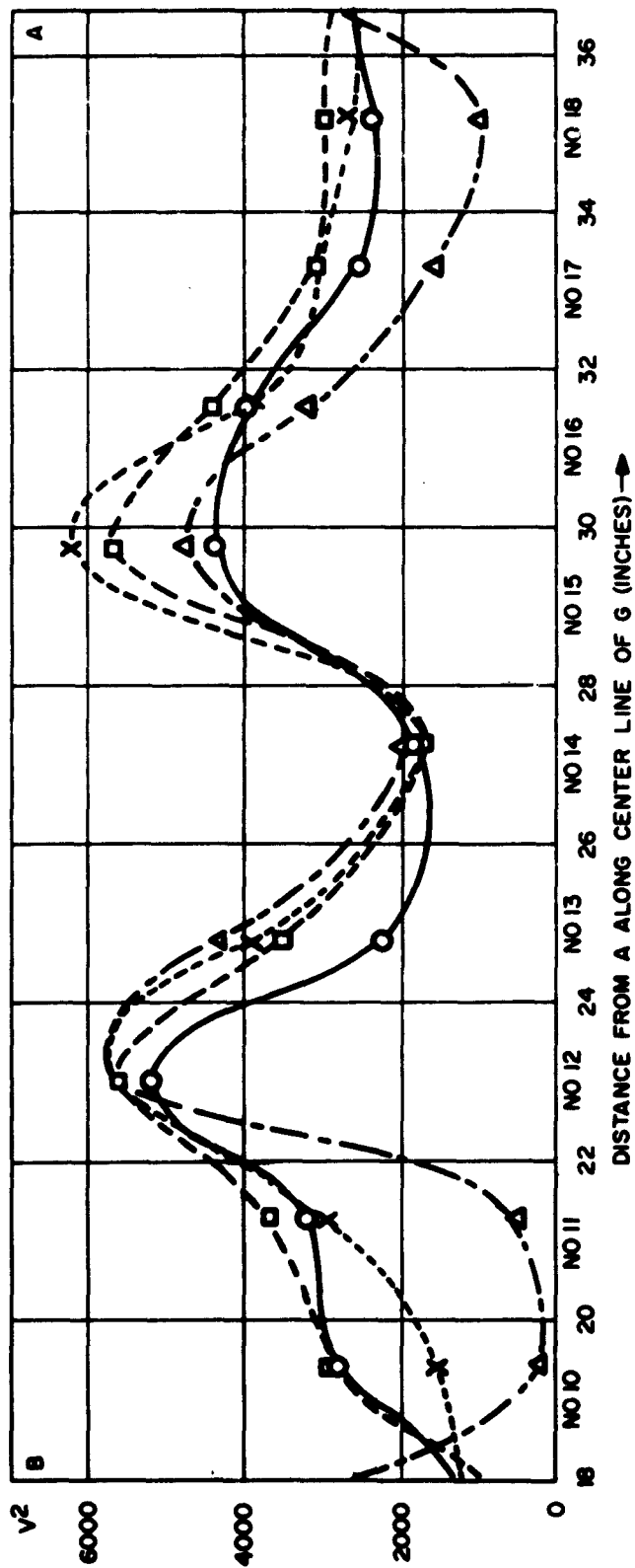


Figure 221. Spanwise Flux Distribution from B to A along Trailing Edge

The flight data was recorded by the photographic technique (Ref. 1) and is reproduced in Figures 222 to 227 inclusive.

This data was obtained by taking a 16 mm movie picture of the model as it flew past a reference grid. By analysing the behaviour of three reference points on the model, the dynamic behaviour of this GEM can subsequently be obtained. A full treatment as to methods of analysis is presented in Ref. 1 and thus will not be discussed here.

Figures 224 to 227 are the reduced records showing angle of pitch and height of a reference point above the ground. The CG. position and other model parameters are given in Appendix A.

The tests showed that the model occasionally contacted the ground board. The reasons for this behaviour cannot be definitely stated, but it is suspected that inadequate pitch stability may be the cause. The hits were not clearly evident to observers watching the flights, which to the unaided eye appeared to be reasonably smooth and steady.

#### REFERENCES

1. Liiva, J.                    A Facility for Dynamic Testing of Models of Airborne Vehicles with Ground Effect. UTIA Technical note 53, Oct. 1961.
2. Dau, K.                    Characteristics of a Rectangular Wing with a Peripheral Jet in Ground Effect, Part I. (in preparation)

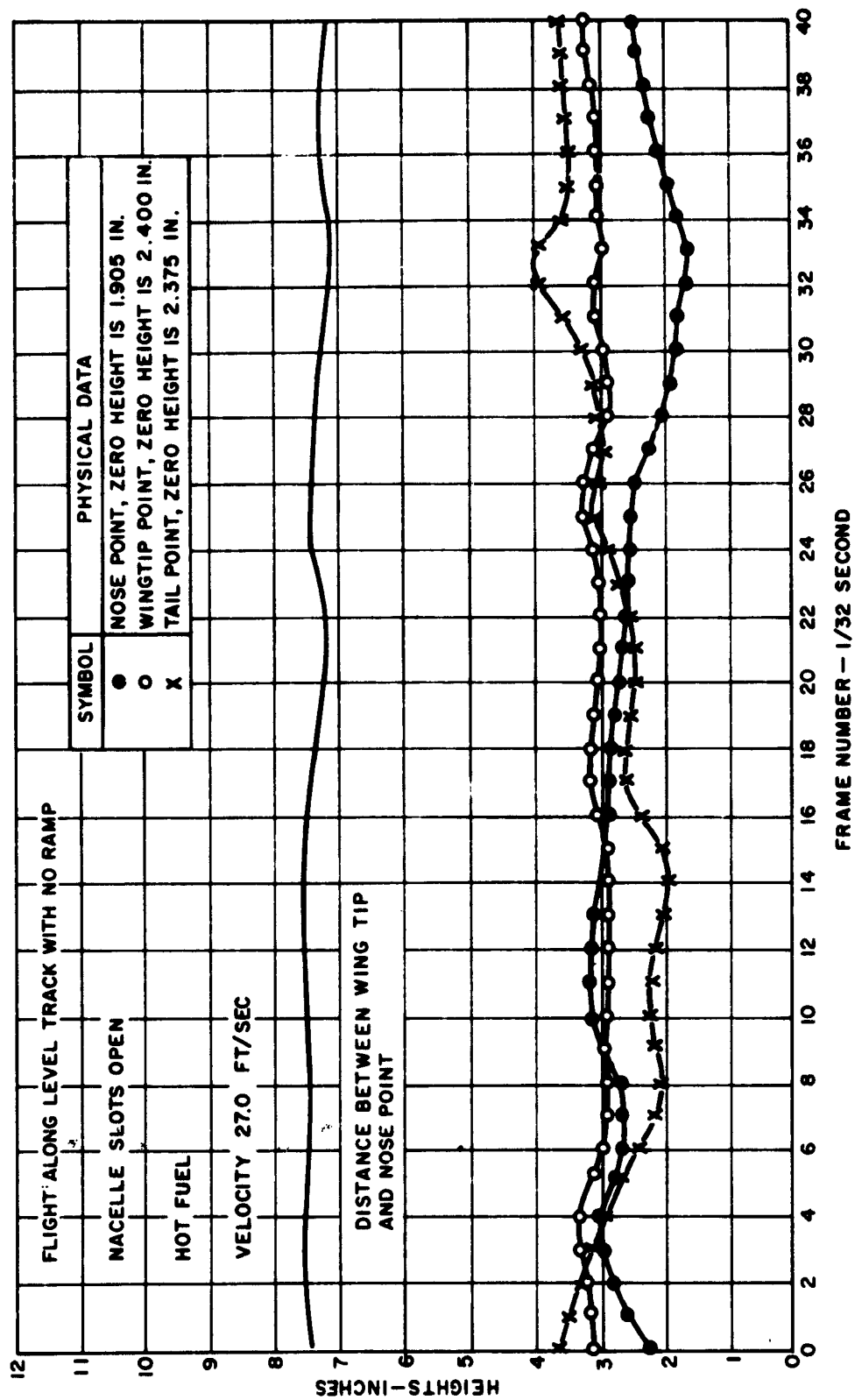


Figure 222. Unreduced Record Taken from Flight along Track with No Ramp Installed

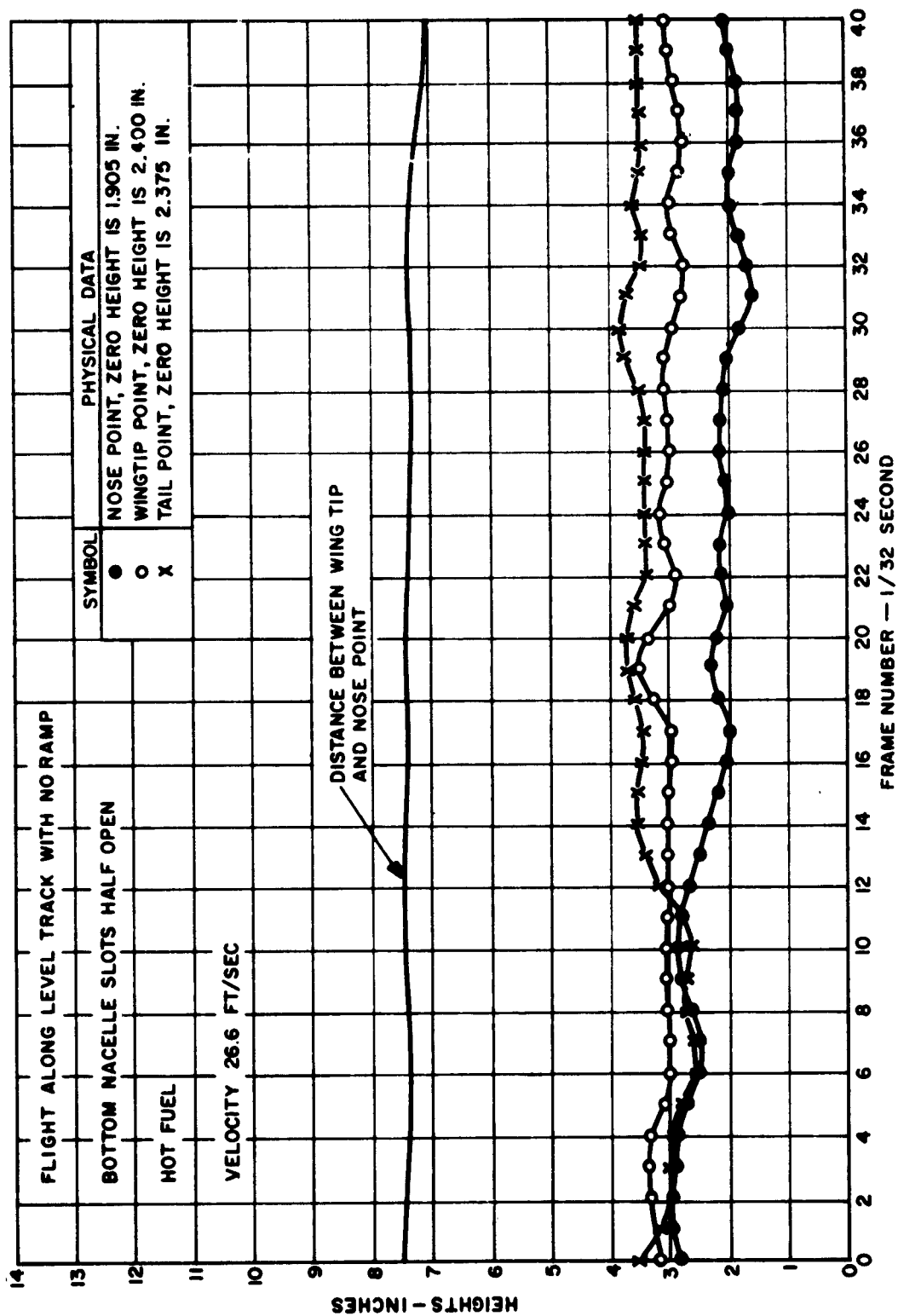


Figure 223. Unreduced Record Taken from Flight along Track with No Ramp Installed

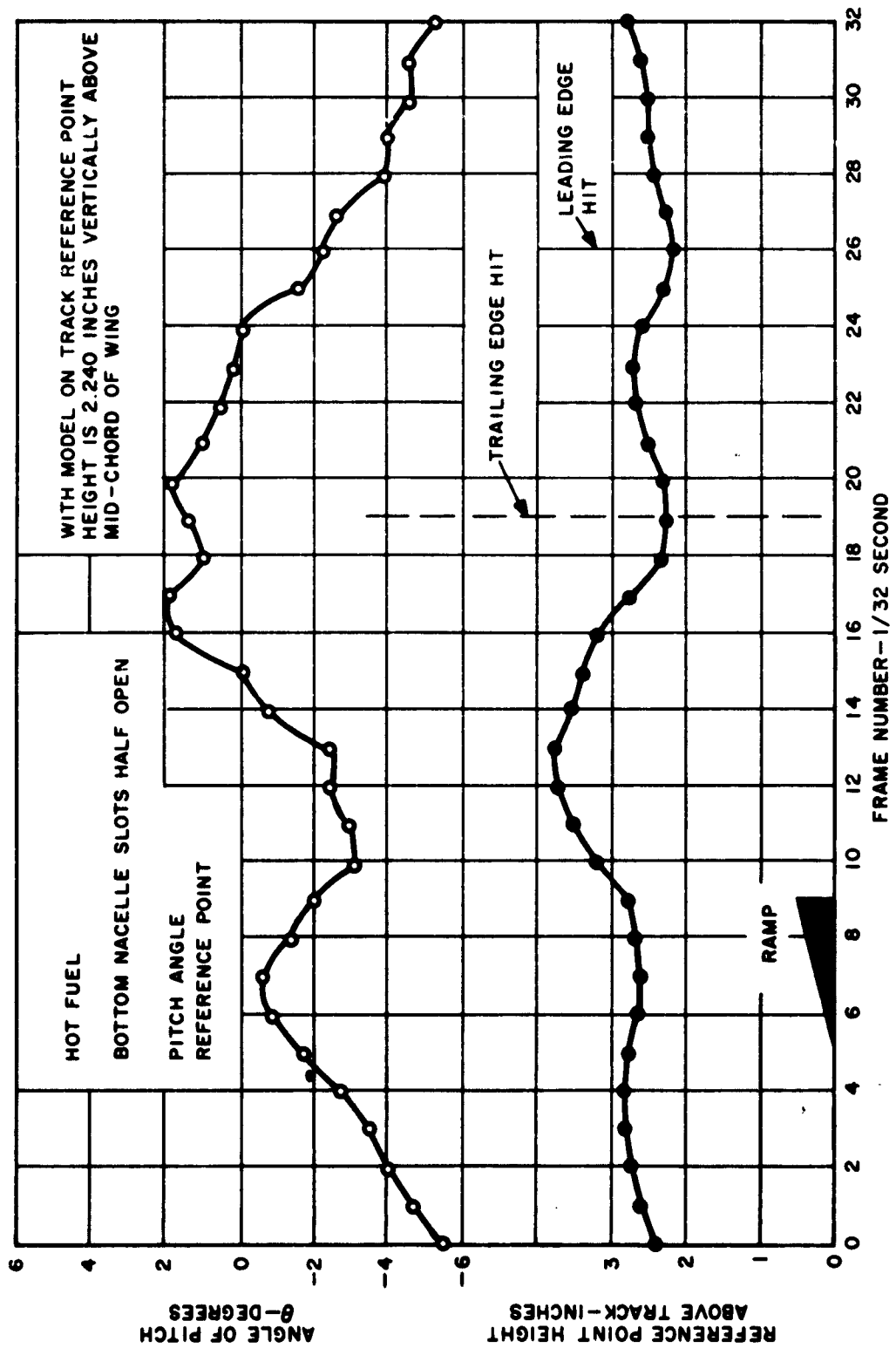


Figure 224. Flight in Plenum Chamber Configuration over .50 inch Ramp in Track

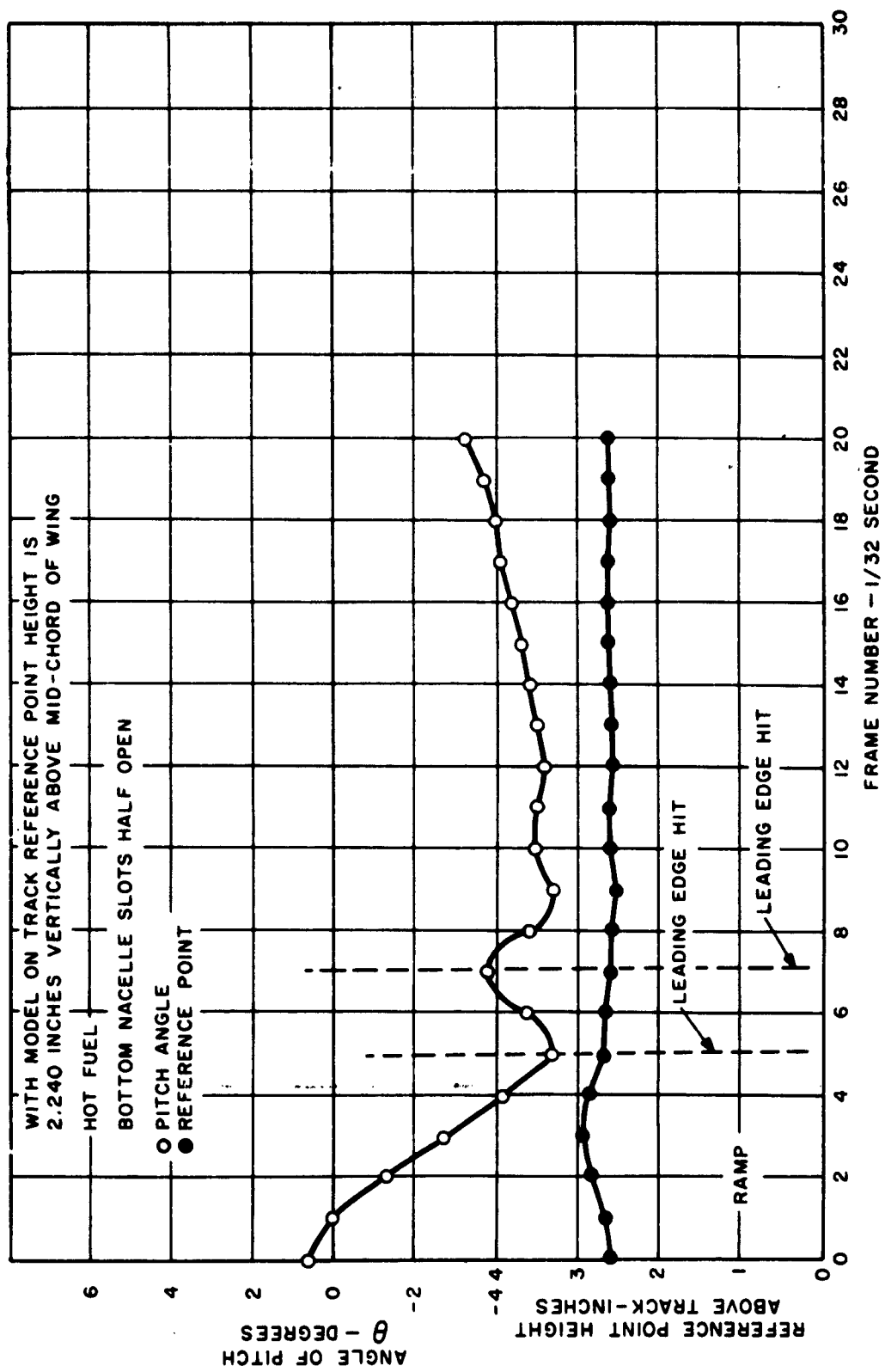


Figure 225. Flight in Annular Jet Configuration over .125 inch Ramp in Track

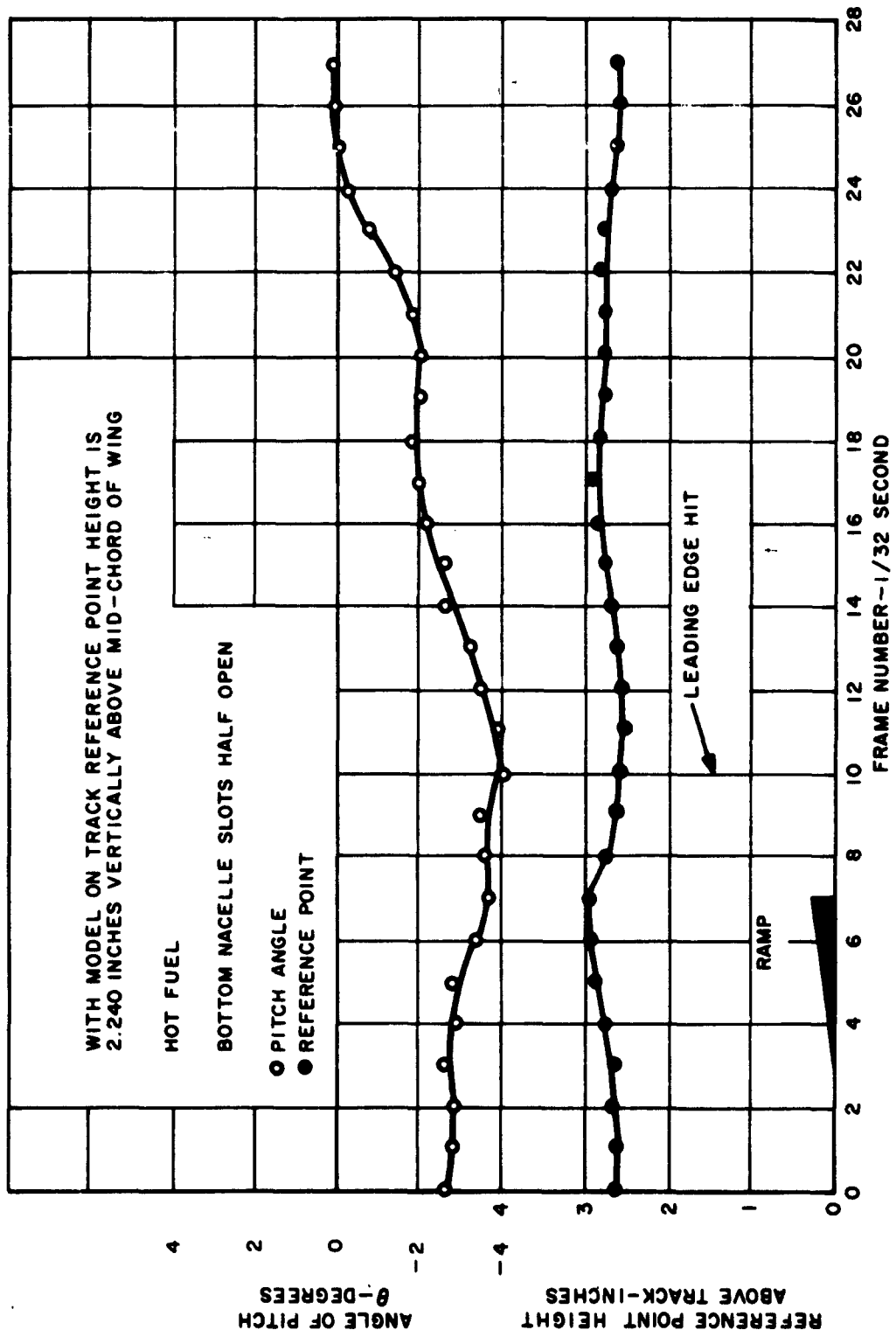


Figure 226. Flight in Annular Jet Configuration over .25 inch Ramp in Track

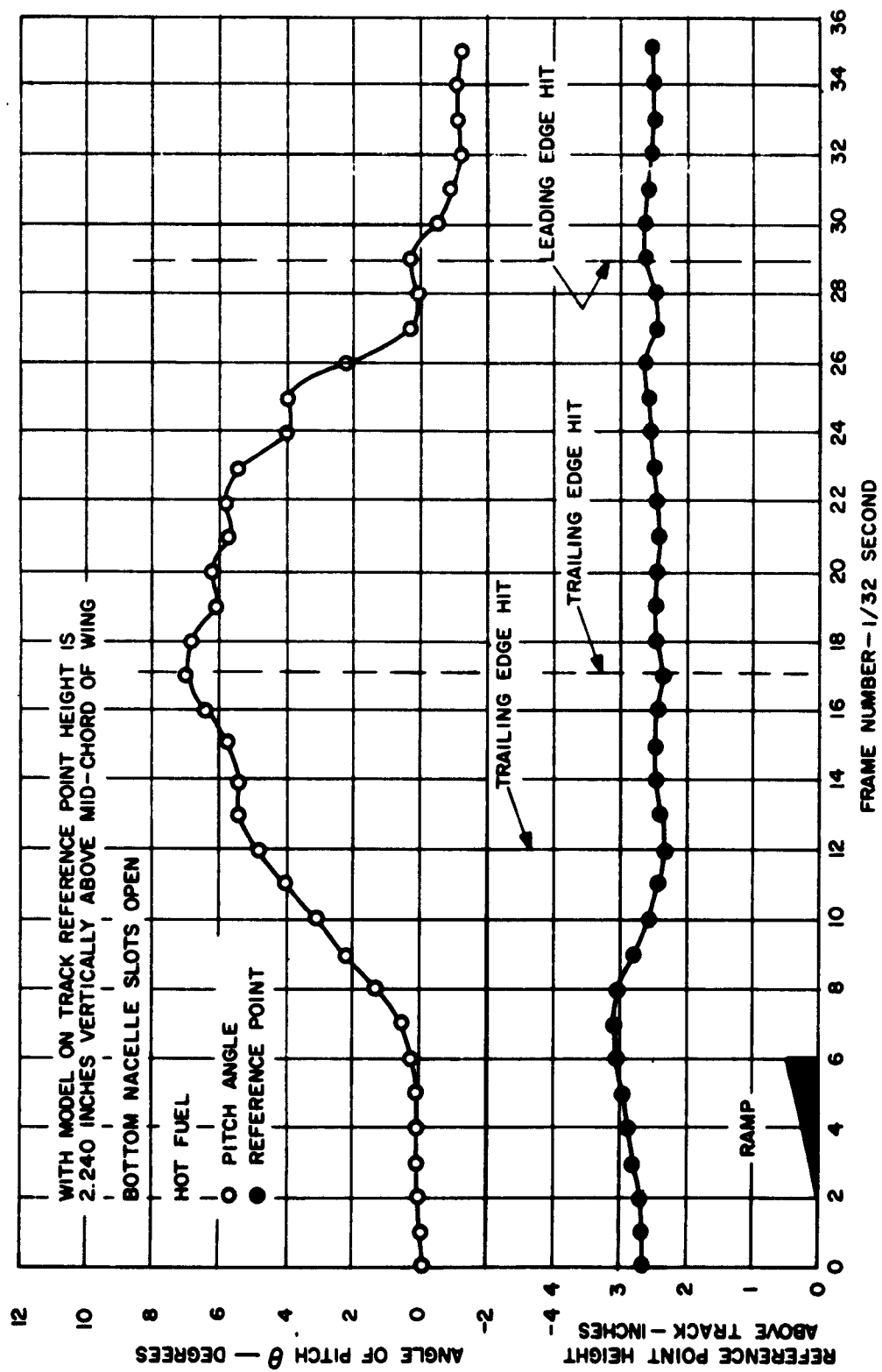


Figure 227. Flight in Annular Jet Configuration over .50 inch Ramp in Track

Appendix A - Data

V = 26.5 fps. in Figures 224 to 227

Model weight = 2.483 #

cg. position is 1/4" behind the midchord and 1.94" above ground  
when model is at rest

$$I_{cgyy} = .0123 \text{ slug ft.}^2$$

$$I_{cgzz} = .018 \text{ slug ft.}^2$$

Jet momentum flux = .68 lbs.

RMS jet velocity = 77.5 fps.

## APPENDIX E

### UNIVERSITY OF TORONTO DYNAMIC MODEL DATA

#### PART II

#### A Facility for Dynamic Testing of Models of Airborne Vehicles with Ground Effect

by

Jaan Liiva

#### ACKNOWLEDGEMENT

The author wishes to thank Dr. G. N. Patterson, Director of the Institute of Aerophysics, for the opportunity to pursue this investigation.

Professor B. Etkin's suggestion of the problem and subsequent supervision is gratefully acknowledged.

Thanks are due to G. Kurylowich for helping to finish construction of the track and for help in vehicle testing; also to R. C. Radford for help during testing, and for drawing graphs.

The discussions with W. Z. Stepniewski, H. Wahl and F. McHugh of Vertol were helpful and illuminating.

Special thanks are extended to members of the Aerodynamic Noise and Ground Effects groups at UTIA for their interest and helpful suggestions.

This work was made possible through the financial assistance of the Defence Research Board of Canada and of the Vertol Division of Boeing Aircraft Corporation.

## SUMMARY

A feasibility study has been carried out of the testing of self-powered models of vehicles with ground effect, on a circular track of 20 ft. diameter. Preliminary testing of a GETOL model with a wing of aspect ratio 3.5 and 17 inch wingspan was performed by flying over ramps in the groundboard of the track. The motion of the vehicle was recorded by filming with a motion picture camera. A theoretical study of the cable derivatives introduced by the harnessing and of their magnitudes relative to the aerodynamic derivatives was made. Problems associated with the model construction and performance are outlined and experimental test results are presented.

## SYMBOLS

a	constant defined in Eq. 4.5
A	augmentation due to ground cushion
b	wing span
$\bar{c}$	mean aerodynamic chord of wing
$C_D^*$	effective drag coefficient of cable, to be added to vehicle drag coefficient
$C_{D_1}$	constant defined in Eq. 4.5
$C_{D_\ell}$	local drag coefficient of cable at local Reynolds number
$C_{D_V}$	drag coefficient of cable at $Re_V$
$C_\ell^*$	additional rolling moment coefficient due to cable
$C_m^*$	additional pitching moment coefficient due to cable
$C_n^*$	additional yawing moment coefficient due to cable
$C_{\ell\varphi}^*$	$\partial C_\ell^* / \partial \varphi$
$C_{m\theta}^*$	$\partial C_m^* / \partial \theta$
$C_{n\psi}^*$	$\partial C_n^* / \partial \psi$
$C_Z^*$	additional vertical force coefficient due to cable
$C_{Z_H}^*$	$\partial C_Z^* / \partial H$
d	perpendicular distance between cables to vehicle
$d_c$	cable diameter
$D^*$	drag of cable
$\Delta D^*$	drag component of cable tension at harness point
g	acceleration of gravity
h	perturbation height of vehicle above ground
H	height parameter $h/\bar{c}$
J	momentum thrust

$\ell_1$	distance from centrepost to point of action of total cable drag
$L^*$	additional rolling moment due to cable
$m$	mass of vehicle
$M^*$	cable restoring moment due to perturbation pitch angle displacement $\theta$
$N^*$	additional yawing moment due to cables
$r$	local distance in cable from centrepost
$R$	distance from vehicle centre of gravity to centrepost
$R_c$	length of cable, centrepost to wingtip point
$Re_\ell$	local Reynolds number of cable due to local cable velocity $V_\ell$
$Re_V$	Reynolds number of cable calculated for flight velocity $V$ by using wingtip speed $V_c$ in Reynolds number relation
$S$	wing surface area
$S_c$	cable cross-sectional area
$T$	cable tension
$T_o$	tension at model end of cable
$V$	flight speed of model
$V_c$	speed of cable end, when model speed is $V$
$V_\ell$	local speed of cable
$W$	gross weight of model and fuel
$y_h$	additional height of cable attachment at centrepost to allow model to fly horizontally, taking cable sag into account
$Z^*$	additional vertical force due to cable
$\alpha$	angle of cable tension at model end with radial line from centrepost
$\theta$	perturbation angle of pitch
$\mu'$	viscosity of air at S. T. P.
$\mu$	mass parameter of vehicle
$\lambda$	characteristic wavelength
$\rho$	atmospheric density at S. T. P.
$\tau$	characteristic time

$\psi$             perturbation angle of yaw  
 $\rho c$            cable linear density in lbs/ft  
 $\Omega$             angular velocity of model around centrepost  
( )\*            cable forces and derivatives

## I. INTRODUCTION

Much work has been completed on the statics of GEM and GETOL aircraft, but so far little is known about the dynamics of these vehicles. To study the dynamic behaviour of models of such vehicles, a circular track facility has been built at UTIA.

The concept of using flying models on a circular path, controlled by a pilot through lines to the centre is not new. It has been in use by "U-Control" model fliers for years. The quality of power plants used for the models has been greatly improved. Consequently, there are glowplug engines now available with horsepower ratings sufficient to power models for most testing purposes.

Testing by this method was proposed by Braun (Ref. 2) in 1949, using models of conventional type aircraft on a 150 foot radius tether. Some of the difficulties that he outlined are not relevant to aircraft of the groundcushion type, where the testing is carried out on a horizontal table at the largest diameter of the testing sphere. The testing sphere is defined as that surface which the tether from the centrepost to the centre of gravity of the vehicle will trace out. Variations in the model's height above groundboard are a small percentage of the radius of the testing sphere. Braun's results show that with the constraint of lines whose weight is small in comparison to vehicle weight, the short-period longitudinal pitching mode can be obtained directly, but that for the long-period mode (the Phugoid) the constraints must be carefully considered.

Rotating-arm devices have been considered, but not used due to the interference of the arm on the derivatives (see Ref. 10).

In wind tunnel testing the "effective" shape of the ground encountered by the peripheral jet depends on the boundary layer on the groundboard. With a Reynold's number that produces a turbulent boundary layer, the ground surface is effectively one of unknown roughness and distance from the jet face.\*

In free flight model testing the pilot in control does not have an absolute knowledge of the attitude of the model when the controls are activated for a response test. Responses of the vehicles could be telemetered to the recording equipment, but the resulting model to house this would then be quite large and heavy. On a circular track one can harness the model to suppress any undesirable modes such as roll and yaw. Continuous recording of flight attitude is possible by the simple arrangement described in this report.

The test data obtained from the track is easy to read and process by direct hand calculation or by automatic analogue and digital computation. Transfer functions and stability derivatives can in principle be obtained by methods similar to those already developed for flight test work.

---

\*The concept of an effective ground surface may actually prove to be inadequate as a representation of the complicated interaction between the jet sheet and the boundary layer.

## II. TESTING TRACK

### 2.1 CONSTRUCTION AND SPECIFICATIONS

The track consists of a level annular table of 9.0 foot radius from the centre of track to centrepost (see Volume I, Figure 25). Eighteen pieces of 1/2" thick plywood from the horizontal table, each subtending an angle of 20 deg. at the centre. The effective table width is 2.5 feet. The framework to support the table is made from Dexion angles for ease of assembly, and also to facilitate adjustment of height when levelling. The bottom of the Dexion framework is fastened to the concrete floor with Ramset bolts and each frame is cross-braced to the two adjacent ones. This combination of interconnected frames, fastened securely to the floor produces a very strong and stiff structure. One of the 18 plywood boards is hinged for access to the interior. The horizontal table is 30 inches above the floor to provide sufficient room for observers to remain inside the track during test runs.

### 2.2 FLIGHT RECORDING

During flight the vehicle was photographed by a 16 mm. Bolex movie camera, with an electric drive. The filming speed was 32 frames per second. The camera is fixed rigidly at the centre of the testing track to the structure which overhangs the track. The optical path from the camera to the model is completed with a mirror, mounted at an angle on a sleeve. This sleeve is fitted with two ball bearings to the top of the centrepost. The lines from the model swing the sleeve and mirror in such a way that the mirror is always aimed at the model; consequently, the model is always in the camera's range of vision.

To obtain quantitative results, there is a vertical background of horizontal lines spaced one inch apart. The background board is 20 inches high, to permit continuous photography of transition to flight outside ground effect.

Floodlights on every second post light the model and background for photography.

To prevent discoloration of the grid and to provide protection against solution of the glues which bind the plywood, the whole structure was covered with several coats of butrate dope.

There are three reference points on the aircraft; a double rectangle on nose and tail and a post on the wingtip closer to the camera. By conducting a frame-by-frame analysis of the film from a test run, the relative heights above ground-board and distances from each other of these points can be determined. Arithmetic operations, performed either by hand calculating machine or electronic digital computer, will yield the angles of pitch, roll and yaw against frame number. The camera filming speed is calibrated by filming the second hand of an electric clock. This procedure gives an accurate measure of time. Centre of gravity position of the model along the track is obtained from the angle of orientation of the track within the film frame. As the model proceeds along the track, the track rotates in the camera frame due to the arrangement of stationary camera and rotating mirror.

The model points were read from the film by using one of two methods.

1. For very accurate results the commercial comparator available at UTIA was used. This procedure is very time-consuming.
2. For quicker but less accurate results the pictures were enlarged by projecting onto a screen at a convenient magnification, such as half, full, or double size. The accuracy of reading is consistent with track construction accuracy and frame magnification. By aligning a sheet of paper with the grid lines on the backboard, the model points were directly plotted against frame number.

### 2.3 CENTREPOST

The centrepost consists of a three-legged frame to hold a 3/4 inch diameter steel rod with set-screws for adjustment of height. The rod is fitted with two ball bearings at the top, and an aluminum sleeve is pressed on the outer races of the bearings. Since the models are self powered it was decided to make the inertia and bearing drag of the rotating part of the centrepost as small as possible. This prevented direct mounting of the camera to the centrepost and the mirror arrangement described in part 2.2 was used instead. The mirror arrangement had the added advantage that distance along the track could be directly obtained as an angular displacement from a reference radius, such as that at the ramp.

The lines to the model are fastened to two nylon-coated steel wires that run through tubular guides and attach to a bellcrank. The guides provide a restoring moment to the mirror mount if the vehicle tends to lead or lag. On the model wingtip there is a bellcrank the height of which is adjustable by a set-screw. There is no additional rolling-moment introduced by the tether, if the lines are adjusted to the height of the vehicle c.g.

One control can be introduced to the vehicle through the control lines. By linking cables from the elevator or engine throttle to the bellcrank on the wingtip of the vehicle, it can be controlled from the outside. This mechanical control through the bellcranks was intended for use as a throttle control for the GETOL model, but since no suitable throttle for the engine was found, the control was not used.

Other controls could be provided by using stepping relays or servos, electrically fed through the control lines and slip-rings on the centrepost, operated from a control-centre outside the test track.

### 2.4 STARTER

An engine starter is indispensable for efficient operation of the test track. In the beginning of the program much time was spent trying to start the engine by hand; the starter subsequently made this a simple operation. The starter consists of an automobile starter motor, a 6 volt battery and charger. The model engine is pressed against a rubber hose fastened to the motor shaft, while the

needle valve on the engine is adjusted for proper fuel flow, as indicated by the sound of the exhaust. Final adjustment can then be made with the engine removed from the starter. Power for the glowplug is obtained from one of the three cells in the battery. While 1.5 volts for the glowplug is recommended by the manufacturer, it was found that 2 volts made starting easier with occasional burnout of plugs.

### III. MODEL

#### 3.1 STRUCTURE

The model used for preliminary feasibility tests was based on a Vertol design. It was made from balsa wood covered with polyester resin. The internal surfaces of the nacelles and ducting were also covered with the resin to provide a smooth surface. The combination of balsa covered with resin makes a strong structure, but it has a tendency to crack. These cracks occurred at many of the joints and had to be repaired by using layer of glass cloth with resin to bond it to the surface of the model.

#### 3.2 SPECIFICATIONS

The wing is of NASA 4418 cross-section with a 6" chord at the root, tapering to a 3" tip chord outboard from the nacelle structures. The wing aspect ratio is 3.5—a compromise chosen to provide both a good ground cushion and a more efficient wing for forward flight than the circular planform, which is more efficient as a GEM. The wing span is 17". The horizontal tail aspect ratio is 4.5, with a tail moment arm of almost 13.0". The long moment arm to the high aspect ratio horizontal tail provides a neutral point at 52% chord (Ref. 1).

This is sufficient to accommodate the shift of the centre of pressure from the midpoint of the wing during hovering, to the more conventional aerodynamic centre near 1/4 chord for forward flight. The C. G. of the vehicle has to be at the midpoint of the wing to provide trim, since the centre of pressure is at the midpoint of the planform enclosed by a peripheral jet during hovering. It may be possible to compensate for a C. G. forward of midchord point during hovering, if the centre of pressure can be shifted by having jet slots of different width at the front and rear of the wing.

The weight of the finished model together with power plant, fans, pulleys, belts and empty fuel tank is 2.4 lbs. Variation of C. G. position and of the moment of inertia can be effected by adding or subtracting lead weights to the tail, nose and wingtips.

The jet slot width can be changed by taping over part of the present opening of .40 inches or by making new bottom covers for the wind with the desired jet slot opening.

#### 3.3 NACELLES, FANS AND DUCTING

The two forward-facing intakes each have a fan driven by a common engine mounted inside the fuselage. There is a twin pulley on the crank-shaft of the

engine. A belt to each fan pulley provides the power transmission. The intake nacelles have built-up lips to prevent separation during hovering. Fixed stator blades behind the fan straighten the flow.

The air supplied by the fans can be directed to either or both of two openings. It can all be used to provide the ground cushion by exhausting the air through the slot around the periphery of the wing, i. e. the hovering mode. Fixed turning vanes inside the nacelle, located at the upper wing cover, turn the air into the wing. At the moment no information is available on their effectiveness in our model. For forward flight, part of the air is used to provide a forward thrust. The back of each nacelle has a set of 4 slots which can be opened or closed to provide various amounts of forward thrust.

The fans are mounted on the shafts with two ball bearings and a thrust bearing each, and are removable. There are commercial fans available to suit model engines of all power ratings. These fans are made to power models of jet aircraft with air passing straight through the body, and were not designed to work against the high internal resistance encountered in our model.

Two types of fans were tried unsuccessfully, since neither allowed the engine to speed up to its full 15,000 r. p. m. and thereby develop its full 3/4 horsepower.

Fair results were obtained from the smaller fan after reducing its solidity by 50% by cutting away six of its twelve blades.

Due to the extremely bad matching of fans to engine and model ducting when the wing bottom cover was on, the hovering heights obtained were small, of the order of .04 to .06 h/ $\bar{c}$ . With the bottom cover removed and the model running as a simple plenum chamber heights of over 3" were obtained during portions of the run.

### 3.4 ENGINE

Installed in the model is a .35 cubic inch displacement Fox Combat Special glow-plug engine delivering 3/4 horsepower at 15,000 r. p. m. This engine has a ball-bearing mounted crank-shaft and a tap on the crank-case for pressurizing the fuel supply. The pressurized supply operated satisfactorily, giving a constant fuel feed and facilitated starting. There was no throttle control on the engine. Two types of butterfly valves were tried on the carburetor, but neither operated satisfactorily. (For efficient control of speed a combination of throttle and exhaust valves can be used. These were not installed on our engine). Runs were therefore taken at full speed, as set by the needle valve on the fuel supply.

Many flexible and springloaded motor mounts were tried unsuccessfully. Not one of them provided enough tension on the belts to prevent slippage. The present mount attaches the engine solidly to the model with four screws and locknuts. The tension to keep the belts tight is provided by the cantilevered fan shafts, fastened into the stator section. Belt tension can be adjusted with shims underneath the engine mounts.

Engine cooling was critical in the preliminary hovering tests. Runs of only a few seconds were obtained before the engine overheated. Glowplug engines are normally cooled by the slipstream from the fan or propeller. In our installation of two fans driven by belts, there was no slipstream cooling of the engine. An ejector was constructed, using the high-velocity exhaust gases from the engine to induce cool air over the cylinder head. During hovering the ejector interfered with the inflow into the fans. With forward flight around the track there was sufficient cooling without the ejector for runs of a few minutes duration. The ejector was discarded, since it added to the weight and did not perform as expected.

The engine performed much better after being thoroughly broken in by running it on a bench stand for several hours with a rich mixture of fuel and added castor oil.

More serious difficulty was caused by the castor oil, which sprayed from the exhaust over pulleys and belts during the runs. This oil caused slippage of the belts after five or six circuits around the track. This slippage could clearly be heard from the change in engine tone. Most of the data was taken on the first three circuits. Between runs the belts and pulleys were cleaned with a commercial window cleaning solvent.

#### IV. MODEL HARNESSING CHARACTERISTICS

##### 4.1 CABLE PROPERTIES

The harnessing arrangement selected consists of two dacron lines from the bellcrank on the centrepost to the wingtip bellcrank. The distance between the lines is 2 inches. The dacron lines have the following properties:

- maximum safe tensile stress per line is 11 pounds
- average diameter  $d_c$  is  $1.51 \times 10^{-3}$  feet
- average lineal weight  $\rho_c$  is  $8.56 \times 10^{-5}$  lb/ft.

##### 4.1.1 Cable Tension

Cable tension for the unbanked and unyawed vehicle in level circular flight around the track is

$$T = \frac{WV^2}{gR} \quad (4.1)$$

If the vehicle is banked, or if control surfaces are deflected, the tension will not be given exactly by equation 4.1, but if the speed of the vehicle is greater than 10 ft/sec the error will be less than 3% for angles of bank up to 5 degrees.

### 4.1.2 Cable Sag

To enable the vehicle to fly with its wings level at any given speed, the height of the centrepost is adjustable to compensate for cable sag.

From Ref. 21 the differential equation of the cable, and the boundary conditions are (see Figure 228(a) ).

$$\frac{d^2y}{dx^2} = \frac{1}{T_0} \rho_c \quad y \Big|_{x=0} = \frac{dy}{dx} \Big|_{x=0} = 0 \quad (4.3)$$

$T = T_0$  at  $x = 0$  and the horizontal component of tension at any point in the cable is assumed to be constant over the length of the cable. This equation neglects the centrifugal force on the cable and gives a pessimistic answer for cable sag. This assumption is good provided the total cable mass is small compared to that of the airplane model, which is the case in the present tests.

Solving Eq. 4.3 gives

$$Y_h = \frac{1}{2T_0} \rho_c R_c^2 \quad (4.4)$$

Using the values for our line the sag is only  $5.69 \times 10^{-3}$  inches at 30 ft/sec testing speed, and decreases rapidly with increasing speed.

## 4.2 HARNESS TO WINGTIP

The pair of lines to the model are harnessed to the wingtip as described in Sec. 2.3, to keep yawing and rolling to a minimum. We are mainly interested herein in obtaining the longitudinal derivatives of the vehicle. The procedure for defining the derivatives is as outlined in Ref. 1, except as otherwise noted. The cable derivatives are compared to the vehicle aerodynamic derivatives to show their relative magnitudes. The comparison will be carried out for the vehicle described in Section II.

### 4.2.1 Cable Drag Coefficient $C_{D_l}^*$

Assuming straight lines to the model, and that the drag coefficient for an infinite cylinder can be approximated by

$$C_{D_l} = C_{D_1} R_{e_l}^a \quad (4.5)$$

$C_{D_1}$  and  $a$  can be found from a log, log plot of  $C_D$  vs.  $Re$  e.g. Refs. 22, 23 or 24, reproduced here for convenience in Figure 235.

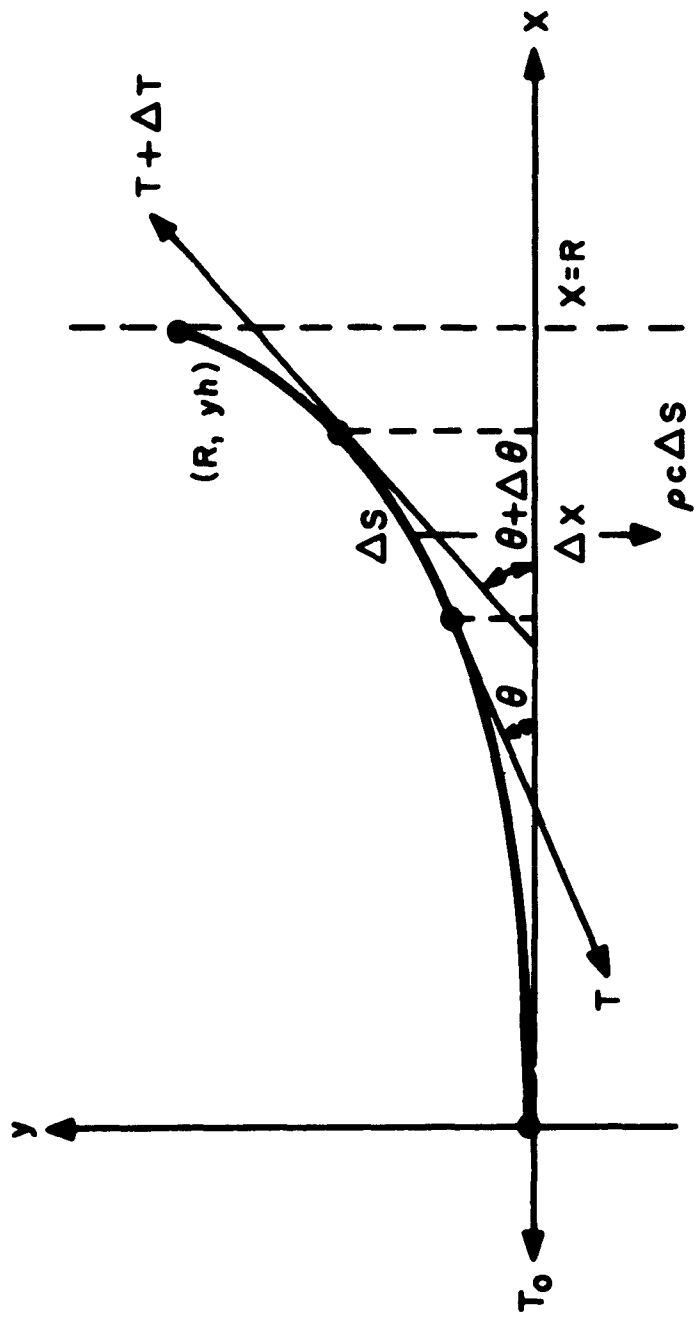


Figure 228(a). Cable Sag Parameter

$$R_{e_l} = \frac{\rho V_l d_c}{\mu} \quad (4.6)$$

The drag on one wire is then

$$D^* = \int_0^{R_c} C_{D_l} \frac{1}{2} \rho V_c^2 \left( \frac{r}{R_c} \right)^2 d_c \cdot dr \quad (4.7)$$

where

$$V_l = V_c \left( \frac{r}{R_c} \right) \quad (4.8)$$

Substituting for  $C_{D_l}$  from Eq. 4.5, using Eq. 4.8 and integrating

$$D^* = C_{D_1} R_{e_v}^a \frac{\rho}{2} V_c^2 d_c \int_0^{R_c} \left( \frac{r}{R_c} \right)^{2+a} dr \quad (4.9)$$

$$D^* = \frac{C_{D_1} V_c}{3+a} (R_c d_c) \frac{1}{2} \rho V_c^2$$

The drag acts at a distance  $l_1$  from the centrepost, where  $l_1$  is given by

$$l_1 = \frac{1}{D^*} \int_0^{R_c} C_{D_l} \frac{1}{2} \rho V_c^2 \left( \frac{r}{R_c} \right)^2 d_c \cdot r \cdot dr \quad (4.10)$$

integrating we get

$$\frac{l_1}{R_c} = \frac{3+a}{4+a} \quad (4.11)$$

Setting up a co-ordinate system as shown in Figure 228(c), we see that by taking moments about the centrepost, the drag component of the cable tension at the wingtip is

$$\Delta D^* R_c = l_1 D^*$$

$$\Delta D^* = D^* \frac{l_1}{R_c} = D^* \frac{3+a}{4+a} \quad (4.12)$$

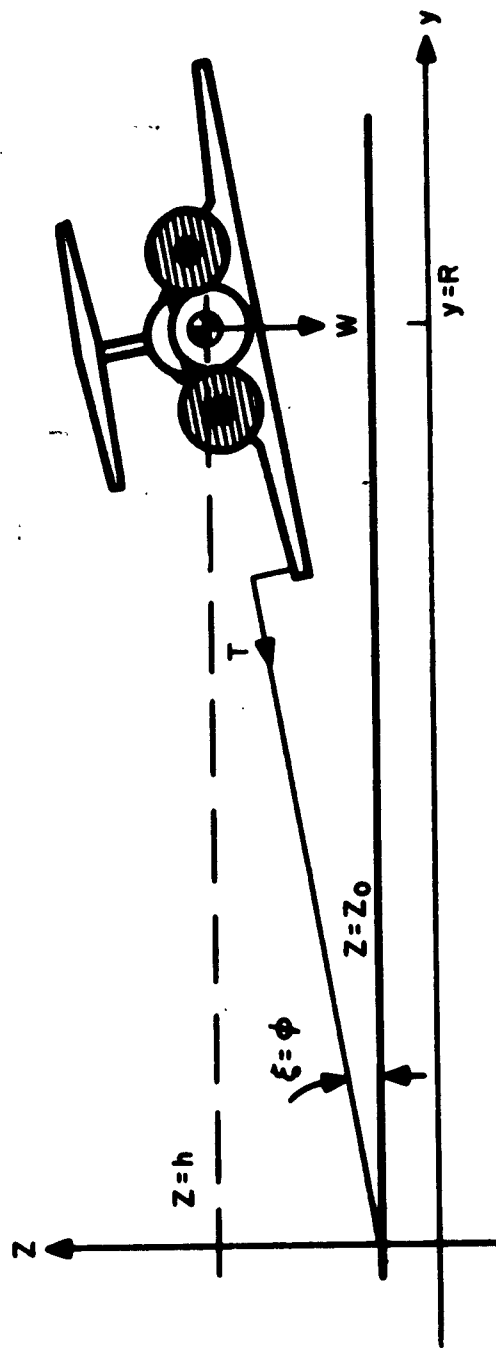


Figure 228(b). Cable Derivative  $C_{2H}^*$

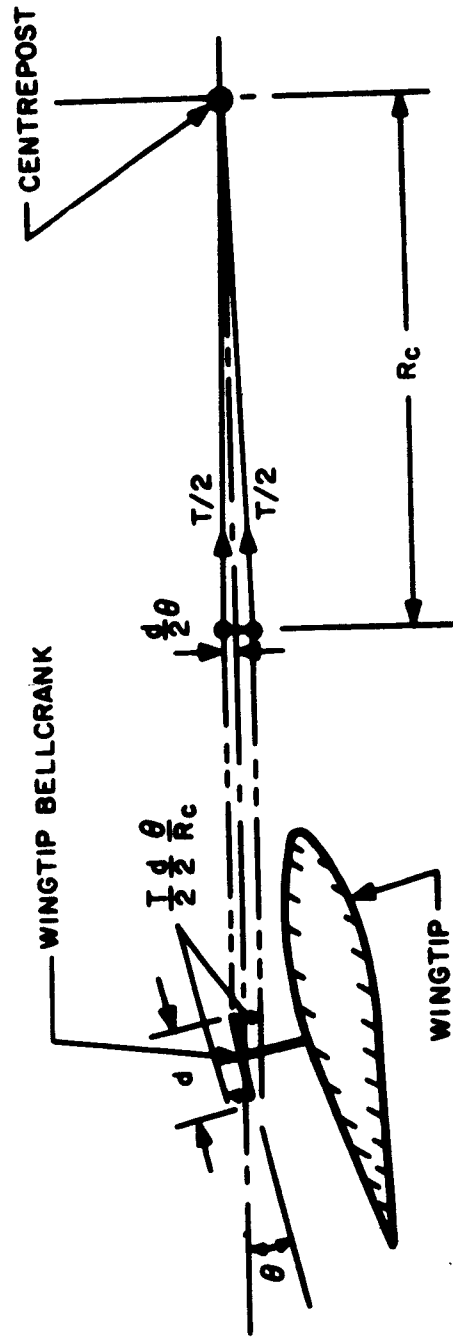


Figure 228(c). Cable Derivative  $C_{m\theta}^*$

This component must be added to the vehicle drag; it produces a yawing moment and a drag force on the vehicle.

The effective additional drag coefficient is then

$$C_D^* = \frac{\Delta D^*}{\frac{1}{2} \rho V^2 S} \quad (4.13)$$

Since two wires are used in the harness

$$C_D^* = \frac{2 C_{Dv} \frac{1}{3+a} \cdot \frac{1}{2} \rho V_c^2 S_c}{\frac{1}{2} \rho V^2 S} \cdot \frac{3+a}{4+a} = \frac{2 C_{Dv}}{4+a} \cdot \frac{S_c}{S} \cdot \left( \frac{R_c}{R} \right)^2 \quad (4.14)$$

we have used

$$V_c = \Omega R_c \quad (4.15)$$

$$V = \Omega R \quad (4.16)$$

Additional drag occurs in the centrepost bearings. This drag is assumed to be small in comparison to vehicle and cable drag.

To find the angle  $\alpha$  (Figure 228(c)) that the cable tension makes with the radius from the centrepost to the end of cable at vehicle, we use Eq. 4.3, but substitute  $D^*(x)$  for  $\rho_c$  using the assumptions of small cable weight compared to vehicle weight

$$\frac{d^2 y}{dx^2} = \frac{D^*(x)}{T_0} \quad (4.17)$$

where  $y$  is now the displacement in the horizontal plane. Using Eq. 4.5 and

$$V_\ell = x \Omega \quad (4.18)$$

we get

$$\frac{d^2 y}{dx^2} = \frac{1}{T_0} C_{D1} \left( \frac{\rho_d \Omega x}{\mu} \right)^a \frac{1}{2} \rho x^2 \Omega^2 d_c \quad (4.19)$$

Integrating we get

$$\frac{dy}{dx} = \frac{1}{T_0} C_{D1} \frac{1}{2} \rho \Omega^2 dc \left( \frac{\rho dc \Omega}{\mu^1} \right)^a \frac{x^{3+a}}{3+a} + C_1 \quad (4.20)$$

and

$$y = \frac{1}{T_0} C_{D1} \frac{1}{2} \rho \Omega^2 dc \left( \frac{\rho dc \Omega}{\mu^1} \right)^a \frac{x^{4+a}}{(3+a)(4+a)} + C_1 x + C_2 \quad (4.21)$$

The boundary conditions are:

$$y = 0 \text{ at } x = 0$$

$$y = 0 \quad x = R_c$$

whence it follows that  $C_2 = 0$  and

$$C_1 = -\frac{1}{R_c T_0} \cdot C_{D1} \frac{1}{2} \rho \left( \frac{\Omega^2 R_c^2}{\mu^1} \right) dc \left( \frac{\rho dc \Omega R_c}{\mu^1} \right)^a \frac{R_c^2}{(3+a)(4+a)}$$

using Eqs. 4.15, 4.6, 4.9

$$C_1 = \frac{-D^*}{T_0 (4+a)}$$

$\alpha$  at  $x = R_c$  is then found from Eq. 4.20

$$\alpha = \left( \frac{dy}{dx} \right)_{x=R_c} = \frac{D^*}{T_0} \left[ 1 - \frac{1}{4+a} \right] = \frac{D^*}{T_0} \frac{3+a}{4+a} = \frac{\Delta D^*}{T_0} \quad (4.22)$$

This result can also be deduced directly from Figure 228(e).

#### 4.2.2 The Cable Derivative $C_{Z_H}^*$

Assuming straight, level, horizontal flight with small perturbations, we see that the vertical force due to the cable is (Figure 228(b) )

$$Z^* = -T \xi = -T \frac{h}{R} \quad (4.23)$$

$\xi$  is approximately the angle of bank  $\varphi$  for the vehicle with wingtip tethering, if wire sag can be neglected as shown in Sec. 4.1.2. Substituting from Eq. 4.1 for T

$$Z^* = -m \frac{V^2}{R} \frac{h}{R} \quad (4.24)$$

$$C_{Z_H}^* = \frac{-mhv^2}{R^2} \cdot \frac{1}{\frac{1}{2} \rho V^2 S} \quad (4.25)$$

m is non-dimensionalized as in (Ref. 1), i.e. let

$$\mu = \frac{m}{\rho S \bar{c} / 2} \quad (4.26)$$

then

$$C_{Z_H}^* = \frac{-\mu \bar{c} h}{R^2} \quad (4.27)$$

Non-dimensionalizing h by dividing by c,

$$\frac{h}{c} = H \quad (4.28)$$

and

$$\frac{\partial C_{Z_H}^*}{\partial H} = C_{Z_H}^* = -\frac{\mu \bar{c}^2}{R^2} \quad (4.29)$$

#### 4.2.3 The Cable Derivative $C_{m_\theta}^*$

If the vehicle's angle of pitch varies by an angle  $\theta$  from  $\theta_0$ , then a restoring moment is set up as shown in Figure 228(c).

$$M^* = -\frac{T}{2} \frac{d}{2} \frac{\theta}{R_c} \cdot d \quad (4.30)$$

Non-dimensionalizing by using Eqs. 4.1 and 4.26, we get

$$C_m^* = -\frac{\mu d^2 \Theta}{4 R R_c} \quad (4.31)$$

$$\frac{\partial C_m^*}{\partial \Theta} = C_{m\Theta}^* = -\frac{\mu d^2}{4 R R_c}$$

#### 4.2.4 The Cable Derivatives $C_{n\psi}^*$ , $C_{l\varphi}^*$

To show that the roll and yaw response will tend to be small,  $C_{n\psi}^*$  is calculated for the vehicle in section 2 with wingtip harness attachment. Figure 228(d) gives the relevant parameters

$$N^* = T l = T R \gamma \quad (4.32)$$

$$\frac{\sin \gamma}{b/2} = \frac{\sin(-\psi)}{R_c} \quad \text{or} \quad \gamma = -\frac{\psi b/2}{R_c} \quad (4.33)$$

$$\therefore N^* = -T \psi \frac{b}{2} \frac{R}{R_c}$$

$$C_n^* = -\frac{\mu b}{2 R_c} \psi$$

Similarly  $\frac{\partial C_n^*}{\partial \psi} = -\frac{\mu b}{2 R_c} = C_{n\psi}^* \quad (4.34)$

$$\frac{\partial C_l^*}{\partial \varphi} = C_{l\varphi}^* = -\frac{\mu b}{2 R_c} \quad (4.35)$$

These derivatives are large, compared to conventional aircraft derivatives, as will be shown in Section 4.3.

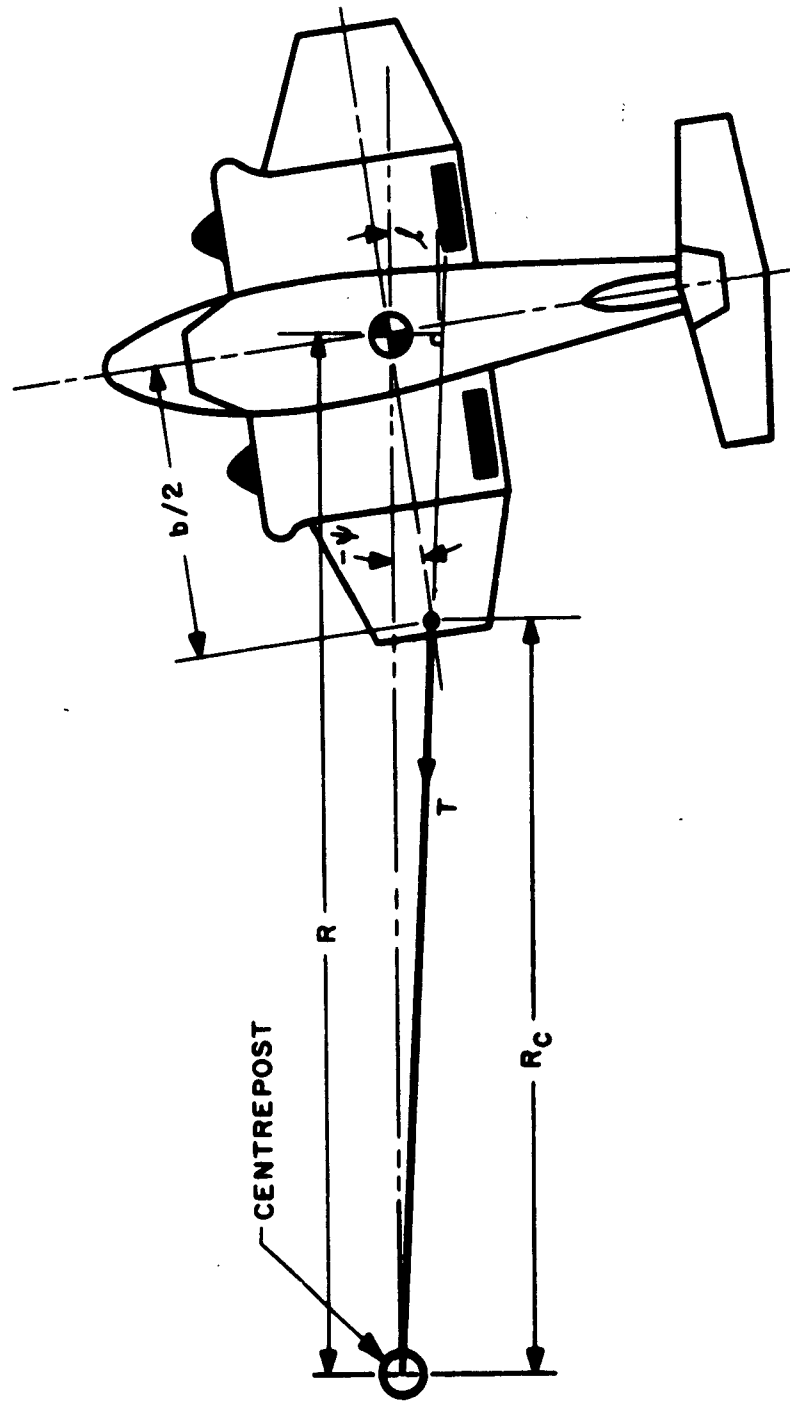


Figure 228(d). Cable Derivative  $C_{n\psi}^*$

### 4.3 COMPARISON OF VEHICLE AERODYNAMIC AND CABLE DERIVATIVES

The calculations will be performed for a 2.0 lb. vehicle at  $h = .25$  inches and forward speed of 30 ft/sec. The following are quantities used in the computations:

$R_c = 8.29$ ft.	$\rho = 2.38 \times 10^{-3}$ slugs/ft <sup>3</sup>
$R = 9.00$ ft.	$\mu$ lateral = $1.16 \times 10^2$
$h = 0.25$ in.	$\mu$ long. = $1.78 \times 10^2$
$V = 30.0$ ft/sec	$Re_V \approx 3.00 \times 10^2$
$W = 2.0$ lbs.	$\mu^1 = 3.73 \times 10^{-7}$
$\bar{c} = 5.56$ in.	$C_{DV} = 1.25$
$b = 17.0$ in.	$C_{D1} = 10.0$
$S = 91.2$ in <sup>2</sup>	$a = -.365$
$d_c = 1.51 \times 10^{-3}$ ft.	$C_{Dl} = 10.0 Re_l^{-3.65}$
$d = 2.00$ in.	$\rho_c = 8.56 \times 10^{-5}$ lbs/ft

$C_{DV}$ ,  $C_{D1}$  are found from Figure 235.

#### 4.3.1 Drag of Cable

$$C_D^* = \frac{2 C_{DV}}{4 + a} \cdot \frac{S_c}{S} \left( \frac{R_c}{R} \right)^2 = 0.0115$$

We can see that the cable drag is a significant fraction of the total drag and must be carefully considered in derivative analysis.

#### 4.3.2 Lift

For equilibrium flight

$$Z = W$$

By the most optimistic theory (in sense that  $\left| \frac{\partial Z}{\partial h} \right|$  is largest) we have  $Z = \frac{k}{h}$  for the cushion. Hence cushion derivative is

$$\left( \frac{\partial Z}{\partial h} \right)_{\text{cushion}} = -\frac{k}{h^2} = -\frac{W}{h}$$

also  $\frac{\partial Z^*}{\partial h} = -\frac{T}{R} = -\frac{WV^2}{gR^2}$  from Eq. 4. 14

Therefore the ratio  $\frac{(Z_h)_{\text{cushion}}}{Z_h^*} = \frac{R^2 g}{V^2 h} = \frac{g}{h \Omega^2}$

hence in our case

$$\text{ratio} = \frac{81 \times 32 \times 12}{900 \times .25} \approx 140$$

This ratio, for the same height  $h$ , falls to 10 when the speed of the vehicle is about 100 ft/sec.

In regimes where the vehicle has little inherent stability in heave, i.e.  $(Z_h)_{\text{cushion}} = 0$  the cable derivative would be the predominant one.

#### 4.3.3 Pitch

Artificial pitch stability is provided by  $C_{m\theta}^*$ .

$$C_{m\theta}^* = \frac{\mu d^2}{4RR_c} = -.0165$$

This value of  $C_{m\theta}^*$  is small, but enough to provide some stability in pitch if vehicle is neutrally stable. By variation of  $d$ , a limited range of pitch stability can be provided. This stabilization increases rapidly with  $d$  since it is squared in the equation.

#### 4.3.4 Roll and Yaw

$$C_{\ell\rho}^* = C_{n\psi}^* = \frac{\mu b}{2R_c} = -5.07$$

Typical values of  $C_{n\beta}$  are .05, therefore the roll and yaw response of the vehicle should be extremely small during flight, i.e. the wingtip harness has the effect of suppressing the roll and yaw degrees of freedom.

#### 4.3.5 Cable Dynamics<sup>(1)</sup>

The speed of propagation of a wave in a cable with tension  $T$  is

$$\nu = \sqrt{\frac{T}{\rho_c}}$$

(1) This analysis is due to Prof. B. Etkin

The characteristic time for this wave to travel the length of the cable and return is

$$\tau_1 = \frac{2R_c}{v} = 2R_c \sqrt{\frac{\rho c}{T}}$$

substituting for T and assuming  $R_c \approx R$

$$\tau_1 = 2R \sqrt{\frac{\rho c R}{mV^2}}$$

The time to complete one cycle in pitch or heave is

$$\tau_2 = \frac{\lambda}{V} \quad \text{where } \lambda = \text{one wavelength}$$

The ratio of these times is

$$\frac{\tau_1}{\tau_2} = \frac{2RV}{\lambda} \sqrt{\frac{m_c}{mV^2}} = \frac{2R}{\lambda} \sqrt{\frac{m_c}{m}}$$

We can see that the ratio of the characteristic times depends only on the length of the cable, the wavelength of an oscillation and the mass ratio of cable and vehicle.

Substituting the values which occurred in the experiments into the equation we get

$$\begin{aligned} \frac{\tau_1}{\tau_2} &= \frac{2 \times 9}{6} \times \sqrt{\frac{9 \times 8.56 \times 10^{-5}}{2}} \\ &= 3 \times 19.6 \times 10^{-3} \\ &= 58.8 \times 10^{-3} \end{aligned}$$

For the cable to adjust instantly to conditions at the end, the ratio of the above times must be small. If the ratio approaches one there may be dynamic interactions between the motion of the cable and that of the model. In the present case it is evident that such interaction can be neglected.

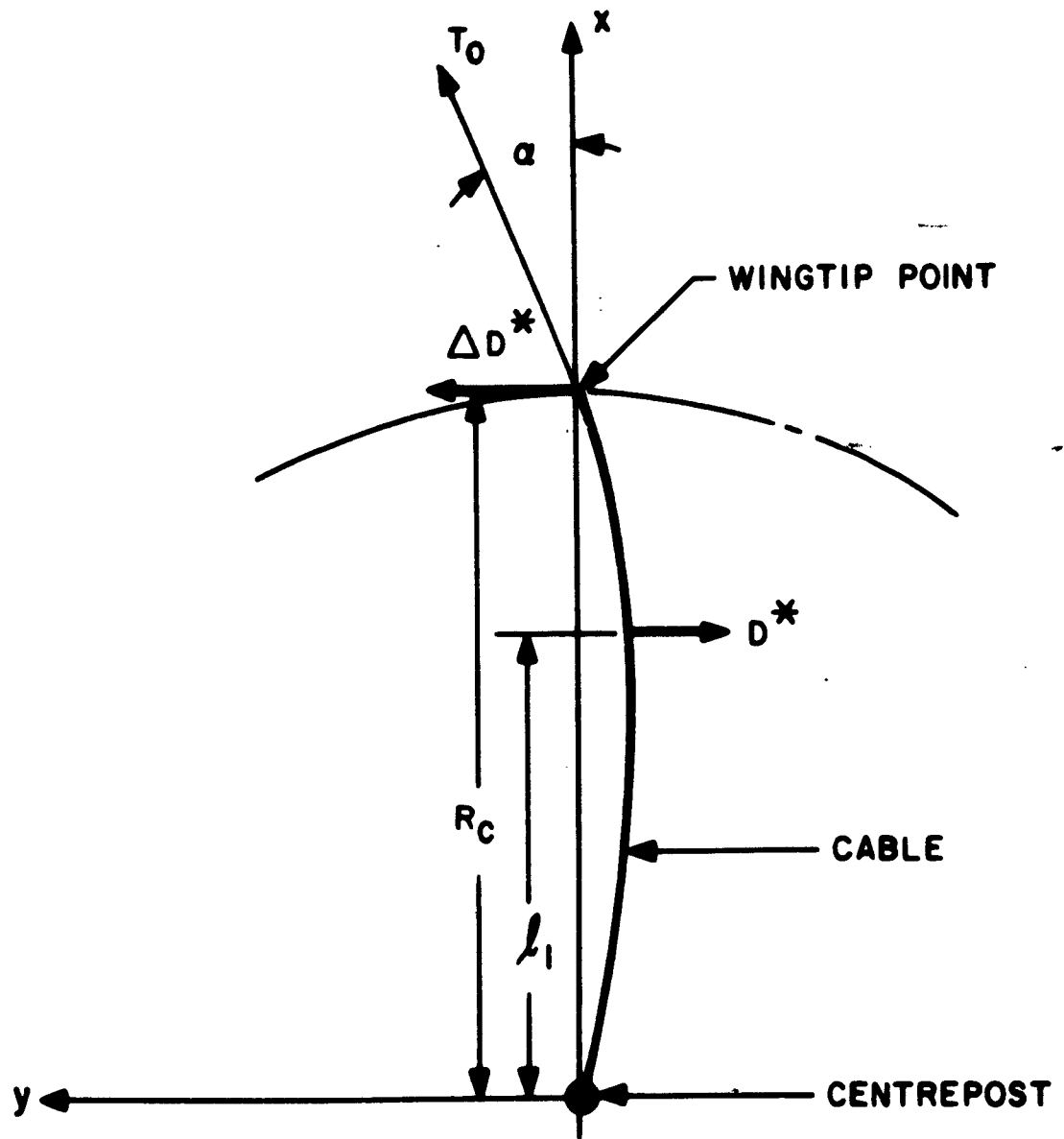


Figure 228(e). Drag Component of Cable Tension

## V. TESTING AND RESULTS

Initial hovering tests with an engine of half power indicated that severe mismatch of fan and load existed, so a new high power engine was installed. Hovering heights of .25 to .75 inches were achieved with the larger engine. Since there was no cooling for the engine without forward motion, as described in Section 3.4, hovering tests were limited to a few seconds before the engine overheated.

The vehicle was tethered to the centrepost and testing on the track began. A ramp was made by raising one edge of the door in the track to the required height. Values of .125, .25, .50 and .75 inches were used. The resulting ramp was set at the required height and the vehicle traversed it during each subsequent pass.

The accuracy of the results was limited by the camera shutter speed. With the electric motor drive the maximum filming rate of the camera was 32 frames per second. The shutter speed of the camera was fixed and proportional to the filming rate. While the filming rate was adequate to record and define the motion, the shutter speed was not fast enough to produce a clear and well defined picture of the reference points on the model. At the testing flight velocity of approximately 30 ft/sec, the background reference lines were fan-shaped, with both ends one inch blurs at the frame edge, due to the fixed camera and rotating mirror arrangement.

Three fan configurations were tested. On all fans the outside diameter of 3.5 inches and hub diameter of 1.5 inches were kept constant. The first fan had 12 fibre blades of .75 inch chord. The results from tests indicated that back pressure on the fan was too great to allow the engine to accelerate up to full speed (12,000 to 15,000 r.p.m.). With the bottom cover of the wing removed, the vehicle hovered at a height of .25 inches.

The second fan tested was of identical construction to the first, except that the blade chord was .50 inches. In the peripheral - jet configuration the hovering heights obtained were very small, but in the plenum chamber configuration the model performed better. A graph of the test run with .50 inch high ramp is given as Figure 231.

The reference point height and angle of pitch  $\theta$ , were calculated from test records similar to the ones in Figures 229 and 230. With the model on the ground the zero angle of pitch  $\theta_0$  is defined by the tailpoint height: 2.375 inches, and nosepoint height: 1.905 inches above the ground. The reference point used for the calculations and shown on Figures 231' to 234 is midway between these two points: 2.240 inches above ground, vertically up from the midchord of the wing at the centreline of the vehicle. Horizontal separation of nose and tail points is 14.25 inches. The wingtip point is 2.406 inches above ground when model's angles of pitch and roll are zero. Because the nose and tail points are on the side of the vehicle the straight line joining them is 1.015 inches out from the centreline of the aircraft toward the camera, at wing midchord (perpendicular to X, Z plane, as defined in Ref. 1 or 20).

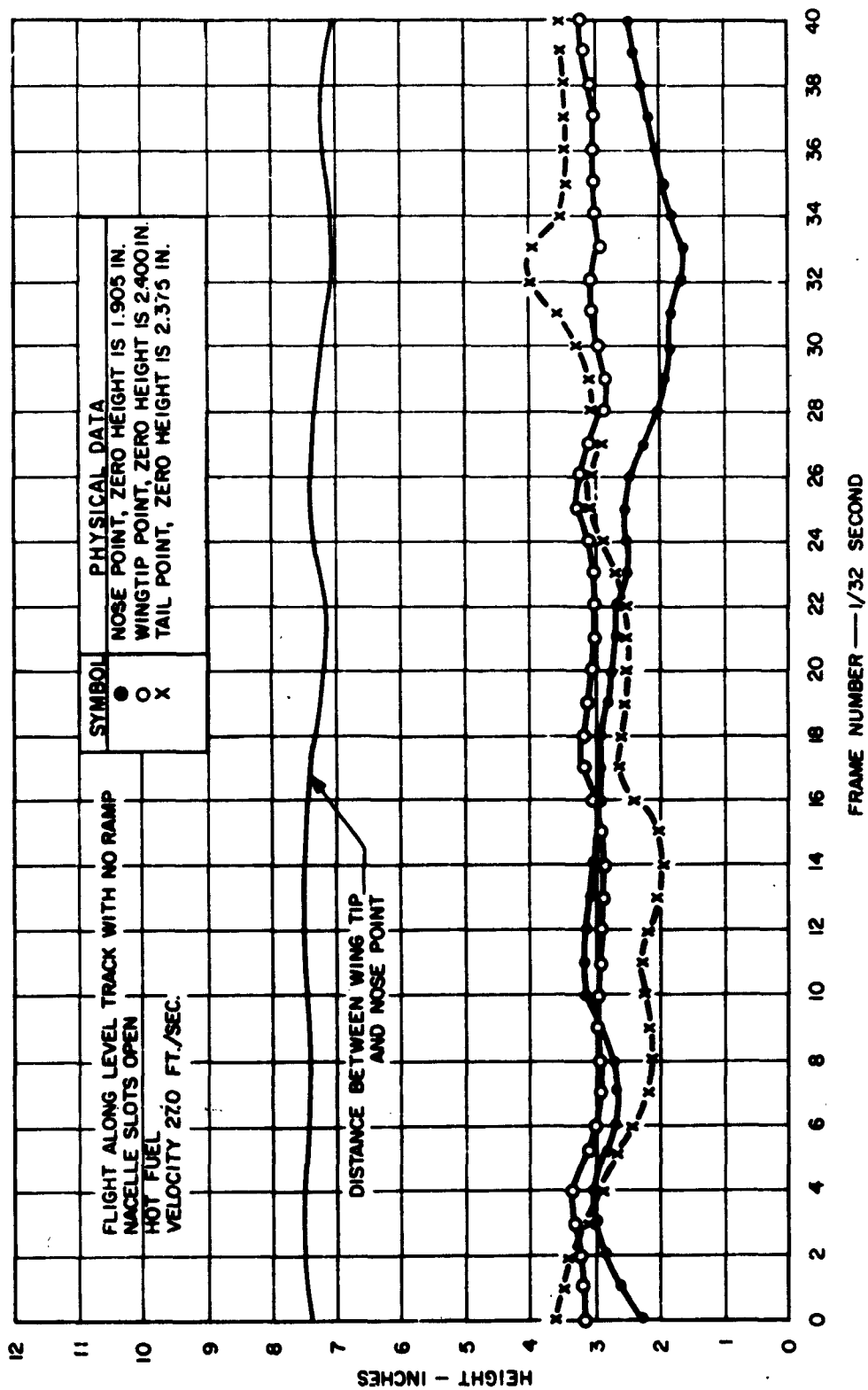


Figure 229. Unreduced Record Taken from Flight along Track with No Ramp Installed

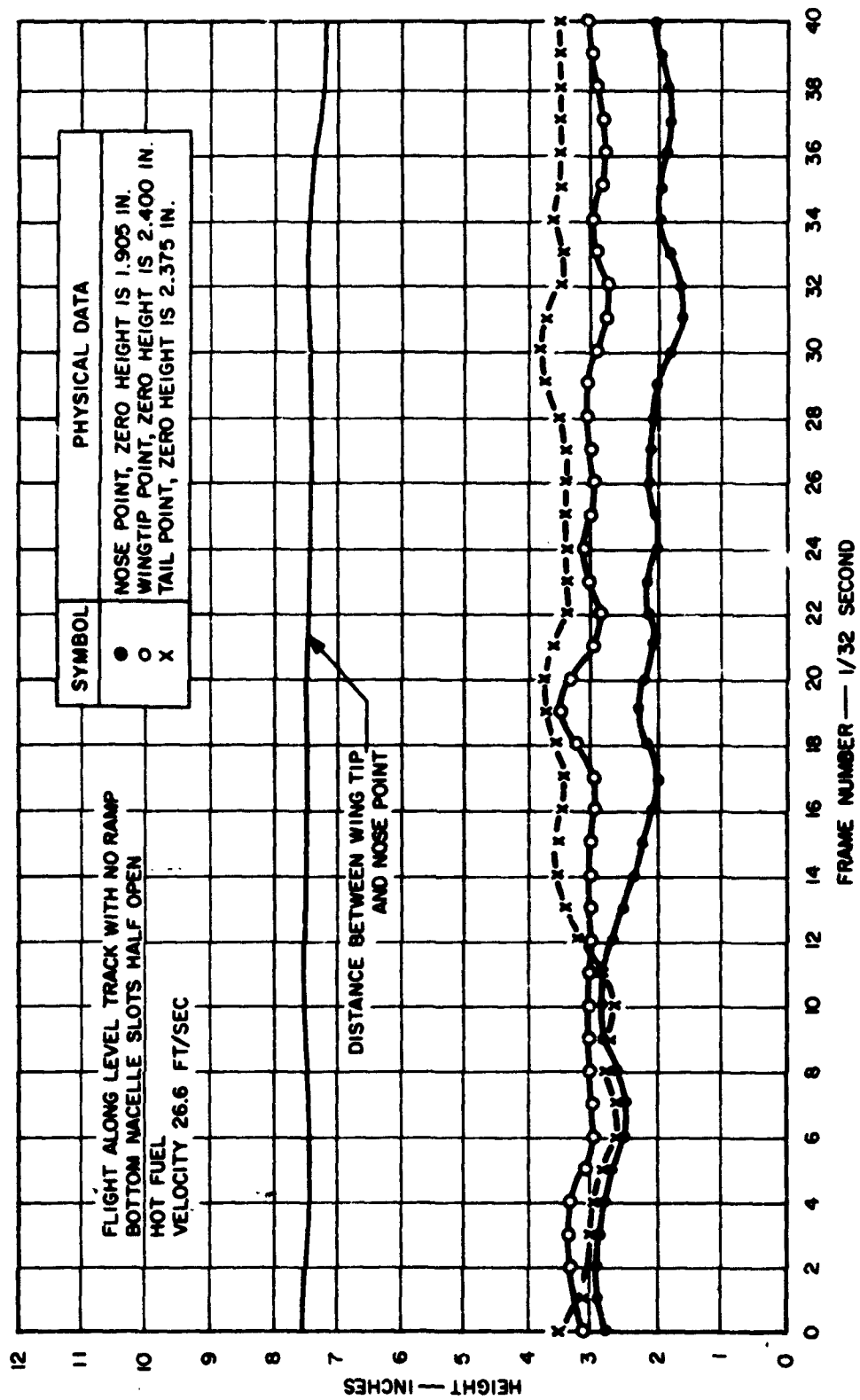


Figure 230. Unreduced Record Taken from Flight along Track with No Ramp Installed

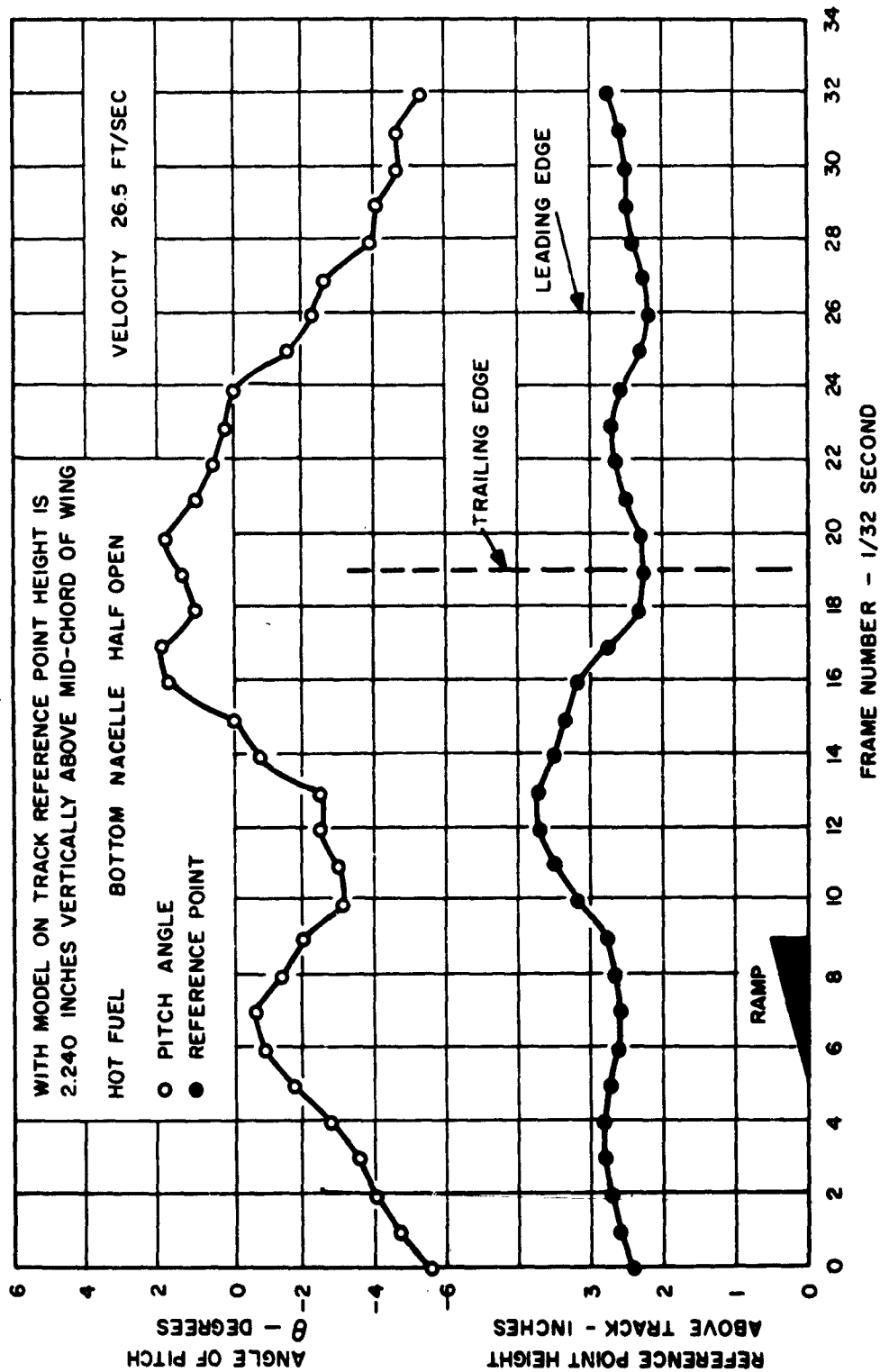


Figure 231. Flight in Plenum Chamber Configuration over .50 inch Ramp in Track

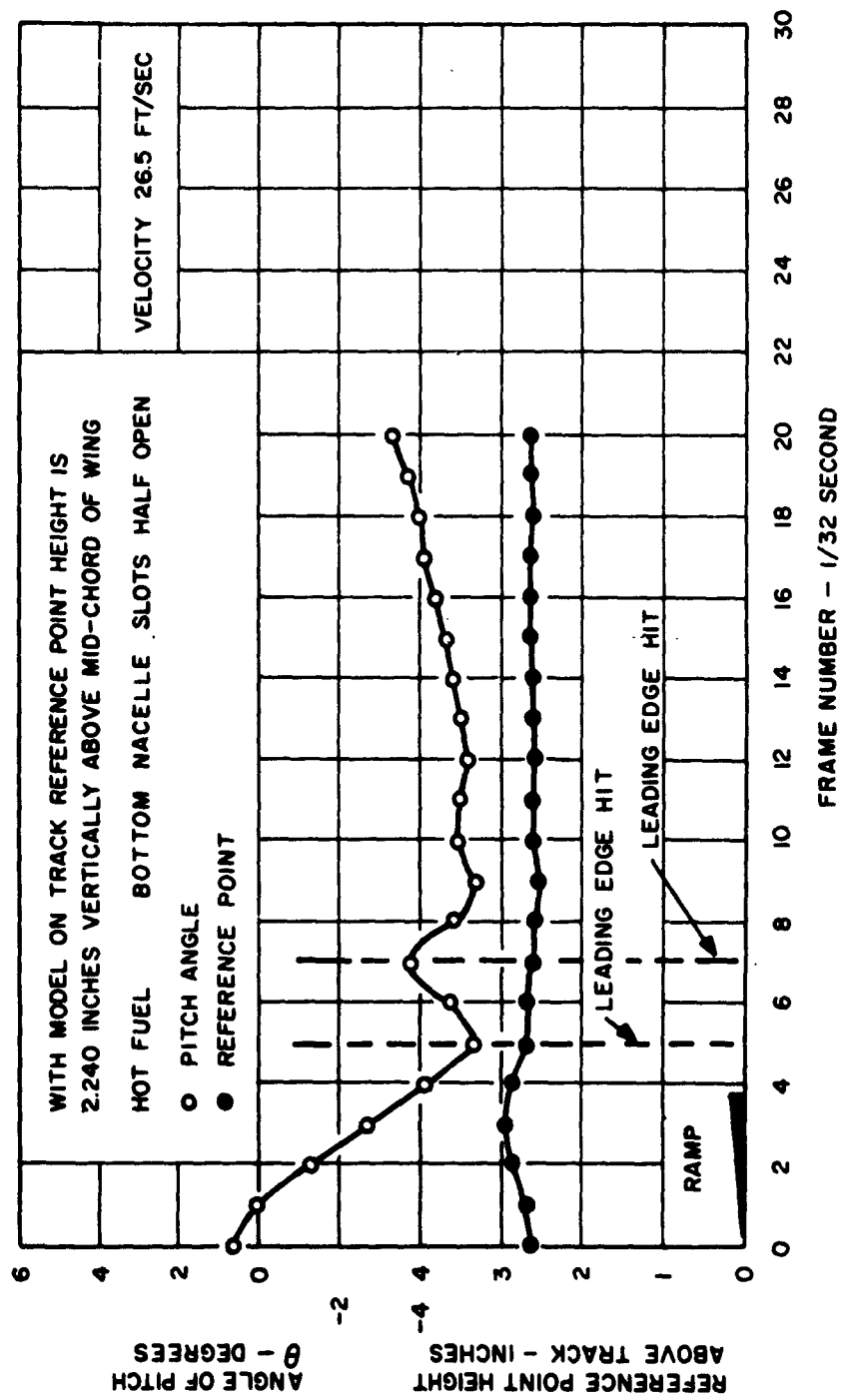


Figure 232. Flight in Annular Jet Configuration over .125 inch Ramp in Track

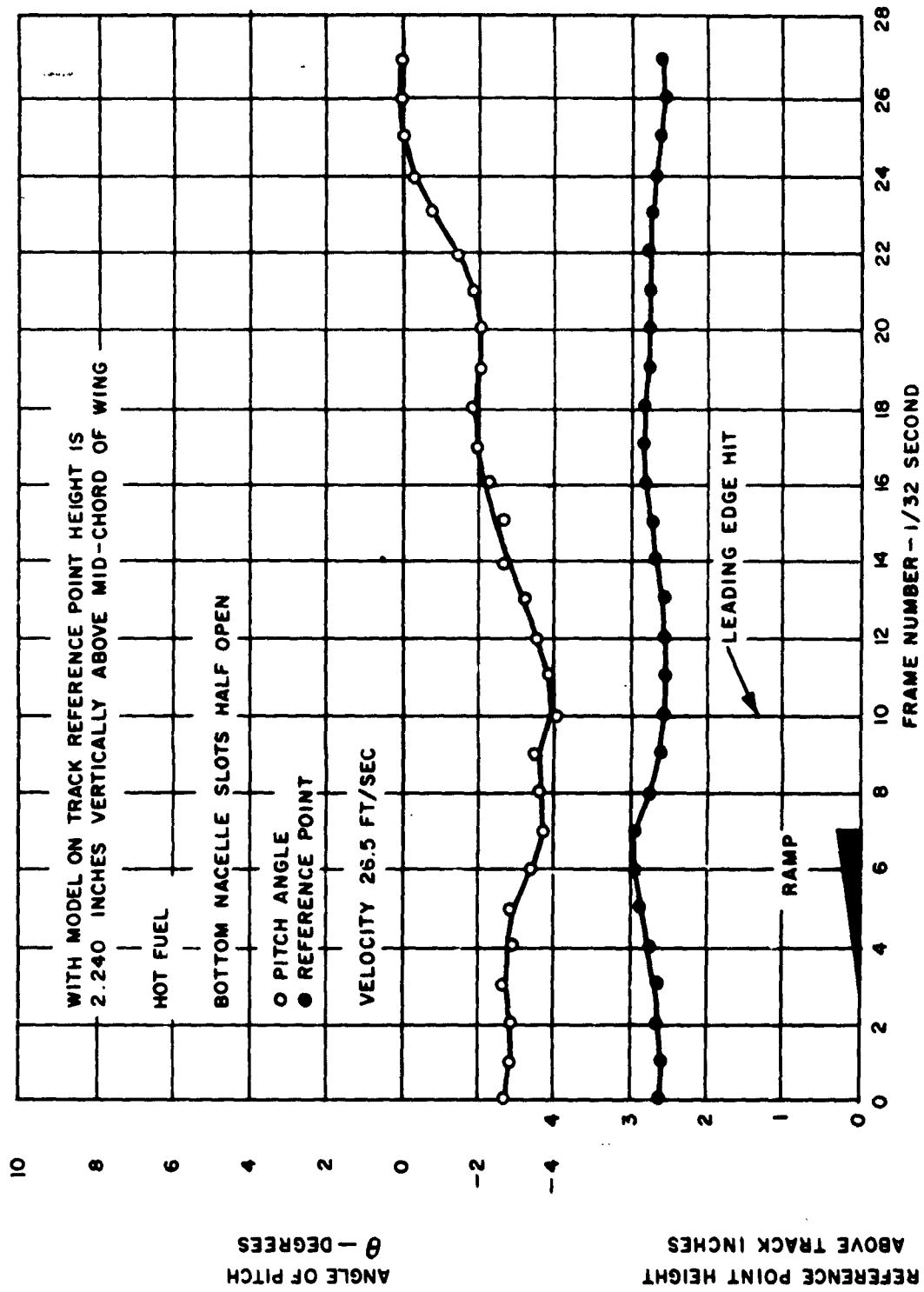


Figure 233. Flight in Annular Jet Configuration over .25 inch Ramp in Track

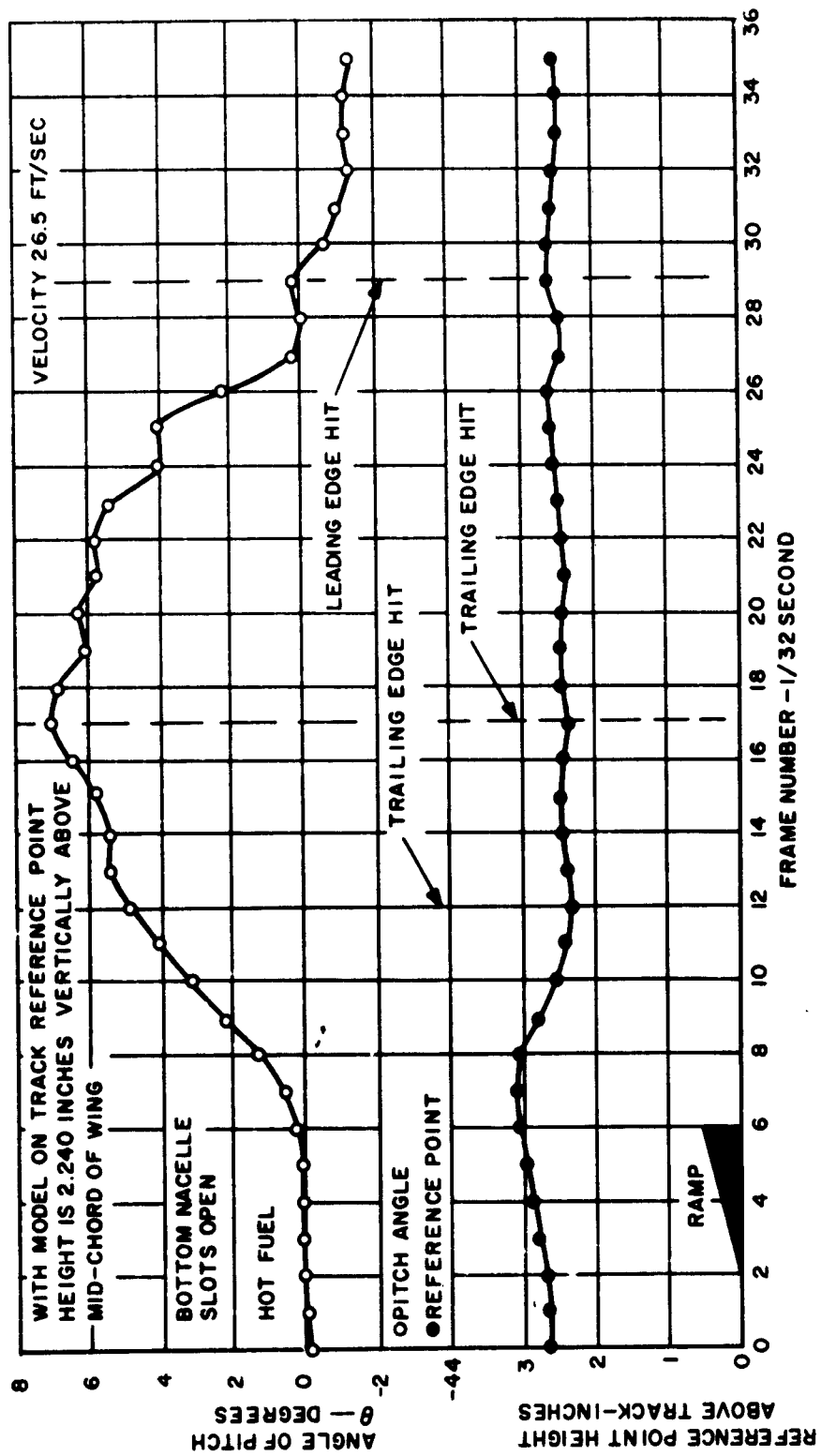


Figure 234. Flight in Annular Jet Configuration over .50 inch Ramp in Track

The centre of gravity of the aircraft was fixed at 54.5% chord for the runs shown in Figures 232 to 234. The pitching moment of inertia was .0123 slugs-ft<sup>2</sup>.

Corrections were made for parallax of the readings due to displacement of the vehicle reference points from the backboard. Yaw and roll angles were calculated but not plotted because the variation was no more than  $\pm 0.8$  degrees. Collisions of the leading and trailing edge of the wing with the groundboard were frequent and have been indicated on all "reduced" graphs of test records.

The solidity of the fan was further decreased by cutting away 6 of the 12 blades from the fan with .50 inch cord. As a result the vehicle's flight in the plenum chamber configuration was highly unstable. Heights of wing bottom above the ground of 3 inches were reached during some of the runs. In the peripheral jet configuration the flight was more stable in height, with .25 to .50 inches ground clearance. Figures 232 to 234 are results from test flights over .125, .25 and .50 inch ramp heights, obtained from frame by frame analysis of the test film. The tests were performed in the peripheral jet configuration with one half of the lower slot on the back of each nacelle open for forward thrust. It was found experimentally that this gave the highest flight above the groundboard without substantial loss of forward velocity. The traces suggest a highly damped heave oscillation and a very lightly damped pitch oscillation, as expected, since the annular jet formed by the wing has little stability in pitch due to the relatively large aspect ratio.

The track was carefully levelled during construction, but due to the butrate dope which was applied for protection against engine fuel, the boards had buckled at the joints. A few runs were taken with no ramp in the track. Two unreduced test records are shown in Figures 229 and 230. The results indicate frequent hits of both leading and trailing edges of the wing with the ground. The pitching mode is very lightly damped, if not unstable. Centre of gravity height is nearly constant, indicating a steady flight height.

A test was performed to see if the wake would linger on the track and disturb the model on subsequent passes. One piece of track was amply equipped with wool tufts on the groundboard, over the background grid and around the edges of board and light fixture. From visual observations, it was seen that the wake was lost through the cracks between backboard and groundboard, and no motion of the tufts was evident after the model had progressed 120° from the tufted section.

## VI. CONCLUSIONS

It can be concluded from the theoretical analysis of cable restraints, and experimental track testing, that this method can be used for testing of vehicles with ground effect, from hovering, through transition, to full forward flight. Longitudinal stability, trim and control effectiveness can be investigated. Additional synthetic stability can be introduced by suitable harnessing the model (e.g. Sec. 4.2.3). Response to gusts and turbulent air could be studied by installing fans at various places around the track.

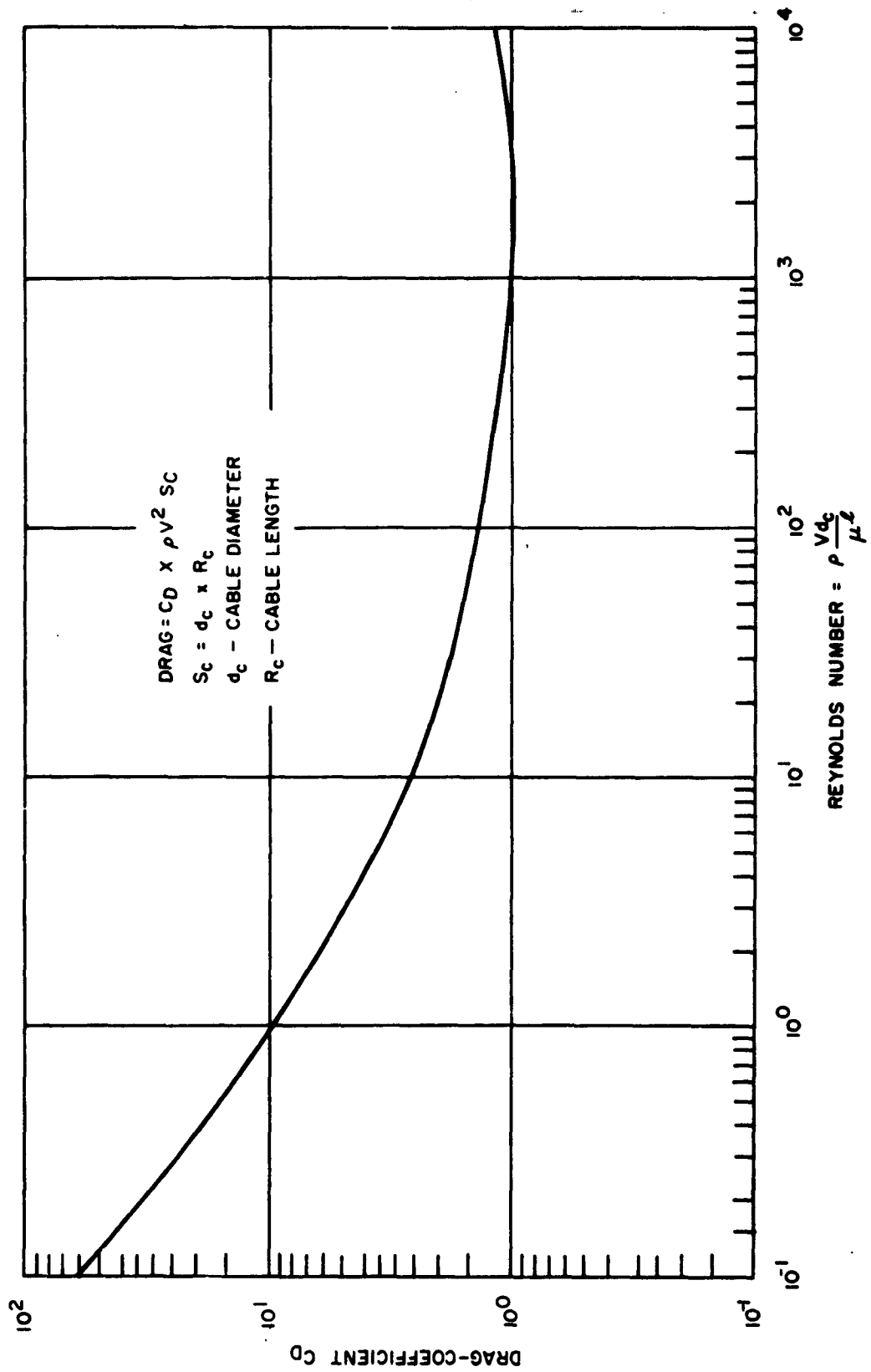


Figure 235. Drag Coefficient for Two-Dimensional Flow around a Cylinder

From the experience gained during this phase of testing it appears that future development of the facility should proceed along the following lines:

- a. Design of a suitable one-fan vehicle of the GETOL type. The vehicle should be designed as an integral unit of fan, powerplant and fuel supply. To this unit planforms of various aspect ratios and shapes could be fastened for testing.
- b. Instrumentation of models to enable outputs of flight results to be directly processed during test runs by analogue equipment.

The photographic method should be improved as outlined in this report, and retained as an absolute check on instrumentation accuracy and response.

#### REFERENCES

1. Etkin, B. Dynamics of Flight: Stability and Control. John Wiley and Sons, 1959.
2. Braun, G. W. Testing Longitudinal Stability on Models in Harnessed Circling Flight. AF Tech. Report. No. 5979, Oct. 1959.
3. Tinajero, A. A. Static Behaviour of a Special Planform GEM Model Utilizing an Integrated System for Lift and Propulsive Thrust. D.T.M.B. Aero Rep. 975 March, 1960.
4. Tinajero, A. A. Fresh, J. N. Aerodynamic Response of a 7-foot GEM Flying Over Uneven Surfaces, D.T.M.B. Aero Rep. 982, June, 1960
5. Eames, M. C. Basic Principles of the Stability of Peripheral Jet Ground Effect Machines. I.A.S. Paper No. 61-71, January, 1961.
6. Walker, N. K. Preliminary Stability, Control and Handling Criteria for Ground Effect Machines (GEMS) I.A.S. Paper No. 61-69, January, 1961.
7. Vogler, R. D. Effects of Various Arrangements of Slotted and Round Jet Exits on the Lift and Pitching Moment Characteristics of a Rectangular-Base Model at Zero Forward Speed. NASA TN-660, February, 1961.
8. Tinajero, A. A. Preliminary Investigation of Planform Effects on Augmentation Parameter for Peripheral-Jet Ground-Effect Machines, D.T.M.B. Aero Rep. 972, February, 1960.
9. Chaplin, H. R. Design Study of a 29-Foot GEM D.T.M.B. Aero Rep. 999, April, 1961.

10. Chaplin, H. R.                   A Preliminary Design Technique for Annular-Jet Ground-Effect Machines (GEMS) D.T.M.B. Aero. Rep. 966, Sept. 1959
11. Various Authors.               Symposium on Ground Effect Phenomena. A  
In this report are               Compilation of the Papers Presented Oct. 21  
contained nearly all             to 23, 1959 at Princeton University.  
references to early  
work on Ground Effect  
Phenomena.
12. Turner, R.                     Ground Influence on a Model Airfoil with a  
Jet-Augmented Flap as Determined by two  
Techniques. NASA TN D-658, Feb. 1961.
13. Campbell, J. P.               Techniques for Testing Models of VTOL and  
STOL Aircraft, AGARD Rep. 61, Aug. 1956.
14. Baals, D. D.                  Model Selection and Design Practices to the  
Development of Specific Aircraft. AGARD Rep.  
21, Feb. 1956
15. Davie, R. P.                  Wind Tunnel Models. AGARD Rep. 19, Aug. 1956.
16. Anscombe, A.                 Some Comments on High-Lift Testing in Wind  
Williams, J.                     Tunnels with Particular Reference to Jet-  
Blowing Models. AGARD Rep. 63, Aug. 1956.
17. Klein, H.                    Dimensionless Parameters for Airplane Model  
Testing. Douglas Rep. SM-14025, March, 1951.
18. Cohen, H.                    Gas Turbine Theory. Longmans, Green and Co.  
Rogers, G. F. C.
19. Durham, F. P.                Aircraft Jet Powerplants, Prentice Hall, 1951.
20.                                 Agard Flight Test Manual Volume II: Stability  
and Control.
21. Sokolnikoff, I. S.           Higher Mathematics for Engineers and Phys-  
and E. S.                       icists. McGraw-Hill, 1941.
22.                                 Mark's Mechanical Engineers Handbook.
23. Eshbach, O. W.               Handbook of Engineering Fundamentals.
24. Binder, R. C.                Fluid Mechanics. Prentice Hall.
25. Gracey, W.                   The Experimental Determination of the Moments  
of Inertia of Airplanes by a Simplified Com-  
pound-Pendulum Method, June 1948, NACA TN  
No. 1629.

## DISTRIBUTION

USAAVNBD	1
ARO, Durham	2
OCRD, DA	1
ARO, OCRD	1
CofT	2
USATCDA	1
USATMC	1
USATRECOM	26
USATRECOM LO, USARDG (EUR)	1
TCLO, USAAVNS	1
AFSC (SCS-3)	1
AFSC (Aero Sys Div)	1
CNR	2
Dav Tay Mod Bas	1
USASGCA	1
Canadian LO, USATSCH	3
BRAS, DAQMG (Mov & Tn)	4
USASG, UK	1
Langley Rsch Cen, NASA	1
NASA, Wash., D. C.	6
Ames Rsch Cen, NASA	2
USGPO	1
ASTIA	10
BUWEPS, DN	1
Wind Tun Br, NASA	1
Institute of Aerophysics	1
Forrestal Research Center	1
AMC	1
MOCOM	3
USSTRICOM	1
Vertol Division, The Boeing Co.,	10

TRECOM

Vertol Division, Boeing Company, Morton, Pennsylvania  
RESEARCH PROGRAM TO DETERMINE THE FEASIBILITY AND POTENTIAL OF  
THE GROUND EFFECT TAKE-OFF AND LANDING (GETOL) CONFIGURATION  
Volume I and II - Research Program to Determine the Feasibility and Potential  
of the Ground Effect Take-Off and Landing (GETOL) Configuration by W.  
Stepniowski, H. Wahl, F. McHugh, R. Hooper and J. Gaffney, TCRREC 62-63,  
March 28, 1962 Volume I, 207 pages, Volume II, 194 pages (Contract DA44-  
177-TC-663) USATRECOM Task 437-7420.

UNCLASSIFIED REPORT  
Boeing-Vertol final report (R276) has been prepared as Volume I and Volume II  
under Contract DA44-177-TC-663 to describe the effort expended to determine  
the feasibility and potential of the Ground Effect Take-Off and Landing (GETOL)  
configuration. The object of such an aircraft is to combine relatively high  
cruising speeds with the capability of operating from any flat surface (impre-  
pared fields, water, snow, etc.)

The main part of testing was performed by NASA at their Langley Field facilities,  
namely in the static room, low track, and wind tunnel. Princeton and Toronto  
Universities also contributed data as the result of their development testing effort.  
NASA test results were utilized as the basic information. Analytical methods for  
data reduction and presentation were developed, thus permitting evaluation of the  
performance, stability and control characteristics of the GETOL type aircraft.  
The results of the whole GETOL program provided a basis for a subsequent  
design analysis and layouts of the Flight Research Vehicle (FRV).

Acquisition of basic GETOL aerodynamic data and development of method of  
analysis and data presentation should be considered as the most significant  
technical advance achieved under this program.

TRECOM

Vertol Division, Boeing Company, Morton, Pennsylvania  
RESEARCH PROGRAM TO DETERMINE THE FEASIBILITY AND POTENTIAL OF  
THE GROUND EFFECT TAKE-OFF AND LANDING (GETOL) CONFIGURATION  
Volume I and II - Research Program to Determine the Feasibility and Potential  
of the Ground Effect Take-Off and Landing (GETOL) Configuration by W.  
Stepniowski, H. Wahl, F. McHugh, R. Hooper and J. Gaffney, TCRREC 62-63,  
March 28, 1962 Volume I, 207 pages, Volume II, 194 pages (Contract DA44-  
177-TC-663) USATRECOM Task 437-7420.

UNCLASSIFIED REPORT  
Boeing-Vertol final report (R276) has been prepared as Volume I and Volume II  
under Contract DA44-177-TC-663 to describe the effort expended to determine  
the feasibility and potential of the Ground Effect Take-Off and Landing (GETOL)  
configuration. The object of such an aircraft is to combine relatively high  
cruising speeds with the capability of operating from any flat surface (impre-  
pared fields, water, snow, etc.)

The main part of testing was performed by NASA at their Langley Field facilities,  
namely in the static room, low track, and wind tunnel. Princeton and Toronto  
Universities also contributed data as the result of their development testing effort.  
NASA test results were utilized as the basic information. Analytical methods for  
data reduction and presentation were developed, thus permitting evaluation of the  
performance, stability and control characteristics of the GETOL type aircraft.  
The results of the whole GETOL program provided a basis for a subsequent  
design analysis and layouts of the Flight Research Vehicle (FRV).

Acquisition of basic GETOL aerodynamic data and development of method of  
analysis and data presentation should be considered as the most significant  
technical advance achieved under this program.

TRECOM

Vertol Division, Boeing Company, Morton, Pennsylvania  
RESEARCH PROGRAM TO DETERMINE THE FEASIBILITY AND POTENTIAL OF  
THE GROUND EFFECT TAKE-OFF AND LANDING (GETOL) CONFIGURATION  
Volume I and II - Research Program to Determine the Feasibility and Potential  
of the Ground Effect Take-Off and Landing (GETOL) Configuration by W.  
Stepniowski, H. Wahl, F. McHugh, R. Hooper and J. Gaffney, TCRREC 62-63,  
March 28, 1962 Volume I, 207 pages, Volume II, 194 pages (Contract DA44-  
177-TC-663) USATRECOM Task 437-7420.

UNCLASSIFIED REPORT  
Boeing-Vertol final report (R276) has been prepared as Volume I and Volume II  
under Contract DA44-177-TC-663 to describe the effort expended to determine  
the feasibility and potential of the Ground Effect Take-Off and Landing (GETOL)  
configuration. The object of such an aircraft is to combine relatively high  
cruising speeds with the capability of operating from any flat surface (impre-  
pared fields, water, snow, etc.)

The main part of testing was performed by NASA at their Langley Field facilities,  
namely in the static room, low track, and wind tunnel. Princeton and Toronto  
Universities also contributed data as the result of their development testing effort.  
NASA test results were utilized as the basic information. Analytical methods for  
data reduction and presentation were developed, thus permitting evaluation of the  
performance, stability and control characteristics of the GETOL type aircraft.  
The results of the whole GETOL program provided a basis for a subsequent  
design analysis and layouts of the Flight Research Vehicle (FRV).

Acquisition of basic GETOL aerodynamic data and development of method of  
analysis and data presentation should be considered as the most significant  
technical advance achieved under this program.

TRECOM

Vertol Division, Boeing Company, Morton, Pennsylvania  
RESEARCH PROGRAM TO DETERMINE THE FEASIBILITY AND POTENTIAL OF  
THE GROUND EFFECT TAKE-OFF AND LANDING (GETOL) CONFIGURATION  
Volume I and II - Research Program to Determine the Feasibility and Potential  
of the Ground Effect Take-Off and Landing (GETOL) Configuration by W.  
Stepniowski, H. Wahl, F. McHugh, R. Hooper and J. Gaffney, TCRREC 62-63,  
March 28, 1962 Volume I, 207 pages, Volume II, 194 pages (Contract DA44-  
177-TC-663) USATRECOM Task 437-7420.

UNCLASSIFIED REPORT  
Boeing-Vertol final report (R276) has been prepared as Volume I and Volume II  
under Contract DA44-177-TC-663 to describe the effort expended to determine  
the feasibility and potential of the Ground Effect Take-Off and Landing (GETOL)  
configuration. The object of such an aircraft is to combine relatively high  
cruising speeds with the capability of operating from any flat surface (impre-  
pared fields, water, snow, etc.)

The main part of testing was performed by NASA at their Langley Field facilities,  
namely in the static room, low track, and wind tunnel. Princeton and Toronto  
Universities also contributed data as the result of their development testing effort.  
NASA test results were utilized as the basic information. Analytical methods for  
data reduction and presentation were developed, thus permitting evaluation of the  
performance, stability and control characteristics of the GETOL type aircraft.  
The results of the whole GETOL program provided a basis for a subsequent  
design analysis and layouts of the Flight Research Vehicle (FRV).

Acquisition of basic GETOL aerodynamic data and development of method of  
analysis and data presentation should be considered as the most significant  
technical advance achieved under this program.

1. Final Summary Report GETOL Configuration

2. Contract DA44-177-TC-663

1. Final Summary Report GETOL Configuration

2. Contract DA44-177-TC-663

1. Final Summary Report GETOL Configuration

2. Contract DA44-177-TC-663

1. Final Summary Report GETOL Configuration

2. Contract DA44-177-TC-663